# Electrostatic Evaluation of a Unipolar Diffusion and Field Charger of Aerosol Particles by a Corona Discharge

PANICH INTRA<sup>1\*</sup>, ARTIT YAWOOTTI<sup>1</sup>, AND NAKORN TIPPAYAWONG<sup>2</sup>

<sup>1</sup>Research Unit of Electrostatic Applications in Energy and Environment, College of Integrated Science and Technology, Rajamangala University of Technology Lanna,

Chiang Mai 50220 Thailand

<sup>2</sup>Department of Mechanical Engineering, Faculty of Engineering, Chiang Mai University,

Chiang Mai 50200 Thailand

\*Corresponding Author: E-mail: panich\_intra@yahoo.com

A unipolar diffusion and field charger by corona discharge is presented and electrostatically evaluated for charging aerosol particles in the present paper. The electrostatic characteristics of the charger were investigated by measuring the ion number concentrations corresponding to the discharge and charging currents with an electrometer. The discharge and charging currents and ion number concentration in the discharge and charging zones of the charger increased with corona voltage. The magnitudes of the ion number concentration for positive and negative coronas in the discharge zone were in the range from  $1.34 \times 10^{13}$  to  $1.84 \times 10^{15}$  ions/m³ and  $7.34 \times 10^{13}$  to  $2.64 \times 10^{15}$  ions/m³, respectively. For the charging zone, the ion number concentrations for positive and negative coronas were in the range from  $2.95 \times 10^{13}$  to  $1.52 \times 10^{14}$  ions/m³ and  $2.06 \times 10^{13}$  to  $1.47 \times 10^{14}$  ions/m³, respectively. The electric field strength and distribution of the charger in the discharge and charging zones were calculated by a commercial computational fluid dynamics software package to predict the behavior of the electric field strength and lines in the discharge and charging zones of the charger. Numerical calculation results of electric field distribution and lines through the inner electrode showed good agreement with experimental results. Also, the mean

charge per particle for particle diameters in the range from 0.01 to 50 µm for various operating conditions of the charger was theoretically evaluated. For both diffusion and field charging, lower aerosol flow rate and higher corona voltage resulted in an increase in the mean charge per particle within the charger. This simple charger proved to be particularly useful in diffusion and field charging of aerosol particles in particulate matter detector instruments for measuring PM10 and PM2.5 concentration.

**Keywords** aerosol, corona discharge, unipolar charger, diffusion charging, field charging

### Introduction

Any solid or liquid material suspended in air with particles of diameters less than 10 and 2.5 µm are often referred to as PM10 and PM2.5, respectively (Hinds, 1999). The investigation of particulate matter has focused on measuring and monitoring this fraction because the U.S. Environmental Protection Agency (EPA) promulgated a new regulation for the mass concentrations of PM10 and PM2.5. The standards were based on results of recent health effects studies (EPA, 1997); PM10 and PM2.5 could penetrate the alveoli and bypass the upper respiratory tract because they are small enough to allow deposition in places where they can do the most damage. The hazard caused by PM10 and PM2.5 depends on the chemical composition of the particulate matter and on the site where they are deposited within the human respiratory system. In order to evaluate the degree of hazard posed to the atmosphere, measurement of the particulate matter concentration in the ambient atmosphere is an important step in atmospheric particulate matter determination.

A particulate matter detector is one of the valuable tools for these applications. One of the most used instruments is an electrical aerosol detector. A typical detector consists of three key components: a size selective inlet, an aerosol particle charger, and the measurement of the electric current on the charged aerosols, normally with an electrometer. The readout of a detector depends strongly on the electrical charging technique used (Liu and Pui, 1975; Lee *et al.*, 2001; Intra and Tippayawong, 2011). Thus, electrical charging of aerosol particles is an important component of

any detector. Its purpose is to impart the aerosol particles with a known net electric charge. Concentration of particulate matter is commonly determined through the net electrical charge of aerosol particles and prediction of the concentration of particulate matter requires the knowledge of the mean charge per particle (Intra and Tippayawong, 2011a). Corona discharge is one of the most common techniques used to produce high ion concentrations for unipolar aerosol particles charging. A number of unipolar corona chargers for aerosol charging have been developed and used in different applications (Alonso and Alguacil, 2008; Hewitt, 1957; Wiedensohler *et al.*, 1994; Buscher *et al.*, 1994; Biskos *et al.*, 2005; Intra and Tippayawing, 2010; Kruis and Fissan, 2001; Intra, 2012). Intra and Tippayawong reviewed the unipolar corona discharger designs for airborne particle charging (Intra and Tippayawong, 2009; Intra and Tippayawong, 2011b). Their review focused on the unipolar charger based on the corona discharge, and covered the operating principles as well gave detailed physical characteristics of these chargers, including the corona-wire and corona-needle chargers.

In the case of PM10 and PM2.5, unipolar chargers are usually based on combined diffusion and field charging (Liu and Kapadia, 1978). For particles larger than 1 µm, field charging was dominant, and for smaller particles smaller than 0.1 µm, thermal diffusion became dominant, and therefore diffusion charging became important (Hinds, 1999). Since diffusion and field charging are proportional to the electric field strength and distribution in the charging zone, the unipolar diffusion and field charger would have a high ion number concentration (usually greater than 10<sup>13</sup> ions/m³) and the presence of a strong electric field (usually greater than 10<sup>4</sup> V/m) (Hind, 1999). However, the loss of charged particles due to high electric field strength in the charging zone is often severe, and needs to be addressed in the development of diffusion and field corona chargers. To avoid these problems, the electrostatic characteristics of the unipolar diffusion and field charger by corona discharge e.g. electric field strength and distribution, current-voltage relationship, ion number concentration, and particle charging should be studied extensively under various operating conditions of the charger.

In this study, a corona diffusion and field charger for unipolar charging of aerosol particles was built and evaluated electrostatically. The electrostatic characteristics of the charger were tested by measuring the discharge and charging current corresponding to the ion number concentration using an electrometer. A commercial computational fluid dynamics (CFD) software package was used to calculate the electric field strength and distribution in the discharge and charging zones of the charger. Mean diffusion and field charge per particle for particle diameters in the range from 0.01 to 50 µm for various operating conditions of the charger were determined. The results are given below.

### Description of corona diffusion and field charger

A schematic diagram of the prototype corona diffusion and field charger is shown in Figure 1. The charger's geometrical configuration is similar to that in the unipolar triode charger used by Intra (2012). However, there are differences between those from Intra (2012) and the present work, as follows; (i) in order to reduce diffusion and space charge losses of the particles inside the charger, aerosol flow guide inlet and outlet geometries were modified to ensure uniform flow distribution across the annular entrance to the charging zone; (ii) the corona wire in the discharge zone was rearranged to ensure a uniform electric field distribution and stability discharge current over the perforated screen openings on the inner cylinder to the charging zone of the charger; and (iii) it is a low complexity and inexpensive system. The prototype triode charger was 126 mm in length and 67 mm in diameter. As Figure 1 shows, it consisted of two concentric cylinders with a corona-wire (20 mm in length and 0.3 mm in diameter) placed along the axis of the cylinders. The inner and outer cylinders were fabricated of stainless steel, and were polished to an extremely fine surface finish to avoid distortion of the electrical field from small surface scratches and imperfections. Stainless steel was used because it is electrically conductive, inert, corrosion resistant and very hard, and therefore resistant to scratching. The inner and the outer radii of the annular charging zone were 17 mm and 30 mm. The electrical insulation was provided by a Delrin spacer between the inner and outer cylinder. The aerosol flows in the space between the cylinders. A DC high voltage was applied to the corona-wire to produce a corona discharge and the generated ions migrated toward the inner cylinder due to the high electric field in the region. In order to allow ions to flow in the charging zone, a section of the inner cylinder was made out of a perforated (2.5 mm diameter) cylindrical tube. The width of the perforated screen opening on the inner cylinder was 20 mm. The ion-driving voltage applied on the inner cylinder forced the ions through the perforated screen openings on the inner cylinder to the charging zone, while the outer cylinder was connected to ground. This ion-driving voltage could regulate the ion current flow through the perforated screen. The fraction of ions drawn into the charging zone is equal to the ratio of the field strengths on either side of the perforated screen opening. In the charging zone, the aerosol particles collided with the ions and were charged electrically.

### Diffusion and field charging theory

In the charging zone of the charger, the ions produced by the corona discharge diffuse by Brownian motion and charge the aerosol particles. It is possible to consider the process of diffusion charging in a simpler way. The mean charge per particle,  $n_d$ , caused by the diffusion charging in a time period, t, as a function of particle diameter is approximately determined by the theory of White (Hinds, 1999)

$$n_d = \frac{d_p kT}{2K_E e^2} \ln \left( 1 + \frac{\pi K_E d_p \overline{c}_i e^2 n_i t}{2kT} \right) \tag{1}$$

where  $d_p$  is the particle diameter, k is the Boltzmann's constant (1.380658 × 10<sup>-23</sup> J/K), T is the operating temperature,  $K_E$  is the Coulomb constant (= 1/4 $\pi\epsilon_0$ ),  $\epsilon_0$  is the vacuum permittivity (8.854 × 10<sup>-12</sup> F/m),  $\overline{c}_i$  the mean thermal speed of the ions, e is the value of elementary charge on an electron (1.61 × 10<sup>-19</sup> C),  $n_i$  is the ion number concentration, and t is the time of exposure of the particles to the ions.

In field charging, ions are transported to suspended particles along the field lines. The field lines are repelled as the particle charge becomes high, and finally no electric field line reaches the particle. This condition causes charge saturation. The effect of the finite electric field used in the charging region can be estimated by a classical field charging equation derived by White (Hewitt, 1957), if the particle is initially neutral, the average number of the elementary units of charge on a particle,  $n_f$ , acquired in an average electric field E is given by

$$n_f = \left(1 + 2\frac{\varepsilon - 1}{\varepsilon + 2}\right) \left(\frac{Ed_p^2}{4K_E e}\right) \left(\frac{\pi K_E e Z_i n_i t}{1 + \pi K_E e Z_i n_i t}\right) \tag{2}$$

where  $\varepsilon$  is the particle dielectric constant, E is the average electric field in the charging zones, and  $Z_i$  is the electrical mobility of ion,  $Z_{ion}^+ = 1.15 \times 10^{-4} \text{ m}^2/\text{V}$  s,  $Z_{ion}^- = 1.425 \times 10^{-4} \text{ m}^2/\text{V}$  s, respectively (Reischl et al., 1996). The first two terms in Equation (2) represent the saturation charge situation, the first term is dependent on the dielectric constant of material, and it may have values from 1 to  $\infty$  as  $\varepsilon$  can have values from 1 (insulating particle) to infinity (conductive particle). For most materials t,  $\varepsilon$  varies from 1 to 10. The second term in the Equation (2) depends on the electric field strength and the surface area of the particle. The third term in Equation (2) represents the time dependence of the charging process.

Both diffusion and field charging occur at the same time. This is known as continuum charging where particle charge is the sum of the contributions from diffusion and field charge (Liu and Kapadia, 1978).

$$n_p = n_d + n_f \tag{3}$$

For the particle diameter is less than 1  $\mu$ m, the electrical field in the charger should have a negligible effect on the charging process. In diffusion and field charging studies it is necessary to know the charging parameter,  $n_i t$  product. It is the product of ion number concentration and charging time, and is given by (Intra, 2012)

$$n_i t = \left(\frac{I}{2\pi r_2 LeEZ_i}\right) \left(\frac{\pi (r_2^2 - r_1^2)L}{Q_a}\right) \tag{4}$$

where I is the charging current,  $r_1$  and  $r_2$  are the radii of the inner and outer cylinders, respectively, L is the width of the screen opening on the inner cylinder, and  $Q_a$  is the aerosol flow rate.

### **Numerical Calculation**

In order to gain a better understanding on the operation of the present charger, a numerical model was developed to investigate the distribution of electric field lines in the two main regions of the charger. The numerical model consisted of Poisson's equation in the 2-D, axisymmetric, cylindrical coordinates for the present charger configurations. The commercial computational fluid dynamic software package, CFDRC<sup>TM</sup> was used in this study (CFDRC Manual, 2004). This software was based on the finite volume method. Computational domain and mesh distribution for electric field calculation of the charger are shown in Figure 2. With respect to the boundary conditions used, constant potentials were applied to the corona-wire electrode from 0 to 10 kV, the inner electrode from 100 to 300 V, and the outer electrode was 0 V. It was assumed that the space charge effect was negligible. The operating gas density was 1.225 kg/m³ and the permittivity constant 1.00054. The insulator permittivity constant was 2.1. The zero gradient condition was applied to the boundaries without walls. A structured mesh was used. A total of about 5,643 meshes were distributed in the computational domain of the charger.

### **Apparatus and Experimental setup**

Figure 3 shows the schematic diagram for the equipment used to evaluate the electrostatic characteristics of the corona diffusion and field charger. An adjustable commercial DC high voltage power supply (Leybold Didactic model 521721) was used to maintain the positive or negative high voltage differences on the corona-wire of the charger. The voltage was generally in the range between 0 and 10 kV. A second adjustable AC power supply (TDGC2-1kVA) incorporating the isolation transformer and the full-wave rectifier circuit was used to maintain the ion-driving voltage difference on the inner cylinder in the range between 100 and 500 V. This was necessary to

investigate the charging current through the perforated screen openings on the inner cylinder into the charging zone. In this experiment, the Keithley 6517A electrometer was used to measure the ion currents flowing in the discharge and charging zones of the charger. For the discharge current measurement, the electrometer was connected to the inner cylinder, while the outer cylinder was connected to ground, shown in Figure 3 (a). An insulated foil at the inner surface of the outer cylinder opposite to the perforated screen opening was connected to the electrometer for measuring the charging current as shown in Figure 3 (b). Measurement of the currents of ions flowing between the inner and outer cylinders was similar to those performed in the previous work (Intra, 2012). Therefore, the mean concentration of ions in the discharge or charging zone,  $n_{is}$  of the present charger could be estimated from the following equation,

$$n_i = \frac{I}{2\pi r LeEZ_i} \tag{5}$$

where *r* is the radius of the inner or outer cylinder. Table 1 gives the limits of the evaluated variables. The measurements of the discharge and charging currents were repeated at least three times for each set of operating conditions.

### **Results and Discussion**

Figure 4 shows the current–voltage characteristics of the charger in the discharge and charging zones for positive and negative coronas. In the discharge zone, the discharge current was increased monotonically with increasing corona voltage. The corona onset voltage was 8.5 kV at a current of  $2.4 \times 10^{-6}$  A and 7.5 kV at a current of  $1.1 \times 10^{-6}$  A for of the positive and negative coronas, respectively. At a 10 kV corona voltage, the discharge current magnitude was about  $1.5 \times 10^{-5}$  A for the positive corona and  $2.1 \times 10^{-5}$  A for the negative corona. Because negative ions had higher electrical mobility than positive ions, the magnitude of the negative discharge current was markedly higher than the positive discharge current at the same corona voltage. In the charging zone, the increase of the corona voltage to the charging current increased accordingly. The onset voltage in

the charging zone of both positive and negative coronas for the ion-driving voltage of 100, 300 and 500 V was 8.5 kV at  $5.7 \times 10^{-8}$ ,  $8.0 \times 10^{-8}$ , and  $8.3 \times 10^{-8}$  A, respectively, and 7.5 kV at  $2.3 \times 10^{-8}$ ,  $2.3 \times 10^{-8}$ , and  $2.2 \times 10^{-8}$  A, respectively. At the same corona voltage, a higher ion-driving voltage was observed at a higher charging current, presumably because increasing the ion-driving voltage resulted in the increase of the electric field strength in the charging zone. The electric field strength was a function of the charging current and the charging currents of the positive corona were 1.7 times smaller than the charging currents of the negative corona. The magnitude of the charging current was in the range from  $1.8 \times 10^{-8}$  to  $4.5 \times 10^{-7}$  A, and  $1.6 \times 10^{-8}$  to  $5.4 \times 10^{-7}$  A for positive and negative coronas, respectively.

In order to investigate the distribution of the electric field in the discharge and charging zones of the charger, Figure 5 shows the radial variation of the electric field in the two regions of the charger at different corona voltage from 7 to 10 kV and the ion-driving voltage of 100, 300 and 500 V. Increasing the radial distance away from the corona wire resulted in marked discrepancy in the electric field strength in both zones. The electric field strength appeared to depend on corona voltage only in the discharge zone. For the charging zone, the electric field strength practically became a constant. The electric field strength in the charging zone increased with increasing iondriving voltage corresponding to the numerical calculation of the electric field line in the discharge and charging zones at different ion-driving voltages between 100 and 300 V (Figure 6). As shown in Figure 6, it was evident that the number of the electric field flow lines that pass from discharge zone to charging zone can be increased by increasing the ion-driving voltage. Figure 7 shows variations of the average electric field strength in the discharge and charging zones of the charger at different ion-driving voltages. In the discharge zone, the electric field strength increased with increasing corona voltage and decreased with increasing ion-driving voltage. For the charging zone, the electric field strength appeared to depend on ion-driving voltage only. Increasing the ion-driving voltage resulted in an increase in the electric field strength. The average electric field strength in the discharge zone was about  $3.3 \times 10^5$  to  $4.5 \times 10^5$  V/m for corona and ion-driving voltages between 7

and 10 kV, and 100 and 300 V, respectively. In the charging zone, the average electric field strength was from about  $8.9 \times 10^3$  to  $4.3 \times 10^4$  V/m for corona and ion-driving voltages between 7 and 10 kV, and 100 and 300 V, respectively.

Variations in ion number concentrations with corona voltage in the discharge and charging zones of the charger at different ion-driving voltages of 100, 300 and 500 V are shown in Fig. 8. As shown in Figure 8, (a) increasing the corona voltage resulted in the increase of ion number concentration in both zones. The magnitudes of the ion number concentration in the discharge zone were in the range from  $1.34 \times 10^{13}$  to  $1.84 \times 10^{15}$  ions/m<sup>3</sup> and  $7.34 \times 10^{13}$  to  $2.64 \times 10^{15}$  ions/m<sup>3</sup>, for positive and negative coronas respectively. (b) The ion number concentration in the charging zone decreased monotonically with increasing ion-driving voltage. Because of the electrostatic precipitation of ions on the perforated screen is a function of the applied voltage on the inner cylinder it was expected that at higher ion-driving voltage the ion loss by electrostatic deposition onto the perforated screen opening on the inner cylinder became large. The ion number concentrations in the charging zone were in the range of  $2.95 \times 10^{13}$  to  $1.52 \times 10^{14}$  ions/m<sup>3</sup> and 2.06 $\times$  10<sup>13</sup> to 1.47  $\times$  10<sup>14</sup> ions/m<sup>3</sup> for positive and negative coronas, respectively. Figure 9 shows the variations in  $n_i t$  product with corona voltage in the charging zone of the charger at the different aerosol flow rates of 1, 3 and 5 L/min and ion-driving voltages of 100, 300 and 500 V for positive and negative coronas. The charging times were in the range of about 0.4 to 2 s. The higher flow rate, also the shorter residence time, gave rise to a lower  $n_i t$  product. An increase in corona voltage produced a monotonic increase in the ion concentration and also of the  $n_i t$  product.

Figures 10 – 11 show the theoretical prediction of mean diffusion charge per particle as a function of particle diameters from 10 nm to 50 µm at various aerosol flow rates of 1, 3 and 5 L/min, applied voltages of 7 to 10 kV and ion-driving voltages of 100, 300 and 500 V for positive and negative corona voltages. In this study, the mean diffusion charge per particle was calculated from Equation (1). The concentrations of particles were assumed to be uniformly distributed at the entrance of the charger. The mean charge per particle increased with particle diameter. In diffusion

charging the mean charge is proportional to  $d_p$ . Longer residence time (low aerosol flow rate) and higher corona voltage resulted in an increase in the mean charge per particle within the charger. It should be noted that for  $N_i t > 10^{13}$  s/m<sup>3</sup>, the White's charging equation is accurate to within a factor of two for particles with diameters from 0.07 to 1.5  $\mu$ m and  $N_i t > 10^{13}$  s/m<sup>3</sup>, to within a factor of two for particles diameter from 0.05 to 40  $\mu$ m at standard conditions. Diffusion charging was the dominant mechanism for particles with diameters less than 0.1  $\mu$ m, even in the presence of an electric field (Hinds, 1999).

The theoretical prediction of mean field charge per particle as a function of particle diameter from 10 nm to 50  $\mu$ m at various aerosol flow rates of 1, 3 and 5 L/min, applied voltages of 7 to 10 kV and ion-driving voltages of 100, 300 and 500 V for positive and negative corona voltages is shown in Figures 12 – 13. In this study, the mean field charge per particle was calculated using Equation (2) and the dielectric constant of material was assumed to be from fly ash which is about 3.0 for various charging conditions. The mean field charge per particle increased with particle diameter and was proportional to  $d_p^2$ . The field charging was the dominant mechanism for particles with diameters larger than 1.0  $\mu$ m (Hinds, 1999). In the case of ion number concentration greater than  $10^{13}$  ions/m<sup>3</sup>, field charging would be 95% complete in 3 s or less.

### **Conclusions**

In this study, a unipolar diffusion and field charger by corona discharge for aerosol particles charging was constructed and electrostatically evaluated. The discharge and charging current corresponding to the ion number concentration were measured using an electrometer and used to investigate the electrostatic characteristics of the charger. The results showed that that the discharge and charging currents and ion number concentration in the discharge and charging zones of the charger increased with corona voltage. The magnitudes of the ion number concentration for positive and negative corona in the discharge zone were from  $1.34 \times 10^{13}$  to  $1.84 \times 10^{15}$  ions/m<sup>3</sup> and  $7.34 \times 10^{13}$  to  $2.64 \times 10^{15}$  ions/m<sup>3</sup>, respectively. For the charging zone, the ion number concentrations for

positive and negative coronas were from  $2.95 \times 10^{13}$  to  $1.52 \times 10^{14}$  ions/m³ and  $2.06 \times 10^{13}$  to  $1.47 \times 10^{14}$  ions/m³, respectively. The higher flow rate and the shorter residence time gave rise to a lower  $n_i t$  product. A commercial CFD software package was used to predict the behavior of the electric field strength and lines in the discharge and charging zones of the charger. The average electric field strength in the discharge zone was from  $3.27 \times 10^5$  to  $4.45 \times 10^5$  V/m, and in the charging zone, the average electric field strength was from  $8.9 \times 10^3$  to  $4.27 \times 10^4$  V/m. The mean charge per particle for particle diameters in the range from 0.01 to  $50 \, \mu m$  for various operating conditions of the charger was theoretically evaluated with White's theory. The mean diffusion and field charge per particle increased with particle diameter and was proportional to  $d_p$  in diffusion charging and to  $d_p$  in field charging. A lower aerosol flow rate and higher corona voltage resulted in an increase in the mean charge per particle within the charger for both diffusion and field charging. Finally, the developed charger proved to be particularly useful in diffusion and field charging of aerosol particles in particulate matter detector instruments for measuring PM10 and PM2.5 concentration.

### Acknowledgements

The authors wish to express their gratitude to the Hands-on Research and Development Project, Rajamangala University of Technology Lanna, Thailand, contract no. UR2S-006, and the Thailand Research Fund (TRF), contract no. MRG5480001. The author also wishes to thank Dr. Rainer Zawadzki for the valuable contribution during the preparation of this article.

### References

Alonso, M. and Alguacil, F.J. 2008. Particle size distribution modification during and after electrical charging: comparison between a corona ionizer and a radioactive neutralizer.

\*Aerosol and Air Quality Research 8: 366-380.

- Biskos, G., Reavell, K. and Collings, N. 2005. Electrostatic characterization of corona-wire aerosol charges. *Journal of Electrostatics* 63: 69-82.
- Buscher, P., Schmidt-Ott, A. and Wiedensohler, A. 1994. Performance of a unipolar "Square Wave" diffusion charger with variable nt-product. *Journal of Aerosol Science* 25: 651-663.
- CFDRC Manual. 2004. CFDRC 2004, User's Guide.
- EPA., 1997. National Ambient Air Quality Standards for Particulate Matter. Final Rule. *Federal Register* 62: 38651 38760.
- Hewitt, G. W. 1957. The charging of small particles for electrostatic precipitation. *AIEE Transactions*. 76: 300-306.
- Hinds, 1999. W. C. Aerosol Technology. John Wiley & Sons. New York.
- Intra, P. 2012. Corona discharge in a cylindrical triode charger for unipolar diffusion aerosol charging, *Journal of Electrostatics* 70: 136-143.
- Intra, P. and Tippayawong, N. 2009. Progress in unipolar corona discharger designs for airborne particle charging: A literature review. *Journal of Electrostatics* 67: 605-615.
- Intra, P. and Tippayawing, N. 2010. Effect of needle cone angle and air flow rate on electrostatic discharge characteristics of a corona-needle ionizer. *Journal of Electrostatics* 68: 254-260.
- Intra, P. and Tippayawong, N. 2011a. Performance evaluation of an electrometer system for ion and aerosol charge measurements. *Korean Journal of Chemical Engineering* 28: 527-530.
- Intra, P. and Tippayawong, N. 2011b. An overview of unipolar charger developments for nanoparticle charging. *Aerosol and Air Quality Research* 11: 186-208.

- Kruis, F. E. and Fissan, H. 2001. Nanoparticle charging in a twin Hewitt charger. *Journal of Nanoparticle Research* 3: 39-50.
- Lee, Y. J., Kim, H. T. and Lee, K. W. 2001. Development of monitoring technology for airborne particulate matter. *Environmental Monitoring and Assessment* 70: 3-20.
- Liu, B. Y. H. and Pui, D. Y. H. 1975. On the performance of the electrical aerosol analyzer. *Journal of Aerosol Science* 6: 249–264.
- Liu, B.Y.H. and Kapadia, A. 1978, Combined field and diffusion charging of aerosol particles in the continuum regime. *Journal of Aerosol Science* 9: 227-242.
- Reischl, G.P., Makela, J.M., Harch, R. and Necid, J. 1996. Bipolar charging of ultrafine particles in the size range below 10 nm. *Journal of Aerosol Science* 27: 931-949.
- Wiedensohler, A., Buscher, P., Hansson, H. -C., Martinsson, B. G., Stratmann, F., Ferron, G. and Busch, B. 1994, A novel unipolar charger for ultrafine aerosol particles with minimal particle losses. *Journal of Aerosol Science* 25: 639-649.

**Table 1** Limits of the investigated variables.

Variable	Range
Corona wire diameter	0.3 mm
Inner cylinder diameter	38 mm
Outer cylinder diameter	60 mm
Corona-wire voltage	0 - 10  kV
Ion-driving voltage	100, 300 and 500 V
Ions generated	Positive ion (+), negative ion (-)
Ionized gas	Air
Aerosol flow rate	1, 3 and 5 L/min
Dielectric constant	3.0
Pressure	1 bar

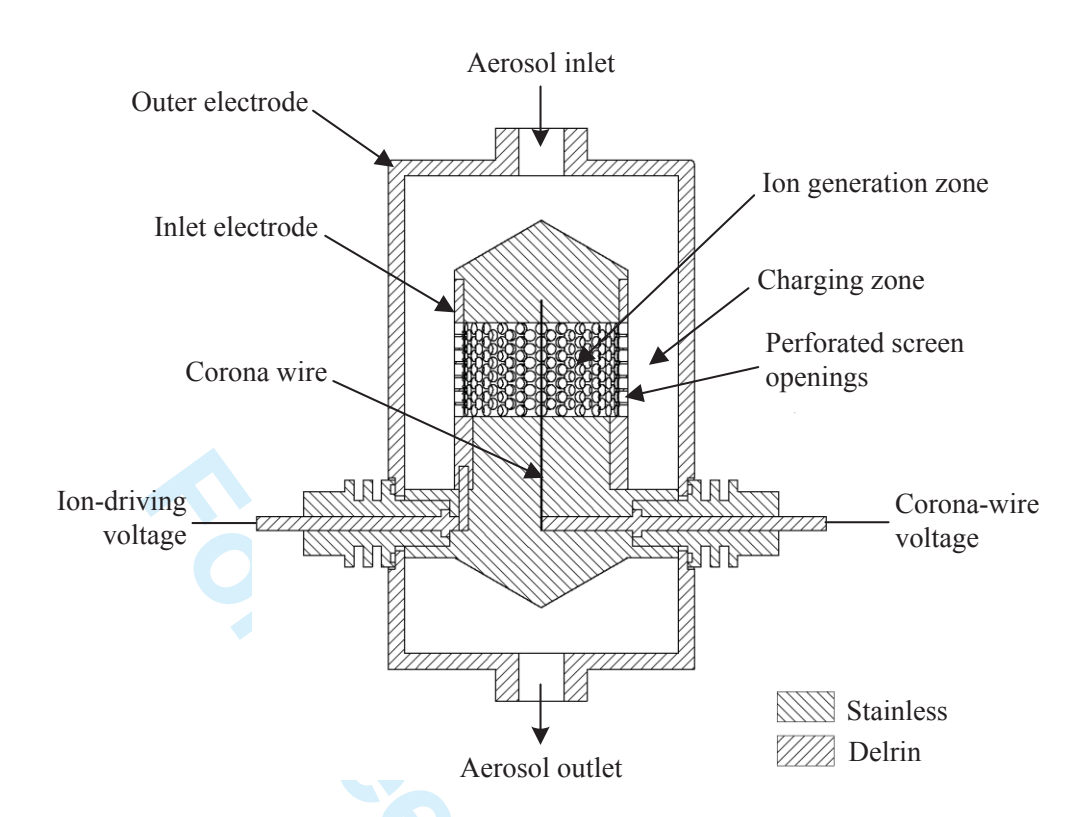


Figure 1. Configuration of the corona diffusion and field charger.

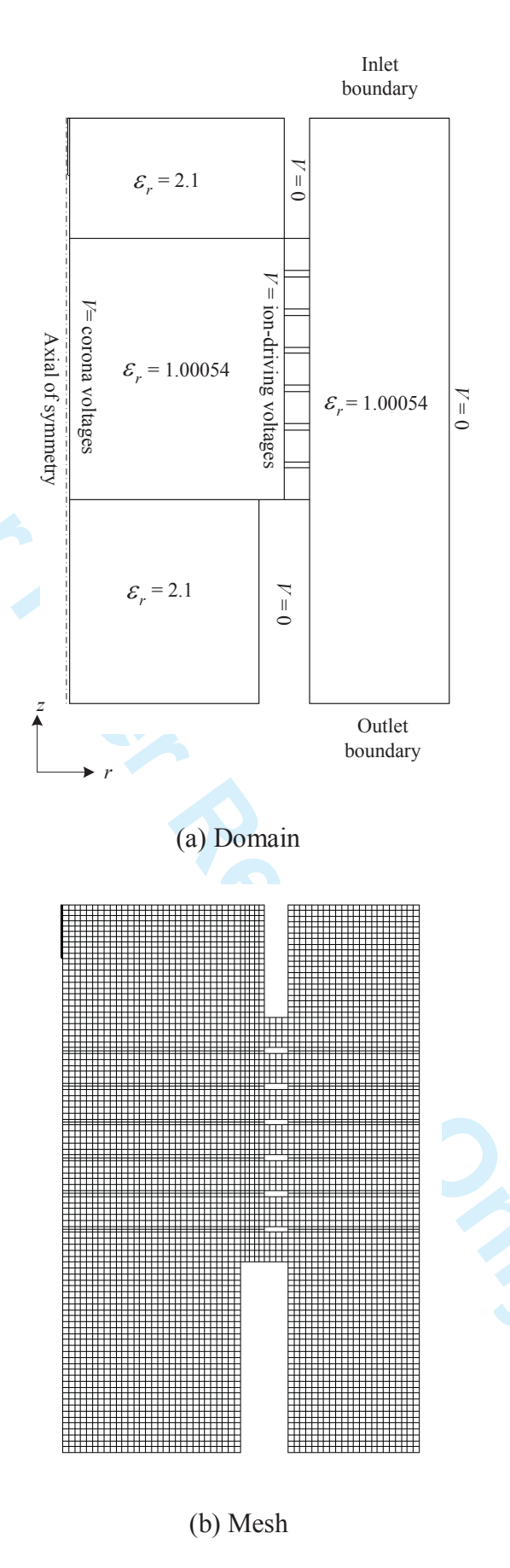
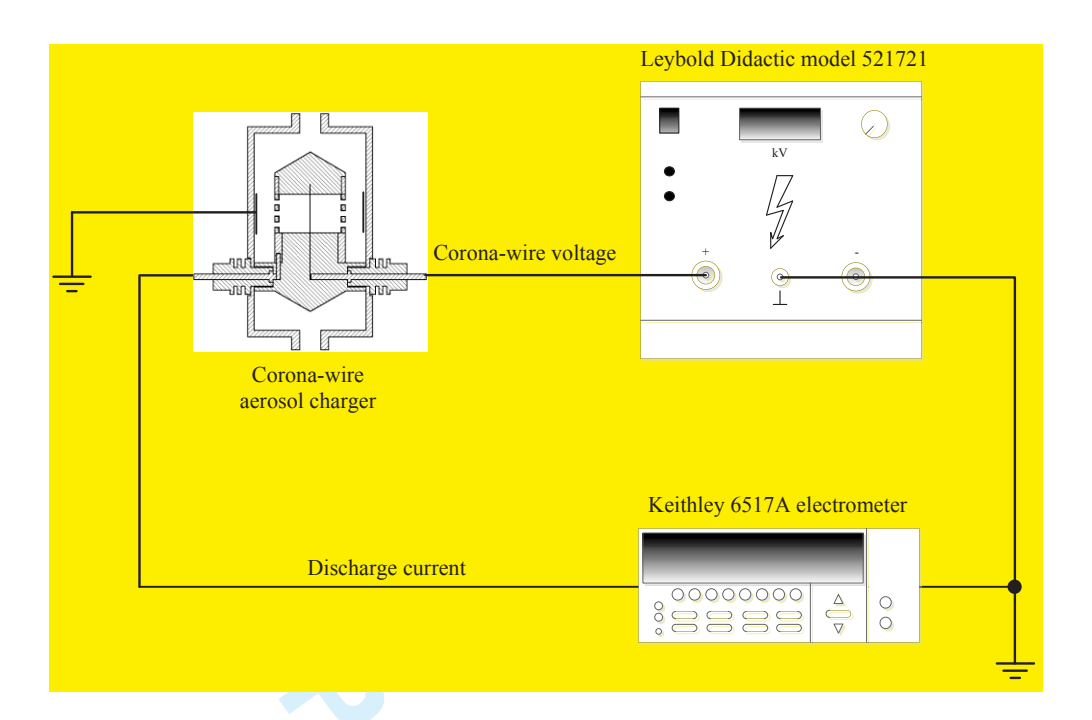
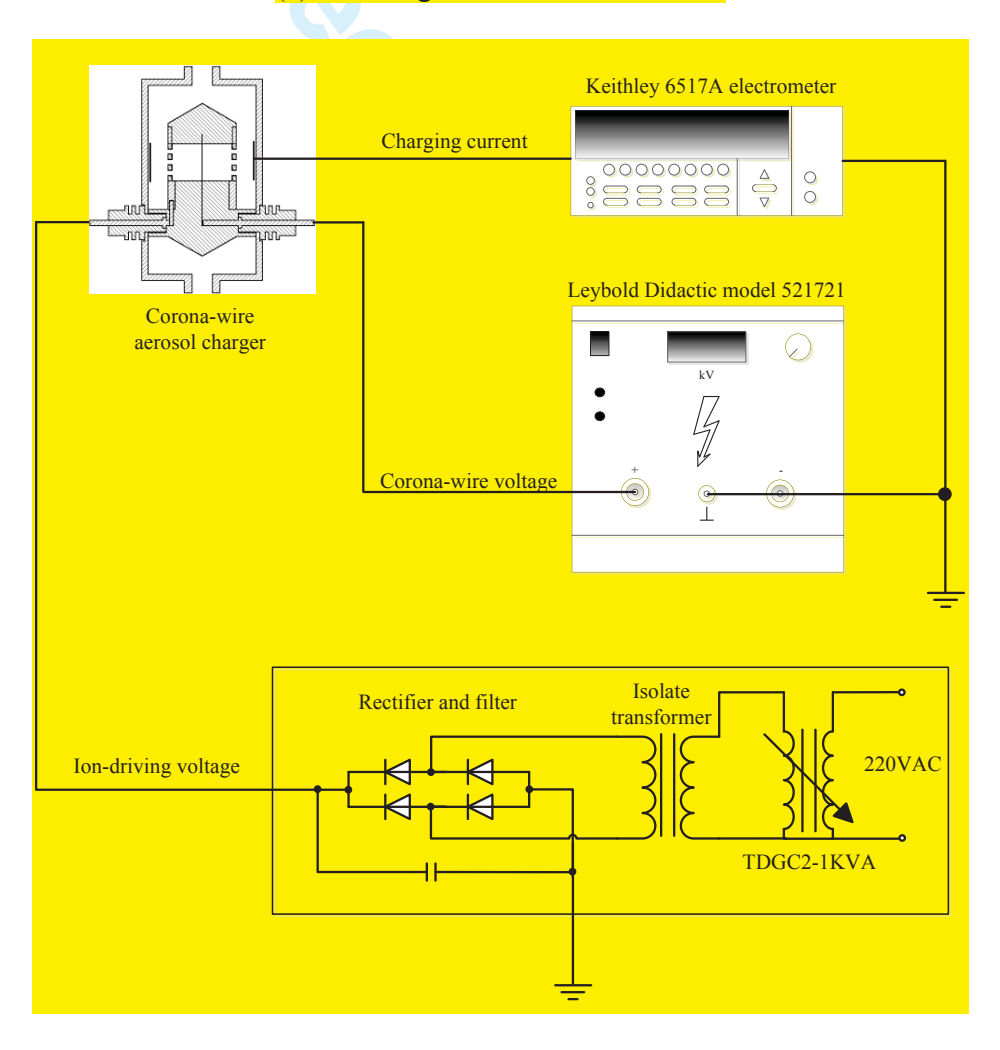


Figure 2. Computational domain and mesh distribution for electric field calculation.



### (a) Discharge current measurement



(b) Charging current measurement

Figure 3. Schematic diagram of the setups for discharge and charging current measurements.

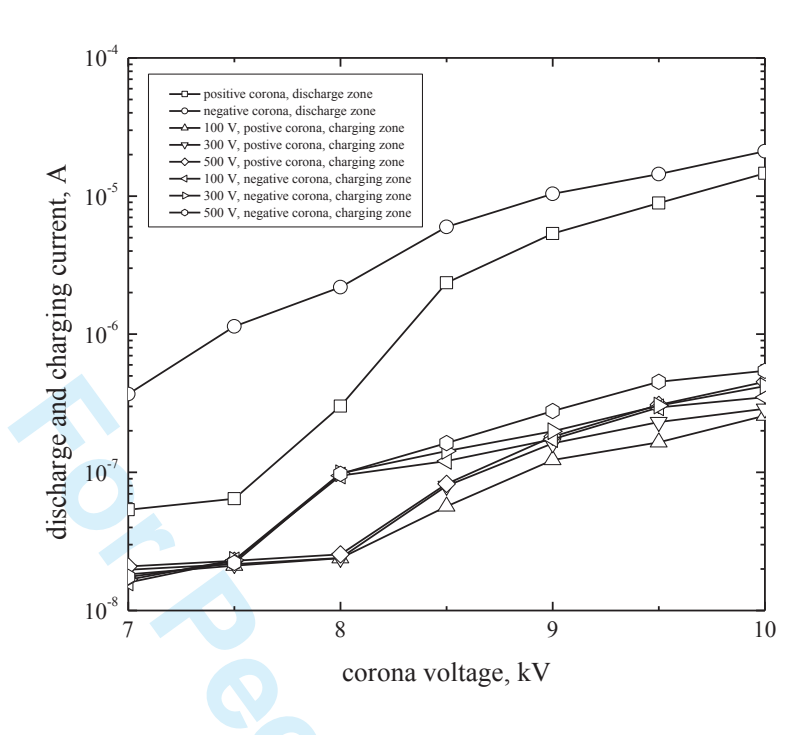
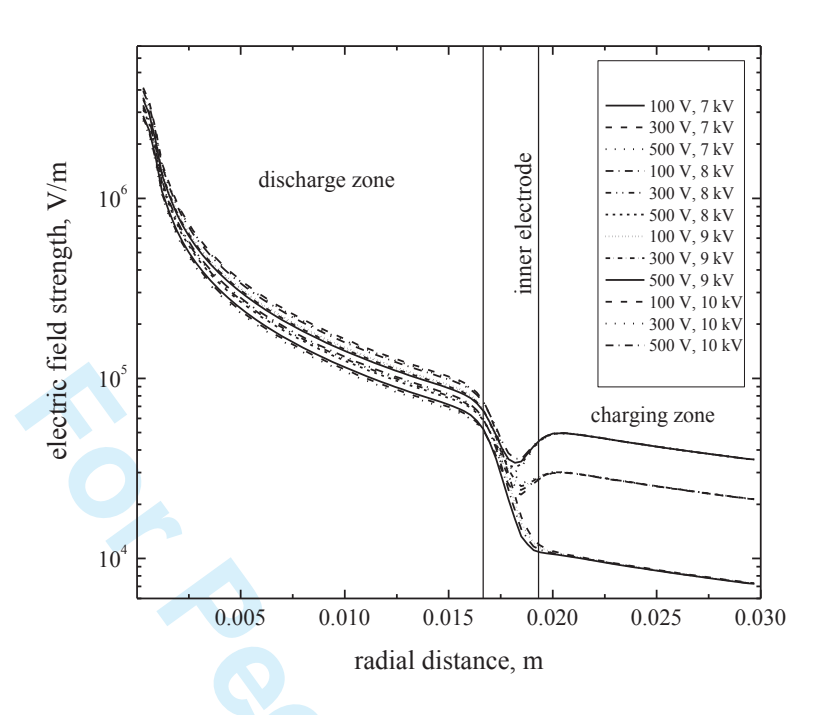


Figure 4. Current–voltage characteristics of the charger.



**Figure 5.** Radial variation of the electric field in the two regions of the charger at different corona and ion-driving voltages.

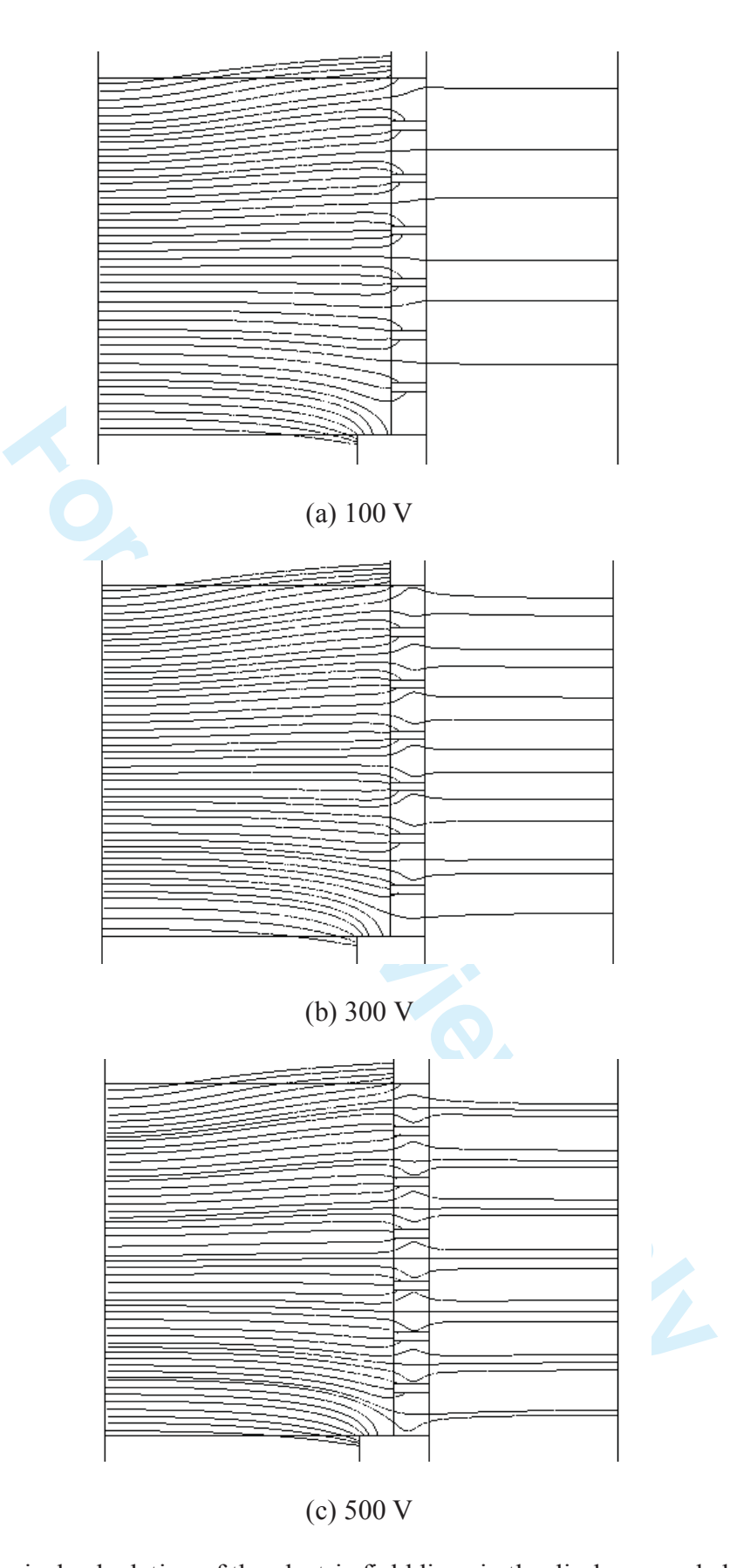
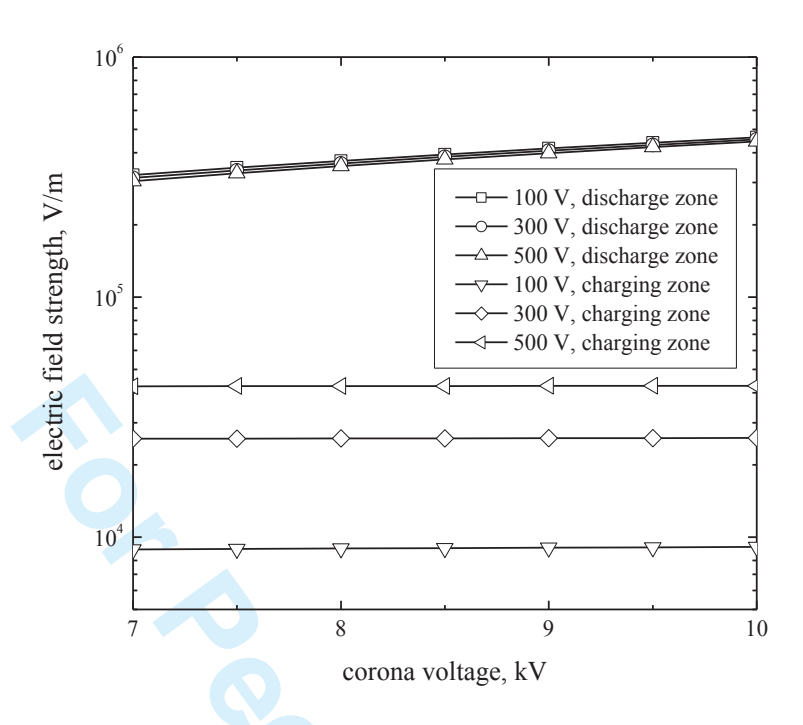
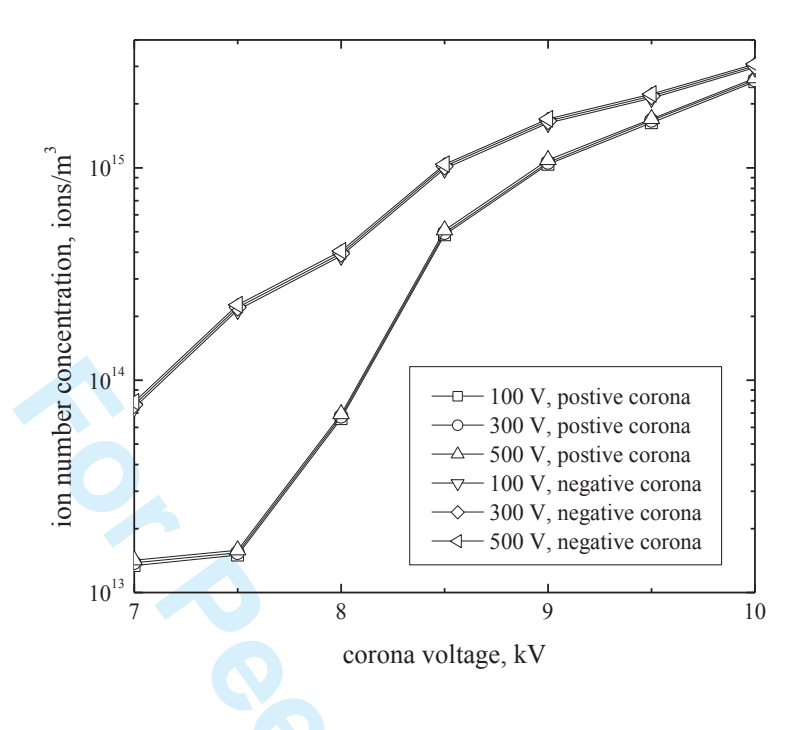


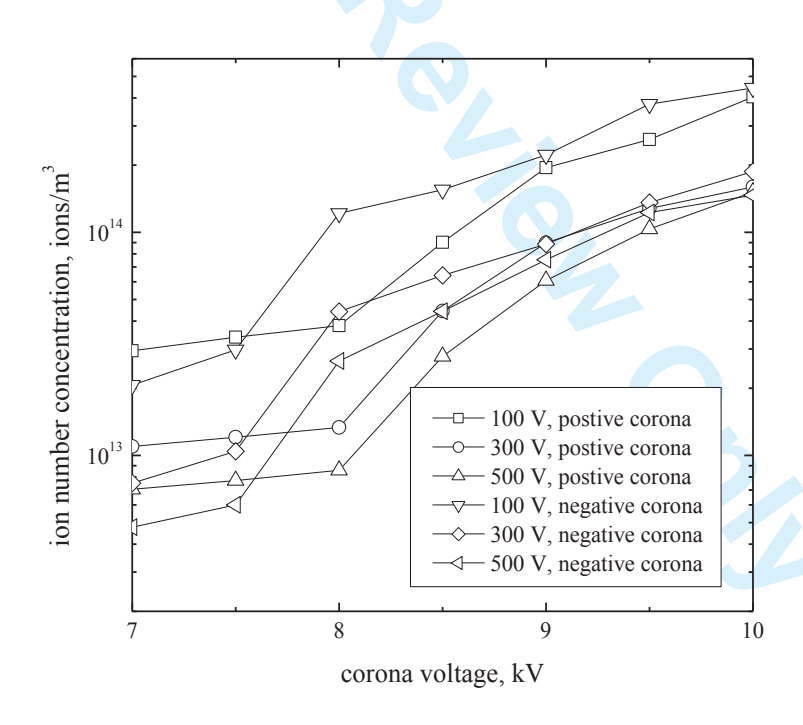
Figure 6. Numerical calculation of the electric field lines in the discharge and charging zones.



**Figure 7.** Variations of the average electric field strength of the charger at different ion-driving voltages.

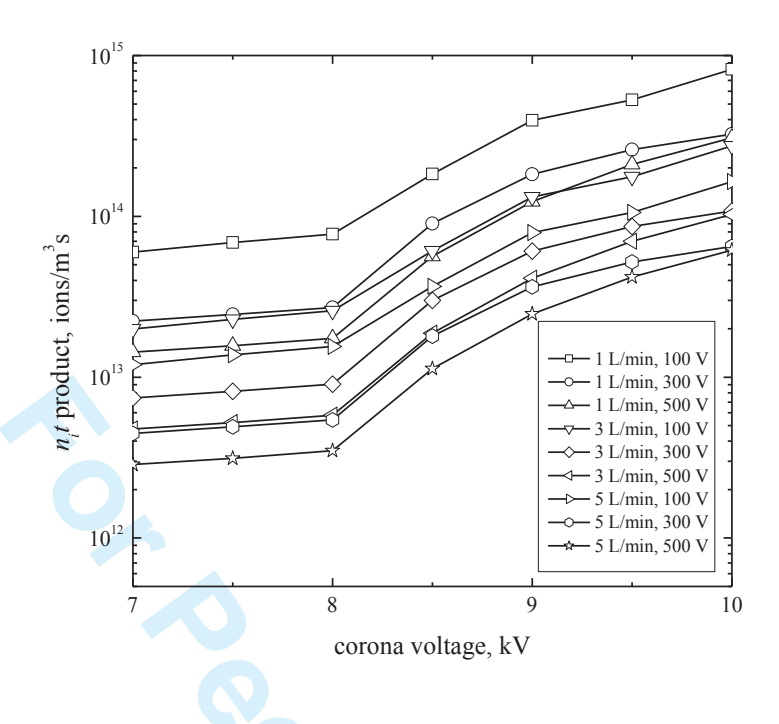


(a) discharge zone

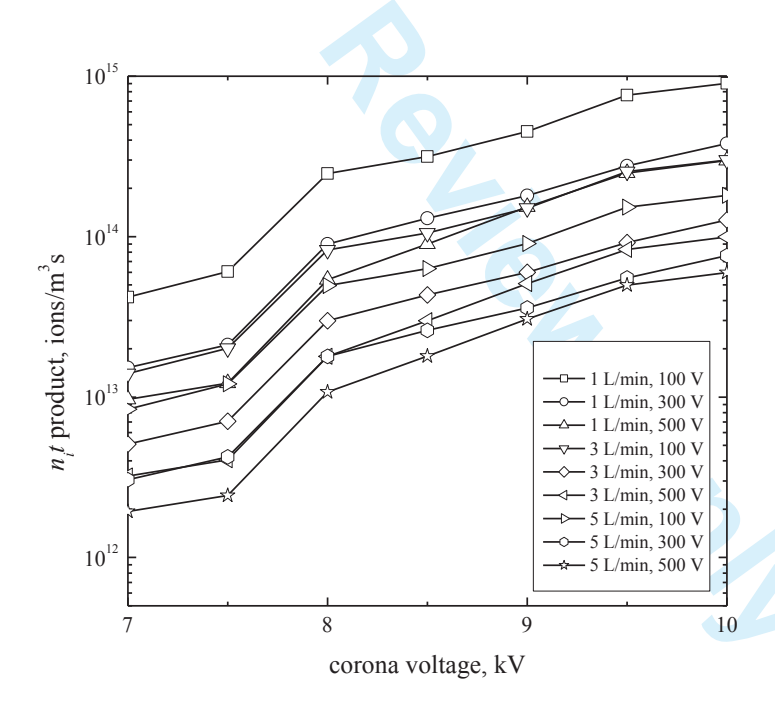


(b) charging zone

**Figure 8.** Variations in ion number concentrations with corona voltage in the charger.

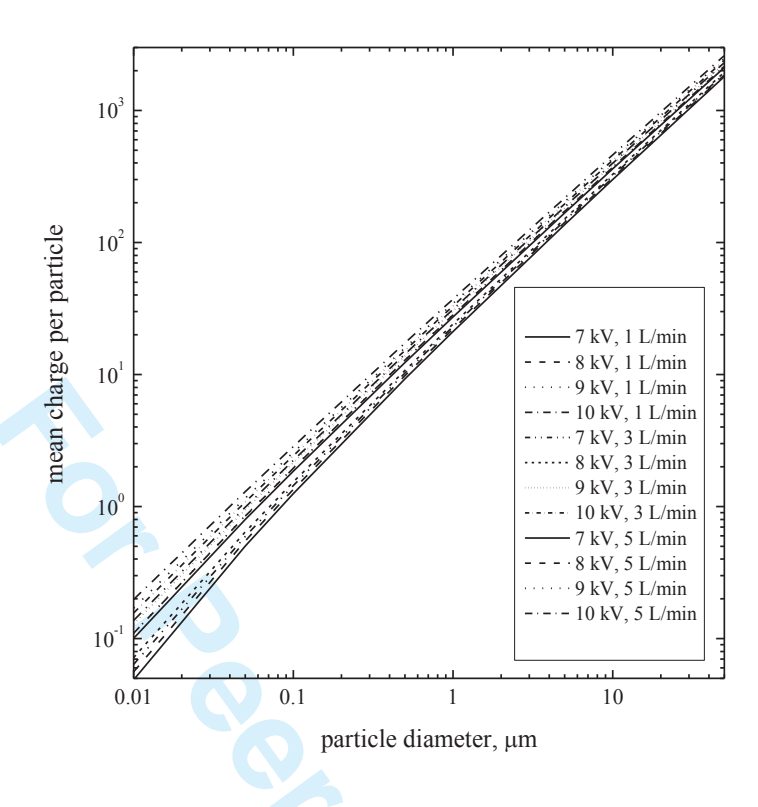


(a) positive corona

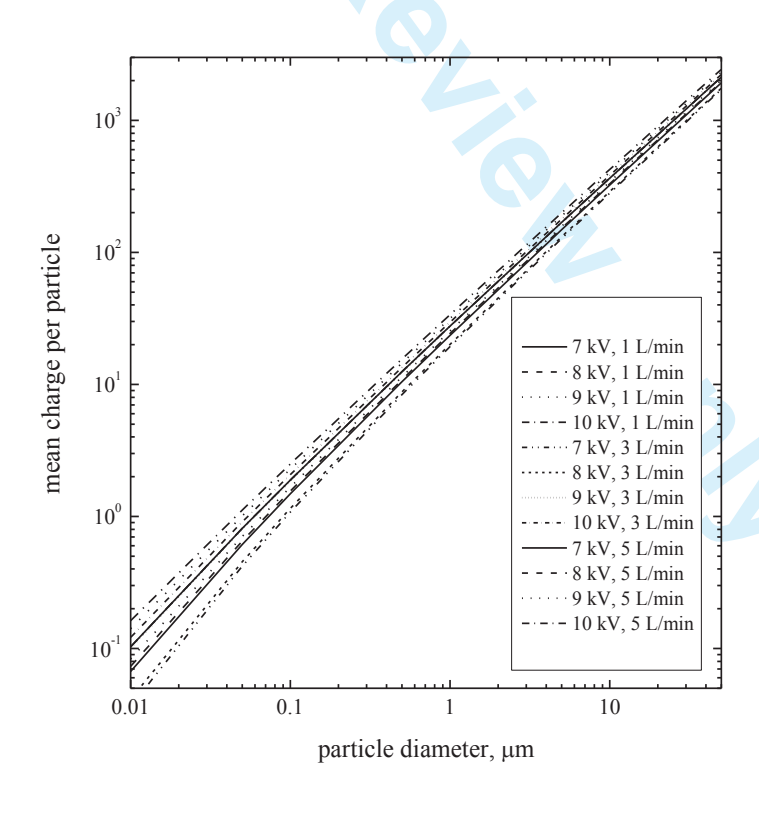


(b) negative corona

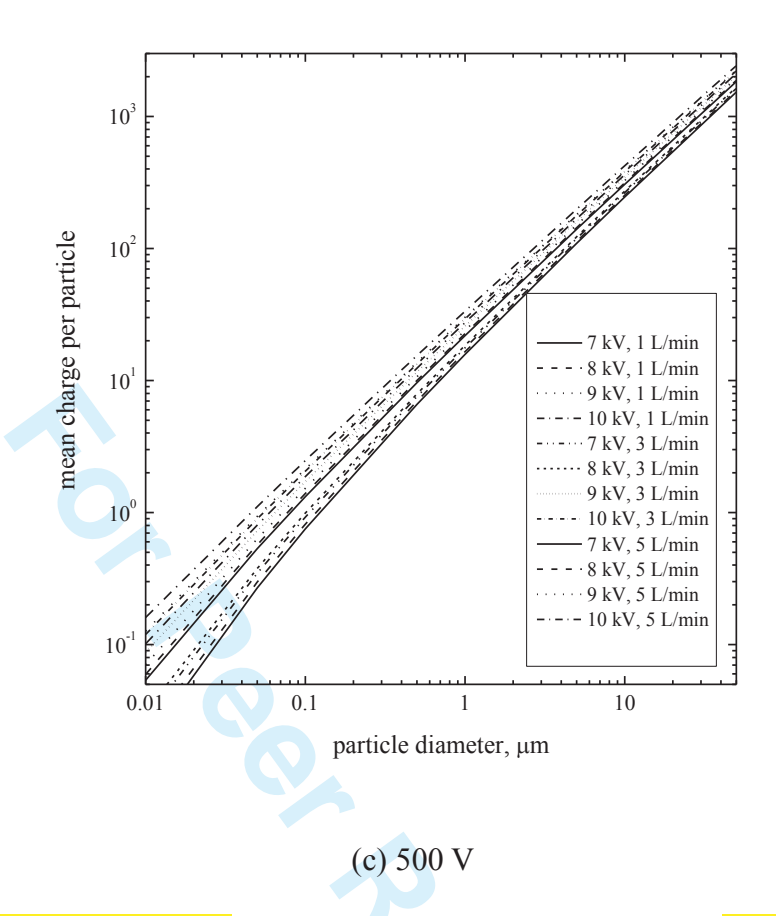
**Figure 9.** Variations in  $n_i t$  product with corona voltage in the charging zone of the charger at different aerosol flow rates and ion-driving voltages.



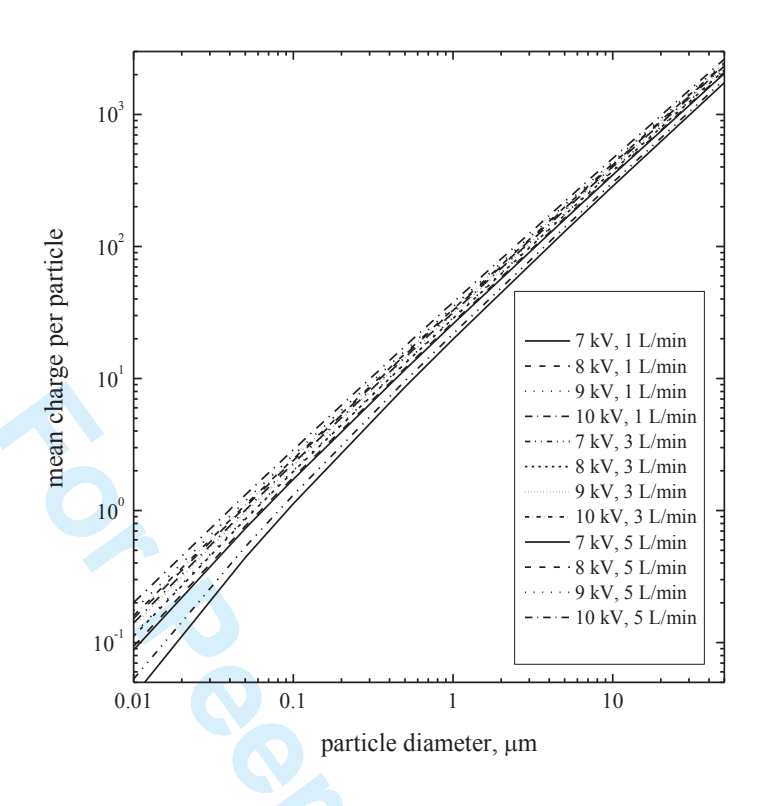




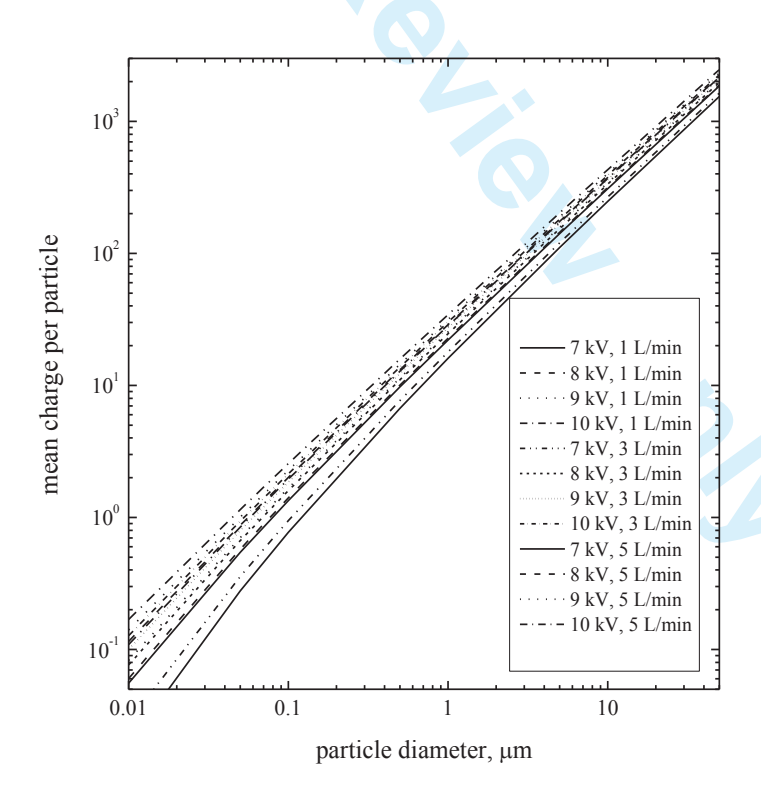
(b) 300 V



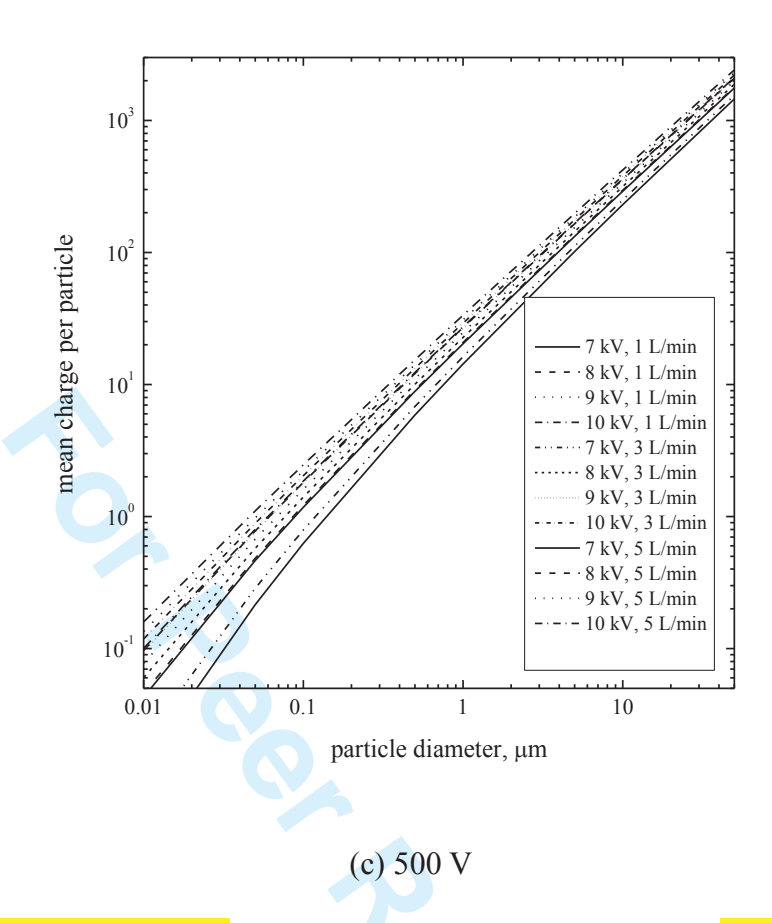
**Figure 10.** Theoretical prediction of mean diffusion charge per particle as a function of particle diameter at various aerosol flow rate and applied voltage for positive corona voltage



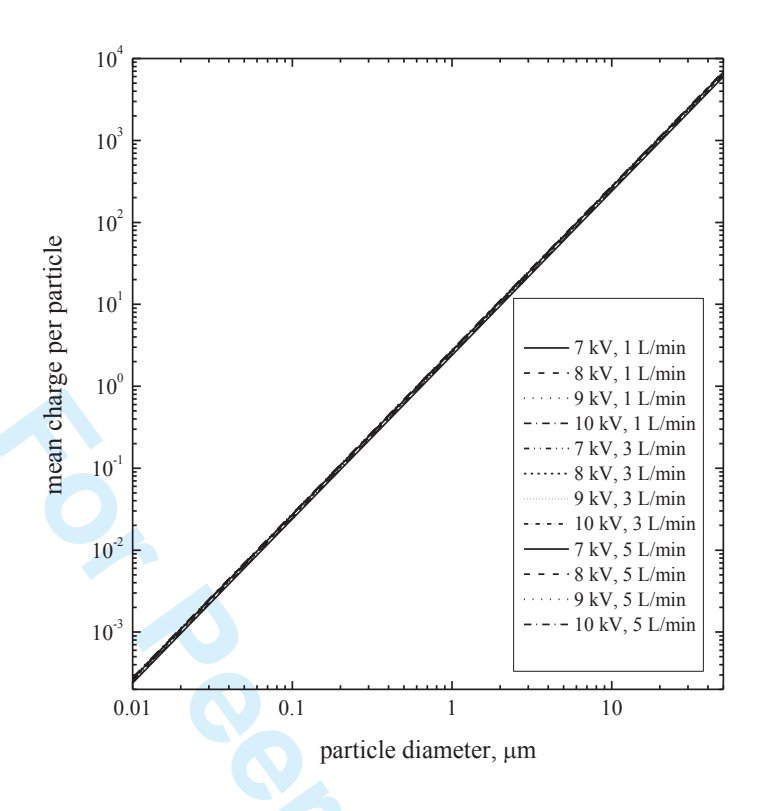




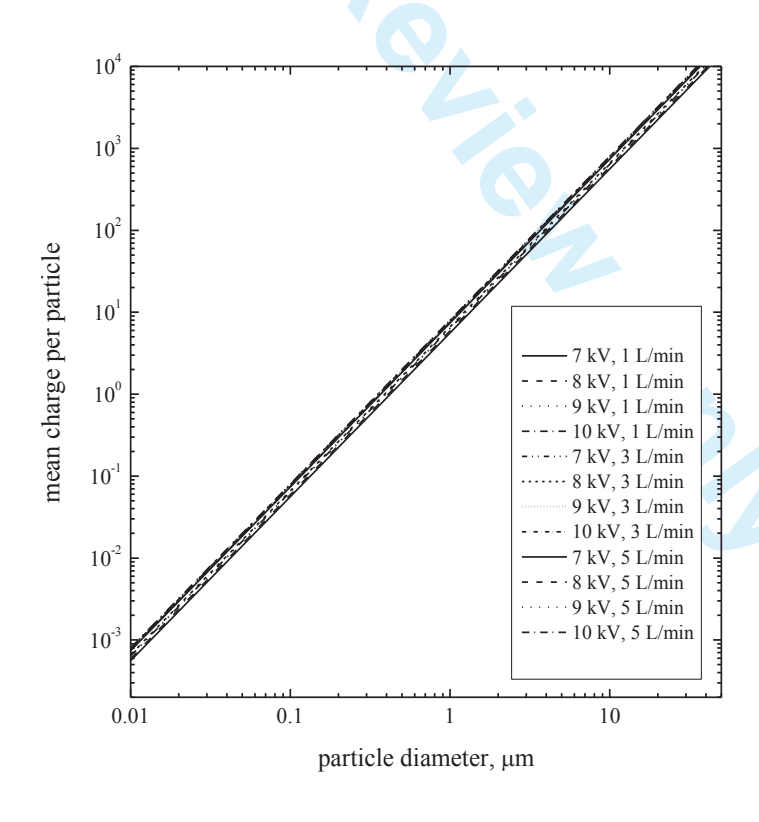
(b) 300 V



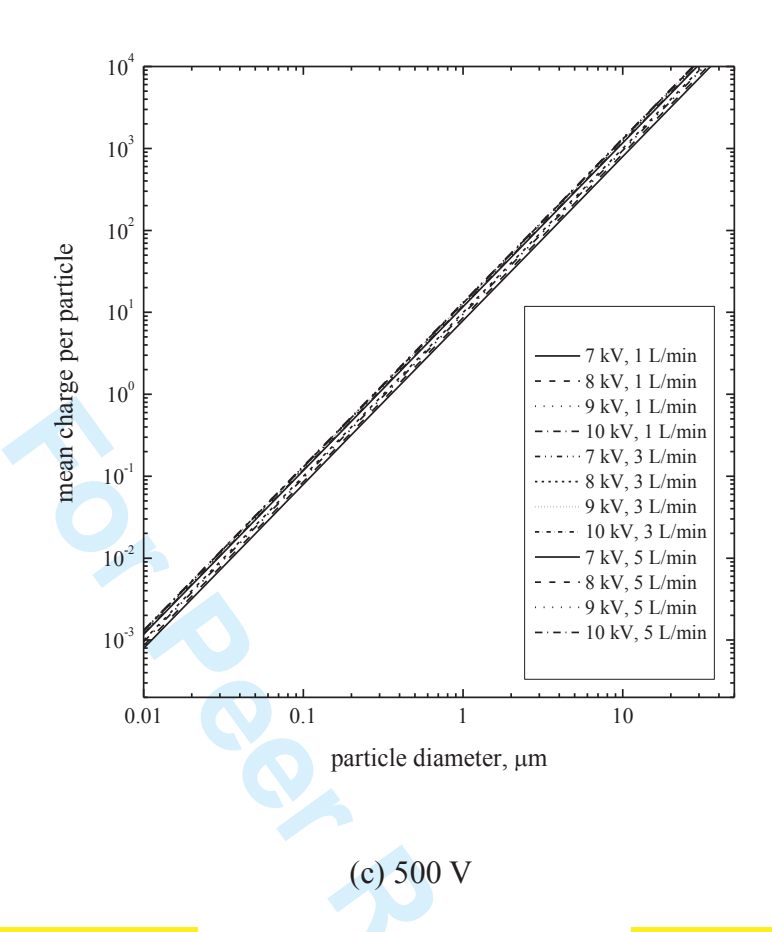
**Figure 11.** Theoretical prediction of mean diffusion charge per particle as a function of particle diameter at various aerosol flow rate and applied voltage for negative corona voltage



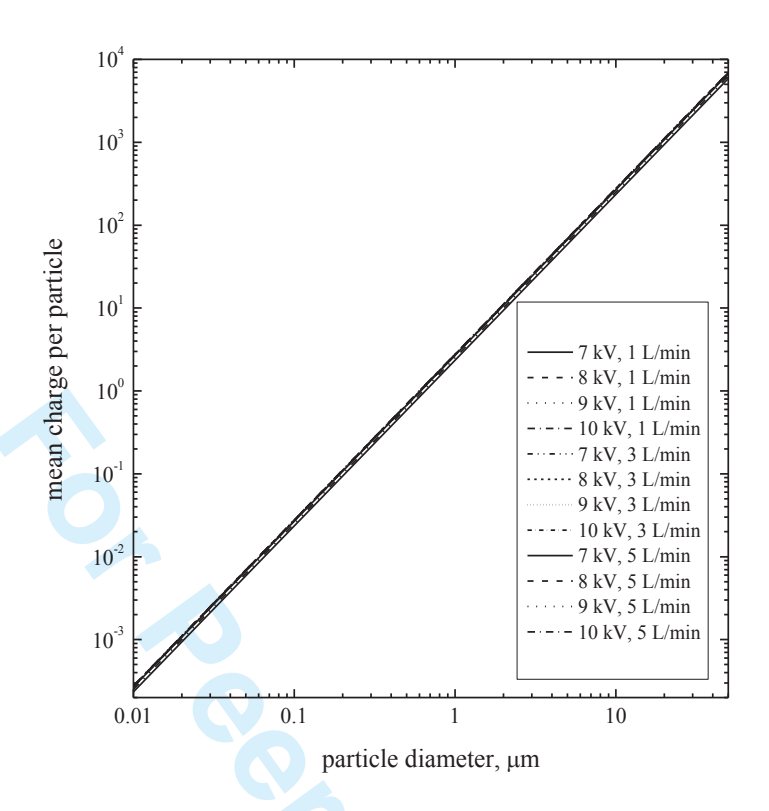




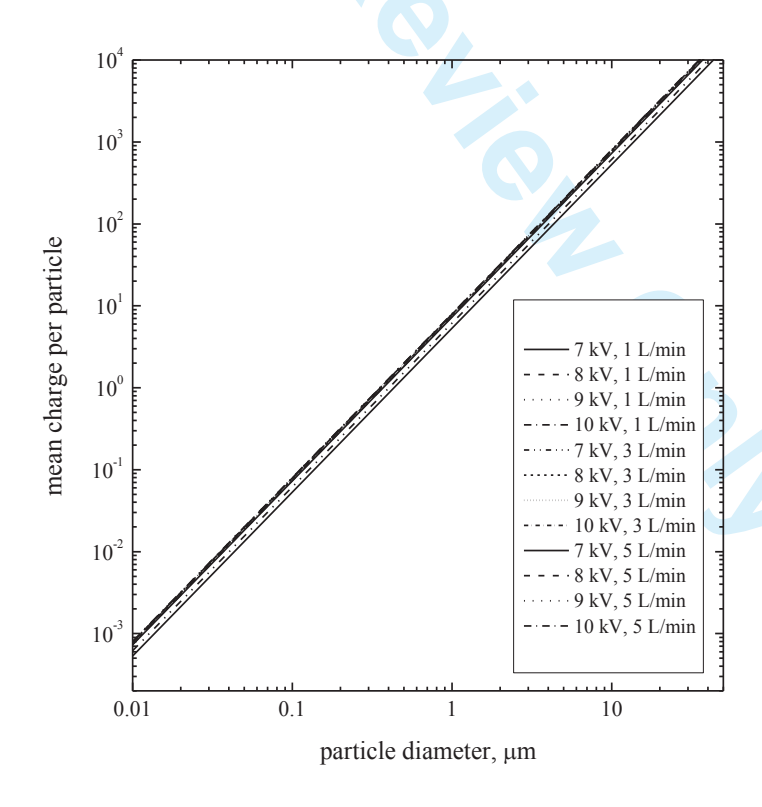
(b) 300 V



**Figure 12.** Theoretical prediction of mean field charge per particle as a function of particle diameter at various aerosol flow rate and applied voltage for positive corona voltage







(b) 300 V

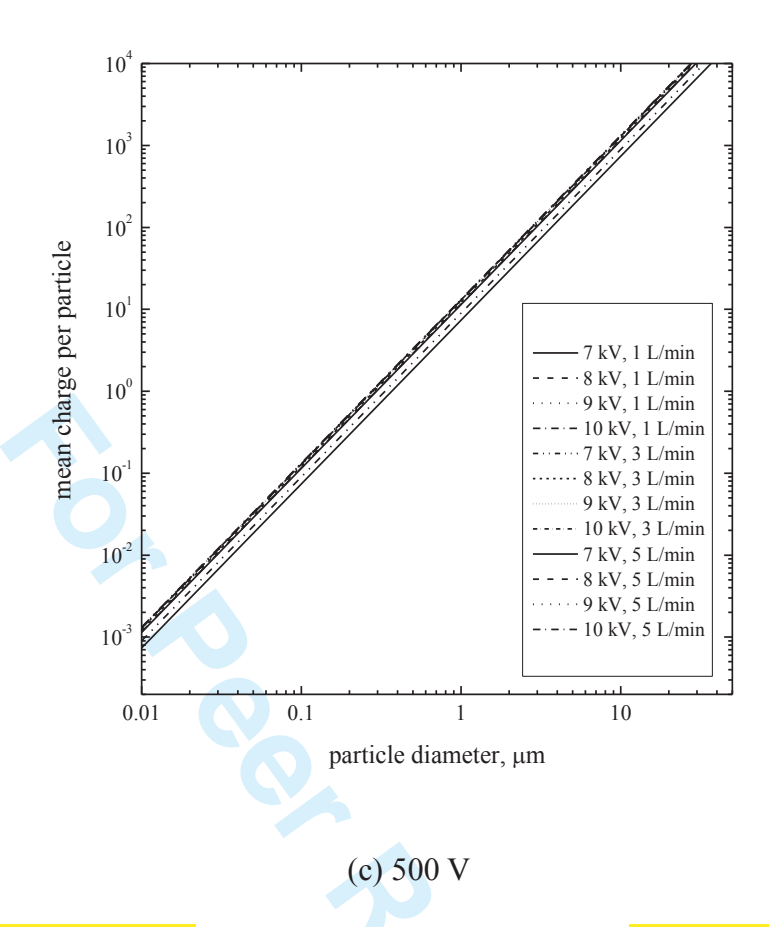


**Figure 13.** Theoretical prediction of mean field charge per particle as a function of particle diameter at various aerosol flow rate and applied voltage for negative corona voltage

# Particulate Science and Technology

## MS id. UPST-2012-0262:

# Response by Authors to review's comment

Comments	Response/Action
1. Nice publication, aside of need for minor grammar corrections.	Thank you for valuable comments. Revision on grammar has been undertaken, taking reviewer advice into consideration.
2. The setup diagram shown in Fig. 3 has the electrometer connected to the charger's enclosure, so the current that is measured is the return current to the ground. Is the current supplied to the corona wire being measured as well? It is unclear to me how the current measured in the way shown in the diagram is related to the ion concentration results. The return current would represent only a portion of the current injected into the system, and unless the injected current is measured simultaneously, it is not clear what is actually used for ion charging (the aerosol is charged and ejected outside of the chamber, correct?). Please elaborate.	For the discharge current measurement, the electrometer was connected to the inner cylinder, while the outer cylinder was connected to ground as shown in Figure 3 (a). Thus, the discharge current flowing between the wire and inner cylinder can be measured. In case of the charging current measurement, an insulated foil at the inner surface of the outer cylinder opposite to the perforated screen opening is connected to the electrometer as shown in Figure 3 (b). The current of ions flowing between the inner and outer cylinders is also measured this way (Intra, 2012). The measured discharge and charging currents were used to predict the concentration of ions in the discharge and charging zones of the charger.  Explanation was added in Page 8, Lines 2 – 9. Additional Figures were also added, Page 18.
3. Authors state that "The discharge and charging currents from the inner and outer cylinders were measured directly with a Keithley 6517A electrometer. Therefore, the discharge and charging current, I, of the present charger could be estimated from the following equation (Intra, 2012), $I = 2\pi$ r2LEZinie" which introduces a bit of confusion: was it measured or estimated? Or, rather, the ion concentration was estimated from this equation, since the current I is known (measured)? Please clarify this part of the manuscript.	The discharge and charging currents were MEASURED directly using the electrometer. And, the ion number concentration was ESTIMATED from the measured discharge or charging current using this Equation 5.  It has been revised and explained more clearly in details, Page 8.
4. To make the picture more complete, could Authors include any information on how the particle diameters were measured? What was the aerosol medium? How was it dispersed before entering the chamber (concern is: were the particles carrying any initial charge)?	In this study, the mean charge per particle as a function of particle diameter was theoretically calculated by Equations (1) and (2). The concentration of particles was assumed to be uniformly distributed at the entrance of the charger. The dielectric constant of material was from fly ash which was about 3.0 for various charging conditions.  Explanation was added in Pages 10 and 11.

### ภาคผนวก ข-4

Intra, P. and Tippayawong, N., "Development and evaluation of a high concentration, high penetration unipolar corona ionizer for electrostatic discharge and aerosol charging", *Journal of Electrical Engineering and Technology*, 2013, accepted for publication, Ms. Ref. No.: J-12-11-017. มี impact factor = 0.579

19/4/2556 Print

Subject:	Journal of Electrical Engineering & Technology- Decision on Manuscript J-12-11-017(Ver. )	
From:	jeet@kiee.or.kr (jeet@kiee.or.kr)	
To:	panich_intra@yahoo.com;	
Date:	Friday, April 19, 2013 12:22 PM	

# Journal of Electrical Engineering & Technology

### Dear Prof. Intra, Panich

It is a pleasure to accept your manuscript entitled "Design and Evaluation of a High Concentration, High Penetration Unipolar Corona Ionizer for Electrostatic Discharge and Aerosol Charging" in its current form for publication in the Journal of Electrical Engineering & Technology. The comments of the reviewer(s) who reviewed your manuscript are included at the foot of this letter.

Thank you for your fine contribution. On behalf of the Editors of the Journal of Electrical Engineering & Technology, we look forward to your continued contributions to the Journal.

Sincerely,

Editor-in-Chief, Prof. Jaeseok Choi Journal of Electrical Engineering & Technology

#### Reviewer 1:

Thank you very much for your response. Through the continuous research, and look forward to the good results of this paper.

http://www.jeet.or.kr//LTKPSWeb/headeditor/headeditormain.aspx

KIEE, Room 901, Science & Technology Building, 635-4, Yeoksam-Dong, Gangnam-Gu, Seoul 135-703 KOREA | TEL: +82-2-553-0151~3 | FAX: +82-2-566-9957 | E-mail: jeet@kiee.or.kr

about:blank 1/1

## KIEE COPYRIGHT FORM

To ensure uniformity of treatment among all contributors, other forms may not be substituted for this form, nor may any wording of the form be changed. This form is intended for original material submitted to the KIEE and must accompany any such material in order to be published by the KIEE. Please read the form carefully and keep a copy for your files.

TITLE OF PAPER/ARTICLE/REPORT/PRESENTATION/SPEECH INCLUDING ALL CONTENT IN ANY FORM, FORMAT, OR MEDIA (hereinafter, "the Work"): Design and Evaluation of a High Concentration, High Penetration Unipolar Corona Ionizer for Electrostatic Discharge and Aerosol Charging

**COMPLETE LIST OF AUTHORS: Panich Intra and Nakorn Tippayawong** 

KIEE PUBLICATION TITLE (Journal): Journal of Electrical Engineering & Technology (JEET)

### Copyright Transfer

The undersigned hereby assigns to the Korean Institute of Electrical and Engineers, Incorporated (the "KIEE") all rights under copyright that may exist in and to the above Work, and any revised or expanded derivative works submitted to the KIEE by the undersigned based on the Work. The undersigned hereby warrants that the Work is original and that he/she is the author of the Work; to the extent the Work incorporates text passages, figures, data or other material from the works of others, the undersigned has obtained any necessary permissions.

### **General Terms**

- The undersigned represents that he/she has the power and authority to make and execute this assignment.
- The undersigned agrees to indentify and hold harmless the KIEE from any damage or expense that may arise in the event of a breach of any of the warranties set forth above.
- In the event the above Work is not accepted and published by the KIEE or is withdrawn by the author(s) before acceptance by the KIEE, the foregoing copyright transfer shall become null and void and all materials embodying the Work submitted to the KIEE will be destroyed.
- For jointly authored Works, all joint authors should sign, or one of the authors should sign as authorized agent for the others.

Author/Authorized Agent for Joint Authors	Date
P. Intra	21/04/2013

PLEASE DIRECT ALL QUESTIONS ABOUT THIS FORM TO:
KIEE, Rm 901, Science Technology B/D, 635-4,
Yeoksam-Dong, Gangnam-Gu, Seoul, 135-703, Korea Tel +82 -2-553-0151

# Design and Evaluation of a High Concentration, High Penetration Unipolar Corona Ionizer for Electrostatic Discharge and Aerosol Charging

## Panich Intra\*, and Nakorn Tippayawong\*\*

**Abstract** – The aim of this paper is to design and evaluate a high concentration, high penetration unipolar corona ionizer. The electrostatic characteristics in terms of voltage-current relationships of the present ionizer in the discharge zones for positive and negative coronas were discussed. Using ion current measurement, the concentration and penetration of ions were evaluated at corona voltages across the needle electrodes between 1 and 4 kV, flow rates between 1 and 5 L/min, and an operating pressure of 1 atm. In the discharge zone of the ionizer, the highest ion concentrations were found to be about  $1.71 \times 10^{14}$  and  $5.09 \times 10^{14}$  ions/m³ for positive and negative coronas, respectively. At the outlet of the ionizer, it was found that the highest ion concentration was about  $1.95 \times 10^{13}$ , and  $1.91 \times 10^{13}$  ions/m³ for positive and negative coronas, respectively. The highest ion penetration for positive and negative coronas through the ionizer was found to be about 98 %, and 33 %, respectively. The  $N_i t$  product for positive and negative coronas was also found to  $1.28 \times 10^{13}$  and  $7.43 \times 10^{13}$  ions/m³ s, respectively. From the findings, this ionizer proved to be particularly useful as an aerosol charger for positive and negative charge before the detector in an electrical aerosol detector.

**Keywords**: Aerosol, Ion, Corona Discharge, Ionizer, Unipolar Charging

## 1. Introduction

Aerosol charging is the first basic step in the aerosol measurement based on electrostatic technique [1]. The objective of the aerosol charging mechanism for an electrical aerosol detector is to impose a known net electric charge on the aerosol particles because number concentration of particles depends on the mean charge level of aerosol particles as a function of particle diameter and the mean residence time of the particles to the ions [2]. There are many mechanisms by which aerosol particles acquire net electric charge. There are several mechanisms by which aerosol particles acquire net charge distributions. These are flame charging, static electrification, diffusion charging and field charging [3]. Diffusion charging is one of the most commonly used mechanisms for charging particles in electrical measurement instruments. Generally, aerosol particles are allowed to collide with ions and the charge carried by these ions is transferred to the particles. There are three conventional ways to produce ions for diffusion charging in a gas; (i) by corona discharge, (ii) by photoelectric/UV-light sources, and (iii) by ionizing radiation from  $\alpha$ -ray or  $\beta$ - particle sources such as  $^{85}$ Kr, <sup>241</sup>Am, and <sup>210</sup>Po.

Received ; Accepted

However, corona discharges are among the most common techniques to produce high ion concentrations and there have been numerous extensive studies in the past [4 – 13]. Corona discharge is produced by a non-uniform electrostatic field such as that between a needle and plate or a concentric wire and a tube. In this corona region, electrons have sufficient energy to knock an electron from gas molecules creating positive ions and free electrons. During this process, aerosol flow is directed across the corona discharge field and is charged by random collisions between the ions and particles due to Brownian motion of ions in space. The amount of ion deposition on the particle surface depends on resident time, particle radius and shape, electric field, etc. This technique has been applied successfully and several designs of aerosol corona ionizer have been employed and described in the published literature [14], both corona-wire and corona-needle ionizers. A widely used ionizer is a corona-needle dischargers because of its simplicity and capability to provide high number concentrations of ions [15]. There have been numerous studies and developments on the corona-needle ionizer, both AC and DC sources [5, 10, 11, 12]. In general, the ideal charger would need a high efficiency charging technique that: (a) produces stable and high ion concentrations, (b) does not damage the aerosol, (c) has low particle losses (d) has no contamination, (e) applies to nanoparticles, and (f) is capable of working at low pressures and in different gases. The geometry, dimension and size of the precipitator should be less complex to keep the unit cost low.

<sup>\*</sup> Research Unit of Electrostatic Applications in Energy and Environment, College of Integrated Science and Technology, Rajamangala University of Technology Lanna, Chiang Mai 50220 Thailand. (panich\_intra@yahoo.com)

<sup>\*\*</sup> Department of Mechanical Engineering, Faculty of Engineering, Chiang Mai University, Chiang Mai 50200 Thailand. (n.tippayawong@yahoo.com)

Reference	Needle electrode diameter	Electrodes distance	Discharge zone length	Aerosol flow rate	Corona voltage range	Aerosol/ion direction
Whitby [5]	n/a	n/a	n/a	0 – 70 L/min	0 – 9.0 kV	Perpendicular
Hernandez-Sierra <i>et al.</i> [10]	3.0 mm	4.0 mm	55 mm	0-10 L/min	2.5 - 4.0  kV	Perpendicular
Alonso et al. [11]	n/a	3.5 mm	25 mm	0-10 L/min	3.1 - 3.7  kV	Circular
Intra and Tippayawong [12]	6.0 mm	3.5 mm	30 mm	0-8 L/min	2.6 - 4.3  kV	Circular
This work	3.0 mm	3.5 mm	20 mm	0-5 L/min	2.2 - 3.6  kV	Circular

**Table 1.** Comparison of different unipolar corona-needle ionizers.

n/a: information not available

This paper presents the work on designing and evaluating the high concentration, high penetration unipolar corona ionizer for electrostatic discharge and aerosol charging. The electrostatic characteristics in terms of voltage-current relationships of the present ionizer in the discharge zones for positive and negative coronas were discussed. Its electrostatic characteristics were determined at corona voltages at the needle electrode between 1 and 4 kV, flow rates between 1 and 5 L/min, and an operating pressure of 1 bar. Based on ion current measurement, the concentration and penetration of ions of the ionizer were also evaluated.

## 2. Description of Unipolar Corona Ionizer

Fig. 1 shows the schematic diagram of the corona-needle ionizer employed in this study. The ionizer's geometrical configuration is similar to the ionizer used by Whitby [5], Hernandez-Sierra et al. [10], Alonso et al. [11], and Intra and Tippayawong [12]. However, differences between the present ionizer and existing ionizers include; (i) the concept of the present ionizer was based on a compact, inexpensive and portable unit. Short column ionizer was used to reduce diffusion effects of the particle inside the ionizer; (ii) the ionizer adopted a tangential aerosol inlet upstream of the charging zone to ensure uniform particle distribution across the annular aerosol entrance to the charging zone of the ionizer column; and (iii) the applied voltage was set to maintain at low level to reduce electrostatic precipitation effects of the particle inside the ionizer. In general, the electrostatic discharge and ionization of the ionizer was dependent on the geometrical configuration, the charging time, the electric field strength and the flow field and behavior of the ionizer. A comparison between the present ionizer and the existing ionizers in terms of the geometrical configuration, the aerosol flow rate, the corona voltage range and the aerosol flow behavior is shown in Table 1. It was shown that the present ionizer is more compact, and operates at lower applied voltage than existing ionizers.

The present ionizer consists essentially of a coaxial needle electrode placed along the axis of a cylindrical tube with tapered end, and divided into three sections. The first and second sections (from top to bottom

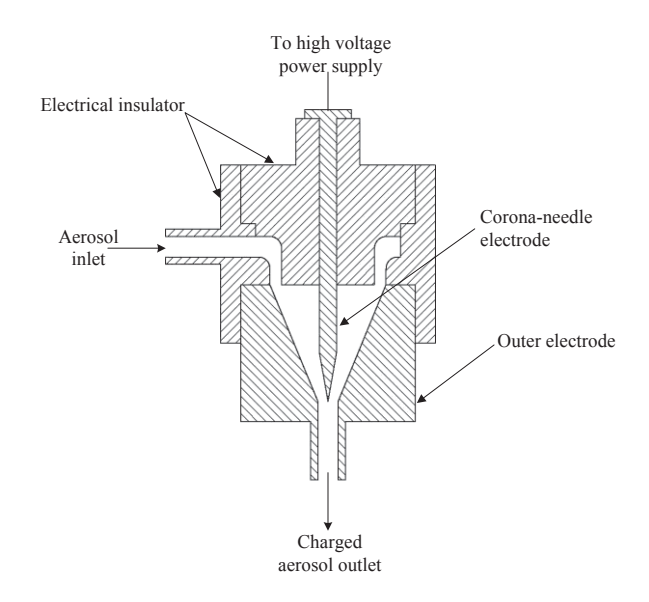


Fig. 1. Schematic diagram of the corona-needle ionizer.

in the drawing) are made of a polytetrafluoroethylene (PTFE), and the third (outlet section) of stainless steel tube. The PTFE tube is an electrical insulator between needle electrode and outer electrode and served to hold the needle electrode coaxial with the outer electrode. The needle electrode could be screwed into the PTFE insulator to connect to a DC voltage supply. The needle electrode is made of a stainless steel rod, 3 mm in diameter, ending in a sharp tip. The tip radius is about 50 µm, as estimated under a microscope. The needle cone angle is about 10°. The diameter of the outer electrode is 20 mm, its length is 20 mm with conical shape. The orifice diameter is about 3.5 mm. The distance between the needle electrode and the cone apex is 1.75 mm. The needle electrode head is connected to a positive high voltage, while the outer electrode is grounded.

## 3. Theory

## 3.1 Ion Number Concentration of the Ionizer

In the absence of aerosol particles, the mean number concentration of ions,  $n_{in}$ , in the discharge zone of the ionizer can be estimated from the discharge current using the expression [12]

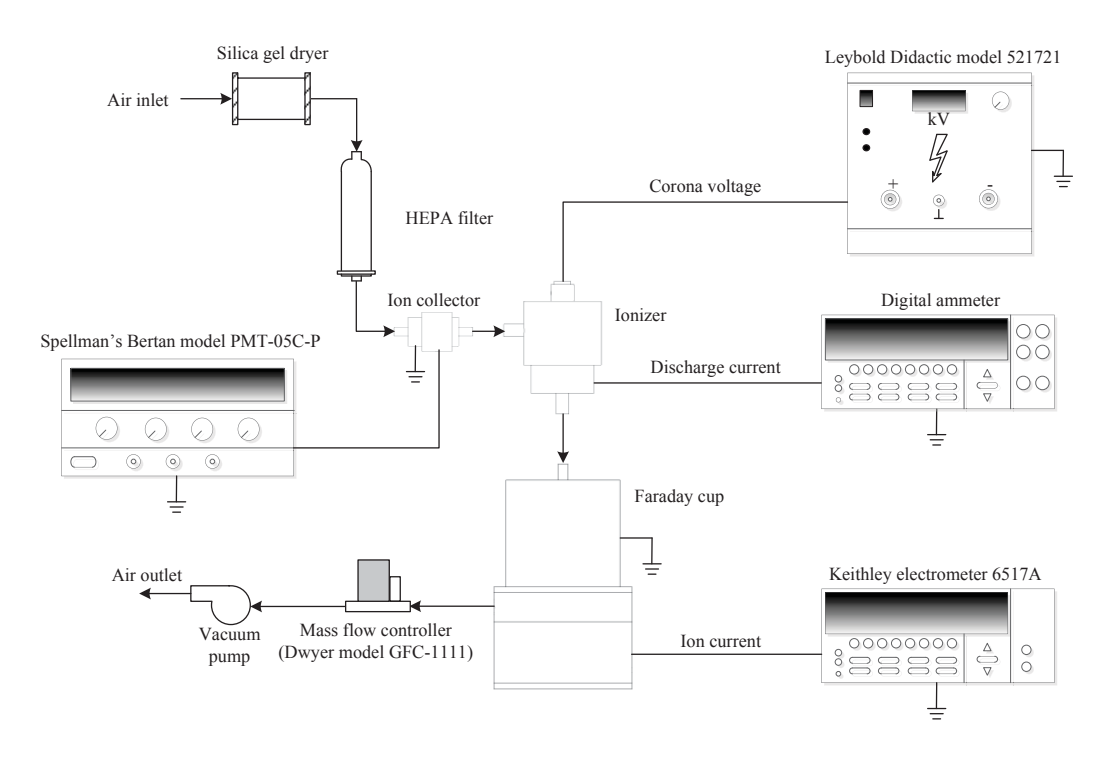


Fig. 2. Experimental setup for the characterization of the corona-needle ionizer.

$$n_{in} = \frac{I_{in}}{eZ_i EA} \tag{1}$$

where  $I_{in}$  is the current deposited on the grounded conical-shaped wall, e is the elementary charge,  $Z_i$  is the electrical mobility of the ions (It has been suggested that the average value for the positive and negative ion electrical mobility at atmospheric pressure were  $Z_i^+ = 1.4 \times 10^{-4} \,\mathrm{m^2/V}$  s and  $Z_i^- = 2.2 \times 10^{-4} \,\mathrm{m^2/V}$  s, respectively [16]), E is the electric field inside the discharge zone, and A is the inner surface area of the metallic cone (ionizer outlet) where the discharge current is collected. In the present ionizer, the inner surface area of the metallic cone (charger outlet) where the ion current is collected, and is given by

$$A = \pi (r_1 + r_2) \sqrt{(r_1 - r_2)^2 + L^2}$$
 (2)

where  $r_1$  and  $r_2$  are the inner and outer radii of a conical-frustum, and L is the length of the discharge zone of the ionizer. The ion number concentration has units of ions/m<sup>3</sup>. The mean residence time or charging time of the particles in the charging zone of this charger is given by

$$t = \frac{\pi L \left( r_1^2 + r_1 r_2 + r_2^2 \right)}{3Q_a} \tag{3}$$

where  $Q_a$  is the volumetric air flow through the ionizer.

The total number concentration of ions at the ionizer outlet,  $n_{out}$ , can be calculated from the ion current by the following equation [10]

$$n_{out} = \frac{I_{out}}{eO} \tag{4}$$

where  $I_{out}$  is the ion current at the ionizer outlet was measured by the Faraday cup electrometer, and Q is the volumetric air flow through the Faraday cup.

#### 3.2 Ion Penetration through the Ionizer

The ions penetration, P, through the ionizer is defined as the ratio of the number concentration of ions at the ionizer outlet over the number concentration of ions in the discharge zone of the ionizer, and can be estimated from the relation [12]

$$P = \frac{n_{out}}{n_{in}} \tag{5}$$

## 4. Experimental Setup and Apparatus

The schematic diagram of the experimental setup for the electrostatic discharge characterization of the present ionizer is shown in Fig. 2. Air flow was regulated and controlled by means of a mass flow controller (Dwyer model GFC-1111) with a vacuum pump, typically in the range between 1.0-5.0 L/min. The air was first dried with the diffusion dryer, any remaining water was removed, and then filtered through a high efficiency particulate-free air (HEPA) filter, Pall HEPA capsule model 12144 with

filtration efficiency of 99.97 % and retention of 0.3  $\mu$ m for air/gas, to remove any particles and then enter the ion trap to remove the air ions. A commercial adjustable DC high voltage power supply (Leybold Didactic model 521721) was used to maintain the positive high voltage difference in the ionizer, generally in the range between 1.0 – 4.0 kV. The discharge current from the corona-needle electrode was measured directly with a digital ammeter. The rate of discharging is proportional to the mean ion number concentration in the discharge zone.

In this study, the ion current at the ionizer outlet was measured by filtration method. An air sample was drawn into a shielded Faraday cup with a HEPA filter through which all the air passed. A Faraday cup was devised using a 47 mm stainless steel filter holder in a 70 mm diameter stainless steel container. The filter was equipped with a fine collection metal grid, and was electrically isolated with Teflon from the container and ground. In the Faraday cup, the 99.99 % of ions were removed from the air stream by the filter and the resulting ion current flow was measured with Keithley 6517A electrometer. The filter holder was connected to the electrometer input that had been carefully shielded against external fields. Triaxial cables (Keithley 237-ALG-2) between the Faraday cup and the electrometer eliminated leakage currents. As shown in Table 2, several sets of experiments were carried out at varying corona polarity and voltage and aerosol flow rates. For each set of operating conditions, measurements were repeated at least three times.

## 5. Results and Discussion

Fig. 3 shows the current-voltage characteristics in the discharge zone of the ionizer for positive and negative ions. The corona voltage was varied from 0 to 4 kV, the flow rate of 0 L/min, and operating pressure of 1 bar. It was found that the discharge currents increased monotonically with an increase in the corona voltage. The corona onset voltages were found to be about 2.4 and 2.2 kV for positive and negative ions, respectively. As shown in the plot, the spark-over phenomena occurred for the positive corona at voltages larger than 3.6 kV at discharge current of about 2.8 × 10<sup>-5</sup> A and negative corona voltages larger than 3.0 kV at discharge current of about  $7.8 \times 10^{-5}$ A. The spark-over phenomena marks electrical breakdown of the gas were observed to release higher discharge current corresponding to ion concentration, but it was undesirable because of higher particles loss inside the ionizer due to high electrostatic field. Above these values, the discharge current was found to exhibit a fluctuation in an uncontrollable and unstable manner. No measurement could be made by available digital ammeter because of higher discharge current of several hundred mA flowing through the air gap

**Table 2.** Ranges and values of variables investigated.

Variable	Range
Corona voltage	0-4  kV
Orifice diameter	3.5 mm
Needle cone angle	10°
Ion generated	positive ion (+), negative ion (-)
Ionized gas	air
Flow rate	1, 3 and 5 L/min
Pressure	1 atm

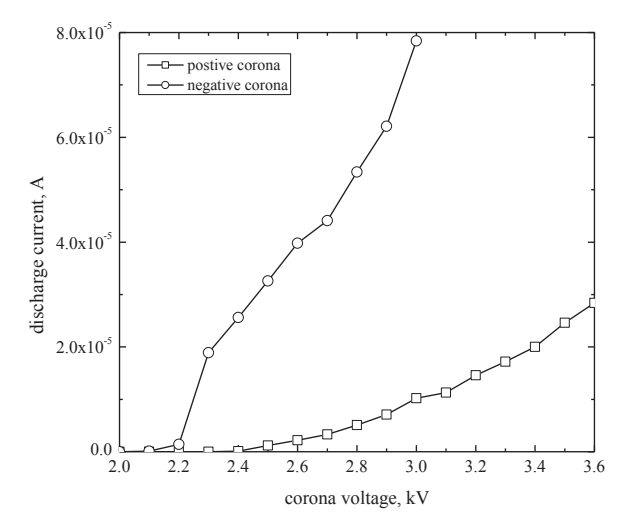


**Fig. 3.** Current-voltage characteristics in the discharge zone of the ionizer.

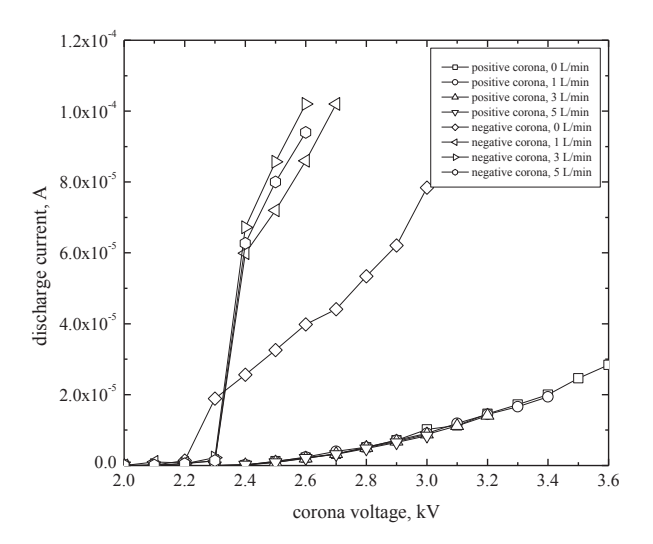


**Fig. 4.** Current-voltage characteristics in the discharge zone of the ionizer at different operating flow rates.

between the electrodes. At the same voltage, the currents for negative ions were slightly higher than those positive ions. This was expected because negative ions have higher electrical mobility than positive ones. It was more likely to

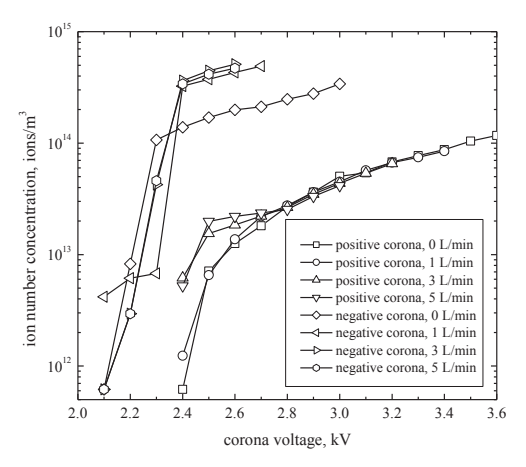


**Fig. 5.** Variation in ion number concentration with corona voltage in the ionizer discharge zone at different operating flow rates.

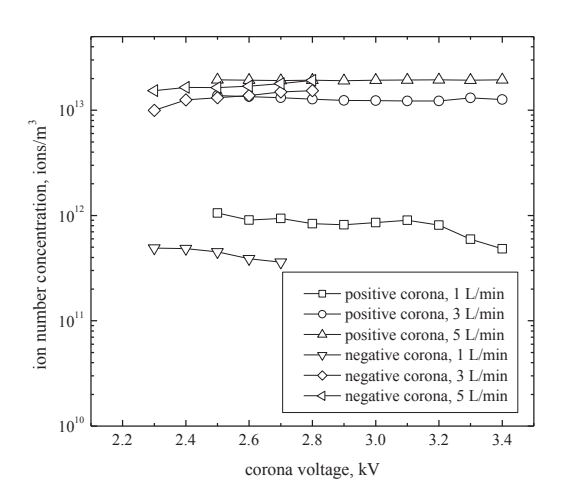


**Fig. 6.** Variation in ion number concentration with corona voltage at the ionizer outlet.

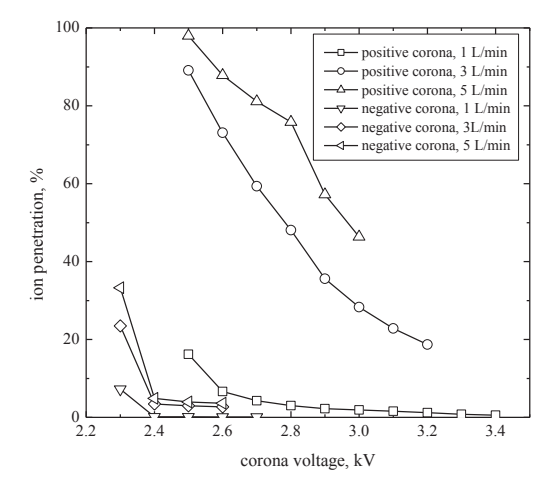


**Fig. 7.** Variation of ion penetration with corona voltage at different operating flow rates.

impact and deposit on the outer electrode wall of the ionizer due to the electrostatic force [16].

, 2011

For different operating flow rates, the currentvoltage characteristics in the discharge zone of the ionizer are shown in Fig. 4. The resultant discharge currents in the discharge zone of the ionizer for both positive and negative coronas were evaluated for 0, 1, 3, and 5 L/min, and 0 - 4kV. Discharge current for positive corona voltage practically became constant, independent of the flow rate. Meanwhile, negative discharge currents were found to depend on flow rate, increased with increasing flow rate, because higher electrical mobility and ion will be moved toward outer electrode by air flowing. However, the electrical breakdown voltages were found to decrease with increasing flow rate for both positive and negative coronas. It was expected that the ion or electron will be accelerated quickly from corona electrode to outer electrode with higher flow velocity according to the flow rate.

With respect to the current-voltage characteristics, the variation in ion number concentration with corona voltage in the ionizer discharge zone at different operating flow rates is shown in Fig. 5. The mean number concentration of ions in the discharge zone of the ionizer was calculated by Equation (1). Obviously, the increase of the ion number concentration depends on the corona voltage. This shows that the highest ion concentration for positive and negative coronas was about  $1.71 \times 10^{14}$  and  $5.09 \times 10^{14}$  ions/m<sup>3</sup>, occurring at corona voltage of about 3.6 and 2.6 kV, respectively. It is commonly known that the number concentration of negative ion is generally larger than positive ion, in a range well above corona onset. Fig. 6 shows the number concentration of positive and negative ions as a function of the corona voltage at the ionizer outlet at operating flow rate between 1 and 5 L/min. The onset voltage for negative corona appeared at about 2.3 kV, while positive corona was needed for the onset voltage of about 2.5 kV. At the flow rate of 1 L/min, it was found that the ion concentration for both positive and negative coronas decreased with increasing corona voltage. For larger operating flow rate, ion number concentration for positive corona practically became a constant, independent of the corona voltage, while negative corona slightly increased with increasing corona voltage, dependent of the corona voltage in narrow range. The highest ion concentration was found to be about  $1.95 \times 10^{13}$ , and  $1.91 \times 10^{13}$  ions/m<sup>3</sup> occurring at the corona voltage of 3.4, and 2.8 kV for positive and negative coronas, and the flow rate at 5 L/min, respectively.

Fig. 7 shows the ion penetration as a function of the corona voltage at different operating flow rates. Both positive and negative coronas, the penetration dropped with increasing corona voltage because the sink flow of air through the discharge zone was no longer able to focus all of ions through the discharge zone and more ions loss due to electrostatic deposition on the inner surface of the outer electrode inside the ionizer. When the flow rate increased, the ion penetration through the ionizer was found to slightly increase. This is because the ions can be transported from the ionizer more easily by faster flowing air. Due to high

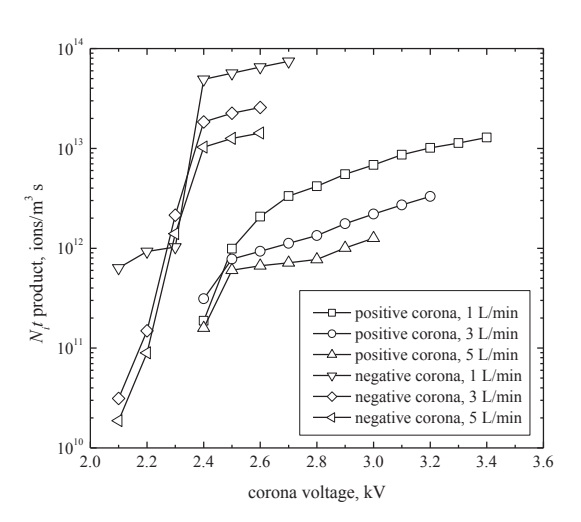


**Fig. 8.** Variation of *N<sub>i</sub>t* product with corona voltage at different operating flow rates.

electrical mobility of negative ion, the penetration of positive ions was found to be higher than negative ions. From Fig. 7, the highest ion penetration for positive and negative coronas through the ionizer was found to be about 98 %, and 33 % occurring at the corona voltage of 2.5 and 2.3 kV, and the flow rate of 5 L/min, respectively. For most applications of the ionizer, stability and the absolute magnitude of the free ion current are more important than the efficiency as long as the efficiency is high.

It should be noted that the aerosol charging efficiency depends on the product of the ion number concentration and the average time the aerosol particles spend in the ionizer. Fig. 8 shows the variation of  $N_i t$ product (product of ion concentration and charging time) with corona voltage at different operating flow rates. In this study, the charging times were found to be about 0.15, 0.05 and 0.03 sec for the flow rates of about 1, 3 and 5 L/min, respectively. It was shown that the  $N_i t$  product decreased with increasing flow rate because higher flow rate or shorter residence time gave rise to lower  $N_i t$  product. Increase in corona voltage produced a monotonic increase in ion number concentration, hence the  $N_i t$  product. It was also shown that the highest  $N_i t$  product for positive and negative coronas was found to  $1.28 \times 10^{13}$  and  $7.43 \times 10^{13}$ ions/m<sup>3</sup> s occurring at the corona voltage of about 3.4 and 2.7 kV, and the flow rate of 1 L/min, respectively.

## 6. Conclusion

The high concentration, high penetration unipolar corona ionizer for electrostatic discharge and aerosol charging was designed and electrostatically evaluated. The electrostatic characteristics in terms of voltage-current relationships of the present ionizer in the discharge zones for positive and negative coronas were discussed. The concentration and penetration of ions of the ionizer were evaluated based on ion current measurement. The experiments were carried out at corona voltages at the needle electrode between 1 and 4 kV, flow rates between 1 and 5 L/min, and an operating pressure of 1 atm. In the discharge zone of the ionizer the highest ion concentration for positive and negative coronas was about  $1.71 \times 10^{14}$  and  $5.09 \times 10^{14}$  ions/m<sup>3</sup> occurring at corona voltage of about 3.6 and 2.6 kV, respectively. At the outlet of the ionizer, it was found that the highest ion concentration was found to be about  $1.95 \times 10^{13}$ , and  $1.91 \times 10^{13}$ 10<sup>13</sup> ions/m<sup>3</sup> occurring at the corona voltage of 3.4, and 2.8 kV for positive and negative coronas, and the flow rate at 5 L/min, respectively. The highest ion penetration for positive and negative coronas through the ionizer was found to be about 98 %, and 33 % occurring at the corona voltage of 2.5 and 2.3 kV, and the flow rate of 5 L/min, respectively. The  $N_i t$  product for positive and negative coronas was also found to  $1.28 \times 10^{13}$  and  $7.43 \times 10^{13}$  ions/m<sup>3</sup> s occurring at the corona voltage of about 3.4 and 2.7 kV, and the flow rate of 1 L/min, respectively. Finally, this shows that this ionizer proved to be particularly useful as an aerosol charger for positive and negative charge before the detector in an electrical aerosol detector.

## Acknowledgements

This research was jointly supported by the Thailand Research Fund (TRF), the Commission on Higher Education (CHE), and Rajamangala University of Technology Lanna (RMUTL), contract no. MRG5480001.

#### References

- [1] P. Intra and N. Tippayawong, "An overview of unipolar charger developments for nanoparticle charging," *Journal of Aerosol and Air Quality Research*, Vol. 11, No. 2, pp. 186 208, 2011.
- [2] W. C. Hinds, *Aerosol Technology*, John Wiley & Sons, New York, U.S.A, 1999.
- [3] P. Intra and N. Tippayawong, "Performance evaluation of an electrometer system for ion and aerosol charge measurements," *Korean Journal of Chemical Engineering*, Vol. 28, No. 2, pp. 527 530, 2011.
- [4] G. W. Hewitt, "The charging of small particles for electrostatic precipitation," *AIEE Transactions*, Vol. 76, pp. 300 306, 1957.
- [5] Whitby, K.T., "Generator for producing high concentration of small ions," *Review of Scientific Instruments*, Vol. 32, No. 12, 1351 1355, 1961.

- [6] H. J. White, *Industrial Electrostatic Precipitation*, Addison-Wesley, Reading, Massachusetts, 1963.
- [7] B. Y. H. Liu, K. T. Whitby and H. H. S. Yu, "Diffusion charging of aerosol particles at low pressures," *Journal of Applied Physics*, Vol. 38, No. 4, pp. 1592 1597, 1967.
- [8] B. Y. H. Liu and D. Y. H. Pui, "On the performance of the electrical aerosol analyzer," *Journal of Aerosol Science*, Vol. 6, pp. 249 264, 1975.
- [9] D. Y. H. Pui, Experimental study of diffusion charging of aerosols, Ph.D. thesis, University of Minnesota, Minneapolis, MN, USA, 1976.
- [10] A. Hernandez-Sierra, F. J. Alguacil, and M. Alonso, "Unipolar charging of nanometer aerosol particle in a corona ionizer," *Journal of Aerosol Science*, Vol. 34, pp. 733 745, 2003.
- [11] M. Alonso, M.I. Martin, and F.J. Alguacil, "The measurement of charging efficiencies and losses of aerosol nanoparticles in a corona charger," *Journal of Electrostatics*, Vol. 64, pp. 203 214, 2006.
- [12] P. Intra and N. Tippayawong, "Effect of needle cone angle and air flow rate on electrostatic discharge characteristics of a corona-needle ionizer," *Journal of Electrostatics*, Vol. 68, No. 3, pp. 254 260, 2010.
- [13] P. Intra, A. Yawootti, U. Vinitketkumnuen and N. Tippayawong, "Investigation of electrical discharge characteristics of a unipolar corona-wire aerosol charger," *Journal of Electrical Engineering and Technology*, Vol. 6, No. 4, pp. 556 562, 2011.
- [14] P. Intra and N. Tippayawong, "Progress in unipolar corona discharger designs for airborne particle charging: A literature review," *Journal of Electrostatics*, Vol. 67, No.4, pp. 605 615, 2009.

- [15] P. Intra and N. Tippayawong, "Comparative study on electrical discharge and operation characteristics of needle and wire-cylinder corona chargers," *Journal of Electrical Engineering and Technology*, Vol. 1, No. 4, pp. 520 527, 2006.
- [16] G.P. Reischl, J.M. Makela, R. Harch, and J. Necid, "Bipolar charging of ultrafine particles in the size range below 10 nm," *Journal of Aerosol Science*, Vol. 27, pp. 931 949, 1996.



## Panich Intra

He received the BS.Tech.Ed. degree in Electrical Engineering from Rajamangala Lanna University of Technology, Thailand in 2001, the M.Eng. degree in Energy Engineering

from Chiang Mai University, Thailand in 2003, and the Ph.D. degree in Mechanical Engineering from Chiang Mai University, Thailand in 2006, respectively. He is currently an Assistant Professor in the College of Integrated Science and Technology, Rajamangala University of Technology Lanna, Thailand. His research interests are electrical aerosol charging and detecting, and applied electrostatic precipitation.



#### Nakorn Tippayawong

He received his B.Eng. and Ph.D. degrees in Mechanical Engineering from Imperial College, UK in 1996 and in 2000, respectively. He is currently an Associate Professor in the Department

of Mechanical Engineering, Chiang Mai University. His research interests are HV applications in aerosol system, renewable energy.

## ภาคผนวก ข-5

Intra, P., "Corona discharge in a cylindrical triode charger for unipolar diffusion aerosol charging", *Journal of Electrostatics*, Vol. 70, No. 1, pp. 136 – 143, 2012. มี impact factor = 1.08



Contents lists available at SciVerse ScienceDirect

## Journal of Electrostatics

journal homepage: www.elsevier.com/locate/elstat



# Corona discharge in a cylindrical triode charger for unipolar diffusion aerosol charging

## Panich Intra\*

Research Unit of Electrostatic Applications in Energy and Environment, College of Integrated Science and Technology, Rajamangala University of Technology Lanna, Chiang Mai, Thailand 50220, Thailand

#### ARTICLE INFO

Article history:
Received 9 July 2011
Received in revised form
3 November 2011
Accepted 25 November 2011
Available online 11 December 2011

Keywords: Aerosol Corona discharge Unipolar charger Diffusion charging

#### ABSTRACT

A cylindrical triode charger for unipolar diffusion charging of aerosol particles was designed, constructed, and evaluated. The corona discharge characteristics were studied in this cylindrical triode charger. For the process the current-voltage characteristics were determined, as were the ion number concentration, the  $n_i t$  product, and the mean charge per particle as a function of particle diameter. The discharge and charging currents, and ion number concentration in the charging zone of the charger increased monotonically with corona voltage. The negative corona had a higher current than the positive corona. At the same corona voltage, the ion number concentration in the discharge zone was larger than the charging current for positive and negative coronas, with values of about 197 and 32 times and 645 and 99 times for the ion-driving voltages of 0 and 310 V, respectively. The average ion penetration for positive and negative coronas was 0.64 and 0.19% and 3.62 and 1.93% for the ion-driving voltages of 0 V and 310 V, respectively. The higher flow rate, shorter residence time, gave a lower Nit product. By calculation 14% of charged particles of 10 nm in diameter were lost to the outer cylinder because of the electrostatic field effect. The charger does not use a sheath of air flow along the walls or the perforated screen opening, it has low diffusion and space charge losses due to the short column charging zone, and is a low complexity and inexpensive system. It worked as well as more sophisticated and expensive commercially available chargers.

© 2011 Elsevier B.V. All rights reserved.

#### 1. Introduction

One of the most important processes in electrical aerosol spectrometry is aerosol particle charging. Its purpose is to impart the aerosol particles with a known net charge distribution. Since particle size distribution is commonly determined through the electrical mobility classification, prediction of particle size requires the knowledge of the charge distribution for every size [1,2]. Diffusion charging is the most commonly used mechanism for charging aerosol particles in electrical aerosol spectrometry. In this type of charging, particles are allowed to collide with ions and the charge carried by these ions is transferred to the particles. The process can be unipolar or bipolar, depending on the polarity of the ions colliding with the particles [2]. Comparing both charging methods, unipolar does not reach an equilibrium charge distribution and potentially gives a higher efficiency. However, in bipolar diffusion charging, particles can grow by Brownian coagulation,

an unwanted complication if the aerosol particle number concentration is above  $10^7/\text{cm}^3$  [3].

There are three conventional methods to generate ions for unipolar diffusion charging in a gas, corona discharge, photoemission from UV-light radiation, and radiation from  $\alpha$ -ray or  $\beta$ -ray sources. Corona discharge is the most common technique used to produce high ion concentrations. Several designs of unipolar aerosol corona chargers have been studied and described. These include both corona-wire and corona-needle chargers [1]. The desirable features of a corona charger are the production of high ion concentrations, low particle losses, no contamination, no gas into particle conversions, nanoparticle applicability and usability under various conditions [2].

The magnitude of the ion number concentration in the discharge and charging zones depends on the charger geometry, i.e., the distance between discharge electrode and the outer electrode, voltage waveform and frequency, and also on the shape and arrangement of the electrode. The corona discharge characteristic of a corona discharge charger is important because of the presence of different electric field profiles in the discharge and charging zones of the charger. Recently, the corona discharge characteristic

<sup>\*</sup> Tel.: +66 0 89 755 1985. E-mail address: panich\_intra@yahoo.com.

of a unipolar aerosol charger has received attention because it improved the extrinsic charging efficiency of nanoparticles [4–7].

The electrostatic loss of charged nanoparticles due to a high electric field is usually severe, and needs to be investigated using unipolar chargers. Ongoing work on improving the performance of these chargers centers on reducing particle losses inside them. Some of this reduction can be achieved by introducing the surrounding sheath air flow at the boundary between the aerosol stream and the wall. It allows more space for the charged particles to flow through the charger without precipitating on the charger walls. However, the large sheath air flow results in dilution of the aerosol. Another approach uses a turbulent jet of unipolar ions in a mixing chamber and applies a sinusoidal or square wave voltage to the electrode instead of a DC voltage [2]. But the mixing chamber again dilutes the aerosol and sinusoidal or square wave voltage generators are expensive and complex to use.

The subject of this work, the cylindrical triode charger for unipolar diffusion charging of aerosol particles, did not use sheath air flow and/or an expensive voltage generator. Its design, fabrication and testing was kept uncomplicated for economic and ease of operation reasons. Its electrostatic discharge characteristics required experimental investigation. Such were the current, the ion number concentration, and the ion penetration through the perforated inner cylinder of the charger. Also, how to get charged particle trajectories in the charging zone of the charger and a model of the particle transport had to be developed. This was the scope of the work.

#### 2. Materials and methods

#### 2.1. Design of cylindrical triode charger

Fig. 1 shows a schematic diagram of the prototype cylindrical triode charger. Its design principle is similar to that in the unipolar diffusion charger used by Hewitt [8], Liu and Pui [9], Buscher et al. [10], Lee et al. [11], and Biskos et al. [12]. Nonetheless, there are differences between the present and each of the existing chargers and they are as follows; (i) the design concept was simple, compact, and inexpensive. A short column charger was used to reduce diffusion and space charge losses of the particles inside the charger; and (ii) the charger does not have sheath gas flow diluting the aerosol. The prototype triode charger was 90 mm in length and

67 mm in diameter. As Fig. 1 shows, it consisted of two concentric metal cylinders with a corona-wire (0.2 mm diameter) placed along the axis of the cylinders. A DC high voltage was applied to the corona-wire to produce a corona discharge and the generated ions migrated toward the inner cylinder due to the high electric field in the region. In order to allow ions to flow in the charging zone, a section of the inner cylinder was made out of a perforated (2.5 mm diameter) cylindrical tube. The ion-driving voltage applied on the inner cylinder forced the ions through the perforated screen openings on the inner cylinder to the charging zone, while the outer cylinder was connected to ground. This iondriving voltage could regulate the ion current flow through the perforated screen. In the charging zone, the aerosol particles collided with the ions and were charged electrically. The inner and the outer radii of the annular charging zone were 15 mm and 30 mm, respectively. The width of the perforated screen opening on the inner cylinder was 20 mm.

#### 2.2. Current and ion number concentration

The discharge and charging current, I, of the charger is related to the ion number concentrations,  $n_i$ , and can be estimated by the following equation [9],

$$I = 2\pi r L E Z_i n_i e \tag{1}$$

where L is the width of the screen opening on the inner cylinder, e is the value of elementary charge on an electron (1.61  $\times$  10<sup>-19</sup> C), E is the local electric field in the discharge and charging zones at a point r from the axis, and  $Z_i$  is the electrical mobility of ion,  $Z_{\rm ion}^+ = 1.15 \times 10^{-4} \, {\rm m}^2/{\rm V}$  s,  $Z_{\rm ion}^- = 1.425 \times 10^{-4} \, {\rm m}^2/{\rm V}$  s, respectively [13]. If the space charge due to the ions is ignored, the radial electric field, E, in the discharge and charging zones is given by

$$E = \frac{V}{r \ln(R)} \tag{2}$$

where V is the applied voltage on the corona-wire or inner cylinder, and  $R = r_2/r_1$ ,  $r_1$  and  $r_2$  are the radii of the inner or corona-wire and outer cylinders. By means of Equation (1), the ion concentration can be calculated when the discharge and charging currents, the corona or screen voltages are known, and is given by

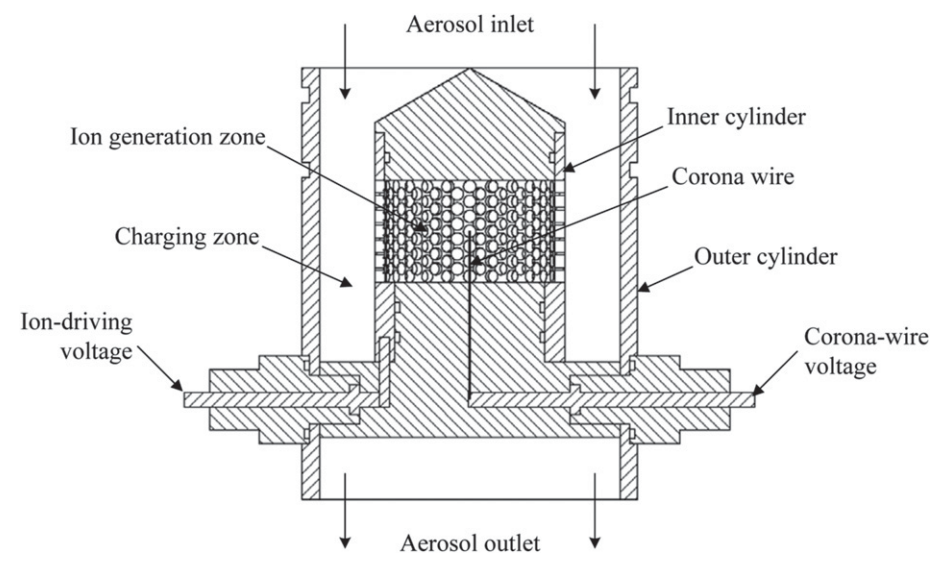


Fig. 1. Configuration of the prototype cylindrical triode charger.

$$n_i = \frac{I}{2\pi r LeEZ_i} \tag{3}$$

In diffusion charging studies it is necessary to know the charging parameter,  $n_i t$ , where t is the time of exposure of the particles to the ions, and can be calculated from the equation,

$$t = \frac{(r_2^2 - r_1^2)L}{Q_a} \tag{4}$$

where  $Q_a$  is the aerosol flow rate.

#### 2.3. Particle charging theory

In the charging zone of the charger, the ions produced by the corona discharge diffuse by Brownian motion and charge the aerosol particles. It is possible to consider the process of diffusion charging in a simpler way. The mean charge per particle,  $n_p$ , caused by the diffusion charging in a time period, t, by a particle diameter is approximately determined by the theory of White [14]

$$n_{\rm p} = \frac{\mathrm{d}_p kT}{2K_E e^2} \ln \left( 1 + \frac{\pi K_E \mathrm{d}_p \overline{c}_i e^2 n_i t}{2kT} \right) \tag{5}$$

where k is the Boltzmann's constant (1.380658  $\times$  10<sup>-23</sup> J/K),  $K_E = 1/4\pi\varepsilon_0$  the vacuum permittivity,  $d_p$  the particle diameter,  $\bar{c}_i$  the mean thermal speed of the ions, and T the operating temperature.

#### 2.4. Ion penetration

The ion penetration,  $P_{\text{ion}}$ , through the perforated screen openings on the inner cylinder to the charging zone of the charger is given by [15]

$$P_{\rm ion} = \frac{n_{\rm charging}}{n_{\rm discharge}} \tag{6}$$

where  $n_{\text{charging}}$  and  $n_{\text{discharge}}$  are the concentration of ions in the discharge and charging zones of the charger.

## 2.5. Transport of charged particle

For the particular case of annular geometries where the charged particles enter the charging zone of the charger on an axial flow and the charged particles migrate along the radial direction of the electrical field, motion of the charged particles in the charging zone of the charger can be described by a system of differential equations as [16]

$$\frac{\mathrm{d}r}{\mathrm{d}z} = \frac{ZV}{ru_{7}(r)\ln(R)}\tag{7}$$

where:

$$u_z(r) = ar^2 + b\ln(r) + c, (8)$$

$$a = \frac{1}{4\mu} \frac{\mathrm{d}p}{\mathrm{d}z},\tag{9}$$

$$b = -\frac{1}{4\mu} \frac{dp}{dz} \left( \frac{r_2^2 - r_1^2}{\ln(R)} \right), \tag{10}$$

$$c = \frac{1}{4\mu} \frac{\mathrm{d}p}{\mathrm{d}z} \left( \frac{r_2^2 - r_1^2}{\ln(R)} \ln(r_1) - r_1^2 \right),\tag{11}$$

where r and z are the radial and axial dimensions of the classifier,  $u_z$  are the radial and axial components of the air flow velocity, Z is the electrical mobility of ions or particles, V is the applied voltage, and dp/dz is the constant pressure gradient and is given by the following equation

$$\frac{\mathrm{d}p}{\mathrm{d}z} = -\frac{\rho \overline{u}^2 f}{2D_h} \tag{12}$$

where:

$$D_h = 2r_2(1 - (\kappa)), (13)$$

$$f = \frac{64}{Re} \left( \frac{1 + (\kappa)^2}{(1 - (\kappa))^2} + \frac{1 + (\kappa)}{(1 - (\kappa))\ln(\kappa)} \right)^{-1},\tag{14}$$

$$Re = \frac{2r_2(1-(\kappa))\overline{u}\rho}{\mu},\tag{15}$$

 $D_h$  is the hydraulic diameter for an annular flow area, f the friction factor,  $\overline{u}$  the mean axial flow velocity,  $\kappa = r_1/r_2$ ,  $\rho$  the gas density and Re the Reynolds number in the annular flow. Substituting Equation (8) into Equation (7) and Integrating Equation (7), the migration paths of the ions can be determined as

$$\int_{r_{in}}^{r_2} ar^3 + b \ln\left(r^2\right) + cr dr = \int_{0}^{z} \frac{VZ}{\ln(R)} dz$$
 (16)

where  $r_{\rm in}$  is the radial position at which the ions enter the precipitator. Therefore, the ions entering the charger at a radial position of  $r_{\rm in}$  have trajectories taking them to an axial position of z, which can be obtained as

$$z = -\frac{g(r_{\rm in})\ln(R)}{4VZ} \tag{17}$$

where:

$$g(r_{\rm in}) = \begin{pmatrix} ar_2^4 - ar_{\rm in}^4 + br_{\rm in}^2 - br_2^2 + 2br_2^2 \ln(r_2) \\ -2br_{\rm in}^2 \ln(r_{\rm in}) + 2cr_2^2 - 2cr_{\rm in}^2 \end{pmatrix}$$
(18)

#### 2.6. Calculation procedure

An analytical model was developed to calculate the ion number concentration and mean charge per particle in the charging zone of the charger. The parameters and operating conditions used are shown in Table 1. The following assumptions applied to the calculations. The flow condition inside the charger was steady, incompressible and laminar. The electric field distribution inside the charger was uniform in the axial direction. At the entrance the particle concentration was uniformly distributed. The particles

**Table 1**Limits of the investigated variables.

Variable	Range
Corona-wire diameter	200 μm
Inner cylinder diameter	30 mm
Outer cylinder diameter	60 mm
Corona-wire voltage	0-10 kV
Ion-driving voltage	0, 310 V
Ions generated	Positive ion $(+)$ , negative ion $(-)$
Ionized gas	Air
Pressure	1 bar
Temperature	30 °C

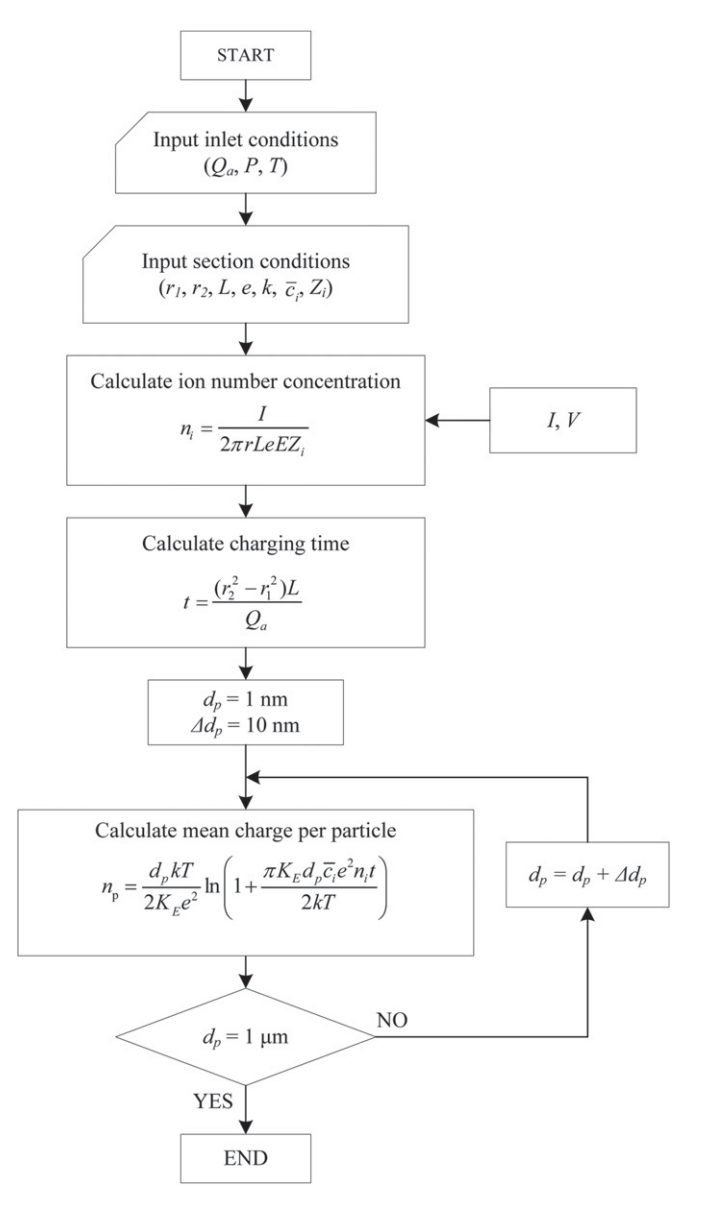


Fig. 2. Flow chart of the analytical model used in this study.

were fly ash with a dielectric constant of 3.0. Air density and viscosity were 1.225 kg/m³ and 1.7894  $\times$   $10^{-5}$  kg/m/s. A temperature of 294 K was used. The operating pressure was 1 bar. The particle size ranged from 1 nm to 1  $\mu m$ , the aerosol flow rates from 5 to 15 L/min, the corona-wire voltage from 1 to 10 kV, and the ion-driving voltage from 0 to 310 V. The ion number concentration and the mean charge per particle were calculated using Equations (3) and (5). The flow chart of the analytical model used is shown in Fig. 2.

#### 2.7. Experimental setup

Fig. 3 shows the schematic diagram for the equipment used to characterize the electrostatic discharge of the cylindrical triode charger. An adjustable commercial DC high voltage power supply (Leybold Didactic model 521721) was used to maintain the positive or negative high voltage differences on the corona-wire of the charger. The voltage was generally in the range between 0 and 10 kV. A second adjustable commercial DC high voltage power supply, Bertan model PMT-05C-P, was used to maintain the iondriving voltage difference on the inner cylinder in the range between 0 and 310 V. This was necessary to investigate the ion penetration through the perforated screen openings on the inner cylinder into the charging zone. The discharge and charging currents from the inner and outer cylinders were measured directly with a Keithley 6517A electrometer. Table 1 gives the limits of the evaluated variables. The measurements of the discharge and charging currents were repeated at least three times for each set of operating conditions.

#### 3. Results and discussion

Fig. 4 shows the current—voltage characteristics of the positive and negative coronas in the discharge and charging zones of the charger. Both discharge and charging currents increased monotonically with increasing corona voltage. As shown in Fig. 4 (a), in the discharge zone the onset voltage of the positive corona was 4.5 kV at a current of  $1.42\times10^{-6}$  A, while in the negative corona it was 3.5 kV at a current of  $1.4\times10^{-6}$  A. Compared with the positive corona, the magnitude of the discharge currents was markedly higher for the negative corona at the same corona voltage. Negative ions had higher electrical mobility than positive ions [13]. As Fig. 4 (b) shows, the onset voltage in the charging zone of both positive and negative coronas for the screen voltage of 0 V was about 4.5 kV

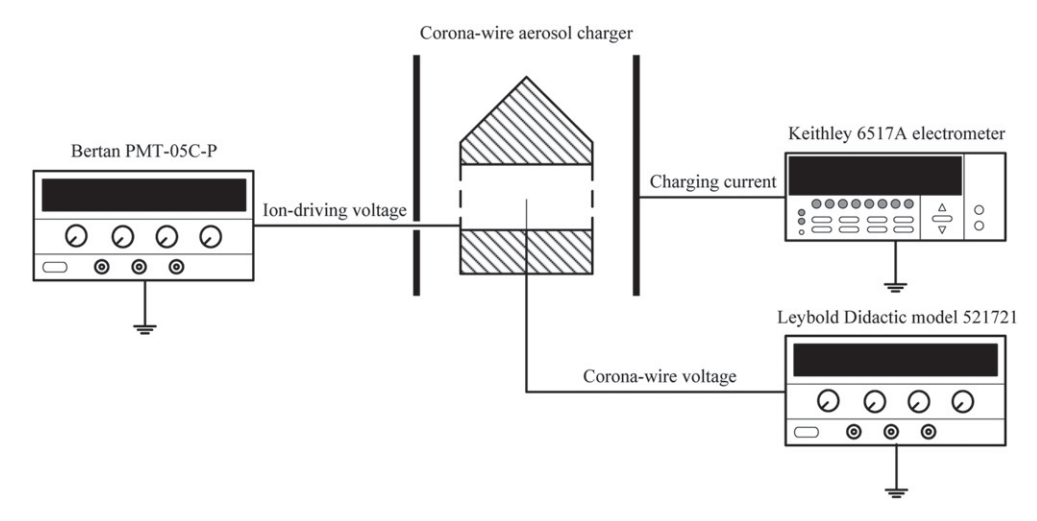
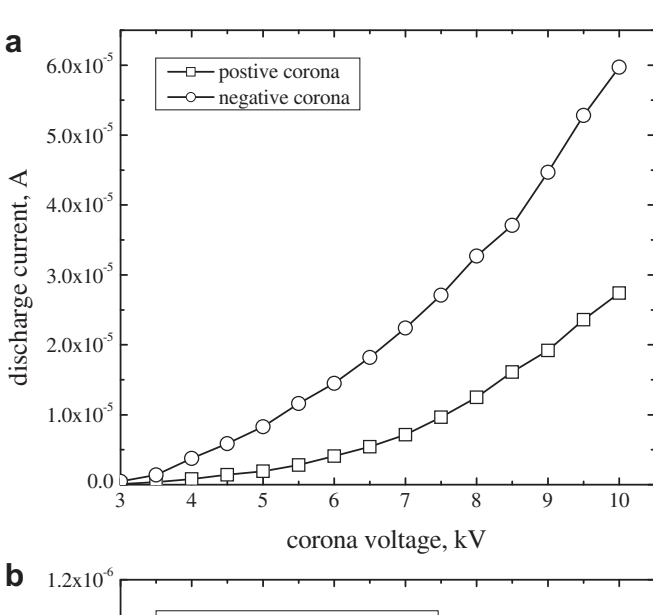
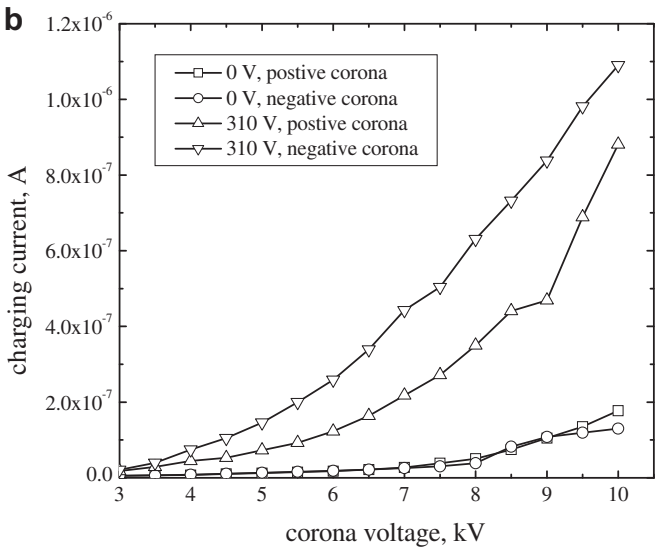


Fig. 3. Schematic instrument diagram for the characterization of the electrostatic discharge of the charger.

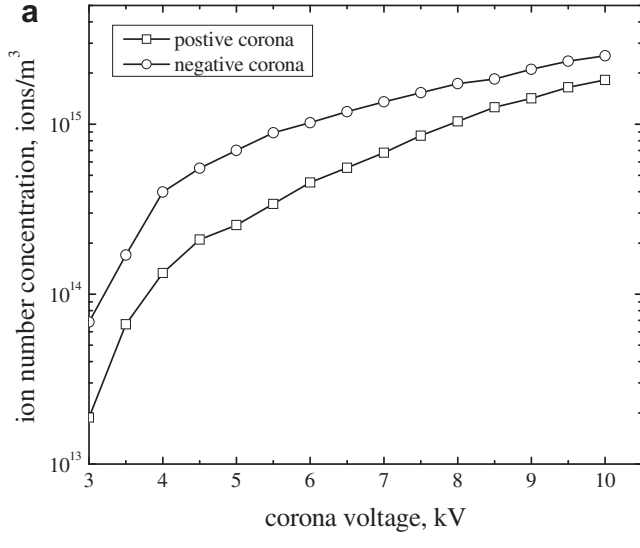
at currents of  $1.03 \times 10^{-8}$  and  $1.09 \times 10^{-8}$  A, respectively. A higher voltage rise was observed for negative charge in the discharge zone, whereas the opposite was true for the charging zone. At the same corona voltage, the magnitude of the charging currents for a positive corona was slightly higher than that of the negative corona, again because negative ions had higher electrical mobility than positive ions. Therefore, negative ions were more likely to deposit on the perforated screen openings on the inner cylinder of the charger by losing their charge.

Based on experimental studies of the ion mobility [17], the electrical mobility of particles 4 nm in diameter is one order of magnitude lower than the mean ion mobility. Nanoparticles essentially "feel" a time-averaged electric field of zero [10]. Therefore, an ion-driving voltage in the range of  $\pm 75$  to  $\pm 600$  V should be applied on the inner cylinder [10,18]. The charging current and ion number concentration in the charging zone increased monotonically with increasing ion-driving voltage [10], but for a higher ion-driving voltage, nanoparticle loss by deposition onto the outer cylinder was significant as the current of the voltage power supply became too high. In order to reduce ion losses on the perforated screen, a 310 V ion-driving voltage was applied to the





**Fig. 4.** Current–voltage characteristics of the charger (a) discharge zone and (b) charging zone.



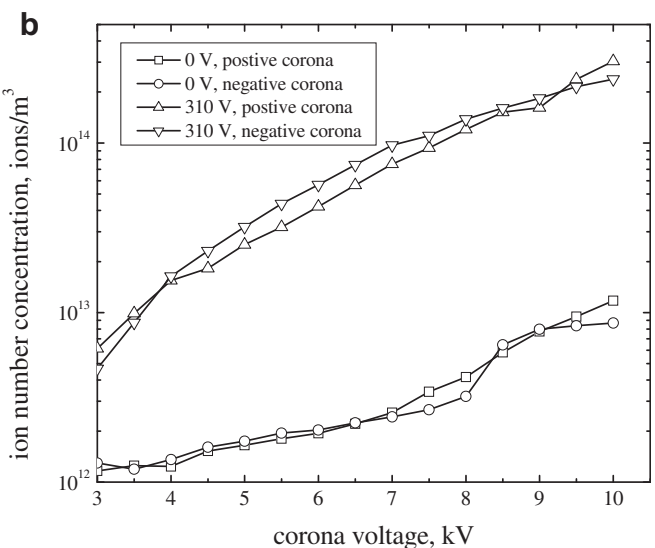


**Fig. 5.** Variations in ion number concentrations with corona voltage in the charger (a) discharge zone and (b) charging zone.

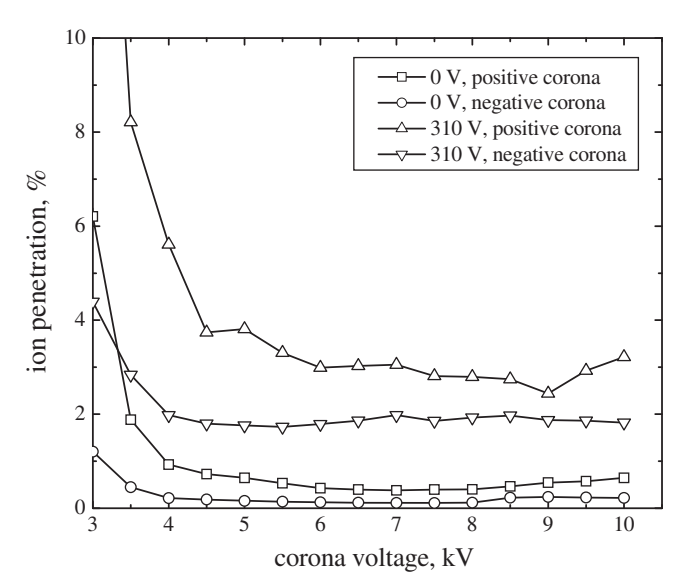
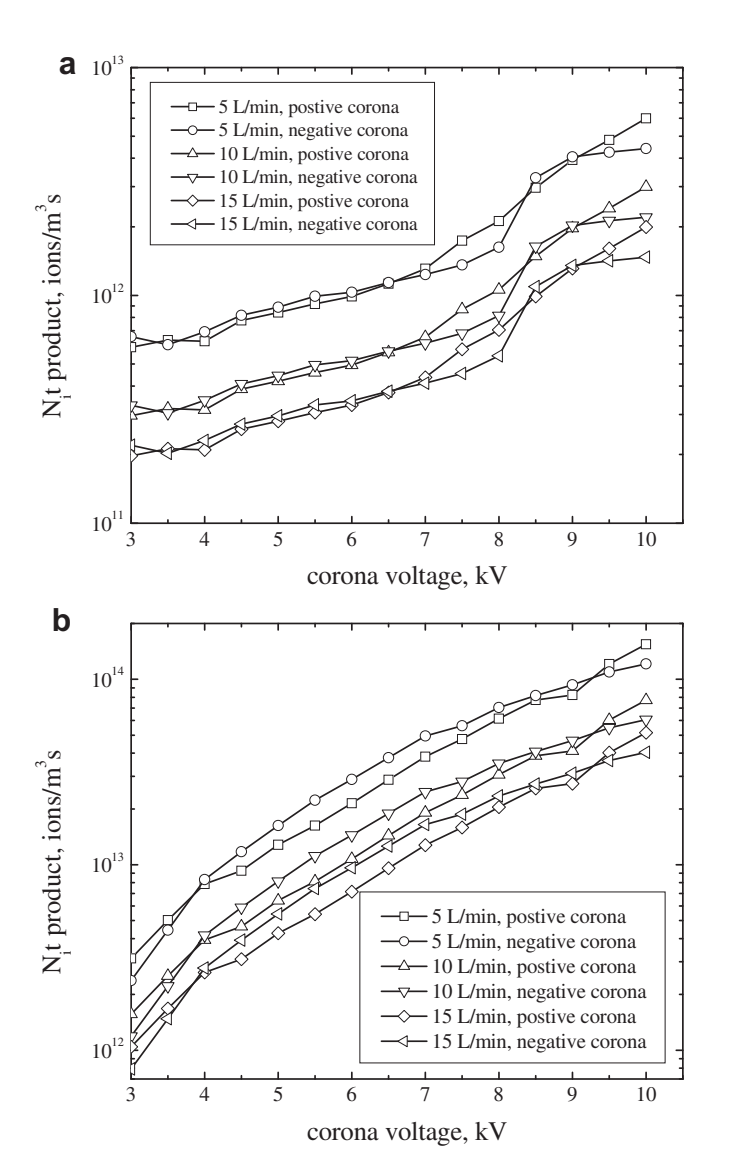


Fig. 6. Variations in ion penetration with corona voltage in the charger at different iondriving voltages.

perforated screen cylinder. The onset voltage in the charging zone of both positive and negative coronas for the ion-driving voltage of 310 V was also about 3.5 kV at currents of 2.87  $\times$   $10^{-8}$  and 3.98  $\times$   $10^{-8}$  A, respectively. In general the operating corona-wire voltage of the charger was in the range of 3.5–10 kV.

Variations in ion number concentrations with corona voltage in the discharge and charging zones of the charger are shown in Fig. 5. The ion number concentration in both zones increased with increasing corona voltage. As shown in Fig. 5 (a), the ion number concentration in the discharge zone was in the range of  $4.40 \times 10^{11}$ to  $1.82 \times 10^{15} \text{ ions/m}^3$  and  $2.80 \times 10^{11} \text{ to } 2.52 \times 10^{15} \text{ ions/m}^3$  for positive and negative coronas, respectively. The number concentration of the negative ions was generally larger than that of the positive ions, and well above the corona onset. In addition, Fig. 5 (b) shows the variation in ion number concentration with corona voltage in the charging zone of the charger at different ion-driving voltages. At 0 V ion-driving voltage, the ion number concentrations in the charging zone were in the range of 7.71  $\times$  10<sup>11</sup> to  $1.17 \times 10^{13}$  ions/m<sup>3</sup> and  $6.25 \times 10^{11}$  to  $8.66 \times 10^{12}$  ions/m<sup>3</sup> for positive and negative coronas, respectively. At 310 V ion-driving voltage, the ion number concentrations in the charging zone were in the range of



**Fig. 7.** Variations in  $N_i t$  product with corona voltage in the charging zone of the charger at different aerosol flow rates (a) 0 V and (b) 310 V.

 $2.01 \times 10^{12}$  to  $3.03 \times 10^{14}$  ions/m³ and  $1.95 \times 10^{12}$  to  $2.38 \times 10^{14}$  ions/m³ for positive and negative coronas, respectively. The ion number concentrations in the discharge zone were larger than the charging currents for positive and negative coronas. These were 197 and 32 times and 645 and 99 times respectively for ion-driving voltages of 0 and 310 V. More ions were lost electrostatically on the perforated screen openings of the inner cylinder of the charger.

Fig. 6 shows the ion penetration through the screen openings of the inner cylinder to the charging zone at different screen voltages. The ion penetration depended on the ion-driving voltage only within a narrow applied voltage interval. For larger ion-driving voltages, ion penetration became practically constant and independent of the ion-driving voltage. The average ion penetrations for

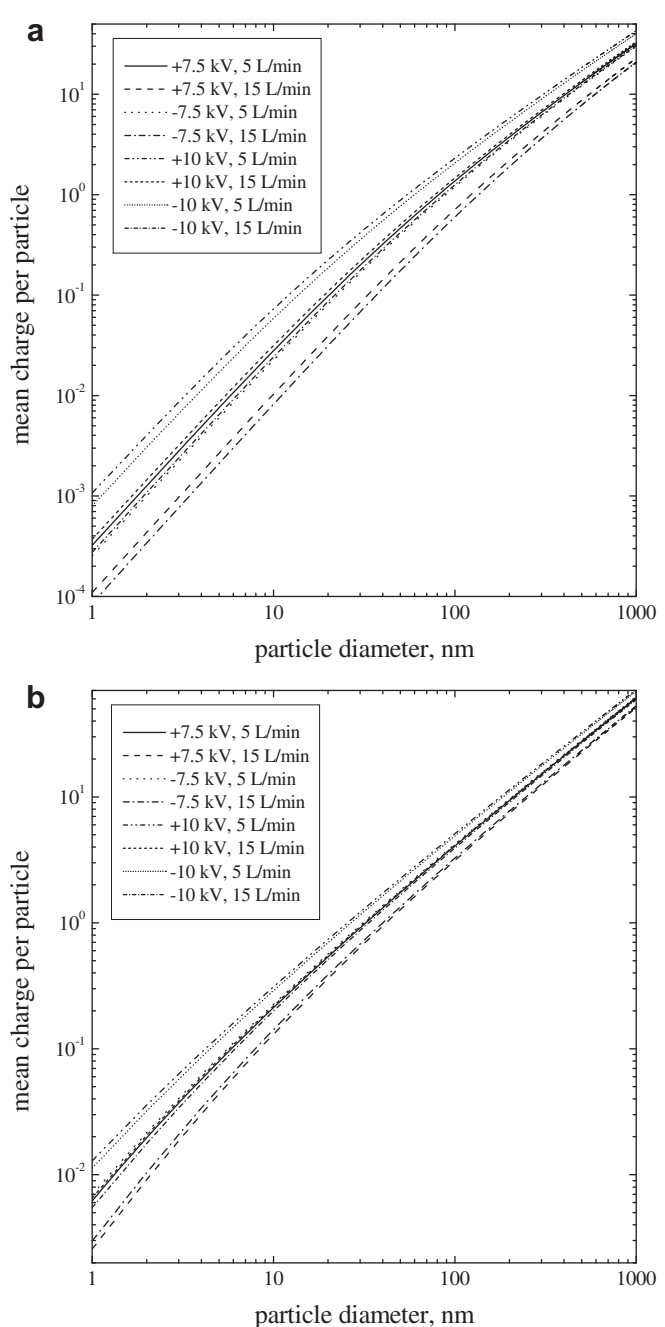


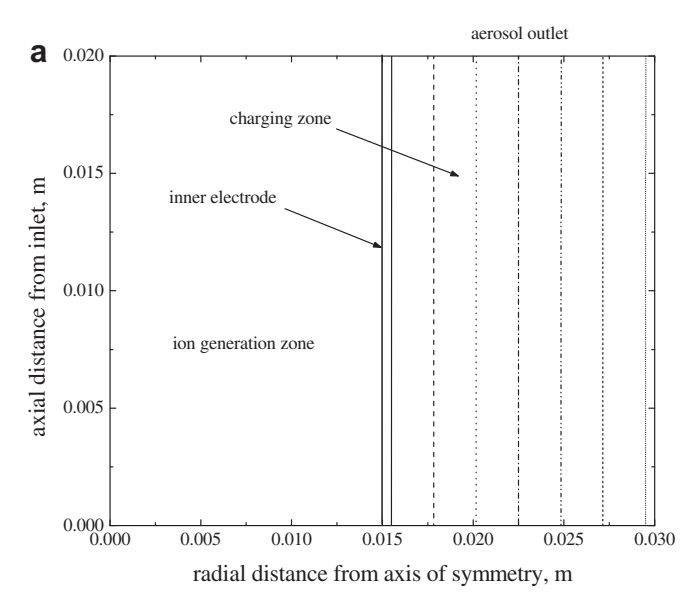
Fig. 8. Variation of mean charge per particle with particle diameter at different aerosol flow rate and applied voltage (a) 0 V and (b) 310 V.

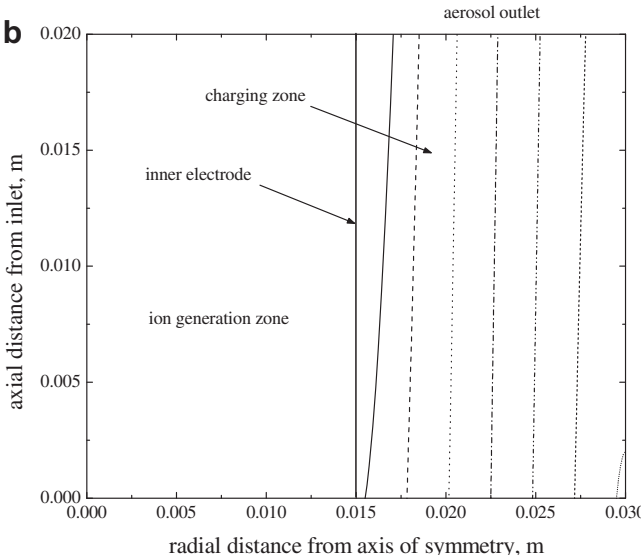
positive and negative coronas were 0.64 and 0.19% and 3.62 and 1.93% for the ion-driving voltages of 0 V and 310 V, respectively.

Fig. 7 shows the variations in the  $n_i t$  products with corona voltages in the charging zone of the charger at aerosol flow rates of 5, 10 and 15 L/min and ion-driving voltages from 0 to 10 kV. The higher flow rate, also the shorter residence time, gave rise to a lower  $n_i t$  product. An increase in corona voltage produced a monotonic increase in the ion concentration and also the  $n_i t$  product.

Fig. 8 shows the variation of the mean charge per particle with particle diameter from 1 nm to 1  $\mu m$  at different aerosol flow rates, applied voltages and ion-driving voltages. The mean charge per particle increased monotonically with particle diameter. Longer residence time (low aerosol flow rate) and higher corona voltage resulted in an increase in the mean charge per particle within the charger.

Fig. 9 shows the charged particle trajectories in the charging zone of the charger, starting from different initial locations. The governing Equation (11) of the particle trajectory was used in the





**Fig. 9.** Variation of charged particle trajectories along the charger length with inlet radial distance (7.5 kV corona-wire voltage, 10 nm particle diameter, and 5 L/min total flow rate), (a) 0 V and (b) 310 V.

calculations. The particle diameter was 10 nm, while the coronawire voltage and aerosol flow rate were 7.5 kV, and 5 L/min, respectively. Sets of seven different trajectories were plotted depending on the radial inlet distances of the charged particles in the charger. At a 0 V ion-driving voltage, all charged particles passed through the charging zone without deposition onto the outer cylinder. At an ion-driving voltage of 310 V, one of the trajectories migrated toward the outer cylinder and deposited, while the other six trajectories passed through the charger without deposition. It should be noted that the charged particle deposition onto the outer cylinder due to the effect of the electrostatic field was 14%.

#### 4. Conclusion

A cylindrical triode charger for unipolar diffusion aerosol charging was designed, constructed, and experimentally studied. The corona discharge characteristics of a triode type corona aerosol charger were determined by a semi-empirical method based on discharge current measurement and electric charging theory. Current-voltage characteristics were determined as were ion number concentration,  $n_i t$  product, and mean charge per particle with particle diameter. The discharge and charging currents and ion number concentration in the charging zone of the charger increased monotonically with corona voltage. The negative corona had a higher current than the positive corona. At the same corona voltage, the ion number concentration in the discharge zone was larger than the charging current for positive and negative coronas by 197 and 32 times and 645 and 99 times for the ion-driving voltage of 0 and 310 V, respectively. The average ion penetrations for positive and negative coronas were 0.64 and 0.19% and 3.62 and 1.93% for the ion-driving voltage of 0 V and 310 V, respectively. Higher flow rate, shorter residence time, gave a lower Nit product. By calculation about 14% of charged particles of 10 nm in diameter were lost onto the outer cylinder due to the electrostatic field effect.

This simple charger proved to be particularly useful in charging aerosol particles in electrical aerosol instruments for measuring aerosol size distribution. It performed as well as other unipolar chargers of more complex and costlier design. Its overall dimensions and weight made it easy to handle and move around. The advantages of the charger are:

- It does not use a sheath of air flow along the walls or the perforated screen opening.
- It has low diffusion and space charge losses because the charging zone consists of a short column.
- It is a low complexity and inexpensive system.

## Acknowledgements

This work was supported by the Thailand Research Fund (TRF), contract no. MRG5480001. The author wishes to thank Assoc. Prof. Dr. Nakorn Tippayawong, Department of Mechanical Engineering, Chiang Mai University and Dr. Rainer Zawadzki, Institute of Research and Development, Rajamangala University of Technology Lanna for the valuable contribution during the preparation of this article.

#### References

- P. Intra, N. Tippayawong, Progress in unipolar corona discharger designs for airborne particle charging: a literature review, Journal of Electrostatics 67 (2009) 605–615.
- [2] P. Intra, N. Tippayawong, An overview of unipolar charger developments for nanoparticle charging, Aerosol and Air Quality Research 11 (2011) 186–208.

- [3] M. Alonso, F.J. Alguacil, Particle size distribution modification during and after electrical charging: comparison between a corona ionizer and a radioactive neutralizer, Aerosol and Air Quality Research 8 (2008) 366-380.
- [4] C.L. Chien, C.J. Tsai, H.L. Chen, G.Y. Lin, J.S. Wu, Modeling and validation of nanoparticle charging efficiency of a single-wire corona unipolar charger, Aerosol Science and Technology 45 (2011) 1468–1479.
- [5] G.Y. Lin, C.J. Tsai, Numerical modeling of nanoparticle collection efficiency of single-stage wire-in-plate electrostatic precipitators, Aerosol Science and Technology 44 (2010) 1122–1130.
- [6] A. Aliat, C.J. Tsai, C.T. Hung, J.S. Wu, Effect of free electrons on nanoparticle charging in a negative direct current corona charger, Applied Physics Letters 93 (2008) 154103-154103-3.
- [7] A. Aliat, C.T. Hung, C.J. Tsai, J.S. Wu, Implementation of Fuchs' model of ion diffusion charging of nanoparticles considering the electron contribution in dc-corona chargers in high charge densities, Journal of Physics D: Applied Physics 42 (2009) 125206.
- [8] G.W. Hewitt, The charging of small particles for electrostatic precipitation, AIEE Transactions 76 (1957) 300–306.
- [9] B.Y.H. Liu, D.Y.H. Pui, On the performance of the electrical aerosol analyzer, Journal of Aerosol Science 6 (1975) 249–264.

- [10] P. Buscher, A. Schmidt-Ott, A. Wiedensohler, Performance of a unipolar "Square Wave" diffusion charger with variable nt-product, Journal of Aerosol Science 25 (1994) 651–663.
- [11] Y.J. Lee, H.T. Kim, K.W. Lee, Development of monitoring technology for airborne particulate matter, Environmental Monitoring and Assessment 70 (2011) 3–20.
- [12] G. Biskos, K. Reavell, N. Collings, Electrostatic characterization of corona-wire aerosol charges, Journal of Electrostatics 63 (2005) 69–82.
- [13] G.P. Reischl, J.M. Makela, R. Harch, J. Necid, Bipolar charging of ultrafine particles in the size range below 10 nm, Journal of Aerosol Science 27 (1996) 931–949.
- [14] W.C. Hinds, Aerosol Technology, John Wiley & Sons, New York, 1999.
- [15] P. Intra, N. Tippayawing, Effect of needle cone angle and air flow rate on electrostatic discharge characteristics of a corona-needle ionizer, Journal of Electrostatics 68 (2010) 254–260.
- [16] P. Intra, N. Tippayawing, Use of electrostatic precipitation for excess ion trapping in an electrical aerosol detector, Journal of Electrostatics 69 (2011) 320–327.
- [17] A. Wiedensohler, P. Buscher, H.-C. Hansson, B.G. Martinsson, F. Stratmann, G. Ferron, B. Busch, A novel unipolar charger for ultrafine aerosol particles with minimal particle losses, Journal of Aerosol Science 25 (1994) 639–649.
- [18] F.E. Kruis, H. Fissan, Nanoparticle charging in a twin Hewitt charger, Journal of Nanoparticle Research 3 (2001) 39–50.

## ภาคผนวก ข-6

Intra, P. and Tippayawong, N., "Use of electrostatic precipitation for excess ion trapping in an electrical aerosol detector", Journal of Electrostatics, Vol. 69, No. 4, pp. 320 – 327, 2011. มี impact factor = 1.08



Contents lists available at ScienceDirect

## Journal of Electrostatics

journal homepage: www.elsevier.com/locate/elstat



# Use of electrostatic precipitation for excess ion trapping in an electrical aerosol detector

Panich Intra a,\*, Nakorn Tippayawong b

<sup>a</sup> College of Integrated Science and Technology, Rajamangala University of Technology Lanna, Chiang Mai 50300, Thailand

#### ARTICLE INFO

Article history: Received 17 August 2010 Received in revised form 28 March 2011 Accepted 14 April 2011 Available online 4 May 2011

Keywords:
Ion trap
Electrostatic precipitator
Electrical aerosol
Collection efficiency

#### ABSTRACT

In this paper, the technique of electrostatic precipitation was used to remove excess ions from a mixture with charged particles before collection on a filter in a Faraday cup electrometer of an electrical aerosol detector. The ion precipitator part of the detector was designed, constructed, and evaluated. An analytical model was developed to investigate ion and particle transports due to diffusion and space charge effects inside the ion precipitator. Experimental investigations were carried out for positive ions, the positively applied voltage at the wire electrode ranged from 10 to 150 V, ion flow rates ranged from 5 to 15 L/min, and the radial distance of the inlet was 0.15 and 14 mm at a fixed separation between the wire and outer electrodes. The calculation results showed that all charged particles of 10 nm in diameter could pass through the ion precipitator smoothly without precipitation at the outer electrode. For all ion flow rates, an increase in ion trap voltage produced an increase in ion collection efficiency of the precipitator. Experiments confirmed that the efficiency of the ion precipitator could increase to 99% at an ion trap voltage larger than 100 V for all ion flow rates.

© 2011 Elsevier B.V. All rights reserved.

### 1. Introduction

Fine aerosols are airborne particles of diameters in the size range of submicron to nanometer. To understand and control fine aerosol dynamics, measurement and characterization are important. Electrical aerosol measurements [1] are the most efficient and widely used techniques to measure or detect these submicron airborne particles, and the instrument widely used is an electrical aerosol detector (EAD). A typical EAD consists of two key components: one for aerosol charging, and the other for measuring the current or charged aerosols with a Faraday cup electrometer. The basis of the EAD is charging the aerosol in which a known net charge distribution is imposed on to the particles. Readout of the EAD depends on the charging technique used. High ion concentrations are usually generated to ensure high charging efficiency. An aerosol charger is always positioned upstream of the EAD and an ion trap removes the excess ions. Prior to collection on the filter in the Faraday cup electrometer of the EAD [2], the ion trap removes the excess free ions mixing with the charged particles. This prevents contamination of the signal current to be measured by free ions potentially reaching the Faraday cup electrometer.

Electrostatic precipitators (ESP) are widely used for removing particles from gas streams in various industrial processes and room air-conditioning systems [3–5]. Typically, it consists of a discharge electrode placed along the axis of the collecting electrode. A high DC voltage is applied to the discharge electrode, while the collecting electrode is grounded. This produces an electric field and causes flow of electric charges or ions from discharge electrode to the collecting electrode. A dirty gas containing particulate pollutants is introduced into the ESP. The particulates get charged by bombardment with unipolar ions from the discharge electrode, the electrostatic force drives them toward the collecting electrode where they deposit on its inner surface. The outgoing gas flow becomes particle-free.

Although ESPs were initially designed to precipitate particles, under certain conditions they are also used for depositing ions; ions, just like the charged particles, carry charges, and can be precipitated with an electrical field. The key to adapting an ESP into an ion precipitator lies in applying the proper voltage to the ESP, allowing only ions to precipitate while charged particles pass through.

Although there have been numerous studies and developments on the wire-cylinder-type ESP related to the particle charger in a number of electrical mobility determining instruments [6], to our knowledge, the design and performance evaluation of the ion trap has received little attention in the literature [7–11]. In the present

<sup>&</sup>lt;sup>b</sup> Department of Mechanical Engineering, Faculty of Engineering, Chiang Mai University, Chiang Mai 50200, Thailand

<sup>\*</sup> Corresponding author. Tel.: +66 086 919 3185. E-mail address: panich\_intra@yahoo.com (P. Intra).

study, a simple and efficient electrostatic precipitator was developed as an ion trap for the EAD. Analytical investigation of the design predicted the ion and particle transports due to diffusion and the space charge effects inside the ion precipitator. The ion precipitator performed experimentally for positive ions, with a positively applied voltage at the wire electrode between 10 and 150 V, a total flow rate of 5–15 L/min, an operating pressure of 1 atm, and a radial distance of the inlet between 0.15 and 14 mm at a fixed separation between wire and outer electrodes. This paper also presents a detailed description of the design of an ion precipitator.

#### 2. Materials and methods

#### 2.1. Description of the ion precipitator

A schematic diagram of the ion precipitator used in this study is shown in Fig. 1. Its geometrical configuration was similar to the unipolar corona-wire charger and the wire-cylinder ESP, and consists of a coaxial wire electrode placed along the axis of a metallic cylindrical tube. The outer electrode, an aluminum tube, was 28 mm in diameter and 15 mm in length. The wire electrode a stainless steel wire was 300  $\mu m$  in diameter and 15 mm in length. The DC voltage supply applied to the wire electrode, typically was in the range between 10 and 150 V, while the outer metallic electrode was grounded. Most importantly for the operation of the ion precipitator, was setting a proper voltage ensuring that all ions can be removed, but most of the charged particles were not affected.

#### 2.2. Experimental setup

The schematic diagram evaluating the performance of the experimental system for is shown in Fig. 2. It consists of an ion generator, a DC high voltage power supply, a Faraday cup, an electrometer, and a flow system. In this study, a high concentration of ions was generated by corona discharge with the corona-needle generator [12], approximately  $10^{13}$  ions/m³. In our experiments, the ion precipitator is connected directly to the ion generator outlet via a very short connecting pipe. The airflow, typically in the range between 5 and 15 L/min, was regulated and controlled by means of

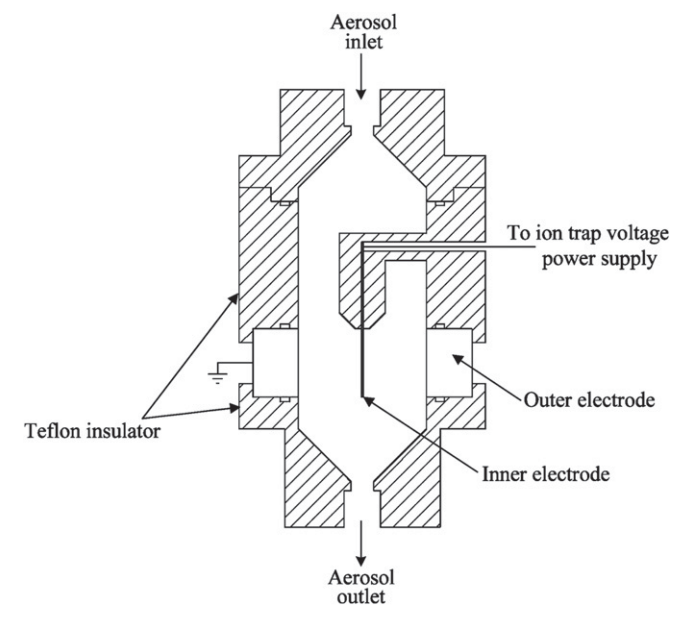


Fig. 1. Schematic diagram of the ion precipitator.

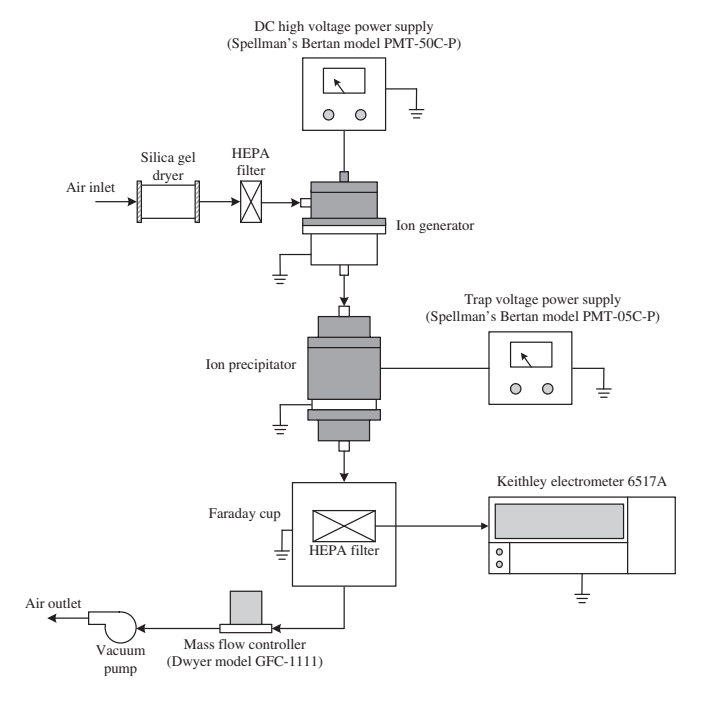


Fig. 2. Experimental setup for evaluating the performance of the ion precipitator.

a mass flow meter and controller (Dwyer model GFC-1111) with a vacuum pump, located at the end of the experimental equipment train. Any remaining water was removed from an air sample using a silica gel drying tube. Dried air samples were filtered through a high efficiency particulate-free air (HEPA) filter (Pall HEPA capsule model 12144 with filtration efficiency of 99.97% and retention of 0.3 µm for air/gas) and were then drawn into the generator. An adjustable commercial DC high voltage power supply, Bertan model PMT-50C-P, was used to maintain the positive corona voltage difference in the generator, generally 3.5 kV. The ions produced inside the generator then entered the ion precipitator. A second adjustable commercial DC high voltage power supply, Bertan model PMT-05C-P, was used to maintain the positive trap voltages difference in the precipitator, generally in the range between 10 and 150 V. After the precipitator, the air sample with ions entered the Faraday cup, where the ions were removed by the filter and the resulting ion current flow was measured with electrometer, Keithley 6517A. It should be noted that the ion current corresponded to the ion concentration at the generator outlet. The ion current measurements were translated into concentrations given the total airflow rate through the generator. Thus, the total concentration of the ion at the generator outlet,  $N_i$ , can be calculated from the expression [12]

$$N_i = \frac{I_i}{e\Omega} \tag{1}$$

where  $I_i$  is the ion current at the generator outlet and  $Q_i$  is the volume flow rate of ions.

## 3. Modeling the transport of ion and particle

#### 3.1. Transport of non-diffusing ion and particle

Transporting ions and charged particles inside an ESP and differential mobility analyzer has been studied and presented in the published literature [11,13–16]. As shown in Fig. 3, the fluid velocity profile in the axial flow influences the axial motion of the ion. The radial motion of the ion is due to the electrical force, by far greater

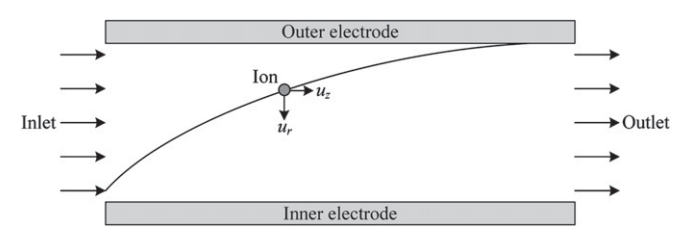


Fig. 3. Ion transport in the precipitator.

than other forces. When ions are introduced into the ion precipitator, any ions under the influence of the electric field will have an electrical mobility. The flow and electric fields were assumed to be axisymmetric and steady. The flow in the precipitator was laminar, fully developed and incompressible. The space charge and Brownian diffusion effects were negligible. It should be also noted that the drag force is important for high Reynolds number or large particles, but for particles smaller than 1.0  $\mu$ m, the drag force is negligible [17]. In this study, the effect of the drag on the trajectory of the ion or particles was not significant and was neglected because the diameters are in the nanometer range.

For the particular case of annular geometries where the ions enter the precipitator on an axial flow and the ions migrate along the radial direction of the electrical field, motion of the ions within the precipitator can be described by a system of differential equations as [13]

$$\frac{\mathrm{d}r}{\mathrm{d}t} = u_r + ZE_r \tag{2}$$

$$\frac{\mathrm{d}z}{\mathrm{d}t} = u_z + ZE_z \tag{3}$$

where r and z are the radial and axial dimensions of the classifier,  $u_r$  and  $u_z$  are the radial and axial components of the air flow velocity. Similarly,  $E_r$  and  $E_z$  are the radial and axial components of the electric field and Z is the electrical mobility of ions or particles. When a uniform electric field is established between the two electrodes of the precipitator, the electric field components are given by the following relations:  $E_r = V/r\ln(R)$  and  $E_z \approx 0$  where V is the applied voltage,  $R = r_2/r_1$ ,  $r_1$  and  $r_2$  are the radii of the wire and outer electrodes. Assuming that the radial velocity component for a laminar annular flow is zero ( $u_r = 0$ ) and combining the above equations, the ions trajectories can be described by

$$\frac{\mathrm{d}r}{\mathrm{d}t} = \frac{ZV}{r\ln(R)} \tag{4}$$

$$\frac{\mathrm{d}z}{\mathrm{d}t} = u_z(r) \tag{5}$$

Using Equations (4) and (5), the trajectory of the ions is given by

$$\frac{\mathrm{d}r}{\mathrm{d}z} = \frac{ZV}{ru_z(r)\ln(R)}\tag{6}$$

where:

$$u_{z}(r) = ar^{2} + b\ln(r) + c \tag{7}$$

$$a = \frac{1}{4\mu} \frac{\mathrm{d}p}{\mathrm{d}z} \tag{8}$$

$$b = -\frac{1}{4\mu} \frac{\mathrm{d}p}{\mathrm{d}z} \left( \frac{r_2^2 - r_1^2}{\ln(R)} \right) \tag{9}$$

$$c = \frac{1}{4\mu} \frac{\mathrm{d}p}{\mathrm{d}z} \left( \frac{r_2^2 - r_1^2}{\ln(R)} \ln(r_1) - r_1^2 \right) \tag{10}$$

 $\mathrm{d}p/\mathrm{d}z$  denotes the constant pressure gradient and is given by the following equation

$$\frac{\mathrm{d}p}{\mathrm{d}z} = -\frac{\rho \overline{u}^2 f}{2D_h} \tag{11}$$

where

$$D_h = 2r_2(1-(\kappa)) \tag{12}$$

$$f = \frac{64}{\text{Re}} \left( \frac{1 + (\kappa)^2}{(1 - (\kappa))^2} + \frac{1 + (\kappa)}{(1 - (\kappa))\ln(\kappa)} \right)^{-1}$$
 (13)

$$Re = \frac{2r_2(1 - (\kappa))\overline{u}\rho}{\mu} \tag{14}$$

 $D_h$  is the hydraulic diameter for an annular flow area, f is the friction factor,  $\overline{u}$  is the mean axial flow velocity,  $\kappa = r_1/r_2$ ,  $\rho$  is the gas density and Re is the Reynolds number in the annular flow. Substituting Equation (7) into Equation (6) and Integrating Equation (6), the migration paths of the ions can be determined as

$$\int_{r_{in}}^{r_2} ar^3 + b \ln(r^2) + cr dr = \int_{0}^{z} \frac{VZ}{\ln(R)} dz$$
 (15)

where  $r_{in}$  is the radial position at which the ions enter the precipitator. Therefore, the ions entering the precipitator at a radial position of  $r_{in}$  have trajectories taking them to an axial position of z, which can be obtained as

$$z = -\frac{g(r_{in})\ln(R)}{4VZ} \tag{16}$$

where:

$$g(r_{in}) = \begin{pmatrix} ar_2^4 - ar_{in}^4 + br_{in}^2 - br_2^2 + 2br_2^2 \ln(r_2) \\ -2br_{in}^2 \ln(r_{in}) + 2cr_2^2 - 2cr_{in}^2 \end{pmatrix}$$
(17)

## 3.2. Transport of diffusing ions and particles

Ions and ultrafine particles (those with diameter below about 20 nm) undergo a strong Brownian motion in the ion precipitator. Thus, the diffusive particle trajectory can be expressed as [17]

$$r = \sqrt{r_{in}^2 + \frac{2VZ}{\overline{u}\ln(R)}} z \pm \sqrt{\frac{2D}{\overline{u}}} z$$
 (18)

where *D*, the diffusion coefficient of ions, is a function of the electrical mobility of the ions and particles, *D*, by the Stokes—Einstein equation:

$$D = \frac{kTZ}{ne} \tag{19}$$

where k is Boltzmann's constant, T is the absolute temperature, n is the number of elementary charges of the ion (n=1 for the type of ions commonly found in the precipitator), and e is the charge of the electron ( $1.6 \times 10^{-19}$  C). In Equation 18, the plus sign indicates the upper limit of the diffusive particle trajectory; the minus sign indicates the lower limit of the diffusive particle trajectory. Ion electrical mobility is a complicated function of the gas density,

**Table 1**Parameter and operating condition values of the model.

Parameter and operating conditions	Values
Diameter of wire electrode, $r_1$ (mm)	0.15
Diameter of outer electrode, $r_2$ (mm)	14
Length of precipitator, $z$ (mm)	15
Wire electrode voltage, V (V)	10, 50, 100, 150
Total flow rate, (L/min)	5, 10, 15
Nature of flow	Laminar
Operating temperature, $T(K)$	294
Operating pressure, P (atm)	1
Gas density, (kg/m³)	1.225
Gas viscosity, μ (kg/m/s)	$1.7894 \times 10^{-5}$
Polarity of ions	Positive
Electrical mobility of ion, $Z_i$ (m <sup>2</sup> /V/s)	$1.425 \times 10^{-4}$
Particle diameter, $d_p$ (nm)	10

electric field strength, and the constituent species of the gas. Based on the work of Reischl et al. [18], the average value for the positive ion electrical mobility at atmospheric pressure was  $Z=1.425\times 10^{-4}~\text{m}^2/\text{V}$  s. Typically, ions and charged particles have different electrical mobility in magnitude, with the electrical mobility of ions in general much higher than that of particles.

## 3.3. Effect of the space charge

When the ion and particle number concentrations are sufficiently high, the space charge field cannot be neglected. The particle trajectory due this effect is given by [19]

$$r = \sqrt{r_{in}^2 + \frac{2Z}{\overline{u}} \left( \frac{eN_0}{2\epsilon_0} r_{in}^2 - \frac{V}{\ln(R)} \right) z \left( 1 + \frac{eZN_0}{2\overline{u}\epsilon_0} z \right)}$$
 (20)

where  $N_0$  is the concentration of ions or particles at the staring point of the trajectory,  $\epsilon_0$  is dielectric constant of the medium, taken to be equal to that in a vacuum (8.854  $\times$  10<sup>-12</sup> F/m).

#### 3.4. Efficiency of ion trapping

The removal or trapping efficiency,  $\eta$ , is defined as the ratio of the difference between inlet and outlet concentrations to the inlet concentration, and is given by

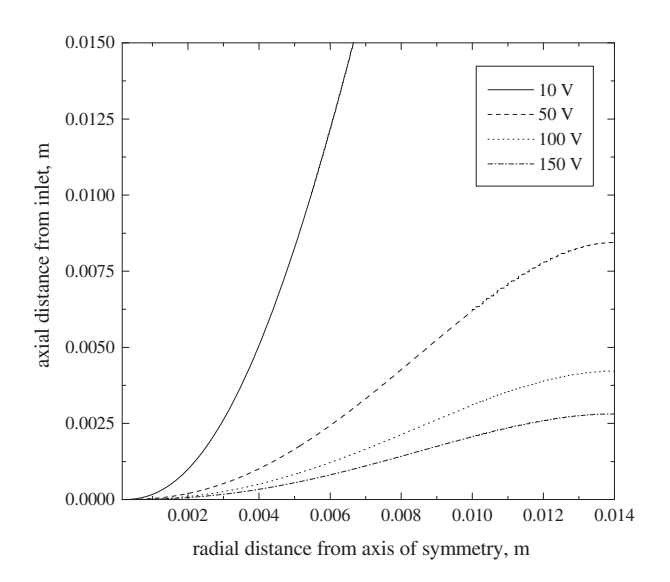
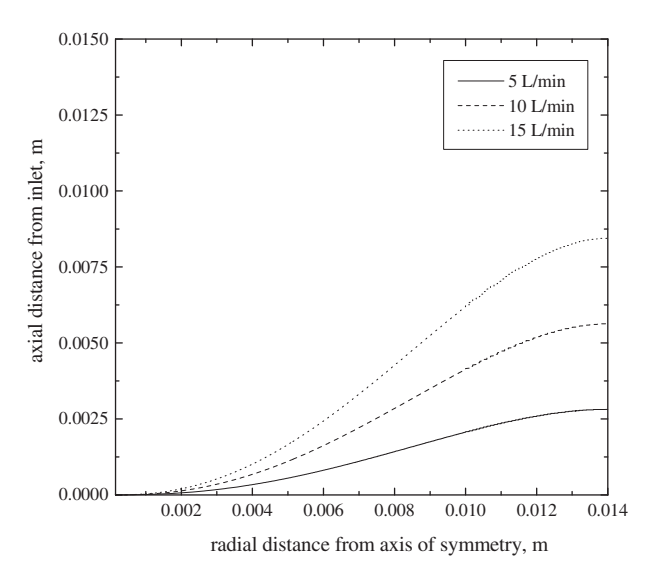


Fig. 4. Variation of ion trajectories along the precipitator length with wire electrode voltage (5 L/min ion flow rate).



**Fig. 5.** Variation of ion trajectories along the precipitator length with total flow rate (150 V ion trap voltage).

$$\eta = 1 - \frac{N_{\text{outlet}}}{N_{\text{inter}}} \tag{21}$$

where  $N_{outlet}$  and  $N_{inlet}$  are concentration of ions at the outlet and inlet.

#### 4. Results and discussion

### 4.1. Transport of ions

An analytical model was developed to investigate the transport of the ions inside the ion precipitator to give a better understanding of its the operation. The calculations were performed for positive ions and charged particles. These calculations were done at positively applied voltages at the wire electrode varying from 10 to 150 V, at a total air flow rate between 5 and 15 L/min, and a radial distance of the inlet between 0.15 and 14 mm at a fixed radial of wire and outer

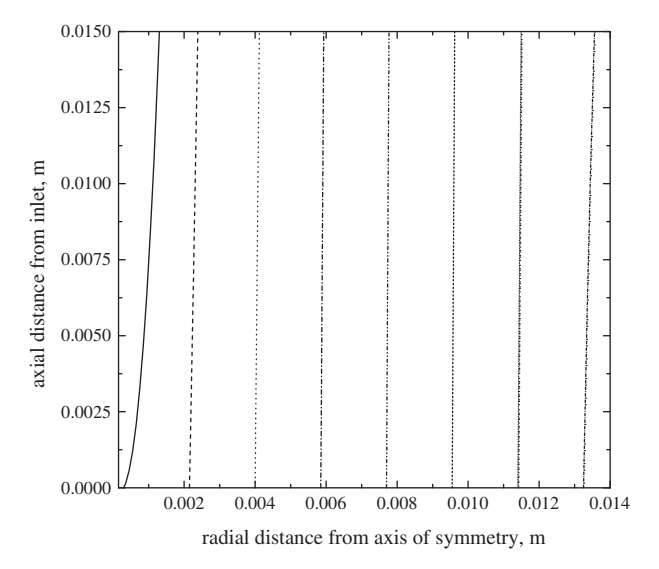


**Fig. 6.** Variation of charged particle trajectories along the precipitator length with inlet radial distance (100 V ion trap voltage, 10 nm particle diameter, and 5 L/min total flow rate).

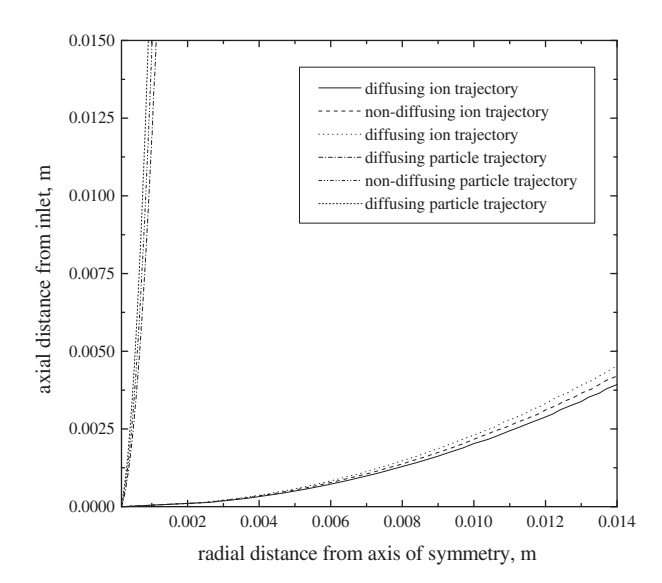


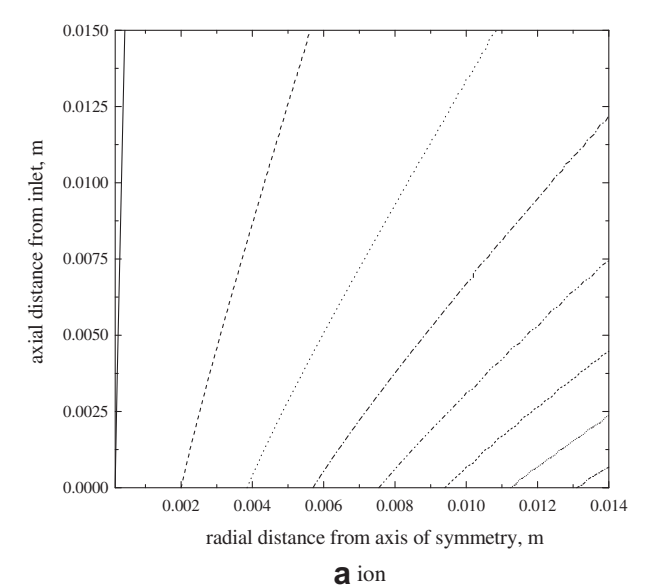
**Fig. 7.** Effect of Brownian diffusion on the ion and particle trajectories in the ion precipitator (100 V ion trap voltage, 10 nm particle diameter, and 5 L/min total flow rate).

electrodes distance of  $r_1$  = 0.15 mm and  $r_2$  = 14 mm. Air density and viscosity were 1.225 kg/m<sup>3</sup> and 1.7894  $\times$  10<sup>-5</sup> kg/m/s. Operating temperature and pressure were 294 K and 1 atm, respectively. Table 1 shows the parameters and operating conditions.

As stated above, the flow conditions inside the ion precipitator were assumed to be steady, incompressible and laminar. The electric field distribution inside the ion precipitator was also assumed to be uniform in the axial direction. The ion and particle trajectories were calculated using Equations (16) and (17) with Microsoft Visual Basic programming. The calculated ion trajectories along the precipitator were compared between the existing models and the present model. The ion trajectory of the present model agreed very well with that proposed by Hagwood et al. [14] and Williams [15]. However, large differences between this model and the models developed by Kulon et al. [16] and Wei [11] were observed. Kulon and Wei models did not take into account the constant pressure gradient effect on the annular flow velocity profile, which could result in significant errors. Fig. 4 shows a number of trajectories of the positive ions as a function of wire electrode voltage. The ions were deflected radially toward the inner surface of the outer electrode of the precipitator. It was found that higher applied wire electrode voltage caused ions to deposit closer to the entrance. This was expected since the applied electrical force mainly influenced the motion of ions. Increasing the applied voltage increased the efficiency of collected ions. Within the range considered, it was clear that the suitable wire electrode voltage was 100 V. For a wire electrode voltage of 150 V or higher, particle loss by deposition onto the precipitator electrode was significant.

After the suitable voltage for the wire electrode was found, the suitable total flow rate through the precipitator was determined. Fig. 5 shows the variation of the ion trajectories along the precipitator with total flow rate: Faster flow rate forced ions to impact the wall further downstream.

It was still necessary to prove that the chosen voltage had a minimum influence on the charged particles. Calculating particle trajectories within the ion precipitator at the same voltage did this. In the calculations, the particle governing equation was identical to ion governing Equation (16) with the exception of the ion electrical mobility Z being replaced by the particle electrical mobility  $Z_p$ . The electrical mobility of particle was calculated as:



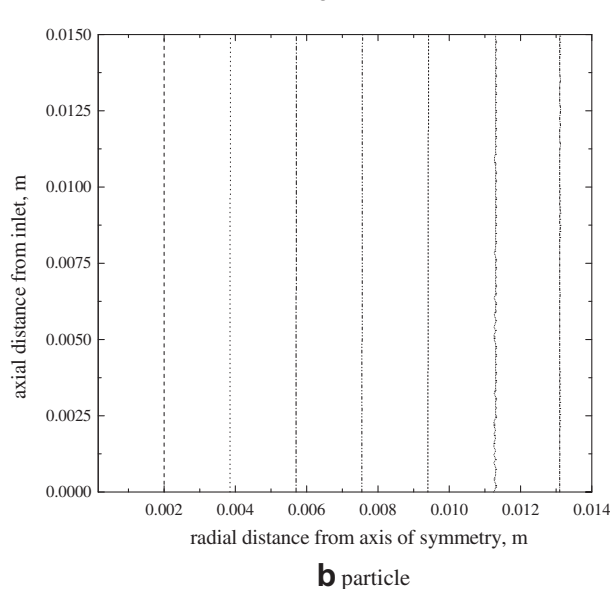


**Fig. 8.** Effect of space charge on the ion and particle trajectories in the ion precipitator (0 V ion trap voltage, 10 nm particle diameter, and 5 L/min total flow rate).

$$Z_p = \frac{n_p e C_c}{3\pi \mu d_p} \tag{22}$$

where  $n_p$  is the net number of elementary charges on the particle, e is the value of elementary charge on an electron,  $C_c$  is the Cunningham slip correction factor,  $\mu$  is the gas viscosity, and  $d_p$  is the particle diameter. The particle tended to have the largest electrical mobility in the extreme case in which the diameter of 10 nm (the lower limit of particle size in the EAD) and a single charge was considered. Fig. 6 illustrates the charged particle trajectories within the ion precipitator, starting from different initial locations. It was shown that all charged particles can pass through the ion precipitator smoothly without deposition onto the precipitator electrode.

The Brownian diffusion effect on the ion and particle trajectories in the ion precipitator is shown in Fig. 7. The particle diameter was 10 nm, while the ion trap voltage and ion flow rate were set at 100 V, and 5 L/min, respectively. The central lines showed the non-diffusing trajectories, while lines on either side of the central ones indicated the diffusion trajectories. Brownian diffusion motion

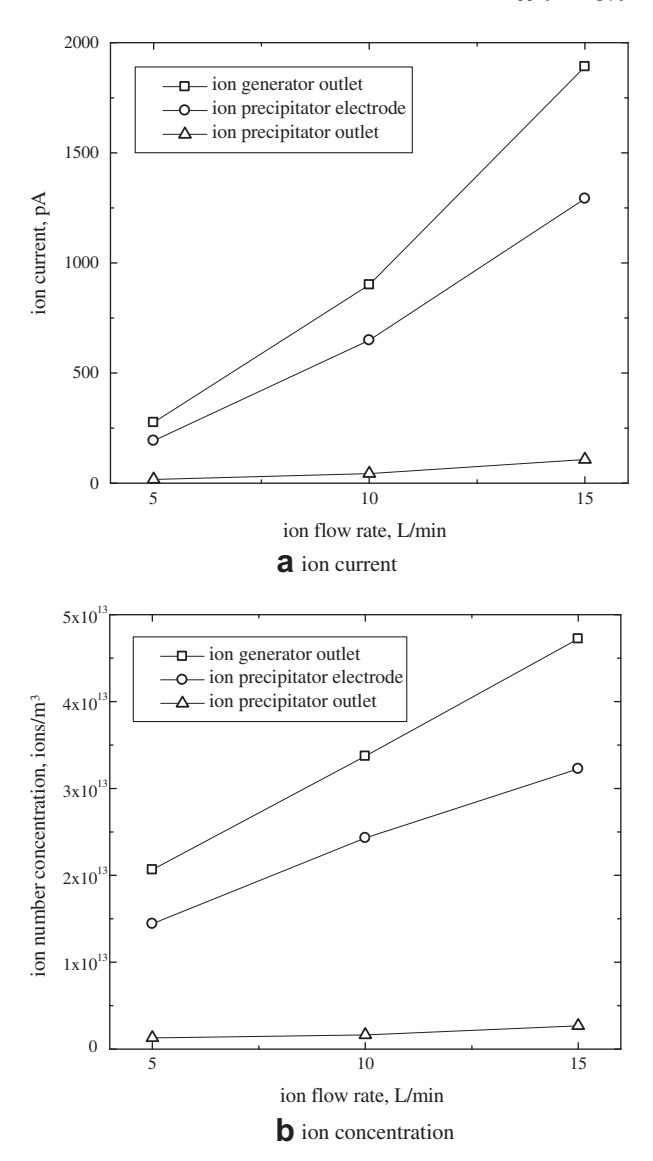


Fig. 9. Signal current and concentration of ions as a function of ion flow rate.

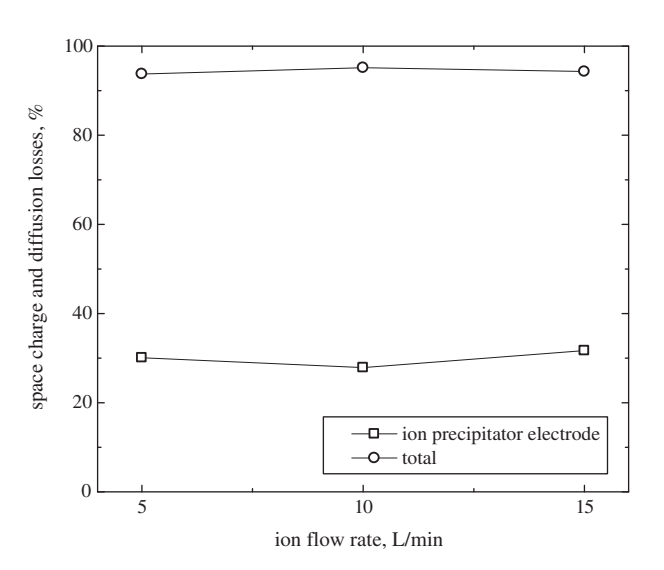
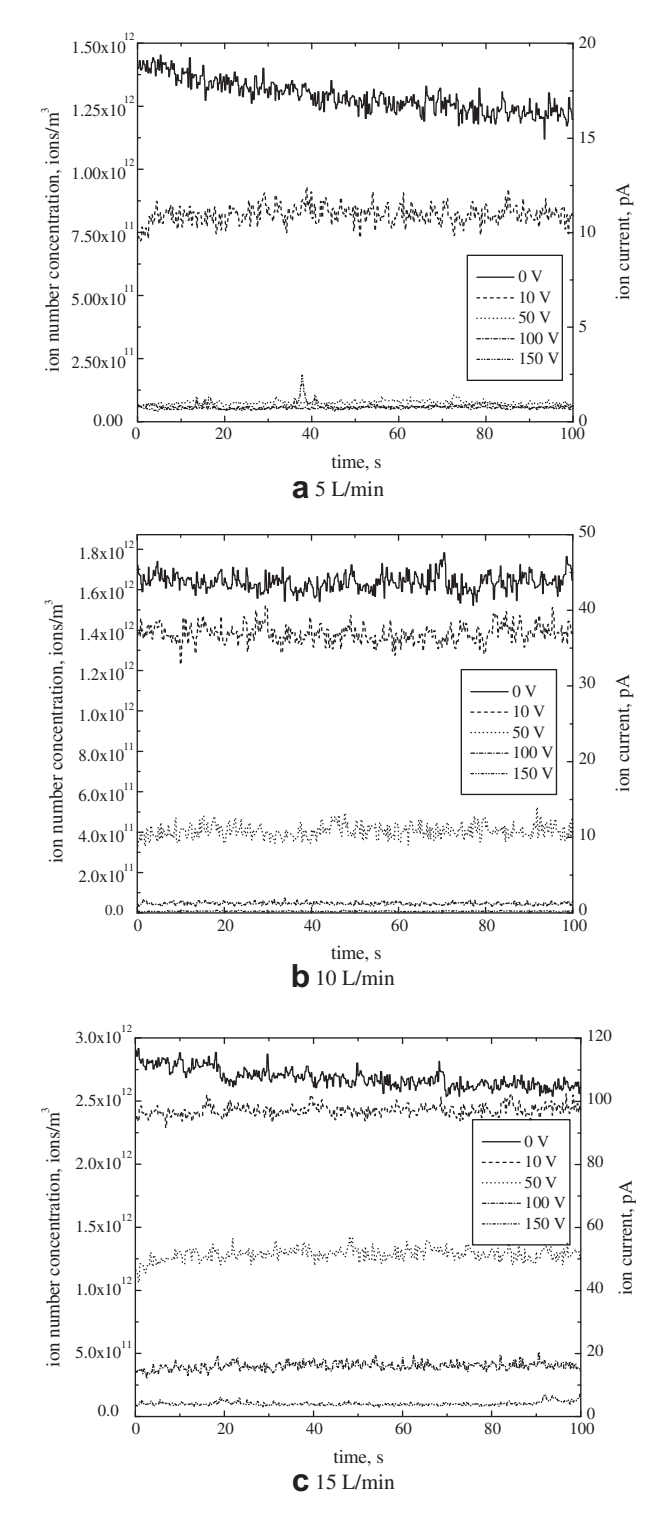


Fig. 10. Space charge and diffusion losses of ions as a function of ion flow rate.

caused ions and particles to deviate from their central trajectories within the precipitator, resulting in ions and particles lost to the precipitator electrode. In addition, ions were found to exhibit higher degree of Brownian diffusion than particles, in the absence of an ion trap voltage.

Fig. 8 shows space charge effect on the ion and particle trajectories in the ion precipitator for ion and particle concentrations of  $10^{13}$  particles/m<sup>3</sup>. A set of eight different trajectories depending on



**Fig. 11.** Time variation of outlet ion concentration and signal current with trap voltage at different operating ion flow rates.

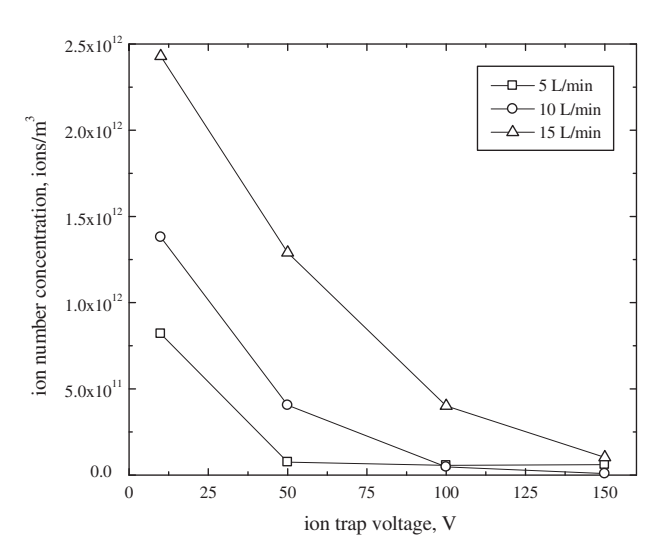


**Fig. 12.** Variation of outlet ion concentration with ion trap voltage at different operating ion flow rates.

the radial inlet distances of the ions and particles in the precipitator were plotted. Five of the trajectories bent towards the precipitator electrode. The particle ended up deposited onto the precipitator electrode, while the other three trajectories passed through the precipitator without deposition. It should be noted that ion deposition onto the precipitator electrode due to space charge effect was about 40%. In case of particle trajectories, it was shown that all particle trajectories can pass through the ion precipitator without deposition onto the precipitator electrode.

## 4.2. Ion trapping

For an applied ion trap voltage of 0 V, Fig. 9 shows the variation of ion concentration and signal current at ion generator outlet, ion precipitator electrode, and ion precipitator inlet with ion flow rate. The concentration of ions was calculated from the measured ion current by Equation (1). The measured current and concentration of ions ranged from 0 to 1900 pA, and 0 to  $5.8 \times 10^{13}$  ions/m<sup>3</sup>. At higher ion flow rates, the ion concentration and signal current were relatively high. The magnitude of the current and concentration of ions at the ion generator outlet was much larger than at the ion precipitator outlet. It was expected that the ions would partially be lost inside the ion precipitator due to Brownian diffusion, electrostatic dispersion (space charge), and an external electric field by electrostatic deposition. With ion concentrations above 10<sup>13</sup> ions/ m<sup>3</sup>, ions may partially deposit onto the ion precipitator electrode by space charge effect in the absence of any applied voltage. As shown in Fig. 8, current and concentration of collected ions on the ion precipitator electrode were  $1.44 \times 10^{13}$  to  $3.22 \times 10^{13}$  ions/m<sup>3</sup>, and 193 to 1300 pA. Space charge and diffusion losses of ions as a function of ion flow rate at an applied ion trap voltage of 0 V are shown in Fig. 10. It was evident that the loss due to space charge and diffusion effects was about 30%, with total losses of about 95%. This implied that about 5% of the ions could get through the ion precipitator.

Fig. 11 shows temporal variation of ion number concentration and signal current of the precipitator outlet at different ion flow rates and trap voltages. The measured current of ions at the precipitator outlet ranged from 0 to 100 pA, corresponding to the concentrations of  $0-2.5\times10^{12}$  ions/m³. Increasing the trap voltage resulted in the decrease of the ion concentration and signal current at the precipitator outlet. Variation of outlet ion number concentration with ion

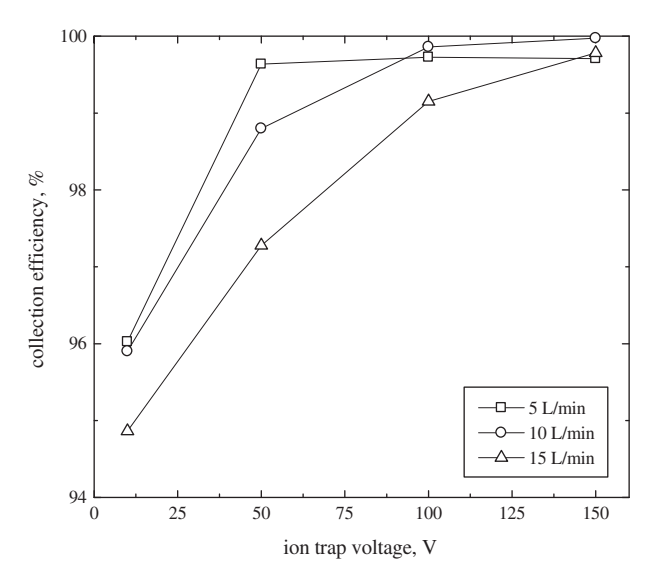
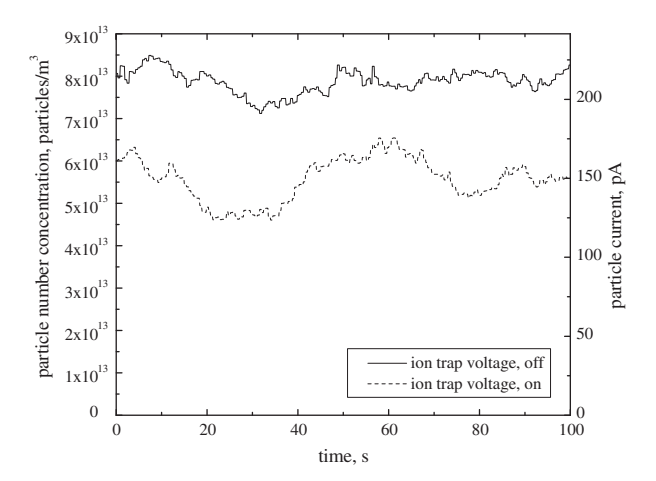


Fig. 13. Variation of total collection efficiency with ion trap voltage at different ion flow rates

trap voltage at different ion flow rates is shown in Fig. 12. Low ion flow rate and high trap voltage resulted in a decrease in the concentration of ions at the precipitator outlet. The ion concentration at the precipitator outlet decreased to about 0 at an ion trap voltage greater than 150 V for all ion flow rates considered. Fig. 13 shows variation of total collection efficiency of the precipitator as a function of ion trap voltage at different operating ion flow rates. The total collection efficiency of the precipitator was calculated using Equation 21. Generally, an increase in ion trap voltage produced an increase in ion collection efficiency of the precipitator. For all ion flow rates, the collection efficiency of the precipitator increased to 99% at an ion trap voltage larger than 100 V.

The measured particle concentration and signal current with and without the ion trap voltage of the precipitator is shown in Fig. 14. In this study, a combustion aerosol generator (CAG) was used to generate a polydisperse aerosol for this experiment. The particle size distribution from the CAG was in the range of 10 nm and 400 nm [20]. An isokinetic sampling system was used. The aerosol was dried, mixed with clean, dry and HEPA filtered air in the mixing chamber and then introduced into the ion generator. The aerosol particles were charged by corona discharge in the ion generator. This



**Fig. 14.** Time variation of particle concentration and current with and without the ion trap voltage.

experimental system was operated at aerosol flow rate of 10 L/min and ion trap voltage of 150 V. The average concentrations of particles with and without the ion trap voltage of the precipitator were  $5.57\times10^{13}\,\mathrm{particles/m^3}$  and  $7.87\times10^{13}\,\mathrm{particles/m^3}$ , corresponding to the measured signal currents of 149.45 pA and 211.27 pA. On one hand, when the ion trap voltage was off, free ions entered the Faraday cup, and were measured together with the charged particles, giving the contaminated signal. On the other hand, when the ion trap voltage was on, most free ions were removed. Hence, only charged particles could pass through the precipitator and give smaller signal currents. This shows that the measured signal current was only derived from charged particles.

#### 5. Conclusion

A wire-cylinder ion precipitator for the EAD was designed, constructed, and investigated in this paper. An analytical model was developed to investigate the ion and particle transports due to diffusion and space charge effects inside the ion precipitator. The experimental study was carried out for positive ions, positively applied voltages at the wire electrode between 10 and 150 V, total flow rates of 5 and 15 L/min, operating pressure of 1 atm, and radial distances of the inlet between 0.15 and 14 mm at a fixed radial distance of wire and outer electrodes. It was found that higher applied wire electrode voltage caused ions to deposit closer to the entrance. Conversely, faster flow rate forced ions to impact the wall further downstream. All charged particles of 10 nm in diameter passed through the ion precipitator smoothly without precipitation at the outer electrode at an ion flow rate of 5 L/min and a trap voltage of 100 V. An increase in ion trap voltage produced an increase in ion collection efficiency of the precipitator for all ion flow rates. The total collection efficiency of the precipitator increased to about 99% at an ion trap voltage larger than 100 V. The ion precipitator proved to be particularly useful in removing excess ions in the EAD.

#### Acknowledgments

This research was financially supported by the Thailand Research Fund (TRF).

#### References

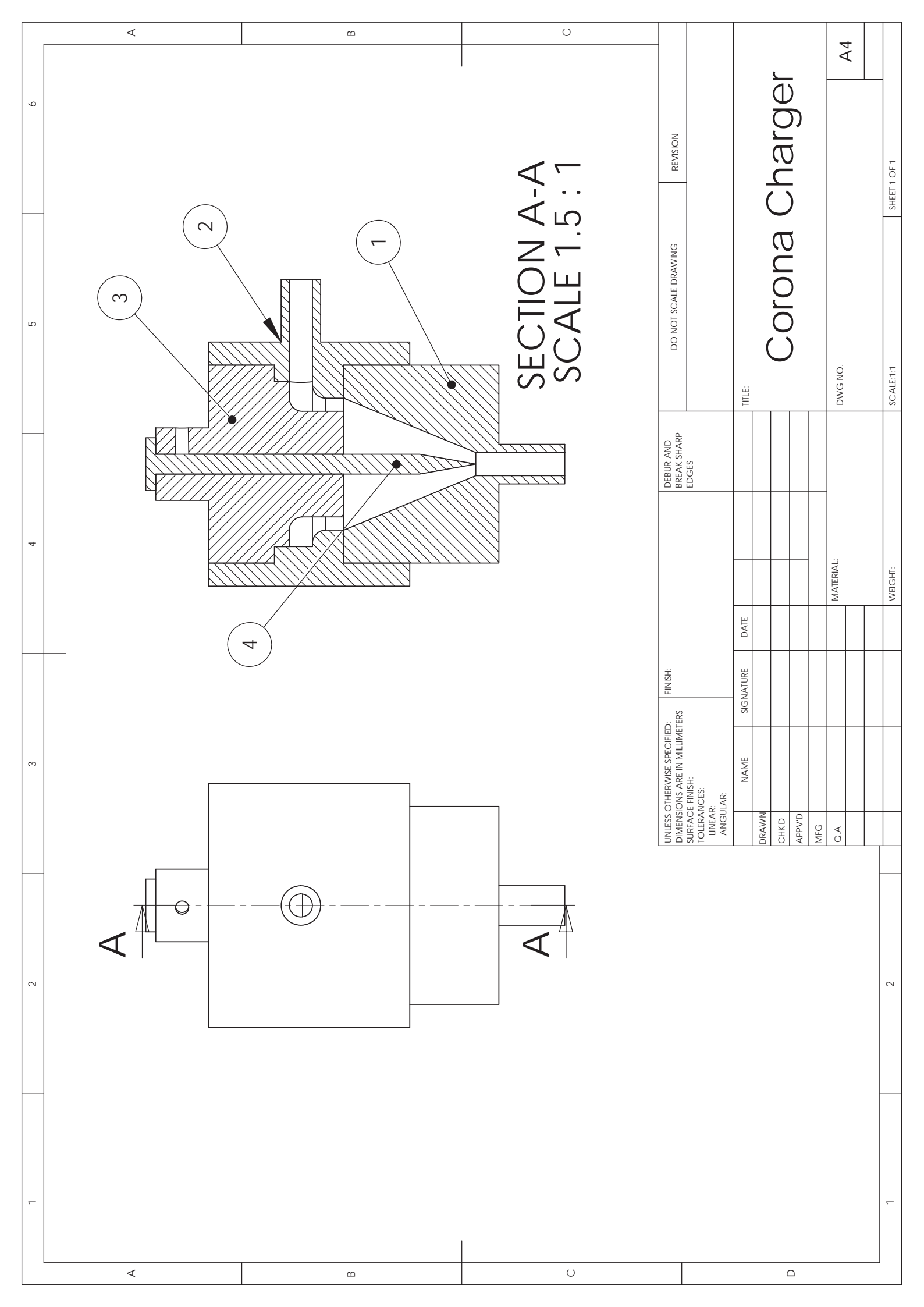
- [1] R.C. Flagan, History of electrical aerosol measurements, Aerosol Science and Technology 28 (1998) 301–380.
- [2] P. Intra, N. Tippayawong, An electrostatic sensor for nanometer-sized aerosol particles detection, Journal of the Japan Society of Applied Electromagnetics and Mechanics 17 (2009) s17–s20.
- [3] H.J. White, Industrial Electrostatic Precipitation. Addison-Wesley, Reading, Massachusetts, USA, 1963.
- [4] K.R. Parker, Applied Electrostatic Precipitation. Blackie Academic & Professional, New York, USA, 1997.
- [5] A. Joworek, A. Krupa, T. Czech, Modern electrostatic devices and methods for exhaust gas cleaning: a brief review, Journal of Electrostatic 65 (2007) 133–155.
- [6] P. Intra, N. Tippayawong, Progress in unipolar corona discharger designs for airborne particle charging: a literature review, Journal of Electrostatics 67 (2009) 605–615.
- [7] J. Keskinen, K. Pietarinen, M. Lehtimaki, Electrical low pressure impactor, Journal of Aerosol Science 23 (1992) 353–360.
- [8] A. Medved, F. Dorman, S.L. Kaufman, A. Pocher, A new corona-based charger for aerosol particles, Journal of Aerosol Science 31 (2000) s616–s617.
- [9] TSI Incorporated, Operation and Service Manual, Revision B, for Electrical Aerosol DetectorTM Spectrometer Model 3070 Minnesota, USA (2004).
- [10] D. Park, M. An, J. Hwang, Development and performance test of a unipolar diffusion charger for real-time measurements of submicron aerosol particles having a log-normal size distribution, Journal of Aerosol Science 38 (2007) 420–430.
- [11] J. Wei, Development of a Method for measuring surface area concentration of ultrafine particles, D.Eng. Thesis, University of Duisburg-Essen, Germany, 2007.
- [12] P. Intra, N. Tippayawong, Effect of needle cone angle and air flow rate on electrostatic discharge characteristics of a corona-needle ionizer, Journal of Electrostatics 68 (2010) 254–260.
- [13] E.O. Knutson, K.T. Whitby, Aerosol classification by electric mobility: apparatus, theory, and applications, Journal of Aerosol Science 6 (1975) 443–451.
- [14] C. Hagwood, Y. Sivathanu, G. Mulholland, The DMA transfer function with Brownian motion a trajectory/Monte-Carlo approach, Aerosol Science and Technology 30 (1999) 40–61.
- [15] P.I. Williams, Construction and Validation of a DMPS for aerosol characterization, Ph.D. Thesis, University of Manchester, UK, 1999.
- [16] J. Kulon, S. Hrabar, W. Machowski, W. Balachandran, A bipolar charge measurement system for aerosol characterization, IEEE Transactions on Industry Applications 37 (2001) 472–479.
- [17] P. Intra, N. Tippayawong, Brownian diffusion effect on nanometer aerosol classification in electrical mobility spectrometer, Korean Journal of Chemical Engineering 26 (2009) 269–276.
- [18] G.P. Reischl, J.M. Makela, R. Harch, J. Necid, Bipolar charging of ultrafine particles in the size range below 10 nm, Journal of Aerosol Science 27 (1996) 931–949.
- [19] M. Alonso, F.J. Alguacil, Y. Kousaka, Space-charge effects in the differential mobility analyzer, Journal of Aerosol Science 31 (2000) 233–247.
- [20] A. Yawootti, P. Intra and N. Tippayawong, A combustion aerosol generator for submicron aerosol production. 3rd Technology and Innovation for Sustainable Development Conference, Nong Khai, Thailand, March 4 – 6, 2010.

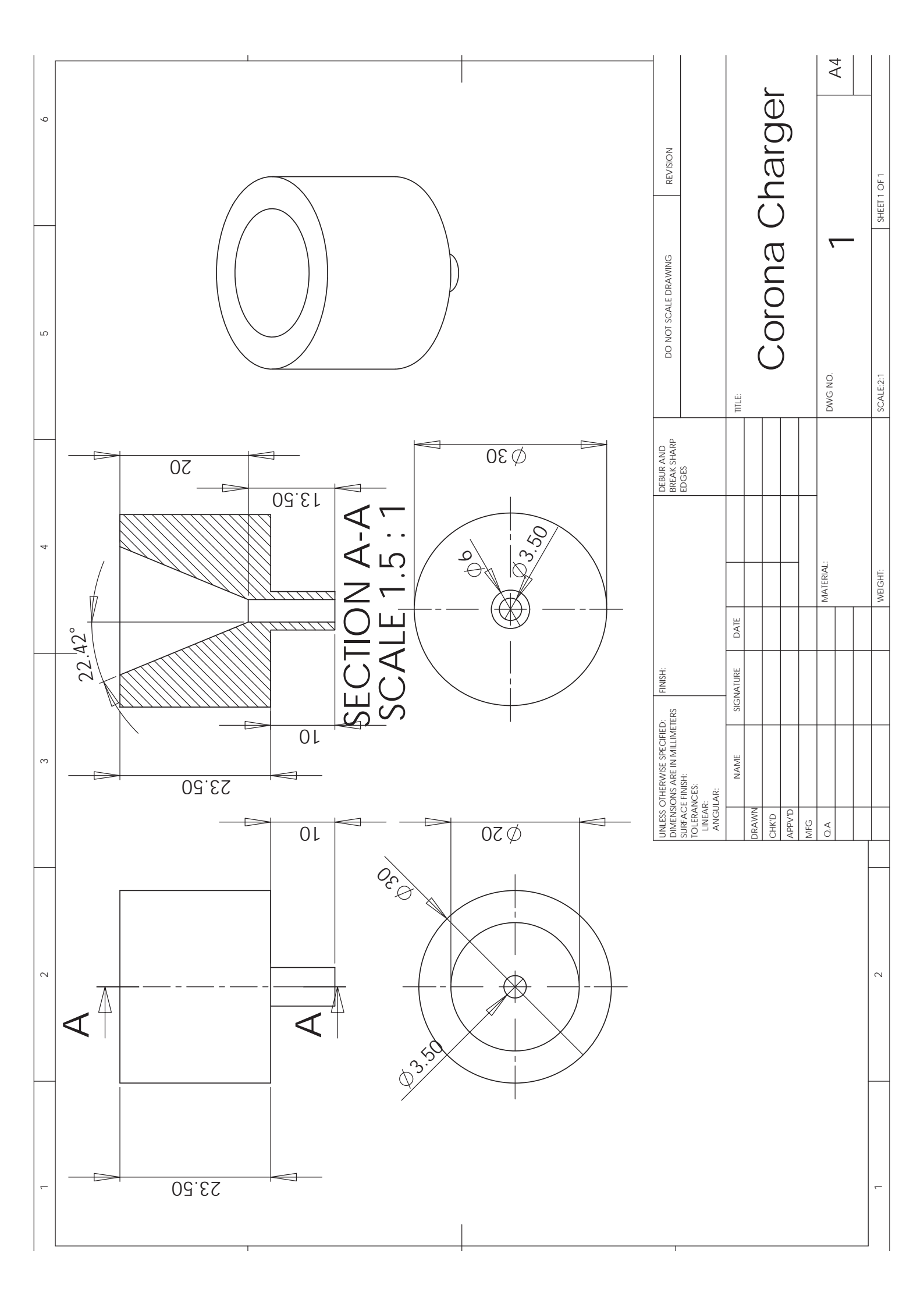
# ภาคผนวก ค

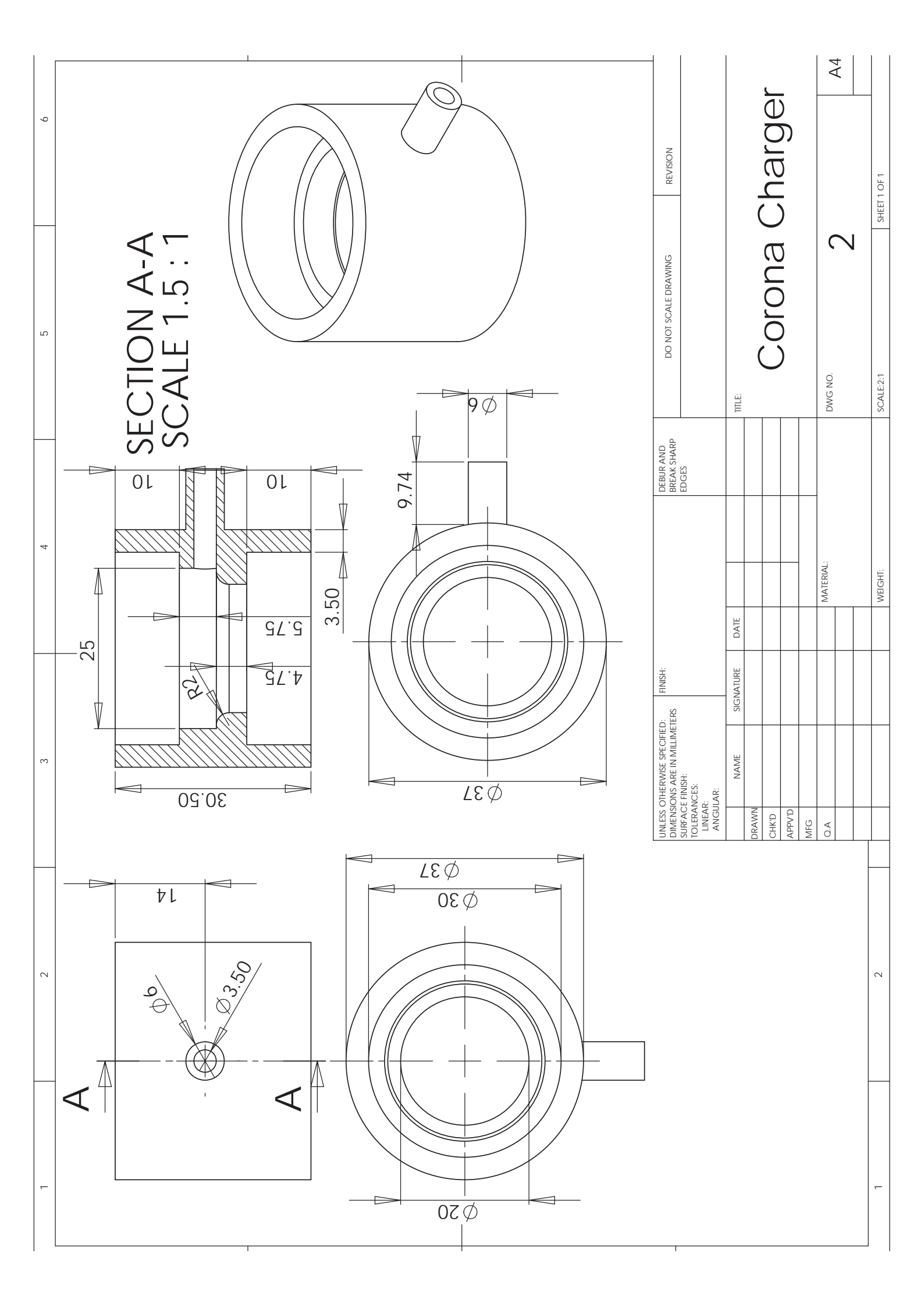
แบบเชิงเทคนิคของอุปกรณ์ประกอบย่อย

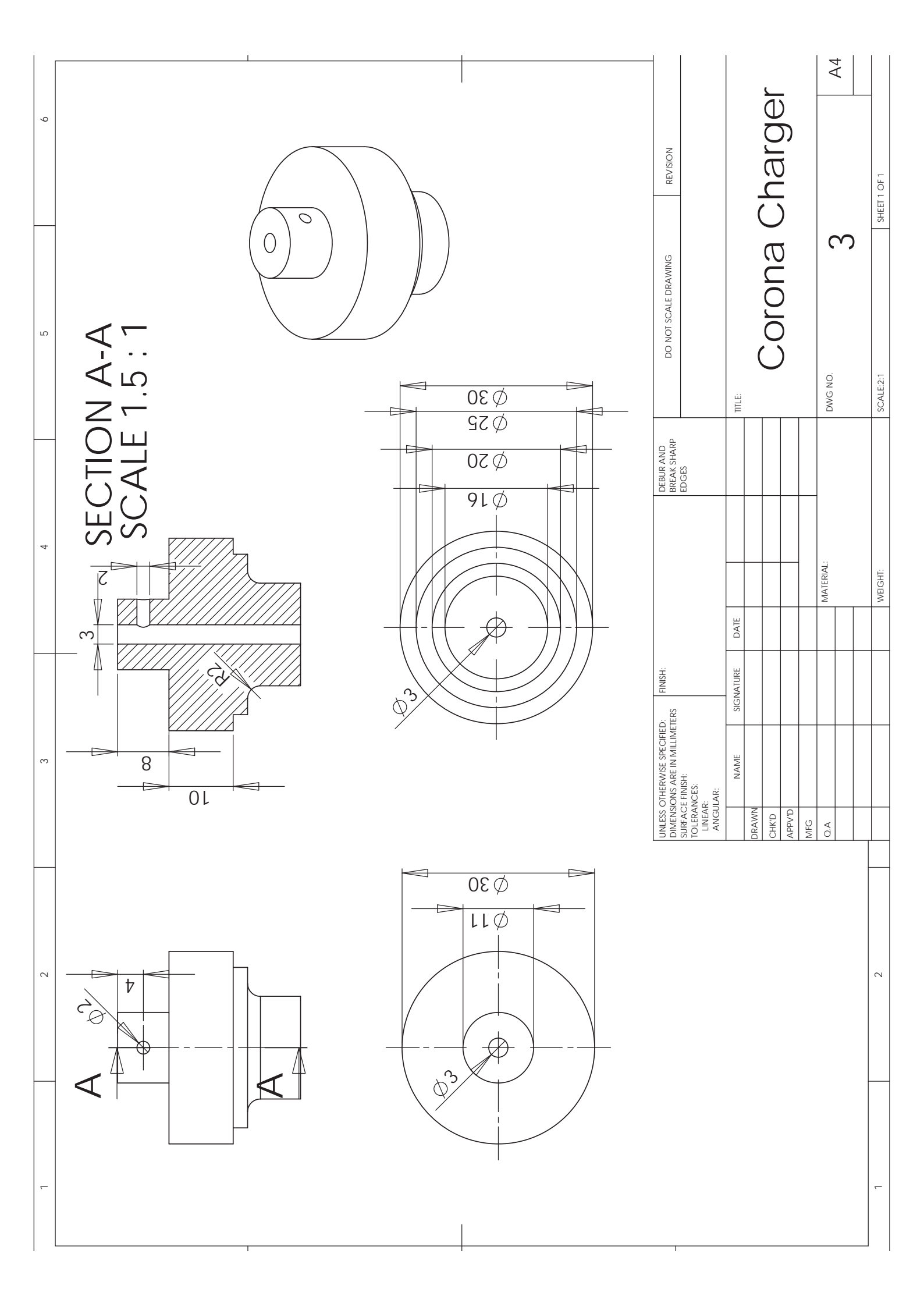
ภาคผนวก ค.1

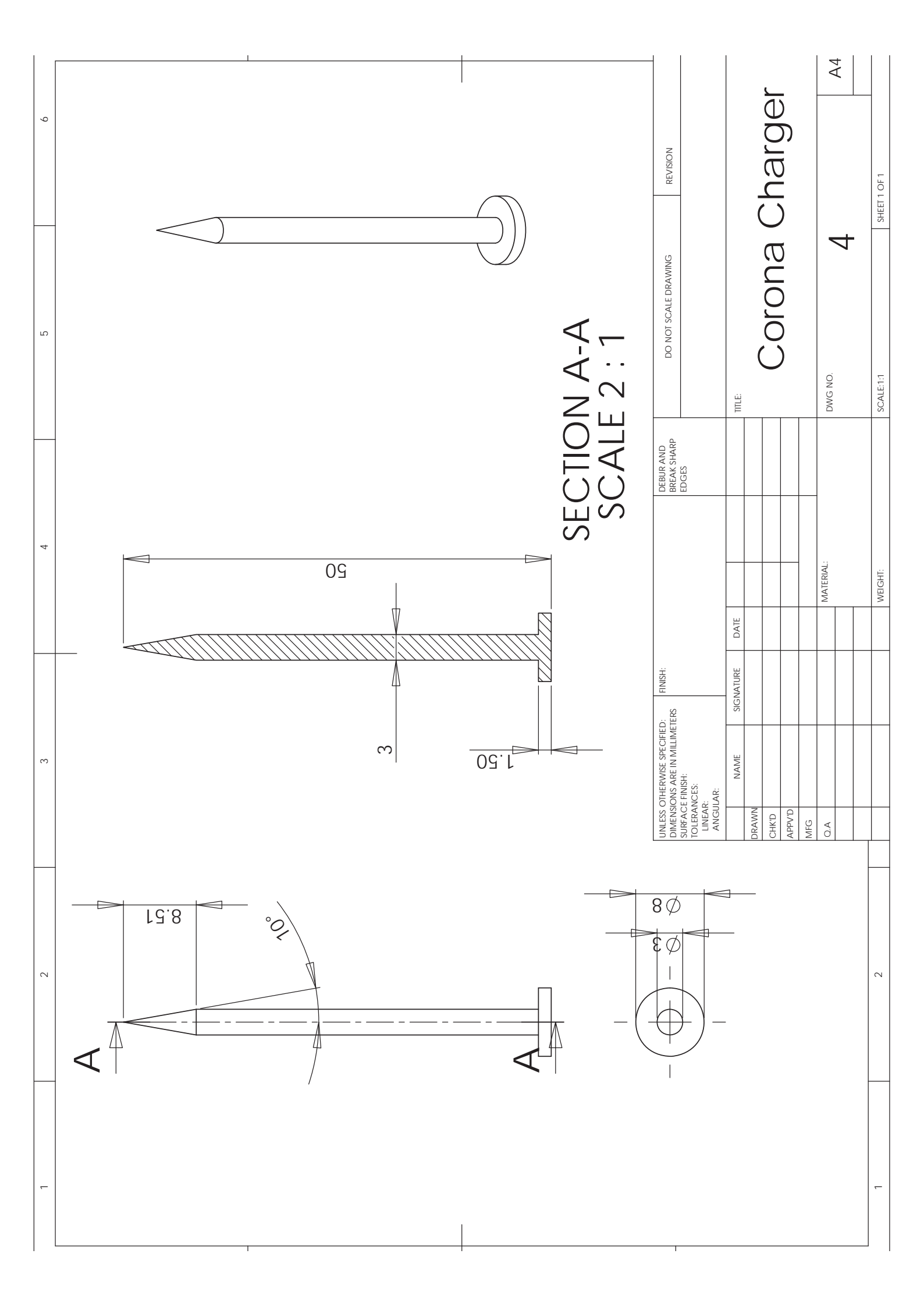
ชุดอัดประจุไฟฟ้าอนุภาคแบบโคโรนา

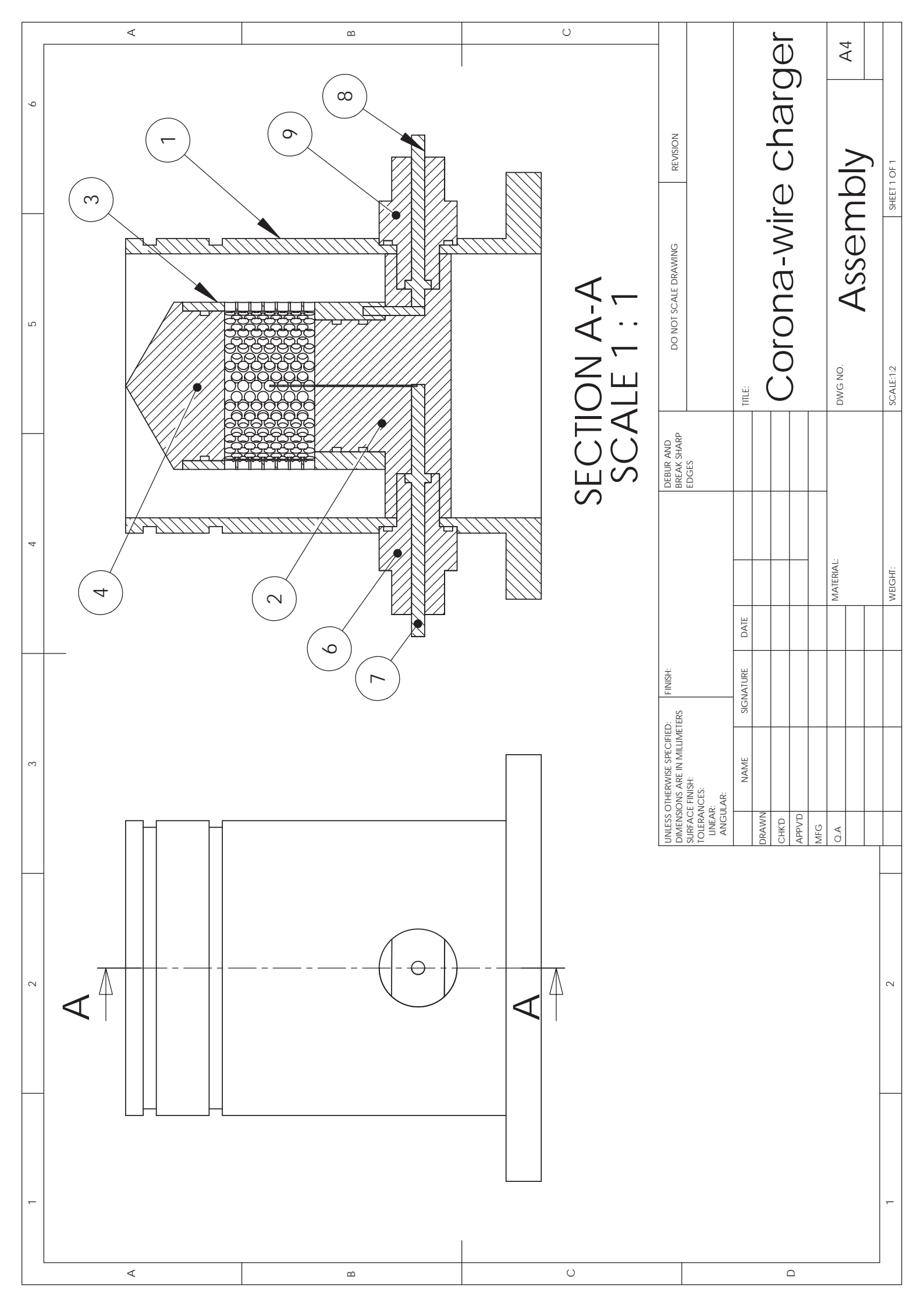


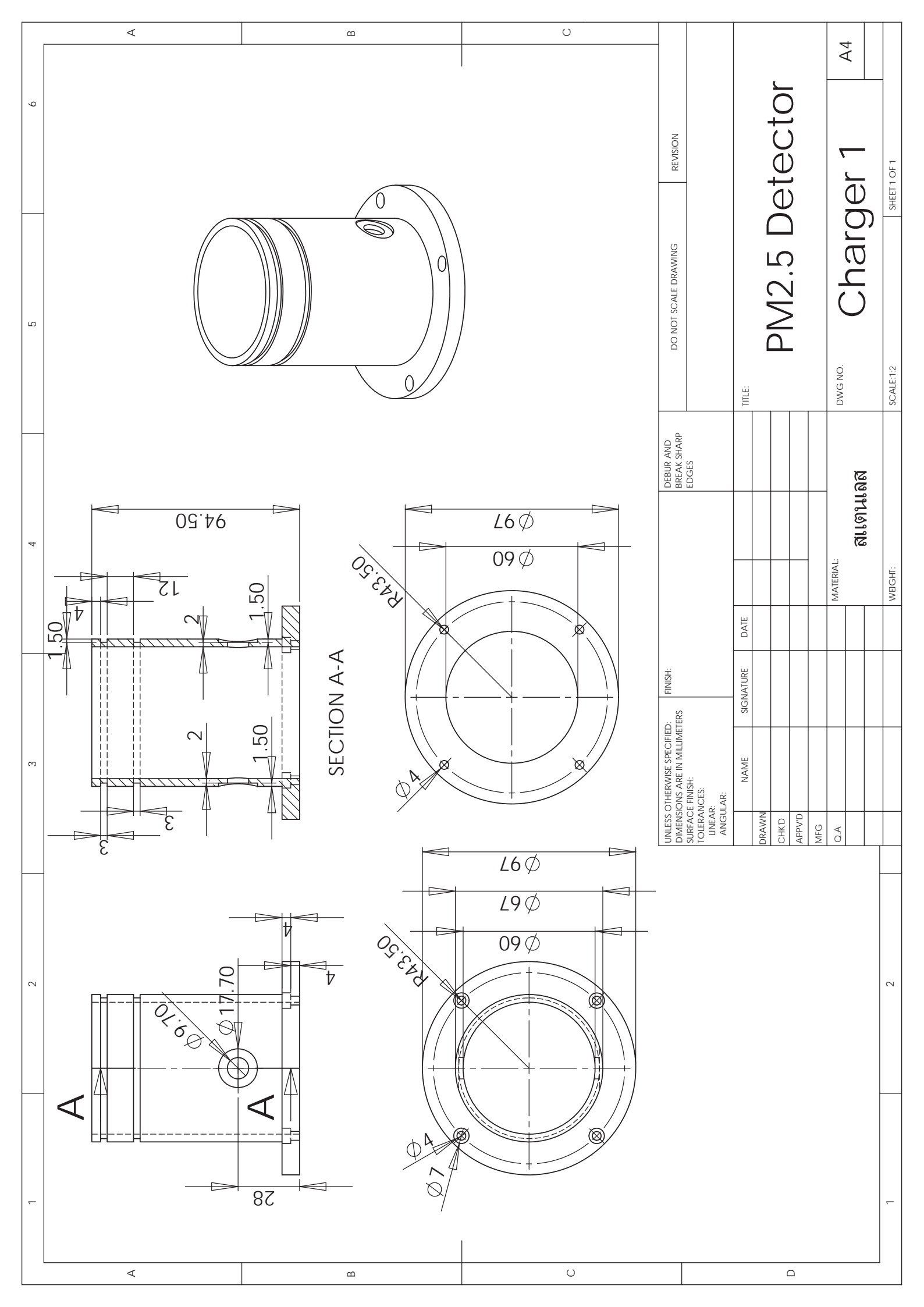


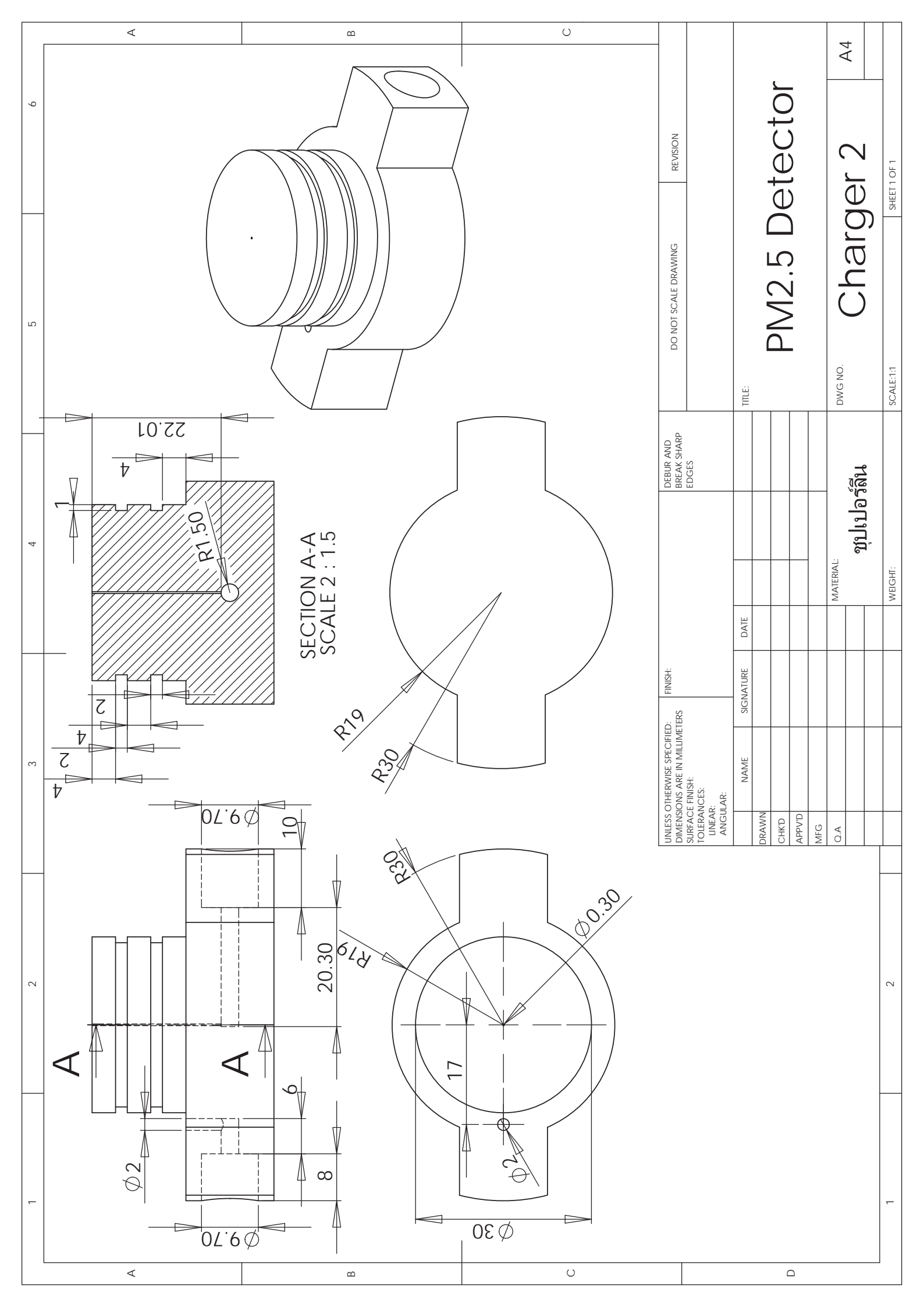


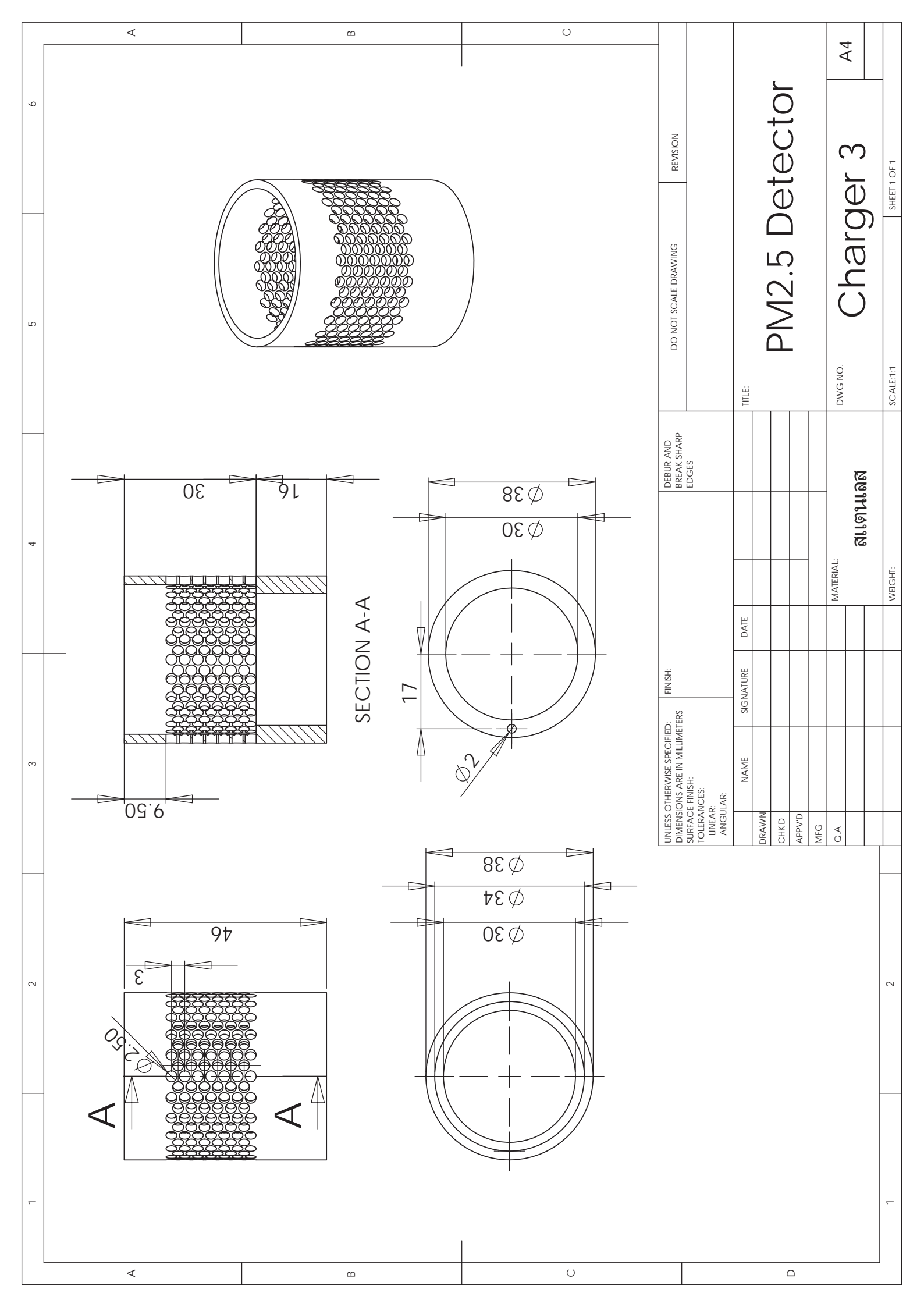


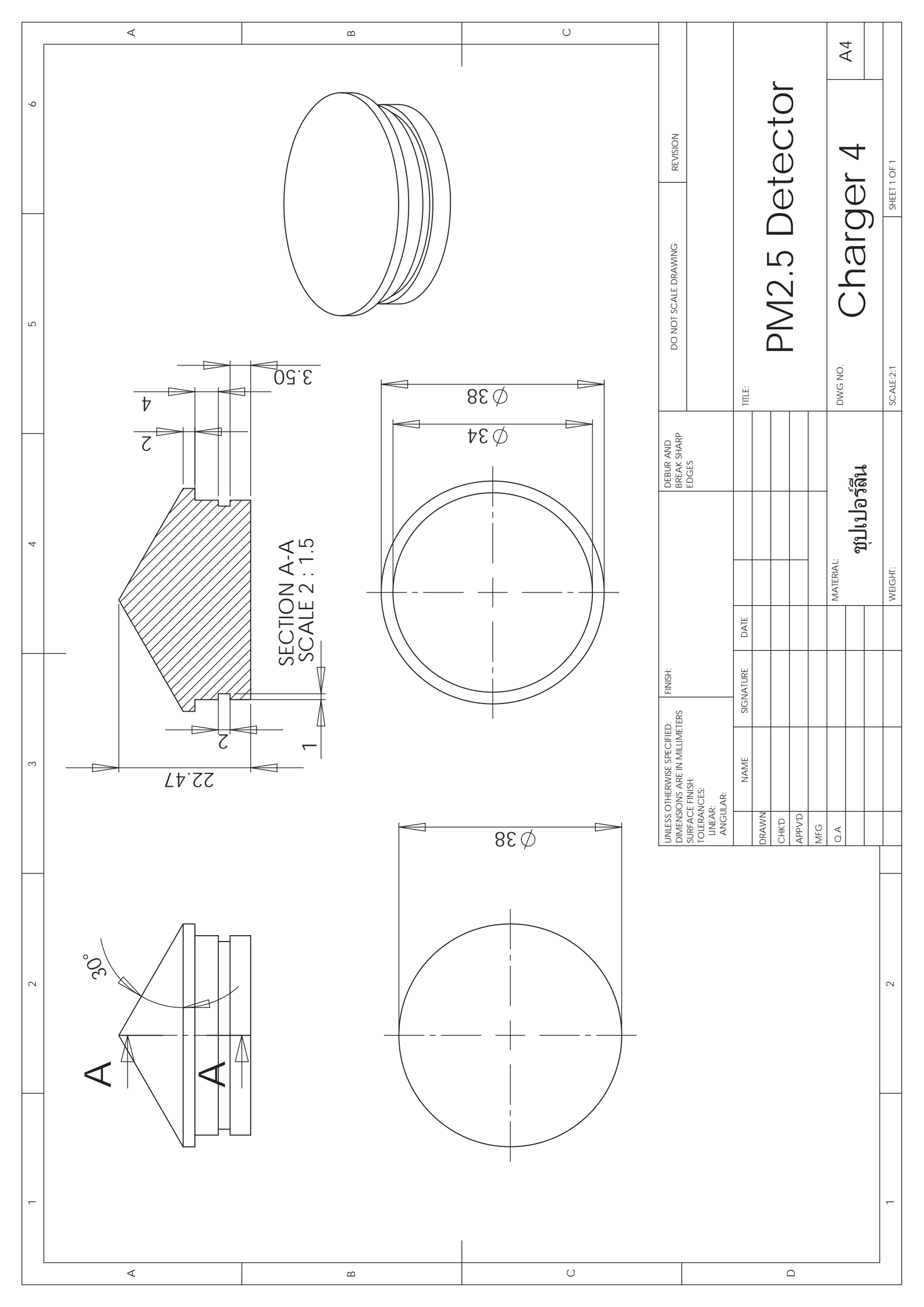


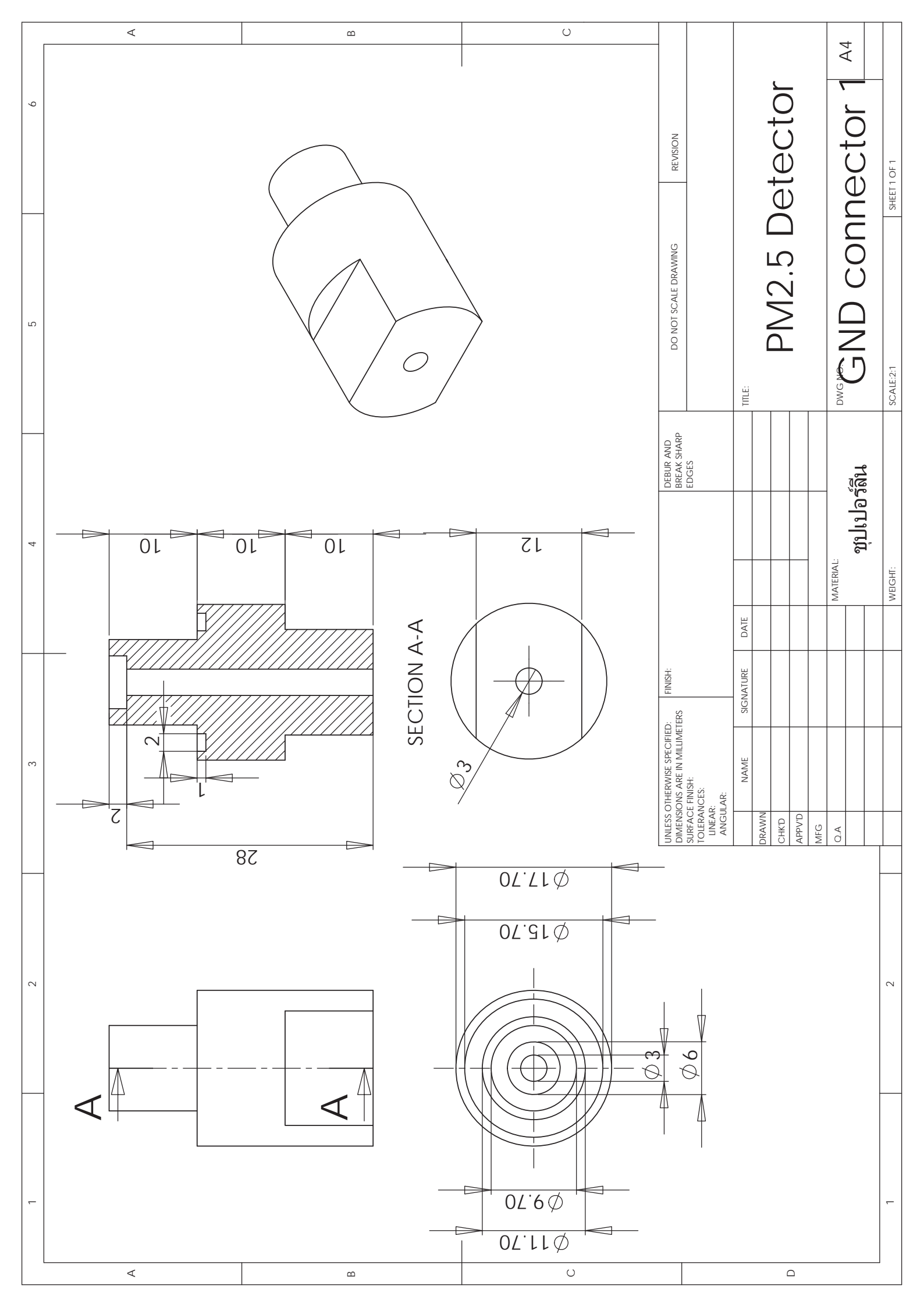


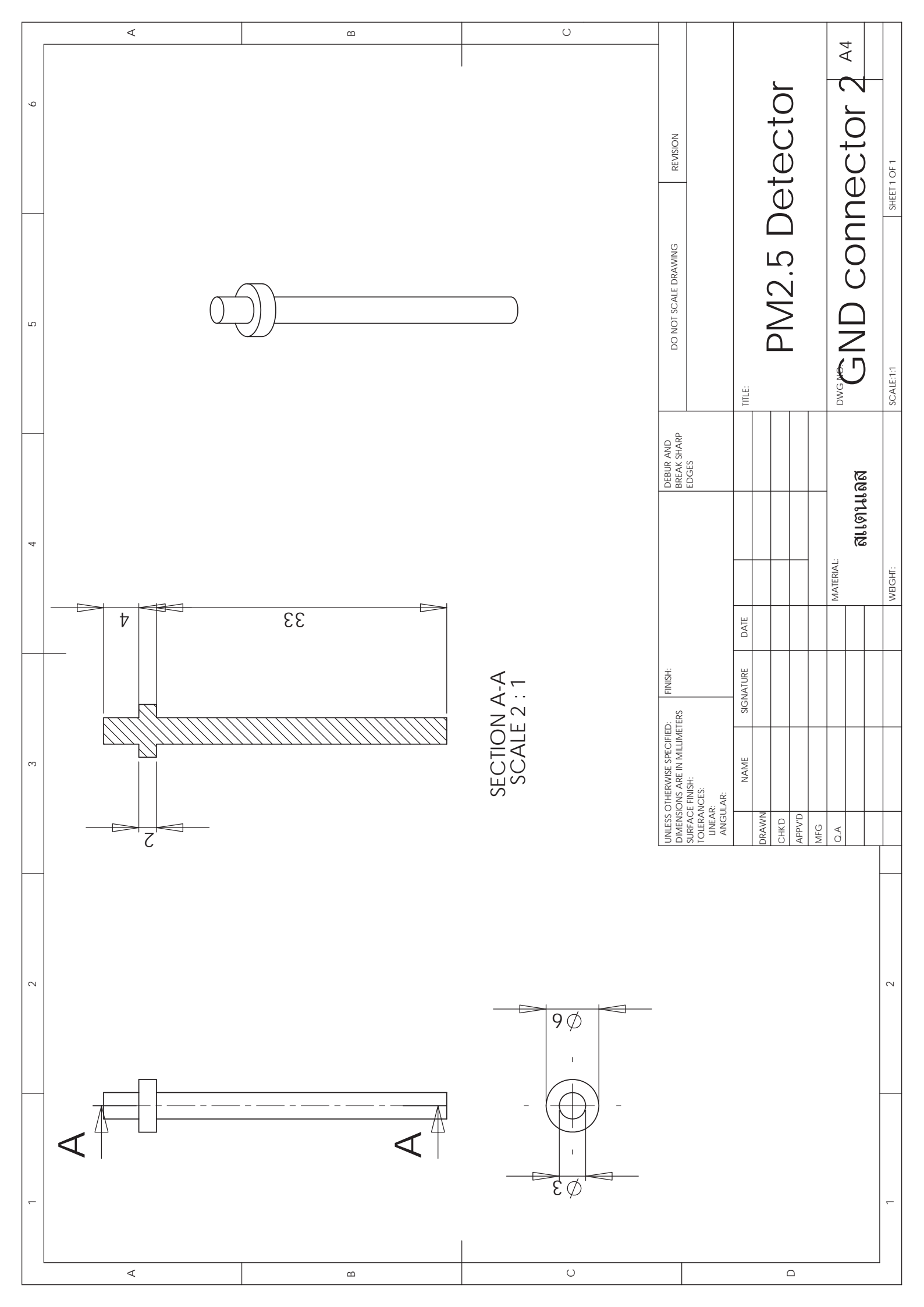


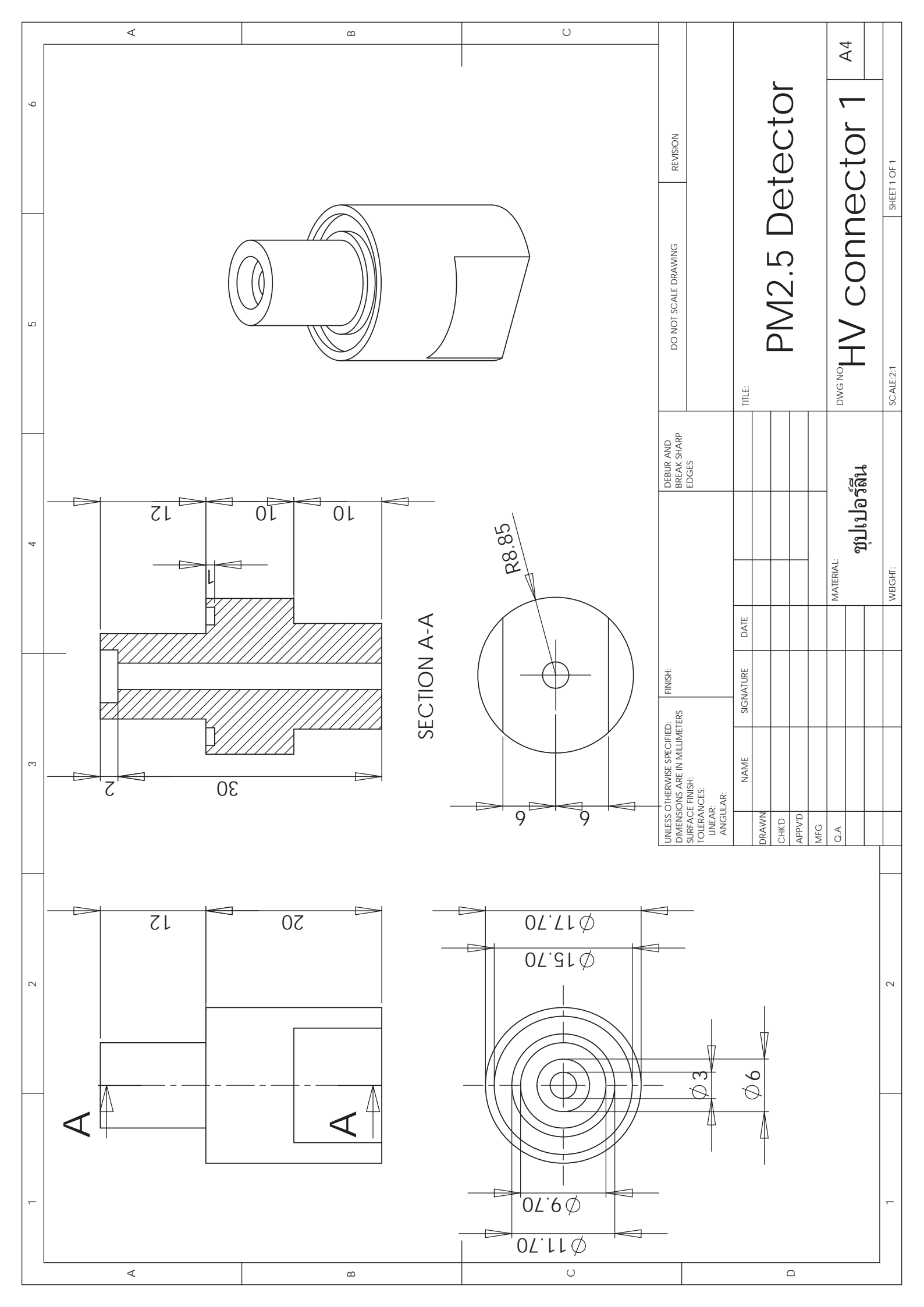


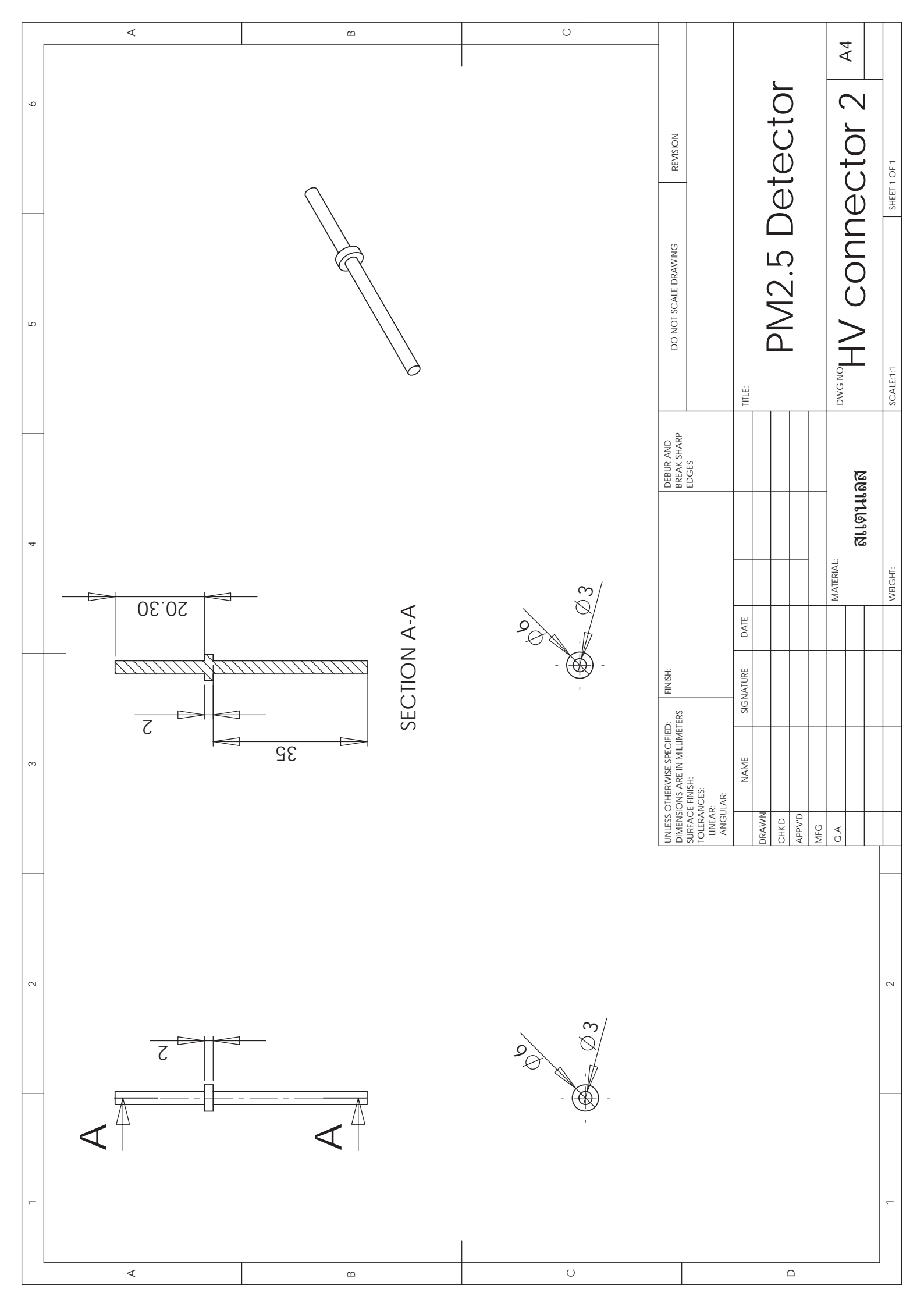






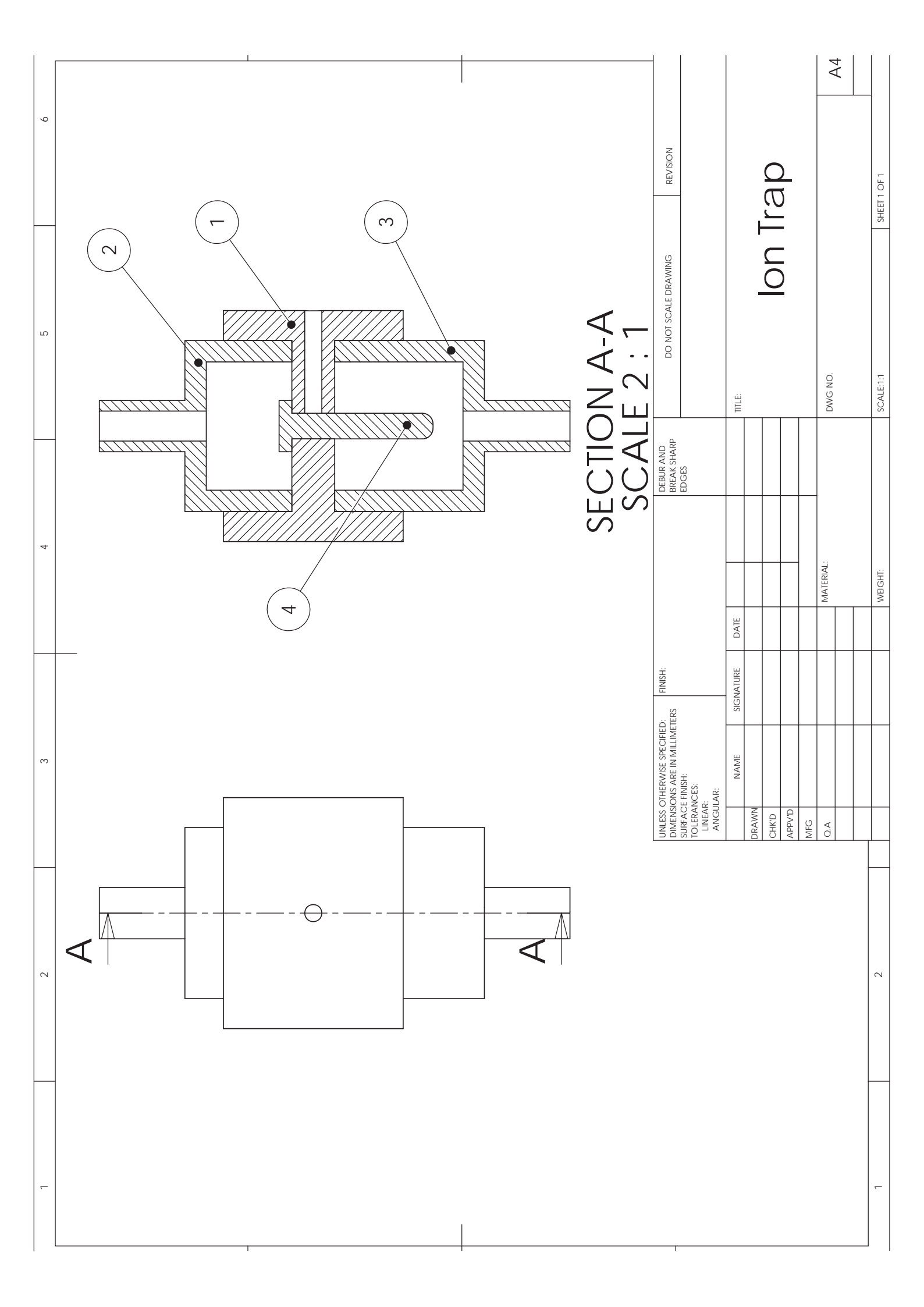


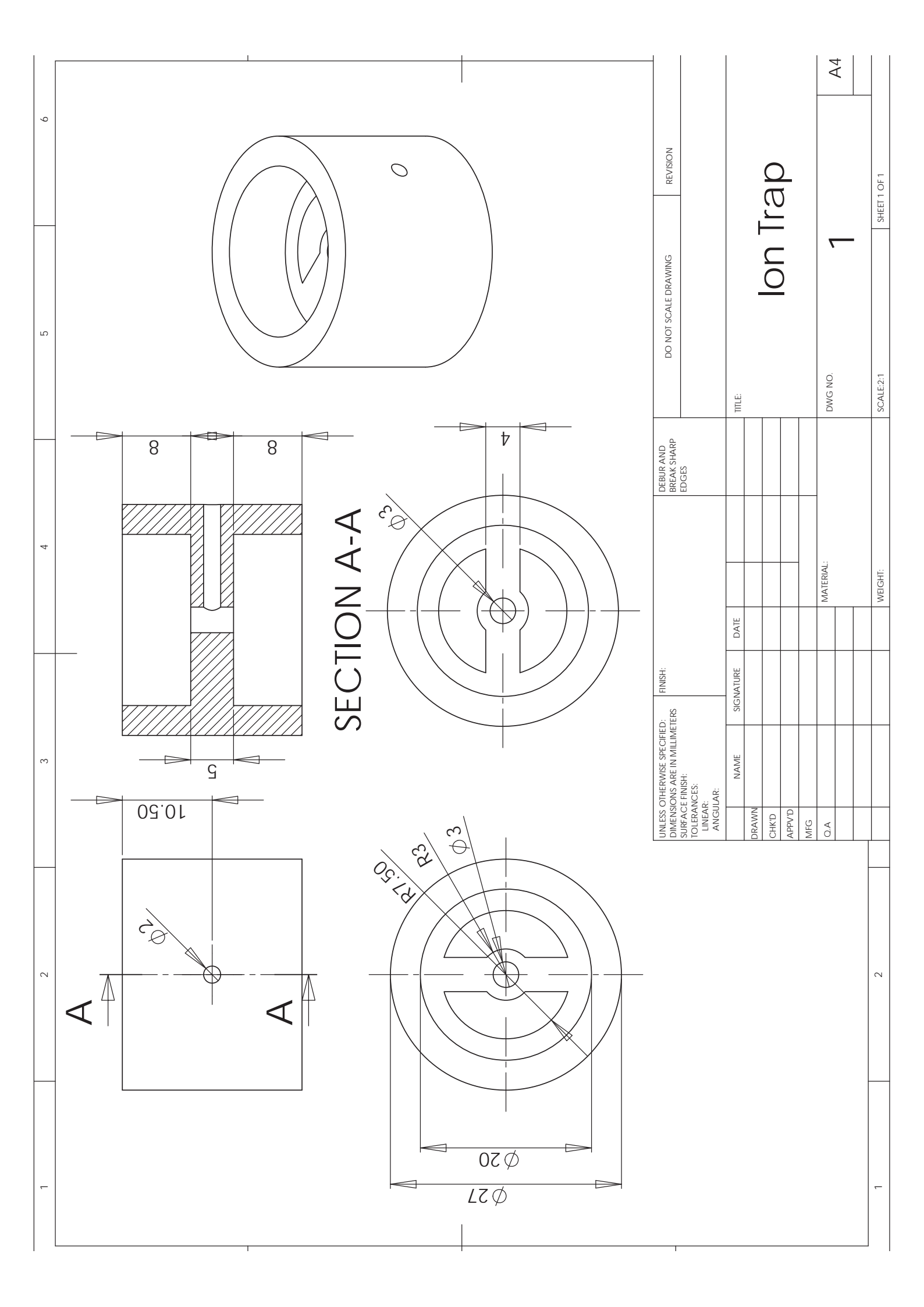


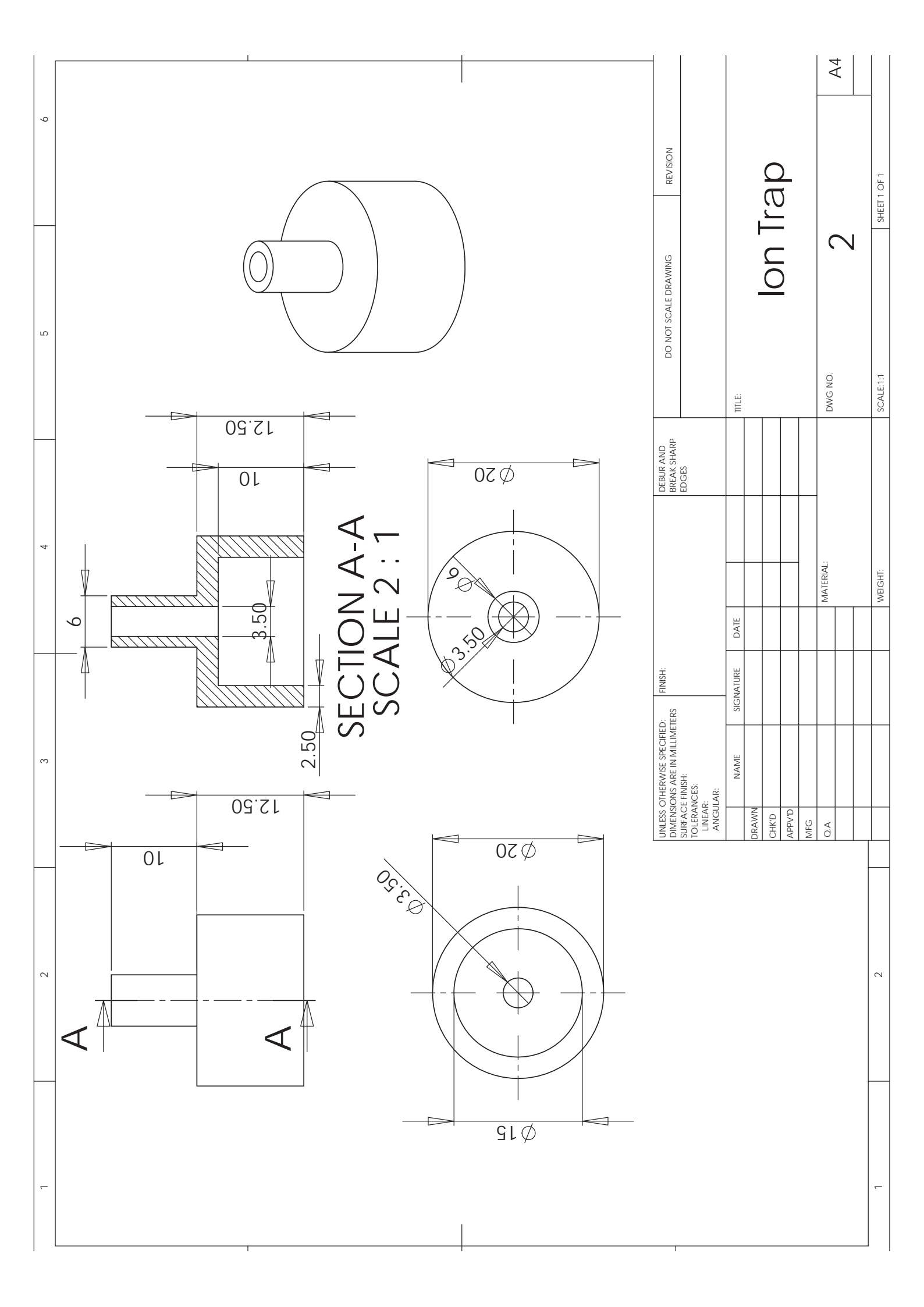


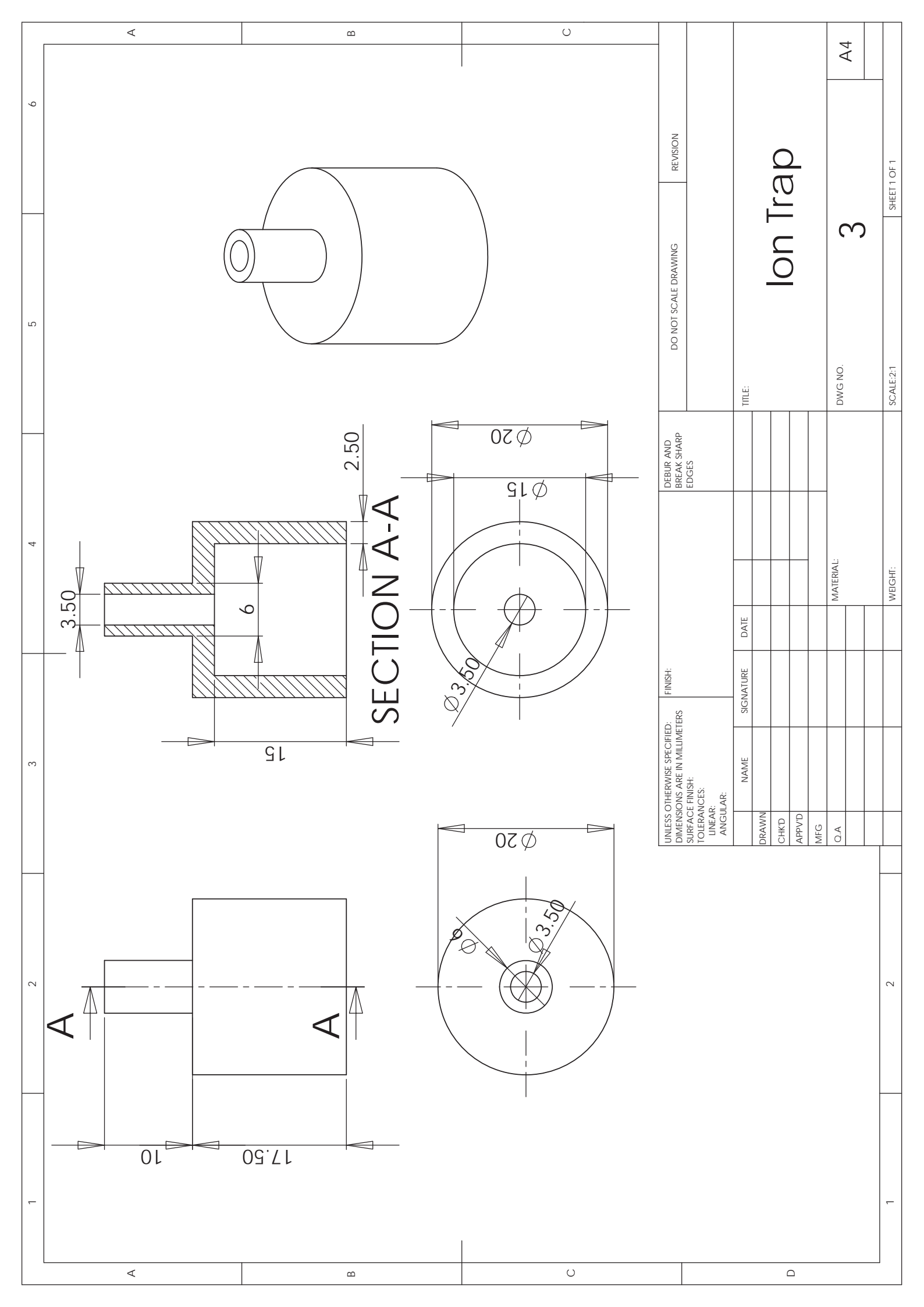
ภาคผนวก ค.2

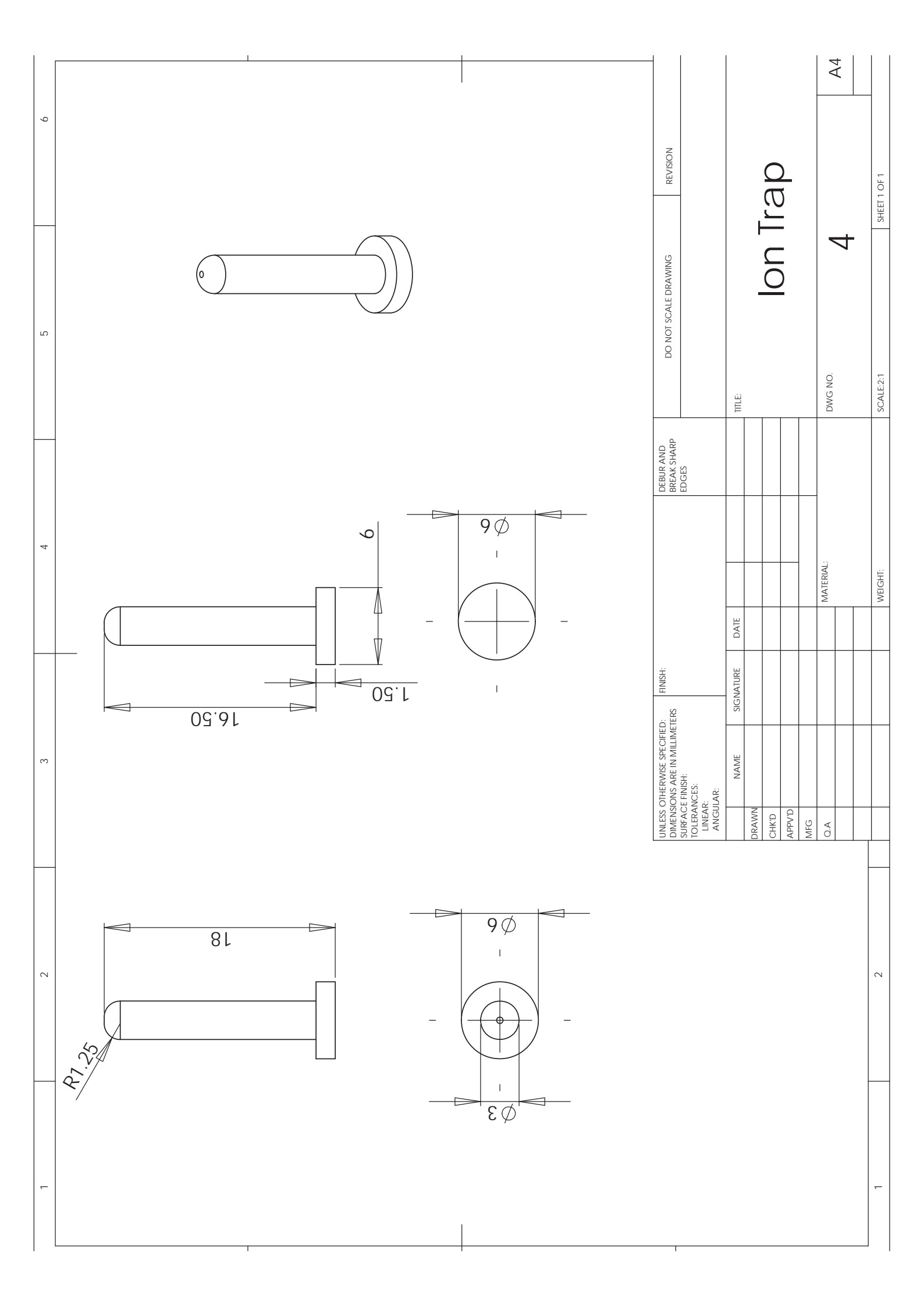
ชุดดักจับไอออนอิสระ





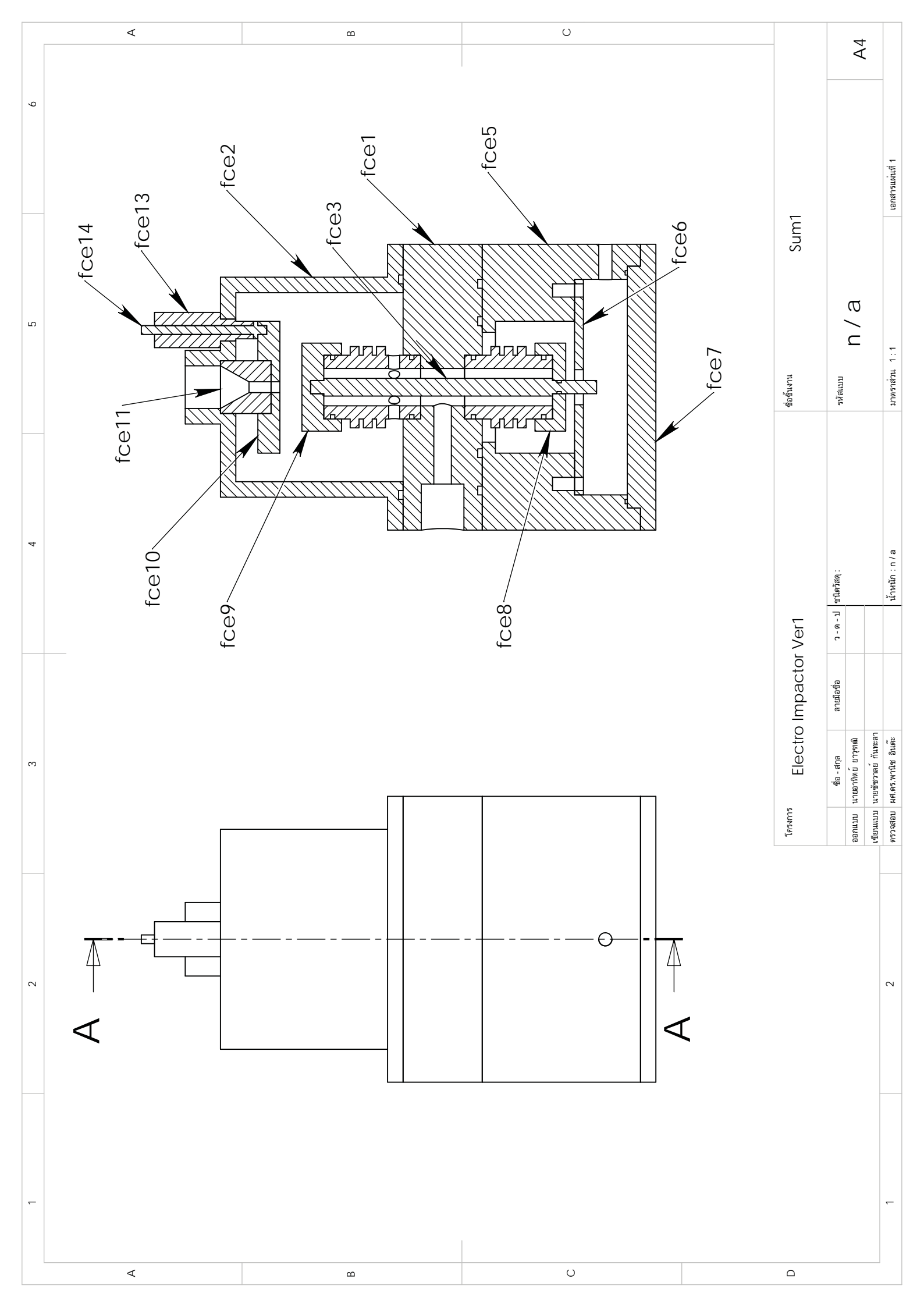


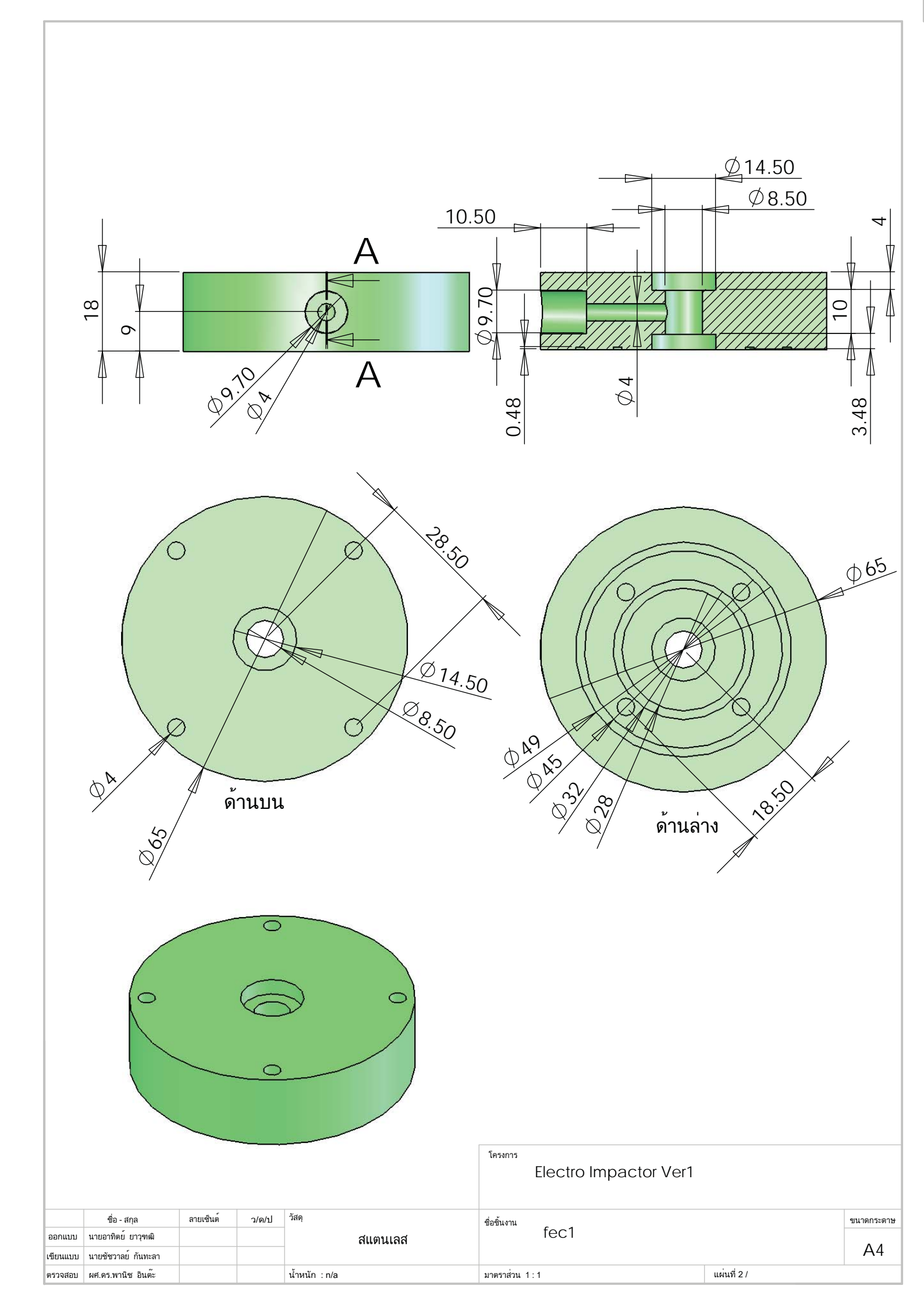


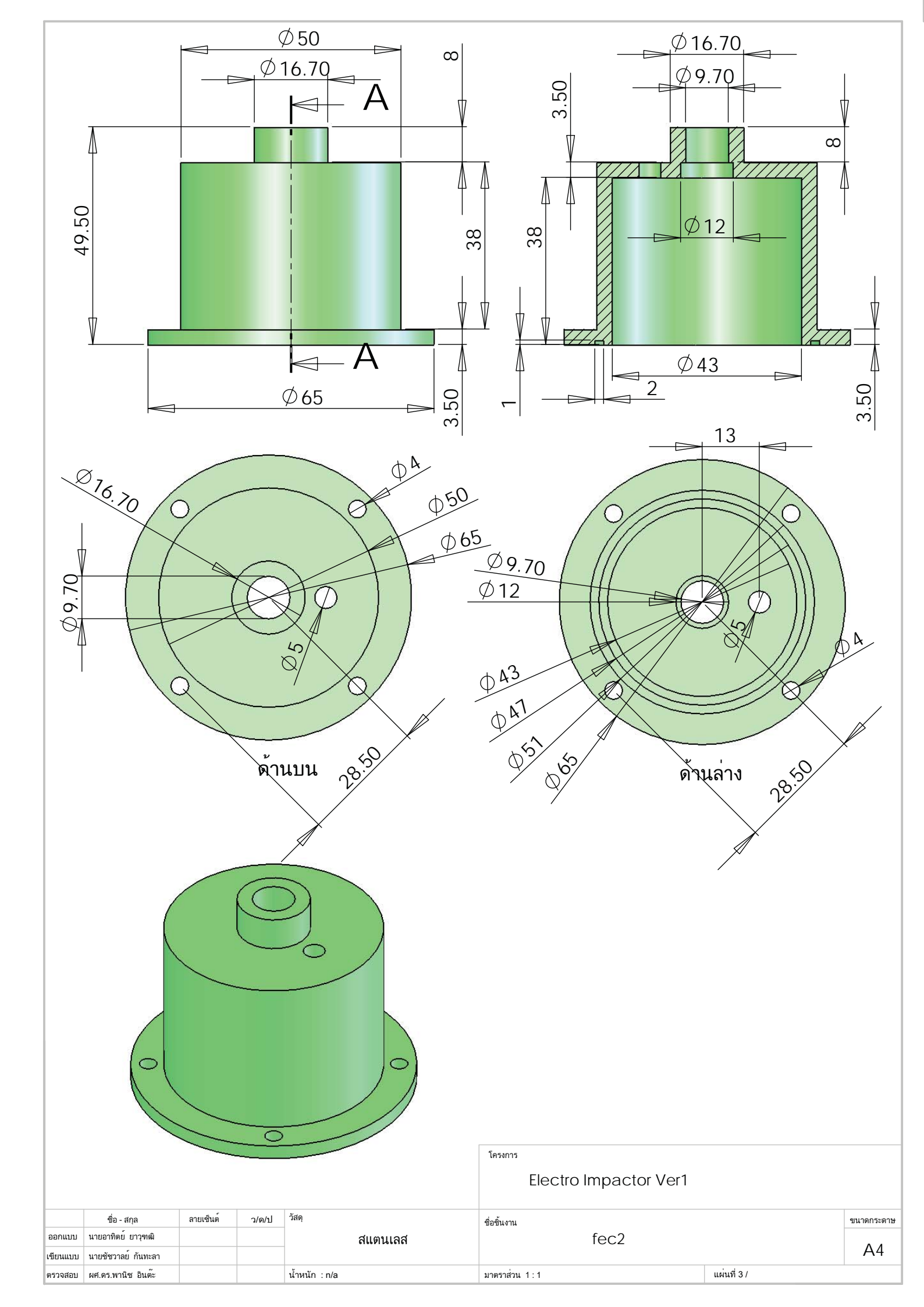


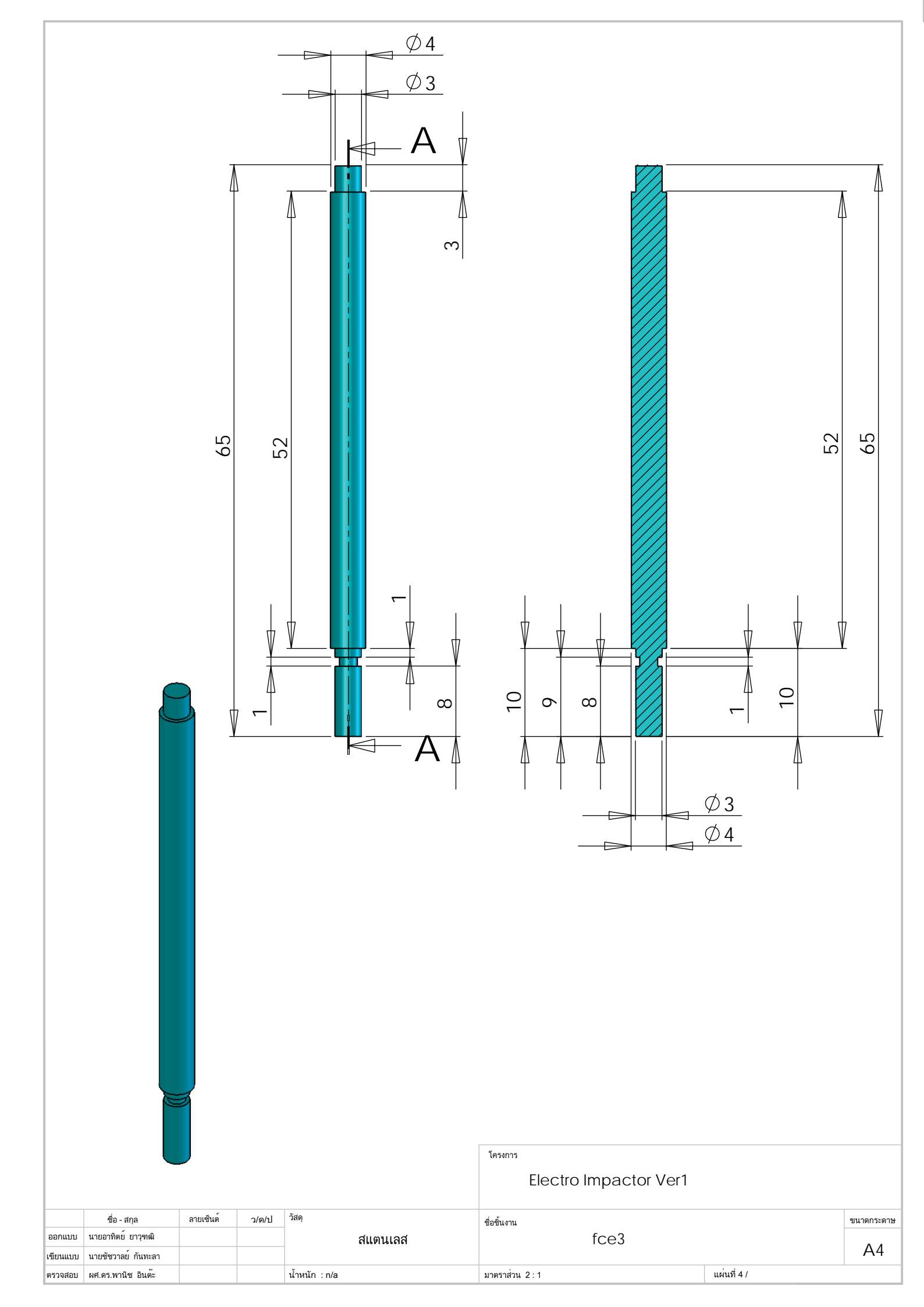
ภาคผนวก ค.3

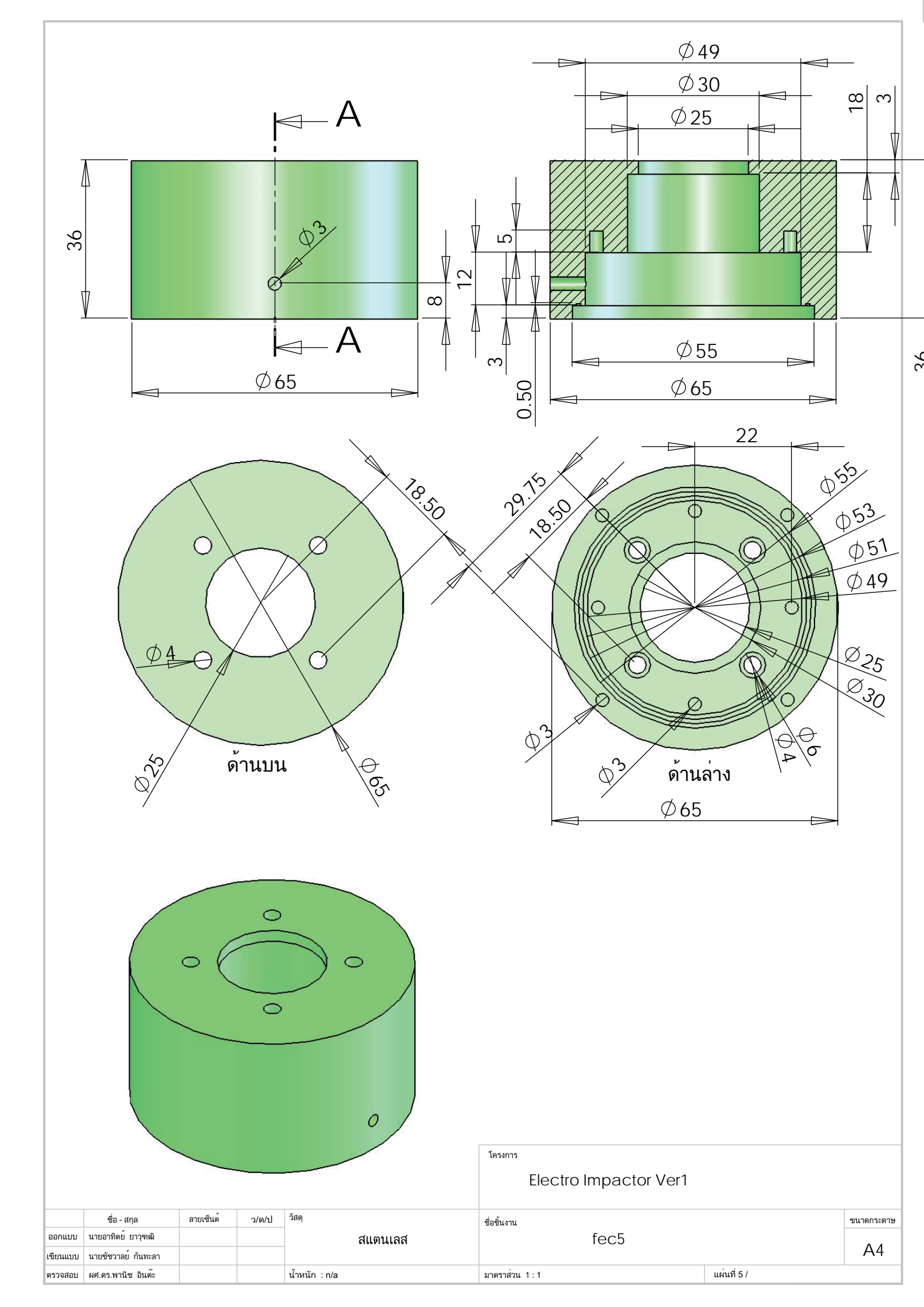
ชุดตรวจจับประจุไฟฟ้าอนุภาคเชิงไฟฟ้า

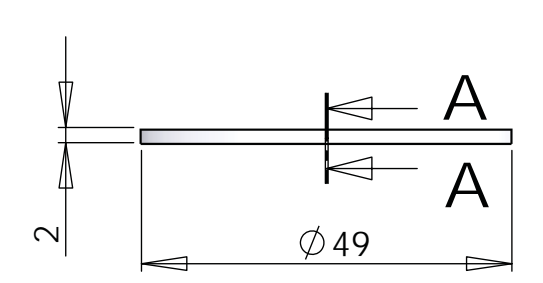


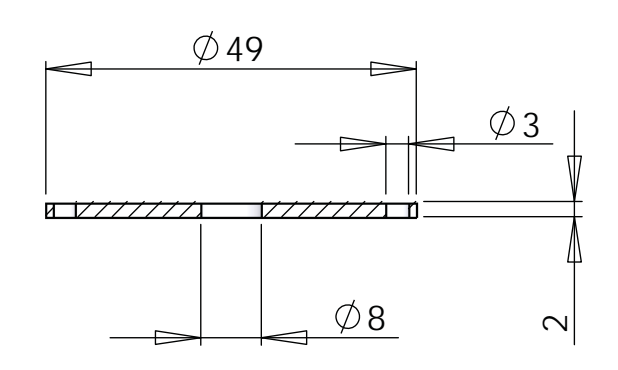


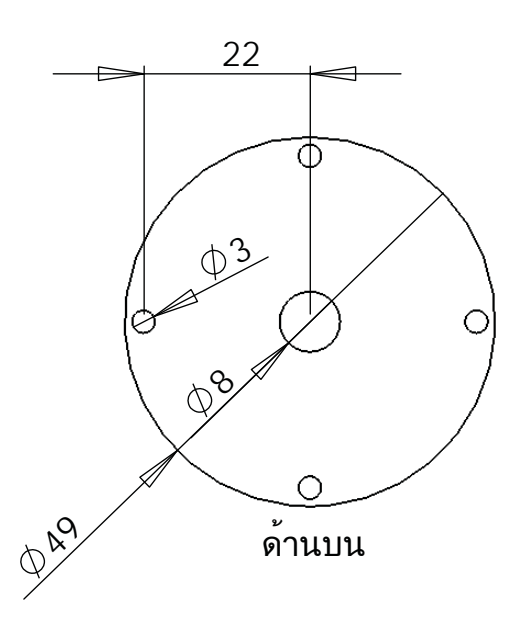


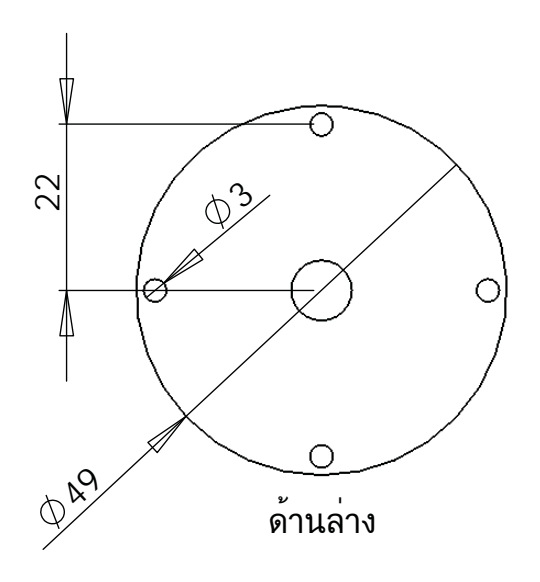


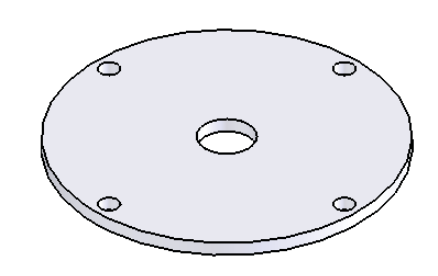






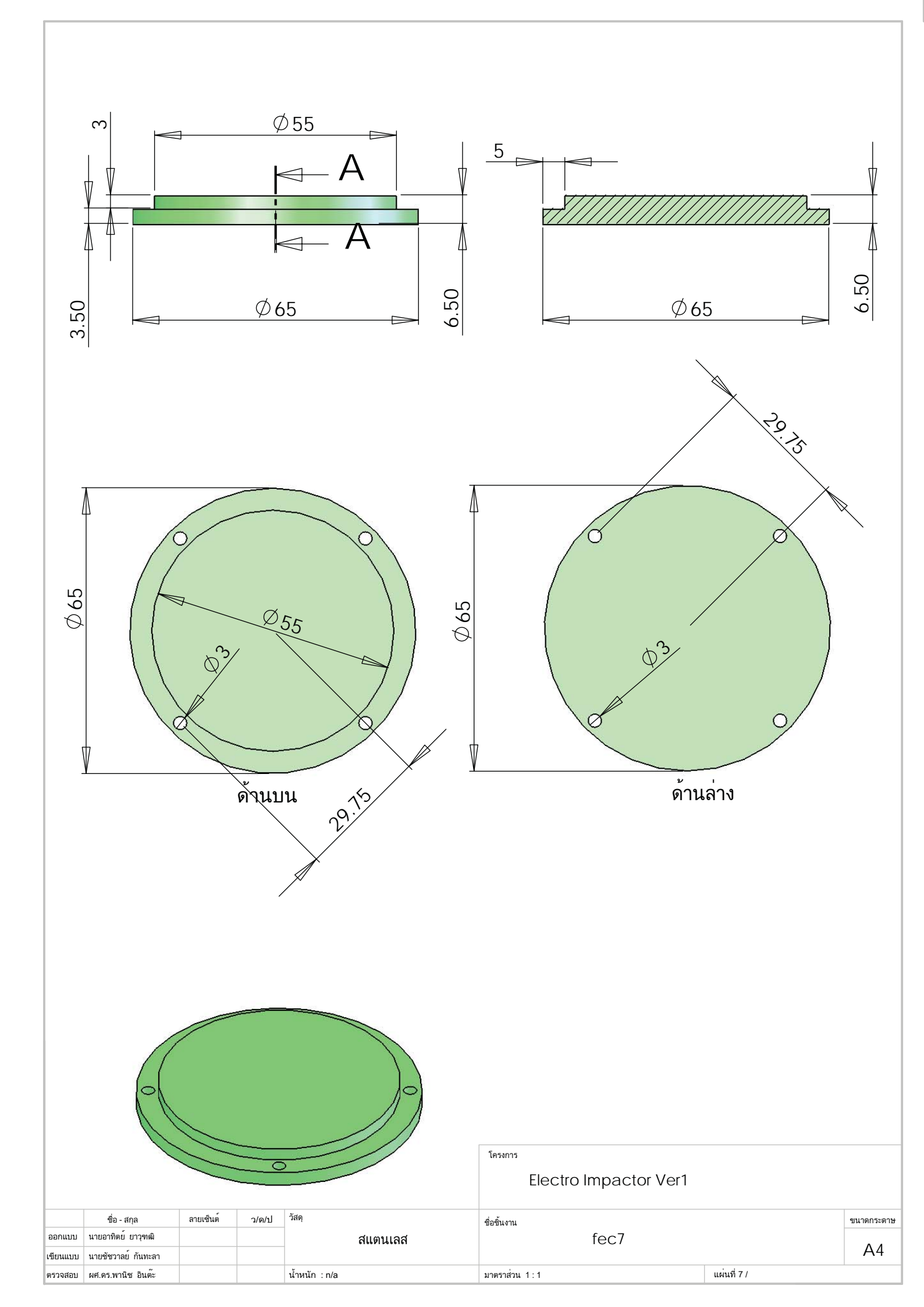


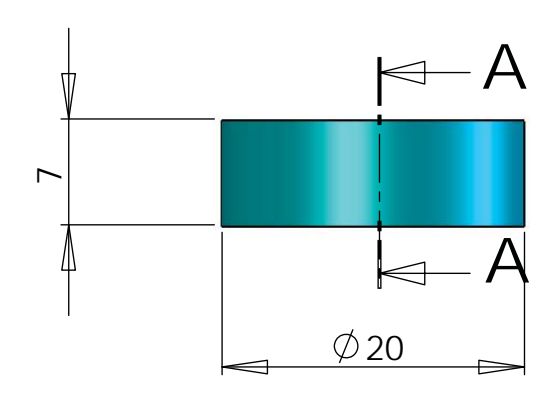


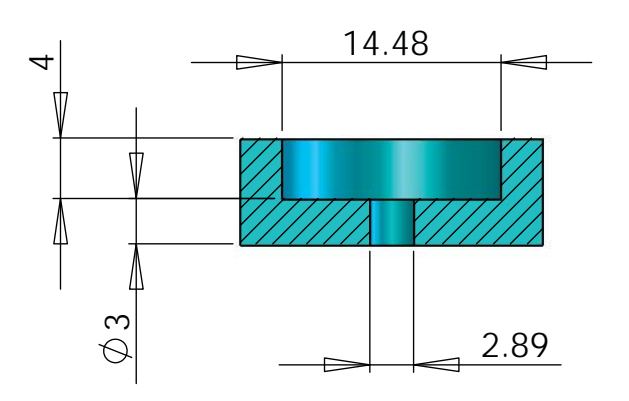


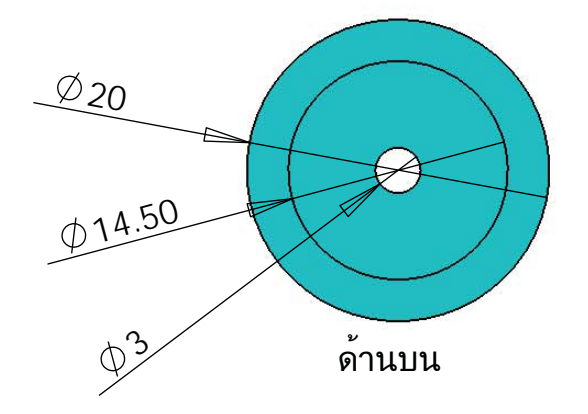
โครงการ		
	Electro Impactor Ver1	

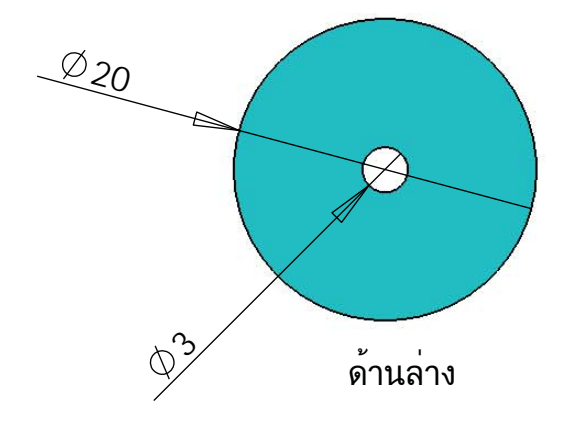
		ชื่อ - สกุล	ลายเซ็นต์	ว/ด/ป	วัสดุ	ชื่อชิ้นงาน		ขนาดกระดาษ
อ	อกแบบ	นายอาทิตย์ ยาวุฑฒิ			สแตนเลส	fce6		
เข็	ขียนแบบ	นายชัชวาลย์ กันทะลา						A4
ต	รวจสอบ	ผศ.ดร.พานิช อินต๊ะ			น้ำหนัก : n/a	มาตราส่วน 1 : 1	แผ่นที่ 6 /	

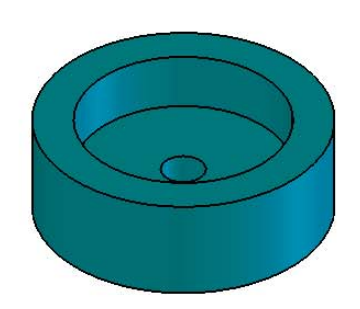




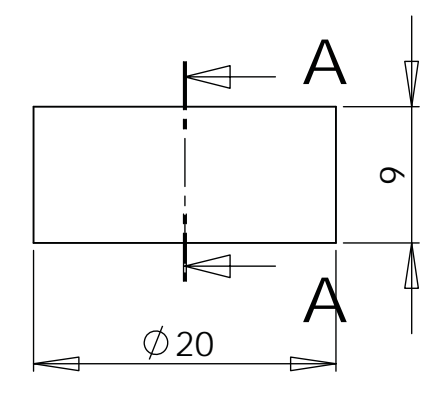


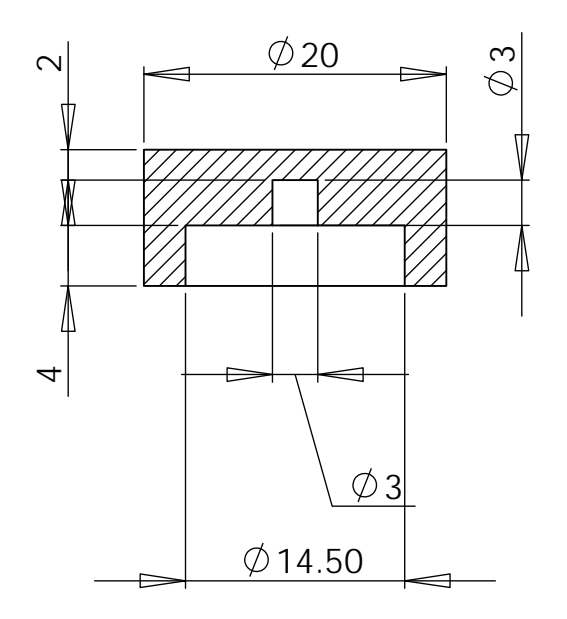


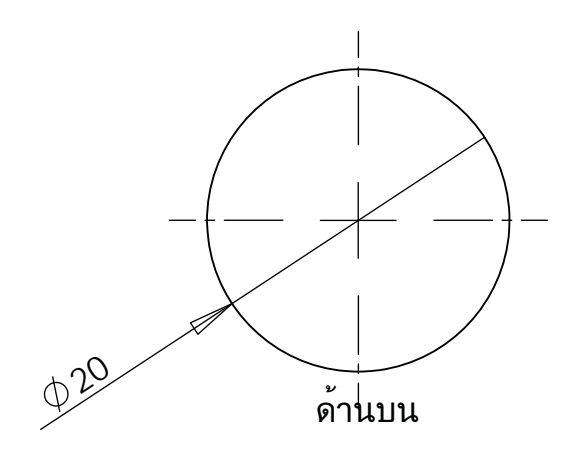


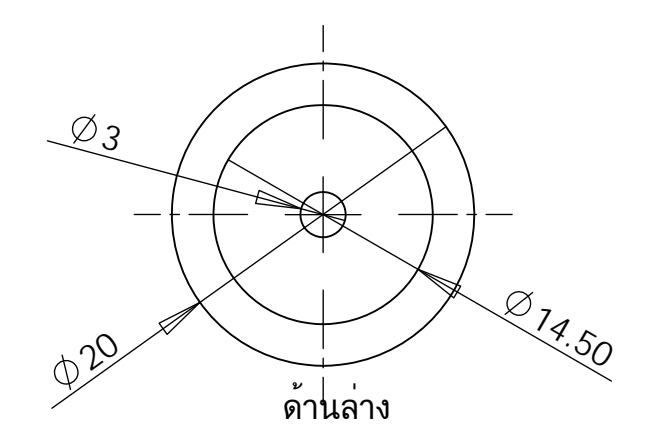


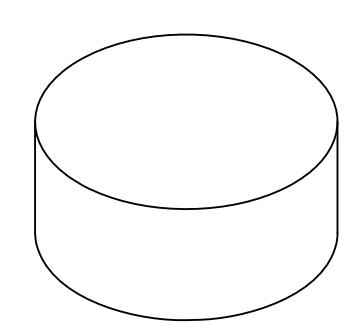
					โครงการ		
					Electro Impactor Ver1		
	ชื่อ - สกุล	ลายเซ็นต์	ว/ด/ป	วัสดุ	ชื่อชิ้นงาน		ขนาดกระดาษ
ออกแบบ	นายอาทิตย์ ยาวุฑฒิ			ดิวลีน	fec8		
เขียนแบบ	นายชัชวาลย์ กันทะลา						A4
ตรวจสอบ	ผศ.ดร.พานิช อินต๊ะ			น้ำหนัก : n/a	มาตราส่วน 2 : 1	แผ่นที่ 8 /	





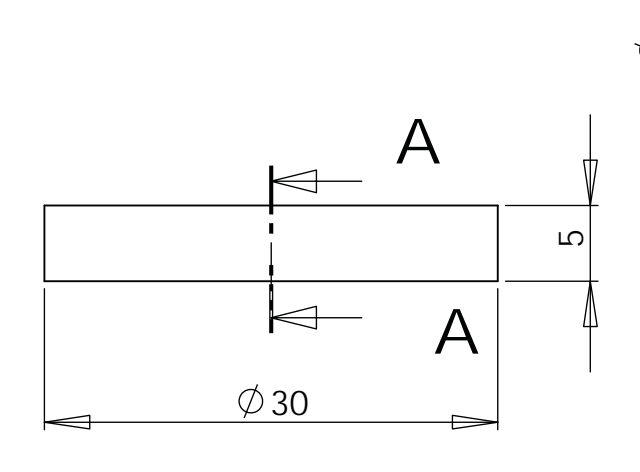


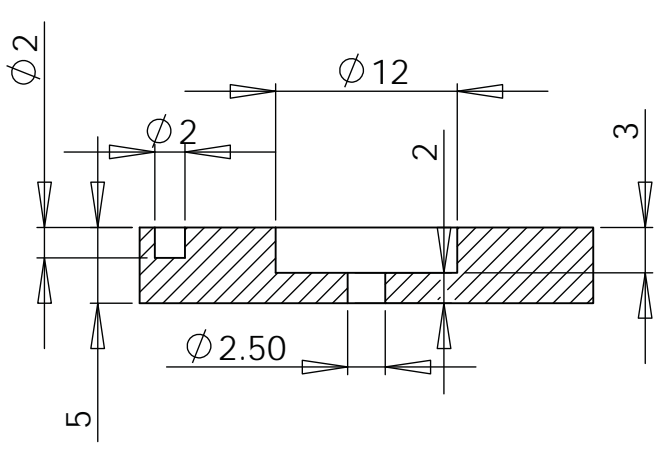


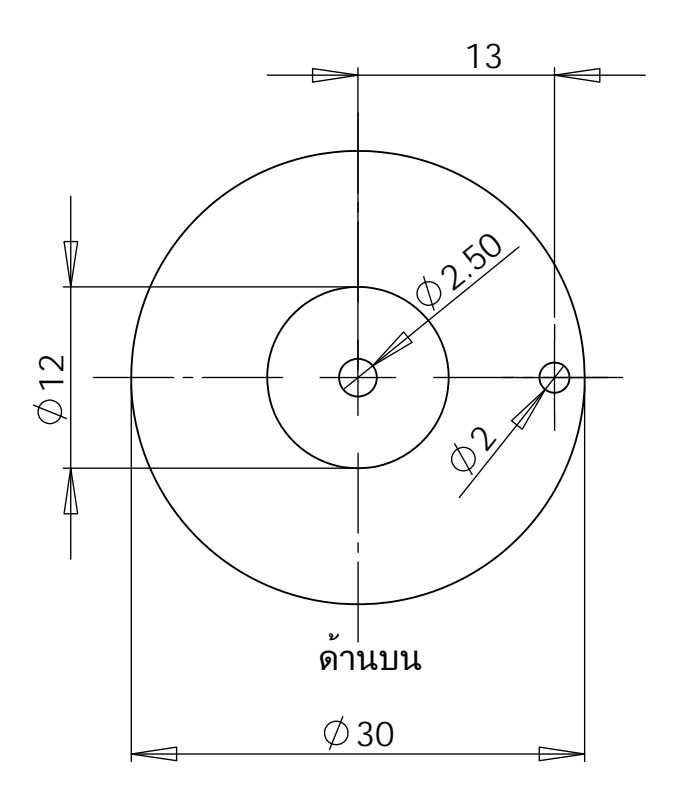


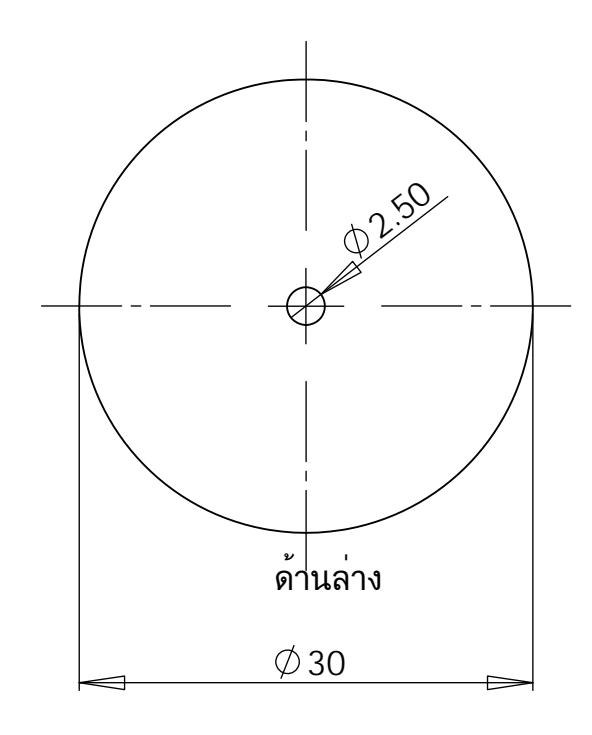
Electro Impactor Ver1

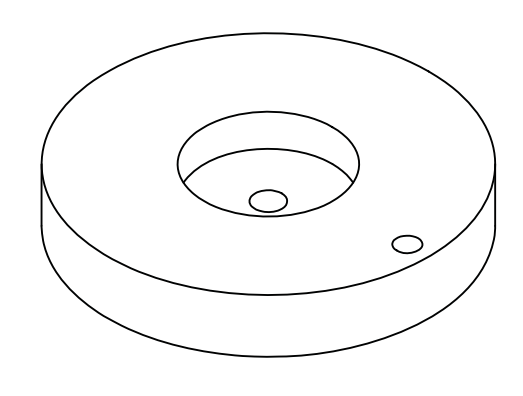
		ชื่อ - สกุล	ลายเซ็นต์	ว/ด/ป	วัสดุ	ชื่อชิ้นงาน		ขนาดกระดาษ
	ออกแบบ	นายอาทิตย์ ยาวุฑฒิ			สแตนเลส	fec9		A 4
1	เขียนแบบ	นายชัชวาลย์ กันทะลา						A4
	ตรวจสอบ	ผศ.ดร.พานิช อินต๊ะ			น้ำหนัก : n/a	มาตราส่วน 2:1	แผ่นที่ 9 /	





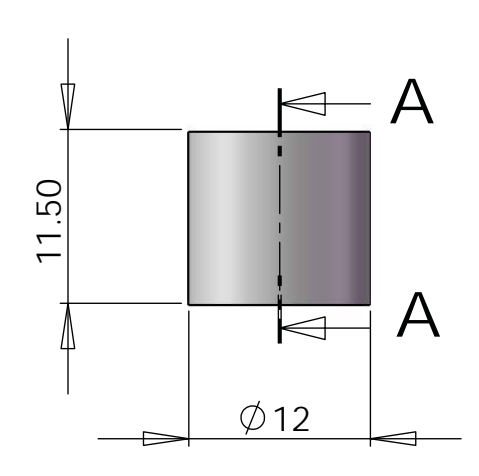


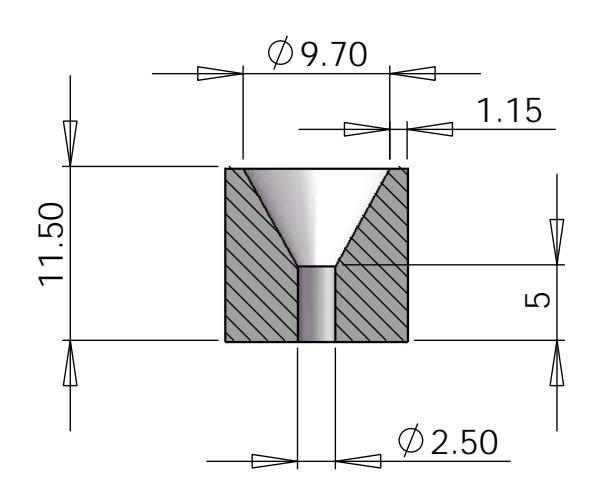


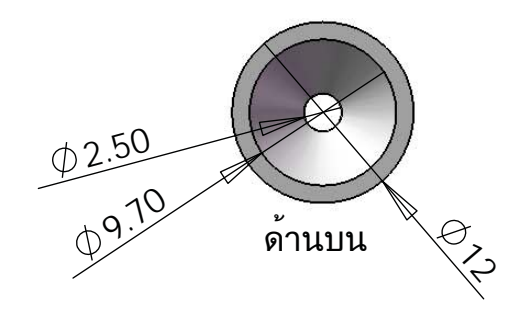


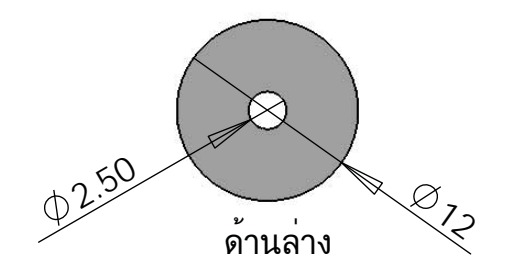
Electro Impactor Ver1

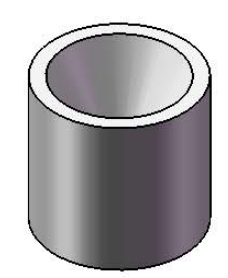
	ชื่อ - สกุล	ลายเซ็นต์	ว/ด/ป	<b>े</b> उंत्तด्	ชื่อชิ้นงาน		ขนาดกระดาษ
ออกแบบ	นายอาทิตย์ ยาวุฑฒิ			สแตนเลส	fec10		
เขียนแบบ	นายชัชวาลย์ กันทะลา						A4
ตรวจสอบ	ผศ.ดร.พานิช อินต๊ะ			น้ำหนัก : n/a	มาตราส่วน 2 : 1	แผ่นที่ 10 /	



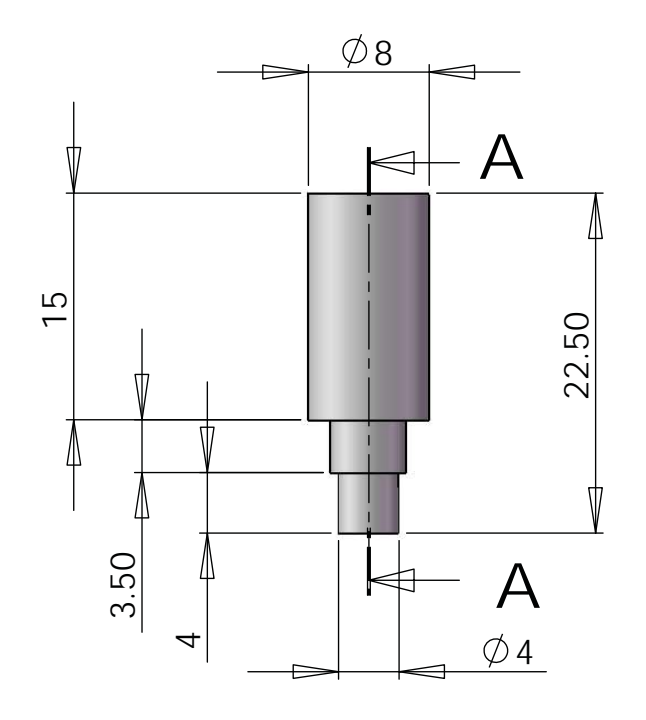


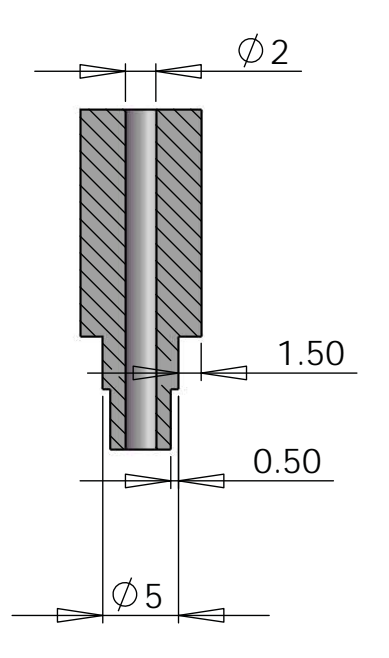






					โครงการ		
					Electro Impactor Ver1		
	ชื่อ - สกุล	ลายเซ็นต์	ว/ด/ป	วัสดุ	ชื่อชิ้นงาน		ขนาดกระดาษ
ออกแบบ	นายอาทิตย์ ยาวุฑฒิ			ดิวลีน	fec11		0.4
เขียนแบบ	นายชัชวาลย์ กันทะลา						A4
ตรวจสอบ	ผศ.ดร.พานิช อินต๊ะ			น้ำหนัก : n/a	มาตราส่วน 2 : 1	แผ่นที่ 11 /	







ว/ด/ป

น้ำหนัก : n/a

ดิวลีน

ลายเซ็นต์

ชื่อ - สกุล

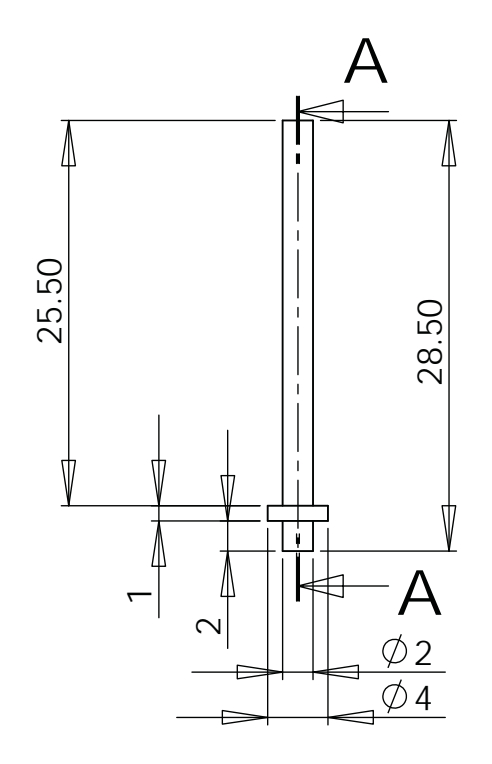
นายชัชวาลย์ กันทะลา

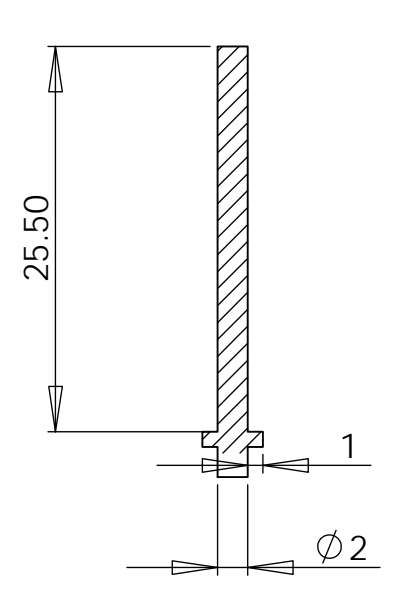
ออกแบบ นายอาทิตย์ ยาวุฑฒิ

ตรวจสอบ ผศ.ดร.พานิช อินต๊ะ

เขียนแบบ

โครงการ	
Electro Impactor Ver1	
ชื่อชิ้นงาน	ขนาดกระดาษ
fce13	A4
มาตราส่วน 2:1 แผ่นร่	i 12 /

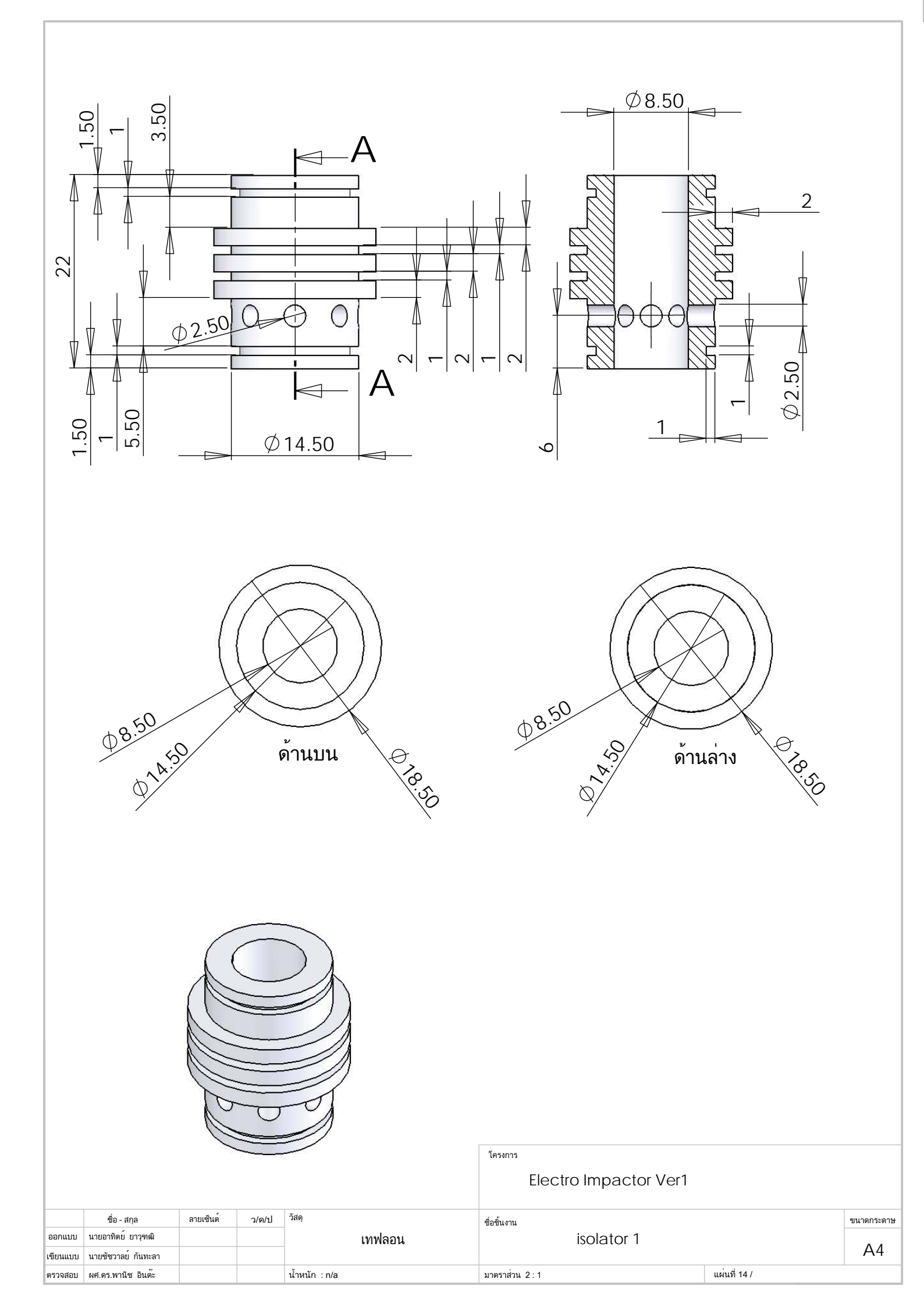


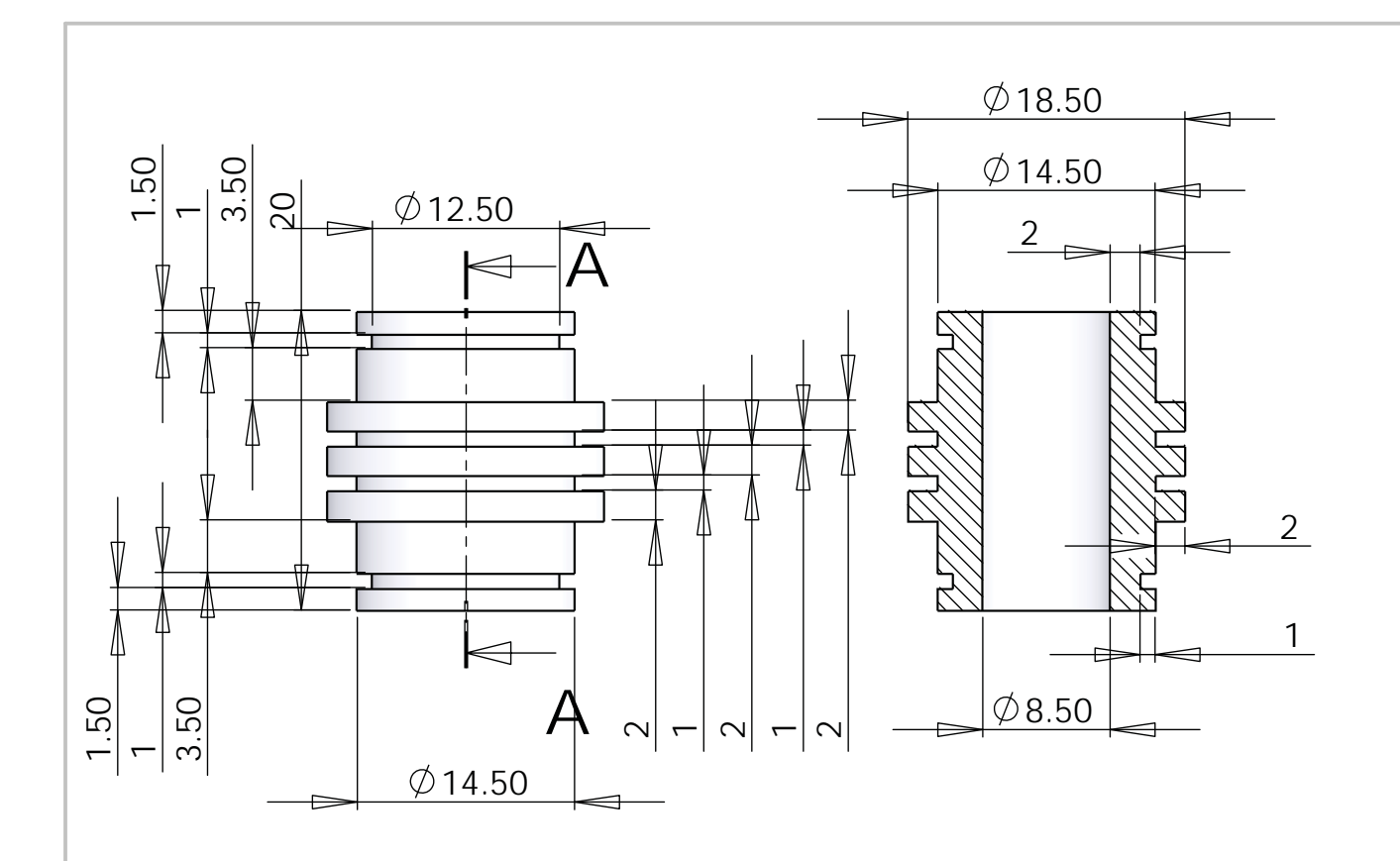


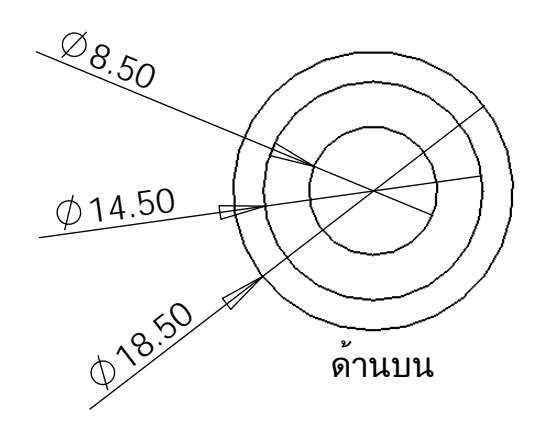


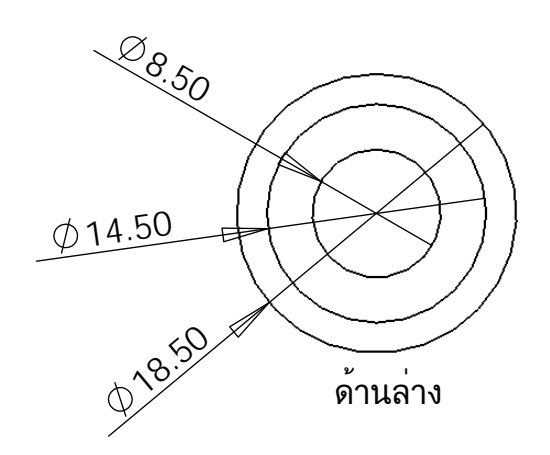
Electio impactor veri	
Electro Impactor Ver1	

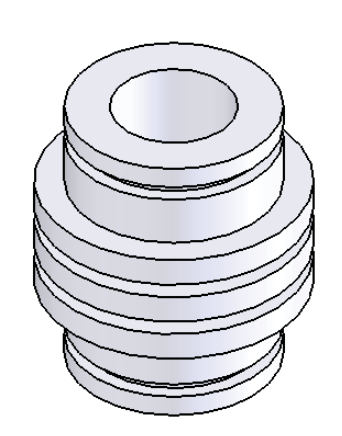
	ชื่อ - สกุล	ลายเซ็นต์	ว/ด/ป	े वेंत्र विक्	ชื่อชิ้นงาน		ขนาดกระดาษ
ออกแบบ	นายอาทิตย์ ยาวุฑฒิ			สแตนเลส	fce14		
เขียนแบบ	นายชัชวาลย์ กันทะลา						A4
ตรวจสอบ	ผศ.ดร.พานิช อินต๊ะ			น้ำหนัก : n/a	มาตราส่วน 2 : 1	แผ่นที่ 13 /	











ลายเช็นต์

ชื่อ - สกุล นายอาทิตย์ ยาวุฑฒิ

นายชัชวาลย์ กันทะลา

ตรวจสอบ ผศ.ดร.พานิช อินต๊ะ

ออกแบบ

เขียนแบบ

ว/ด/ป

น้ำหนัก : n/a

เทฟลอน

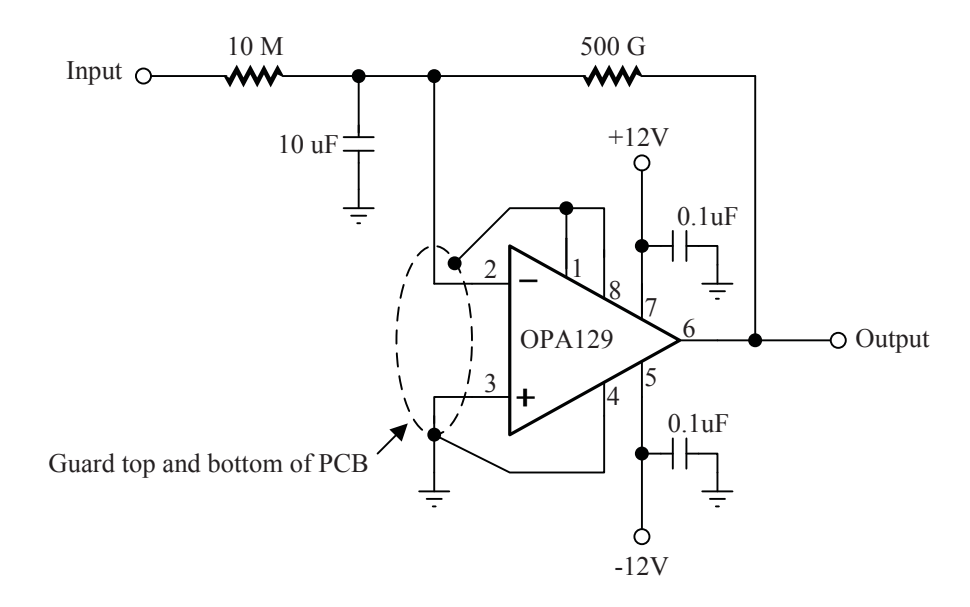
มาตราส่วน 2 : 1

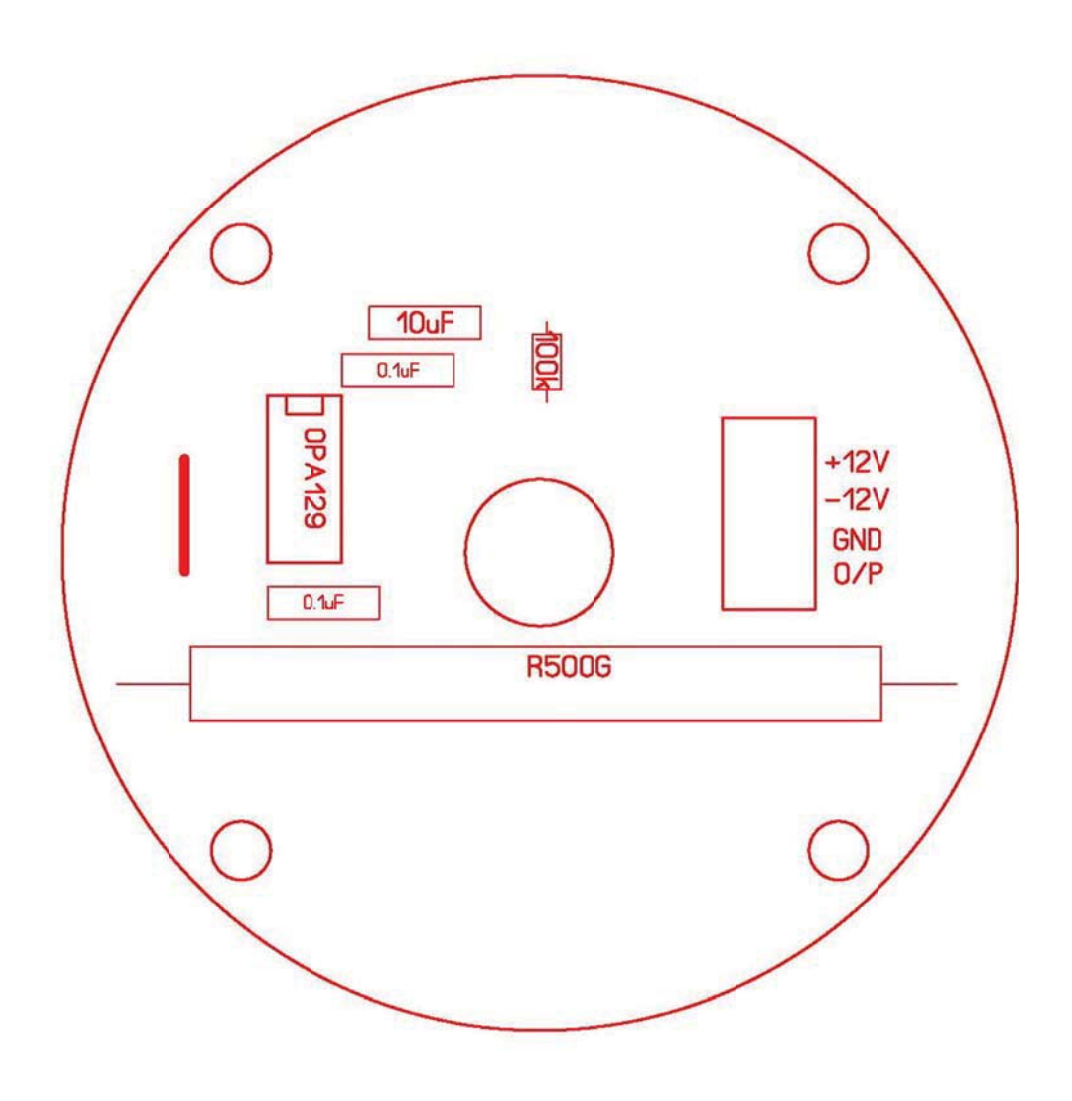
โครงการ	Electro Impactor Ver1	
ชื่อชิ้นงาน		ขนาดกระดาษ
	lsolator2	A4

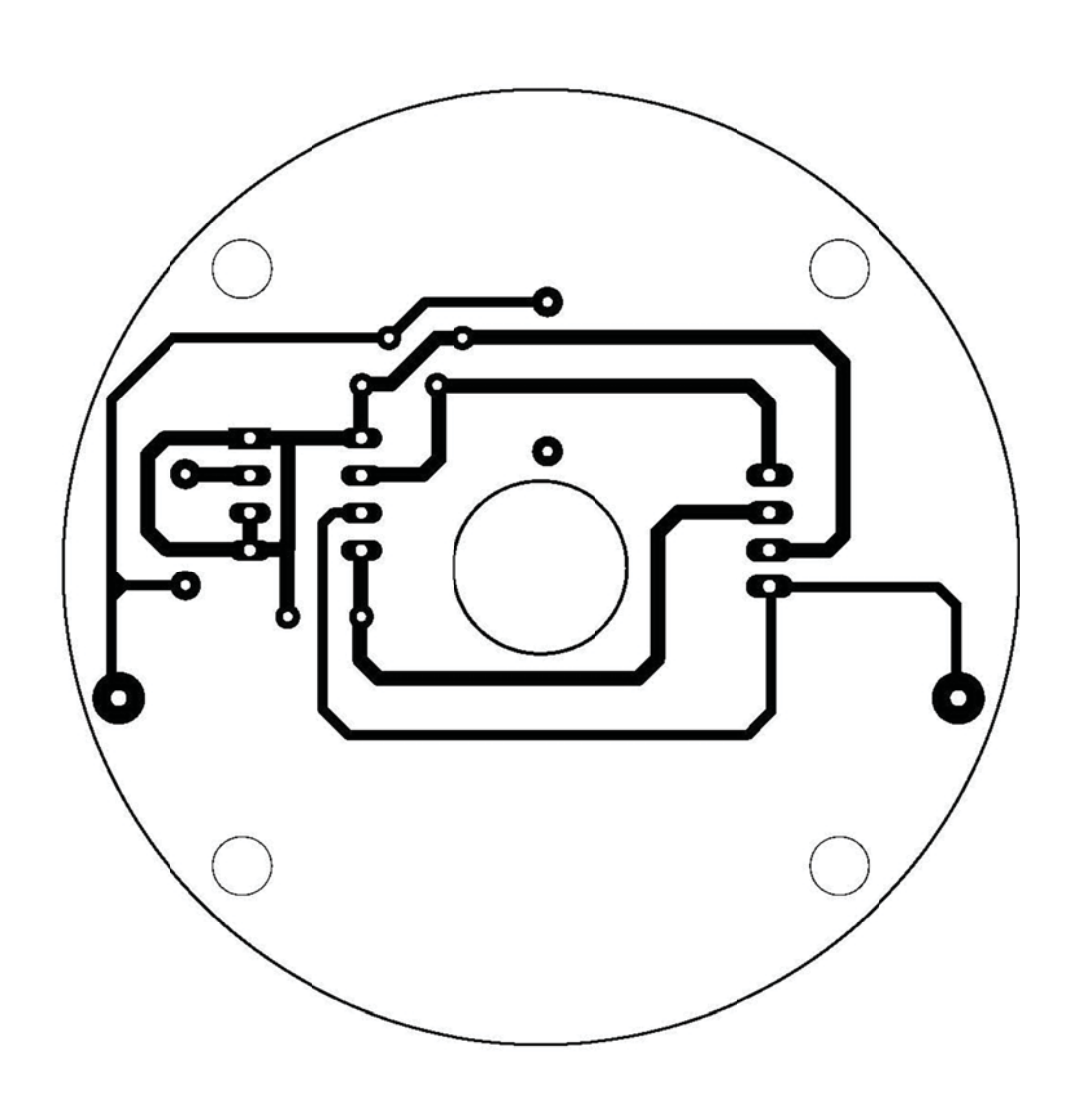
แผ่นที่ 15 /

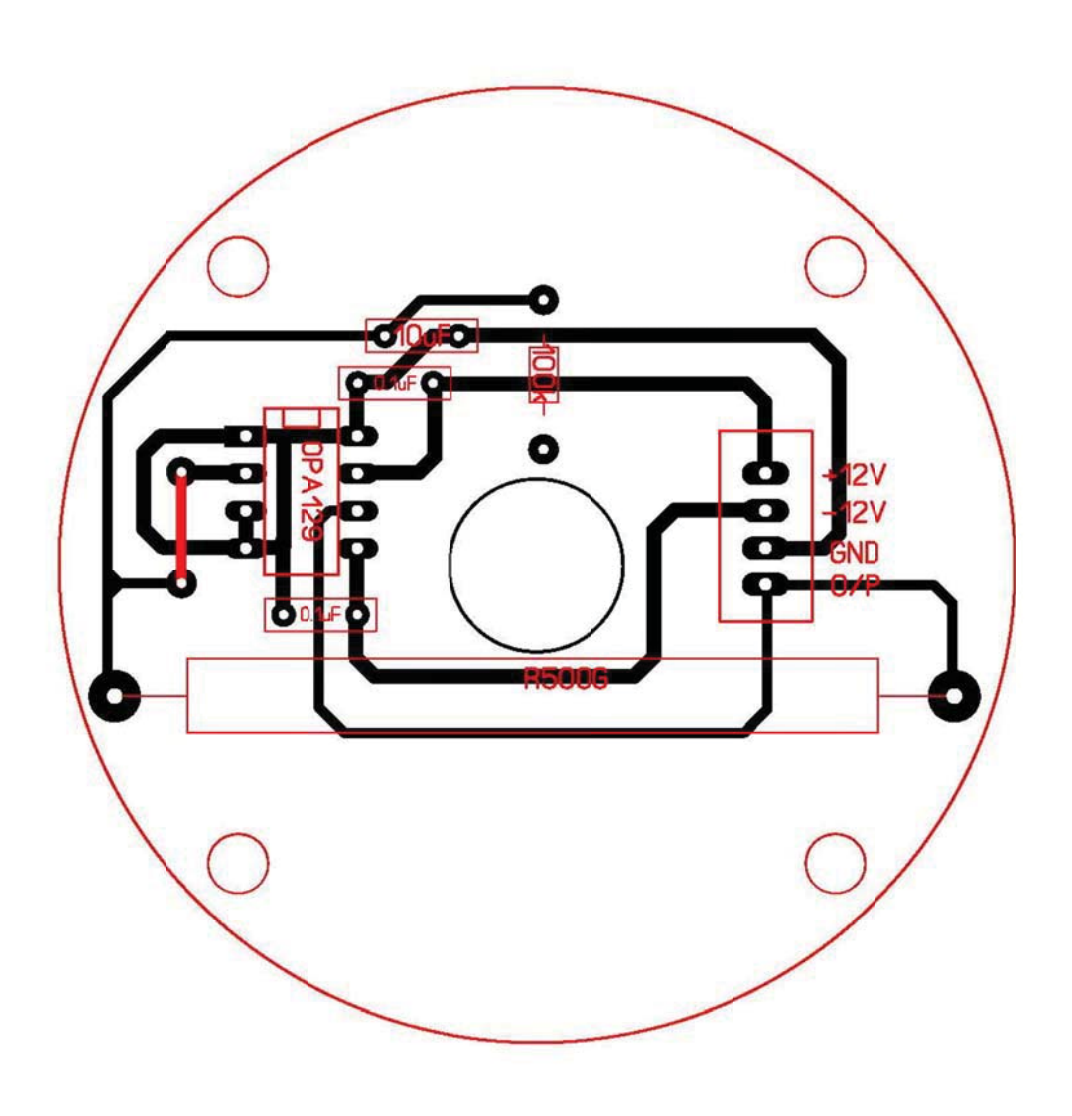
ภาคผนวก ค.4

วงจรอิเล็กโทรมิเตอร์





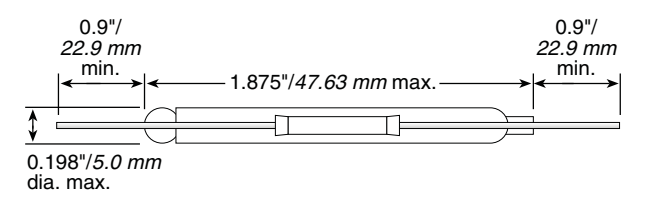


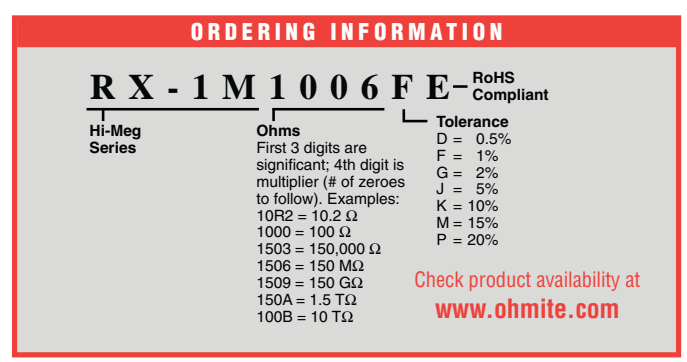


## RX-1M Hi-Meg

#### Ultra High Resistance High Stability Hermetically Sealed







These Hi-Meg resistors are designed for use in electrometer circuits where a high order of performance is required. These resistors achieve a high degree of accuracy and stability, and operate at this high performance level for an extended period of time. By being vacuum sealed in a glass envelope, these Hi-Megs are suitable for ultra-high vacuum applications.

#### **FEATURES**

- Glass sealed hermetric resistors
- Improved temperature stability
- Improved voltage stability
- Metal oxide resistive elements
- No outgassing
- RoHS compliant
- Calibration available

#### APPLICATIONS

- Ultra high vacuum
- Medical instrumentation
- · Current pulse limiters
- Avionics

#### SPECIFICATIONS

Electrical
Resistance Range:
1M to 10,000,000M

Power Rating: 0.5W at 25°C Voltage Rating: 1.0KV Temperature Coefficient: as low as 50PPM/°C

Handling and Cleaning of RX-1M Resistors:

These glass encapsulated resistors, especially those of higher resistance value, require extraordinary cleanliness. These resistors should be handled by the terminals, unless gloves are worn. Fingerprints on the surface of the resistor will attract contaminants and moisture, which will cause a parallel resistance path, reducing the resistance value of the device. If cleaning should become necessary, use isopropyl alcohol and lightly wipe dry with lint free tissues such as Kirnwipes.





SBOS026A - JANUARY 1994 - REVISED APRIL 2007

## Ultra-Low Bias Current Difet® **OPERATIONAL AMPLIFIER**

#### **FEATURES**

ULTRA-LOW BIAS CURRENT: 100fA max

● LOW OFFSET: 2mV max ● LOW DRIFT: 10μV/°C max

● HIGH OPEN-LOOP GAIN: 94dB min ● LOW NOISE: 15nV/√Hz at 10kHz • PLASTIC DIP AND SO PACKAGES

#### DESCRIPTION

The OPA129 is an ultra-low bias current monolithic operational amplifier offered in an 8-pin PDIP and SO-8 package. Using advanced geometry dielectrically-isolated FET (Difet®) inputs, this monolithic amplifier achieves a high performance level.

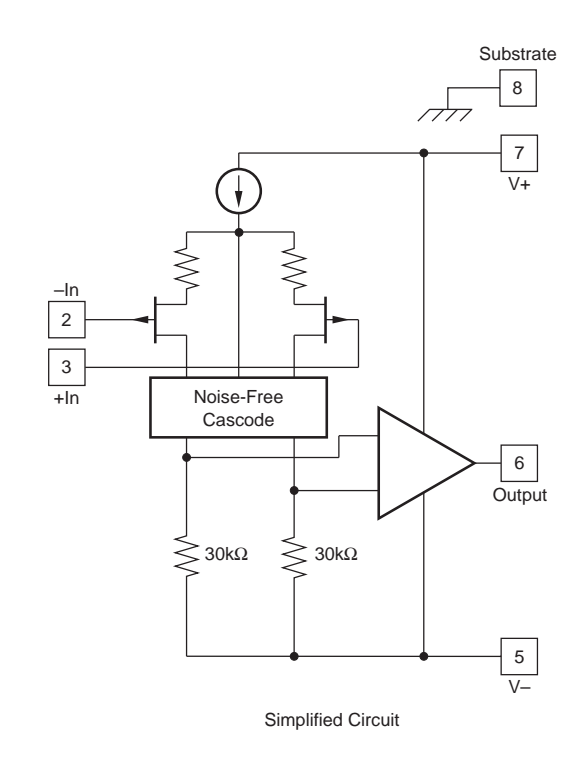
**Difet** fabrication eliminates isolation-junction leakage current—the main contributor to input bias current with conventional monolithic FETs. This reduces input bias current by a factor of 10 to 100. Very low input bias current can be achieved without resorting to small-geometry FETs or CMOS designs which can suffer from much larger offset voltage, voltage noise, drift, and poor power-supply rejection.

The OPA129 special pinout eliminates leakage current that occurs with other op amps. Pins 1 and 4 have no internal connection, allowing circuit board guard traceseven with the surface-mount package version.

OPA129 is available in 8-pin DIP and SO packages, specified for operation from -40°C to +85°C.

#### **APPLICATIONS**

- PHOTODETECTOR PREAMPS
- CHROMATOGRAPHY
- ELECTROMETER AMPLIFIERS
- MASS SPECTROMETERS
- pH PROBE AMPLIFIERS
- **ION GAGE MEASUREMENT**





Please be aware that an important notice concerning availability, standard warranty, and use in critical applications of Texas Instruments semiconductor products and disclaimers thereto appears at the end of this data sheet.

Difet is a registered trademark of Texas Instruments. All other trademarks are the property of their respective owners.



### **SPECIFICATIONS**

#### **ELECTRICAL**

At  $V_S$  =  $\pm 15 V$  and  $T_A$  = +25°C, unless otherwise noted. Pin 8 connected to ground.

		0	OPA129PB, UB		(	OPA129P, U		
PARAMETER	CONDITION	MIN	TYP	MAX	MIN	TYP	MAX	UNITS
INPUT BIAS CURRENT <sup>(1)</sup> vs Temperature	V <sub>CM</sub> = 0V	Doi	±30 ubles every 1	±100 0°C		*	±250	fA
INPUT OFFSET CURRENT	V <sub>CM</sub> = 0V		±30			*		fA
OFFSET VOLTAGE Input Offset Voltage vs Temperature Supply Rejection	$V_{CM} = 0V$ $V_{S} = \pm 5V \text{ to } \pm 18V$		±0.5 ±3 ±3	±2 ±10 ±100		±1 ±5 *	±5 *	mV μV/°C μV/V
NOISE Voltage Current	$f = 10Hz$ $f = 100Hz$ $f = 1kHz$ $f = 10kHz$ $f_B = 0.1Hz \text{ to } 10Hz$ $f = 10kHz$		85 28 17 15 4 0.1			* * * * * * * *		$\begin{array}{c} \text{nV}/\sqrt{\text{Hz}} \\ \text{nV}/\sqrt{\text{Hz}} \\ \text{nV}/\sqrt{\text{Hz}} \\ \text{nV}/\sqrt{\text{Hz}} \\ \text{\muV}_{PP} \\ \text{fA}/\sqrt{\text{Hz}} \end{array}$
INPUT IMPEDANCE Differential Common-Mode			10 <sup>13</sup>    1 10 <sup>15</sup>    2			*		Ω    pF Ω    pF
VOLTAGE RANGE Common-Mode Input Range Common-Mode Rejection	V <sub>IN</sub> = ±10V	±10 80	±12 118		*	*		V dB
OPEN-LOOP GAIN, DC Open-Loop Voltage Gain	$R_L \ge 2k\Omega$	94	120		*	*		dB
FREQUENCY RESPONSE Unity Gain, Small Signal Full Power Response Slew Rate Settling Time: 0.1% 0.01% Overload Recovery, 50% Overdrive(2)	20Vp-p, $R_L = 2k\Omega$ $V_O = \pm 10V$ , $R_L = 2k\Omega$ $G = -1$ , $R_L = 2k\Omega$ , 10V Step G = -1	1	1 47 2.5 5 10 5		*	* * * * * * *		MHz kHz V/µs µs µs µs
RATED OUTPUT Voltage Output Current Output Load Capacitance Stability Short-Circuit Current	$R_{L} = 2k\Omega$ $V_{O} = \pm 12V$ $Gain = +1$	±12 ±6	±13 ±10 1000 ±35	±55	*	* * * *	*	V mA pF mA
POWER SUPPLY Rated Voltage Voltage Range, Derated Performance Current, Quiescent	I <sub>O</sub> = 0mA	±5	±15	±18 1.8	*	*	*	V V mA
TEMPERATURE Specification Operating Storage Thermal Resistance DIP-8	Ambient Temperature Ambient Temperature $ heta_{ m JA}$ , Junction-to-Ambient	-40 -40 -40	90	+85 +125 +125	* *	*	* *	°C °C °C
SO-8			100			*		°C/W



NOTES: (1) High-speed automated test.

(2) Overload recovery is defined as the time required for the output to return from saturation to linear operation following the removal of a 50% input

#### **ABSOLUTE MAXIMUM RATINGS**

Power Supply Voltage	±18V
Differential Input Voltage	V– to V+
Input Voltage Range	V– to V+
Storage Temperature Range	40°C to +125°C
Operating Temperature Range	40°C to +125°C
Output Short Circuit Duration(1)	Continuous
Junction Temperature (T <sub>J</sub> )	+150°C

NOTE: (1) Short circuit may be to power supply common at +25°C ambient.

# ELECTROSTATIC DISCHARGE SENSITIVITY

Any integrated circuit can be damaged by ESD. Texas Instruments recommends that all integrated circuits be handled with appropriate precautions. Failure to observe proper handling and installation procedures can cause damage.

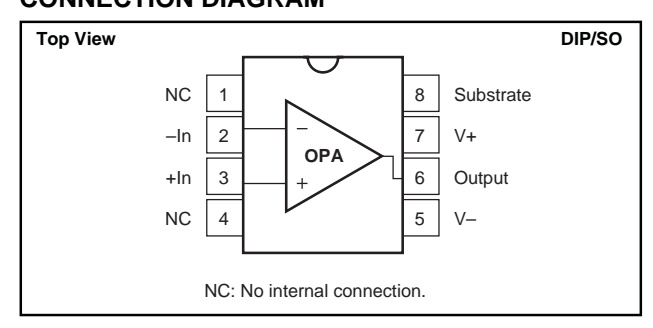
ESD damage can range from subtle performance degradation to complete device failure. Precision integrated circuits may be more susceptible to damage because very small parametric changes could cause the device not to meet published specifications.

#### PACKAGE INFORMATION(1)

PRODUCT	•	PACKAGE-LEAD	PACKAGE DESIGNATOR
OPA129P		DIP-8	Р
OPA129PE	3	DIP-8	Р
OPA129U		SO-8	D
OPA129UE	3	SO-8	D

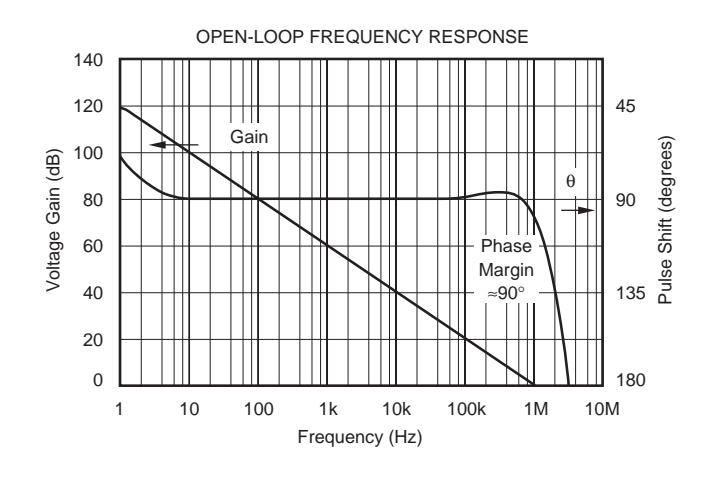
NOTE: (1) For the most current package and ordering information, see the Package Option Addendum at the end of this data sheet, or see the TI website at www.ti.com.

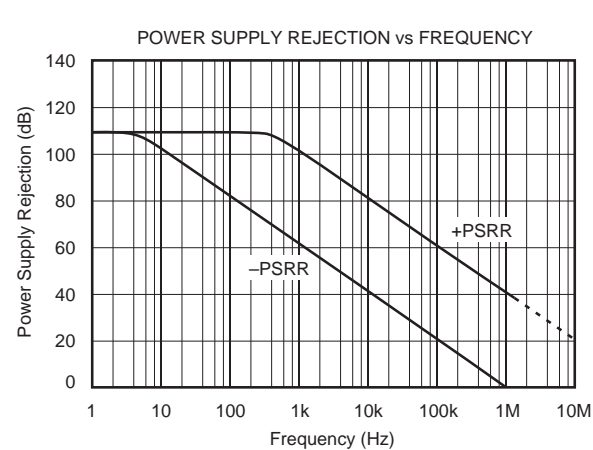
#### **CONNECTION DIAGRAM**



#### TYPICAL PERFORMANCE CURVES

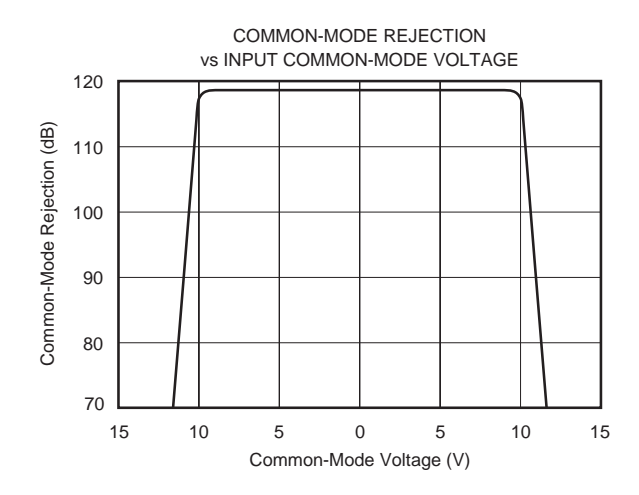
At  $T_A = +25$ °C, +15VDC, unless otherwise noted.

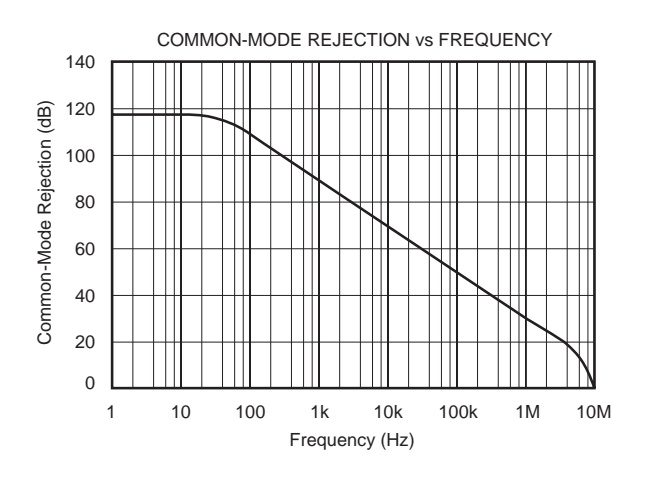


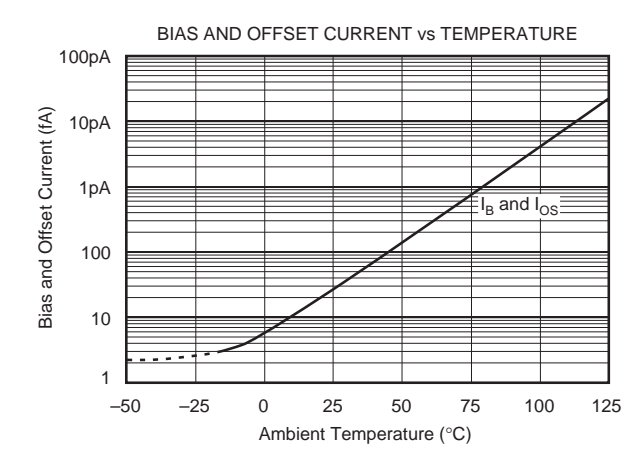


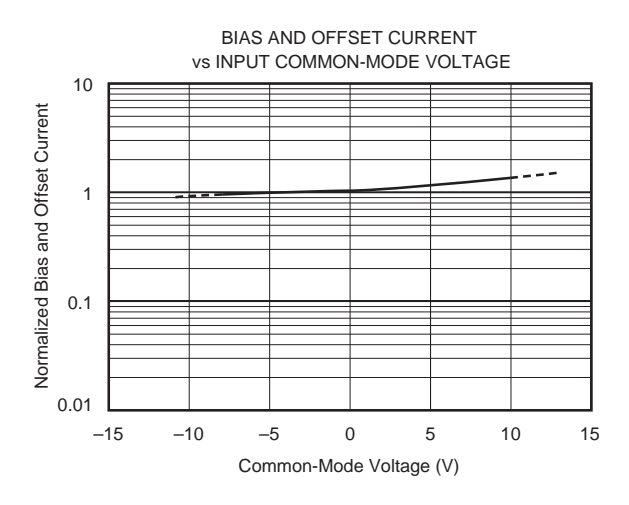
# TYPICAL PERFORMANCE CURVES (Cont.)

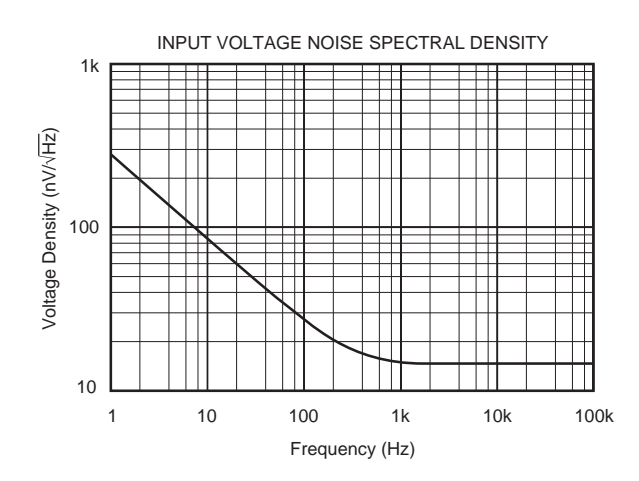
At  $T_A = +25$ °C, +15VDC, unless otherwise noted.

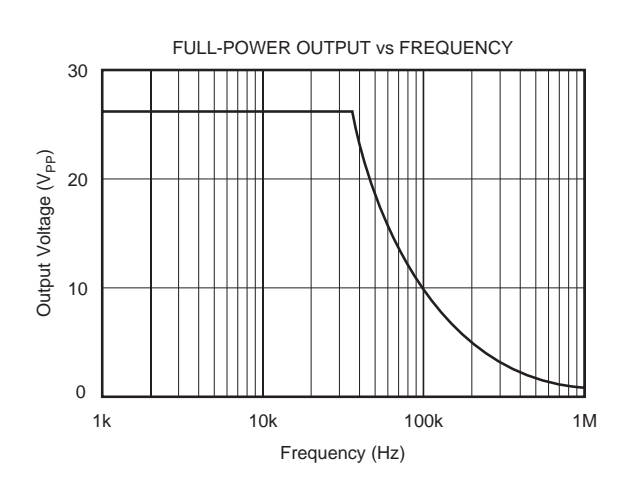








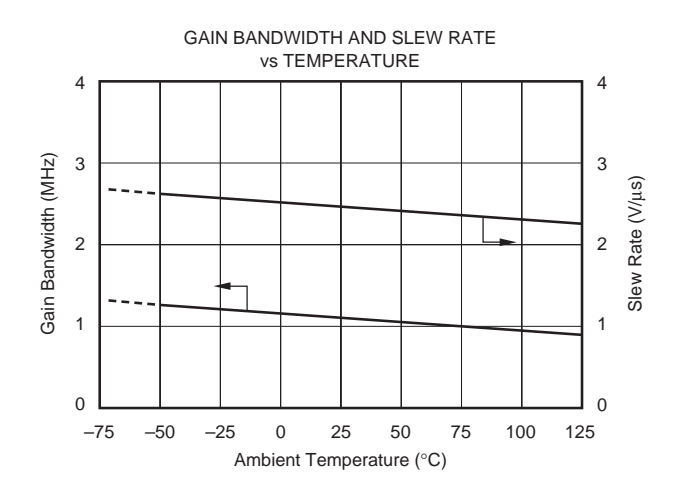


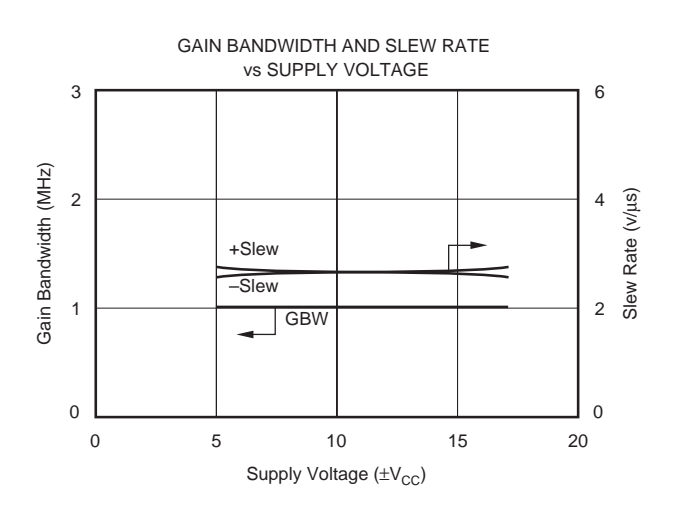


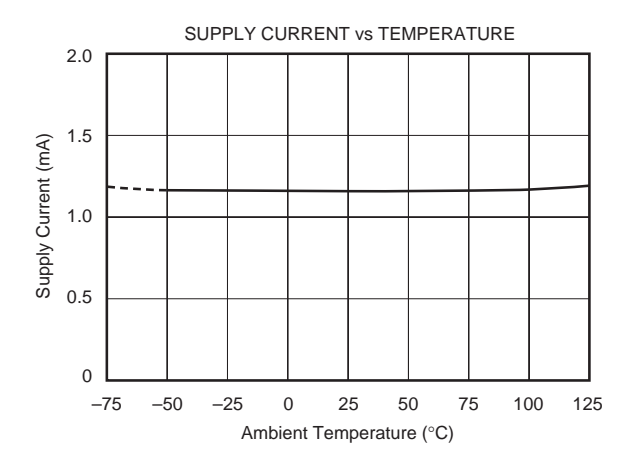


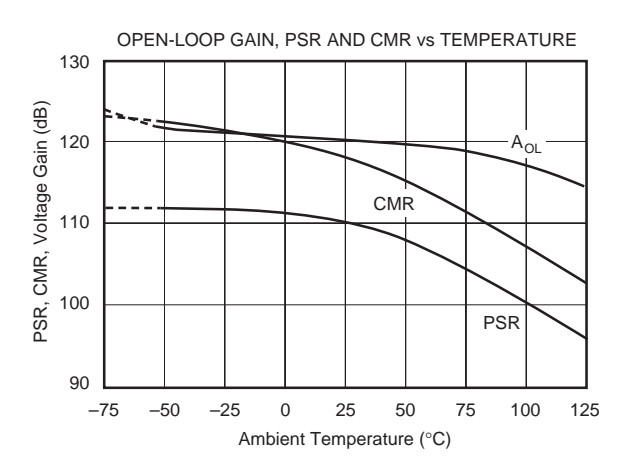
# **TYPICAL PERFORMANCE CURVES (Cont.)**

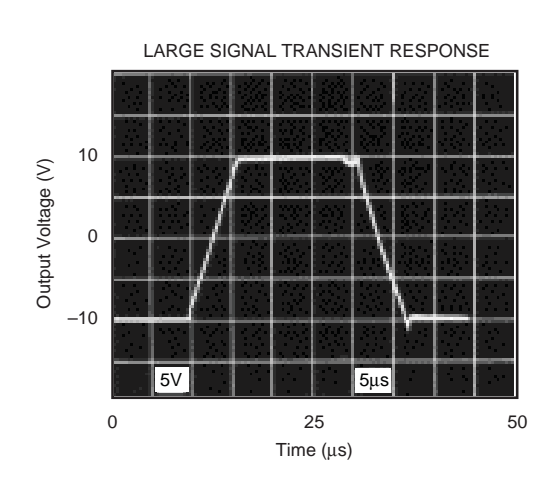
At  $T_A = +25^{\circ}C$ , +15VDC, unless otherwise noted.

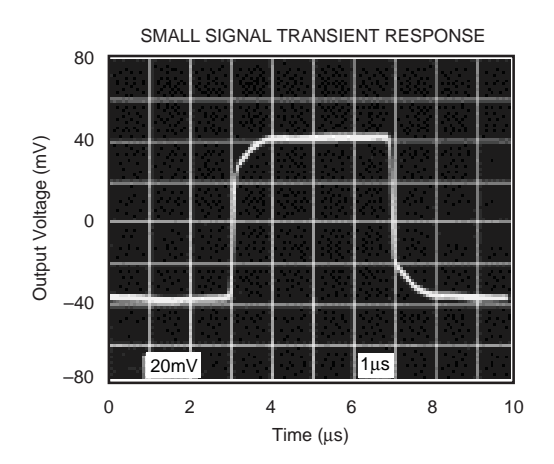








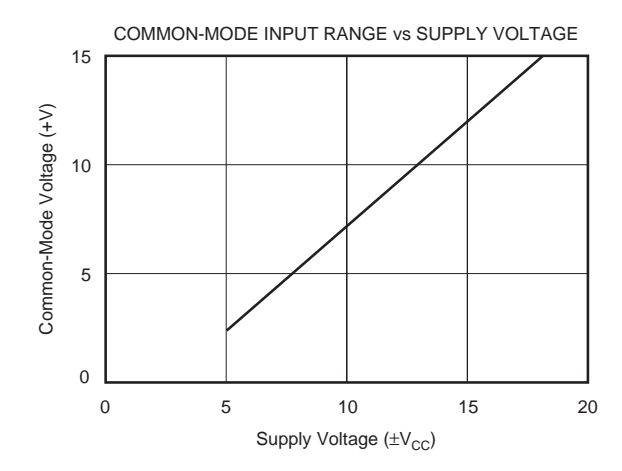


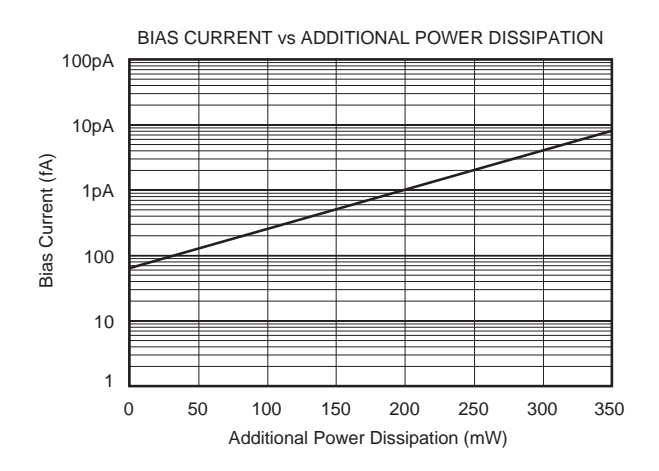




# TYPICAL PERFORMANCE CURVES (CONT)

 $T_A = +25^{\circ}C$ , +15VDC, unless otherwise noted.





#### APPLICATIONS INFORMATION

#### **NON-STANDARD PINOUT**

The OPA129 uses a non-standard pinout to achieve lowest possible input bias current. The negative power supply is connected to pin 5—see Figure 1. This is done to reduce the leakage current from the V- supply (pin 4 on conventional op amps) to the op amp input terminals. With this new pinout, sensitive inputs are separated from both power supply pins.

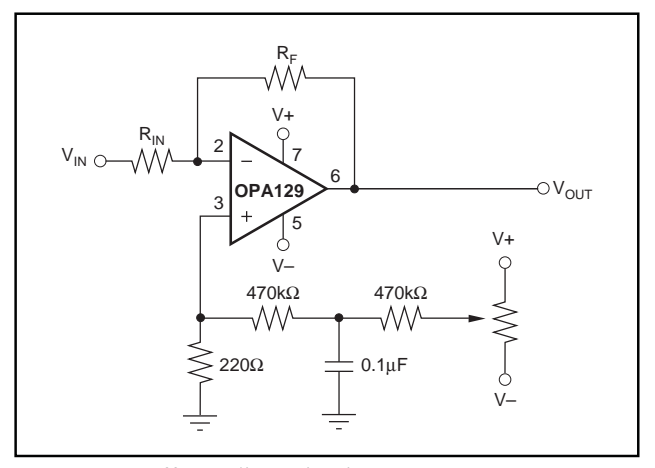


FIGURE 1. Offset Adjust Circuit.

#### **OFFSET VOLTAGE TRIM**

The OPA129 has no conventional offset trim connections. Pin 1, next to the critical inverting input, has no internal connection. This eliminates a source of leakage current and allows guarding of the input terminals. Pin 1 and pin 4, next to the two input pins, have no internal connection. This allows an optimized circuit board layout with guarding—see the *Circuit Board Layout* section.

Due to its laser-trimmed input stage, most applications do not require external offset voltage trimming. If trimming is required, the circuit shown in Figure 1 can be used. Power supply voltages are divided down, filtered and applied to the non-inverting input. The circuit shown is sensitive to variation in the supply voltages. Regulation can be added, if needed

#### **GUARDING AND SHIELDING**

Ultra-low input bias current op amps require precautions to achieve best performance. Leakage current on the surface of circuit board can exceed the input bias current of the amplifier. For example, a circuit board resistance of  $10^{12}\Omega$  from a power supply pin to an input pin produces a current of 15pA—more than 100 times the input bias current of the op amp.

To minimize surface leakage, a guard trace should completely surround the input terminals and other circuitry connecting to the inputs of the op amp. The DIP package should have a guard trace on both sides of the circuit board. The guard ring should be driven by a circuit node equal in potential to the op amp inputs—see Figure 2. The substrate, pin 8, should also be connected to the circuit board guard to assure that the amplifier is fully surrounded by the guard potential. This minimizes leakage current and noise pick-up. Careful shielding is required to reduce noise pickup. Shielding near feedback components may also help reduce noise pick-up.

Triboelectric effects (friction-generated charge) can be a troublesome source of errors. Vibration of the circuit board, input connectors and input cables can cause noise and drift. Make the assembly as rigid as possible. Attach cables to avoid motion and vibration. Special low noise or low leakage cables may help reduce noise and leakage current. Keep all input connections as short possible. Surface-mount components may reduce circuit board size and allow a more rigid assembly.



#### **CIRCUIT BOARD LAYOUT**

The OPA129 uses a new pinout for ultra low input bias current. Pin 1 and pin 4 have no internal connection. This allows ample circuit board space for a guard ring surrounding the op amp input pins—even with the tiny SO-8 surfacemount package. Figure 3 shows suggested circuit board layouts. The guard ring should be connected to pin 8 (substrate) as shown. It should be driven by a circuit node equal in potential to the input terminals of the op amp—see Figure 2 for common circuit configurations.

#### **TESTING**

Accurately testing the OPA129 is extremely difficult due to its high performance. Ordinary test equipment may not be able to resolve the amplifier's extremely low bias current.

Inaccurate bias current measurements can be due to:

- 1. Test socket leakage.
- 2. Unclean package.
- 3. Humidity or dew point condensations.
- 4. Circuit contamination from fingerprints or anti-static treatment chemicals.
- 5. Test ambient temperature.
- 6. Load power dissipation.
- 7. Mechanical stress.
- 8. Electrostatic and electromagnetic interference.

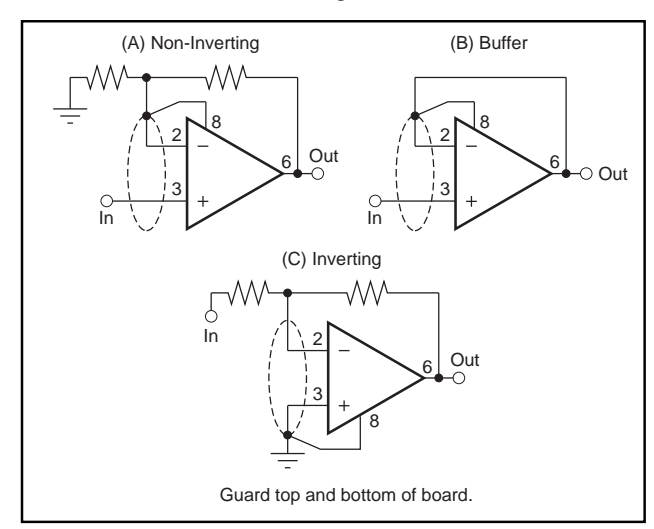


FIGURE 2. Connection of Input Guard.

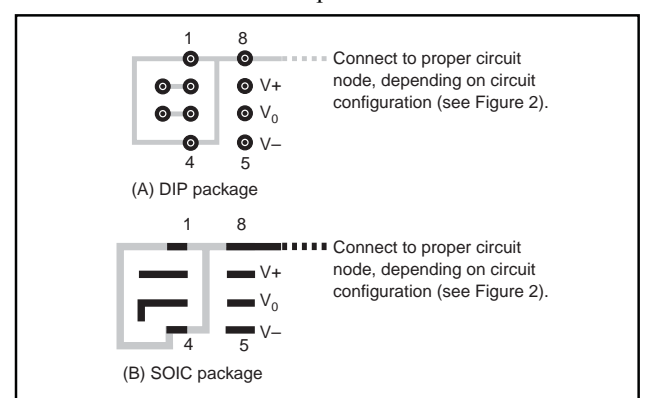


FIGURE 3. Suggested Board Layout for Input Guard.

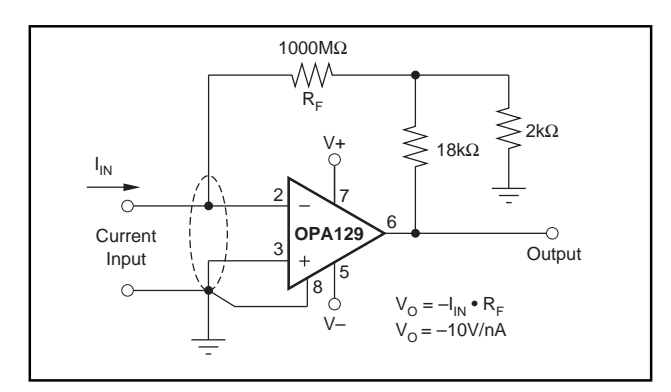


FIGURE 4. Current-to-Voltage Converter.

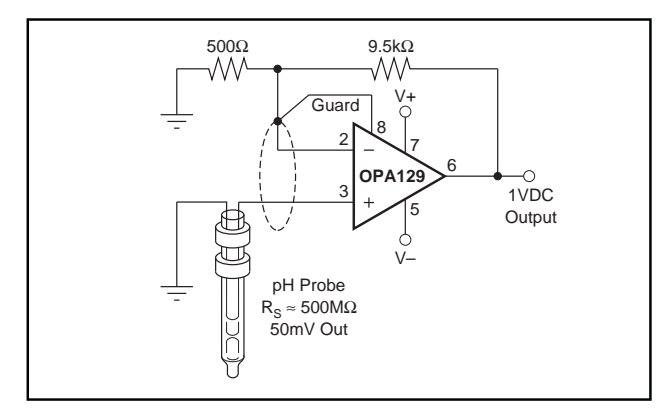


FIGURE 5. High Impedance ( $10^{15}\Omega$ ) Amplifier.

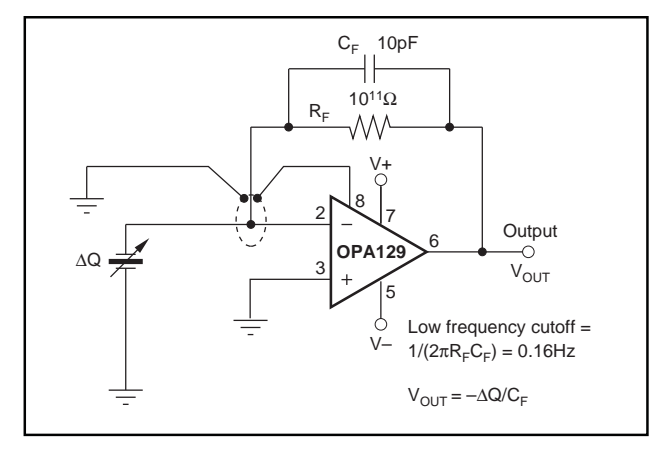


FIGURE 6. Piezoelectric Transducer Charge Amplifier.

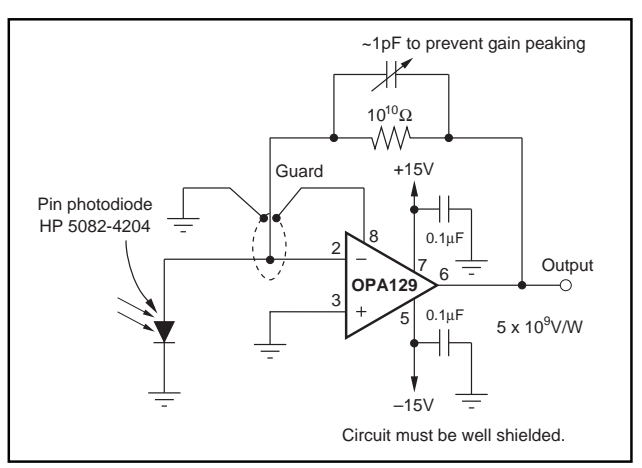


FIGURE 7. Sensitive Photodiode Amplifier.



#### PACKAGE OPTION ADDENDUM

24-Feb-2009

#### PACKAGING INFORMATION

Orderable Device	Status <sup>(1)</sup>	Package Type	Package Drawing	Pins	Package Qty	Eco Plan <sup>(2)</sup>	Lead/Ball Finish	MSL Peak Temp <sup>(3)</sup>
OPA129P	OBSOLETE	PDIP	Р	8		TBD	Call TI	Call TI
OPA129PB	OBSOLETE	PDIP	Р	8		TBD	Call TI	Call TI
OPA129U	ACTIVE	SOIC	D	8	75	Green (RoHS & no Sb/Br)	CU NIPDAU	Level-3-260C-168 HR
OPA129UB	ACTIVE	SOIC	D	8	75	Green (RoHS & no Sb/Br)	CU NIPDAU	Level-3-260C-168 HR
OPA129UB/2K5	ACTIVE	SOIC	D	8	2500	Green (RoHS & no Sb/Br)	CU NIPDAU	Level-3-260C-168 HR
OPA129UB/2K5E4	ACTIVE	SOIC	D	8	2500	Green (RoHS & no Sb/Br)	CU NIPDAU	Level-3-260C-168 HR
OPA129UBE4	ACTIVE	SOIC	D	8	75	Green (RoHS & no Sb/Br)	CU NIPDAU	Level-3-260C-168 HR
OPA129UBG4	ACTIVE	SOIC	D	8	75	Green (RoHS & no Sb/Br)	CU NIPDAU	Level-3-260C-168 HR
OPA129UE4	ACTIVE	SOIC	D	8	75	Green (RoHS & no Sb/Br)	CU NIPDAU	Level-3-260C-168 HR

(1) The marketing status values are defined as follows:

ACTIVE: Product device recommended for new designs.

LIFEBUY: TI has announced that the device will be discontinued, and a lifetime-buy period is in effect.

**NRND:** Not recommended for new designs. Device is in production to support existing customers, but TI does not recommend using this part in a new design.

PREVIEW: Device has been announced but is not in production. Samples may or may not be available.

**OBSOLETE:** TI has discontinued the production of the device.

(2) Eco Plan - The planned eco-friendly classification: Pb-Free (RoHS), Pb-Free (RoHS Exempt), or Green (RoHS & no Sb/Br) - please check http://www.ti.com/productcontent for the latest availability information and additional product content details.

**TBD:** The Pb-Free/Green conversion plan has not been defined.

**Pb-Free** (RoHS): Ti's terms "Lead-Free" or "Pb-Free" mean semiconductor products that are compatible with the current RoHS requirements for all 6 substances, including the requirement that lead not exceed 0.1% by weight in homogeneous materials. Where designed to be soldered at high temperatures, TI Pb-Free products are suitable for use in specified lead-free processes.

**Pb-Free (RoHS Exempt):** This component has a RoHS exemption for either 1) lead-based flip-chip solder bumps used between the die and package, or 2) lead-based die adhesive used between the die and leadframe. The component is otherwise considered Pb-Free (RoHS compatible) as defined above.

Green (RoHS & no Sb/Br): TI defines "Green" to mean Pb-Free (RoHS compatible), and free of Bromine (Br) and Antimony (Sb) based flame retardants (Br or Sb do not exceed 0.1% by weight in homogeneous material)

(3) MSL, Peak Temp. -- The Moisture Sensitivity Level rating according to the JEDEC industry standard classifications, and peak solder temperature.

Important Information and Disclaimer: The information provided on this page represents TI's knowledge and belief as of the date that it is provided. TI bases its knowledge and belief on information provided by third parties, and makes no representation or warranty as to the accuracy of such information. Efforts are underway to better integrate information from third parties. TI has taken and continues to take reasonable steps to provide representative and accurate information but may not have conducted destructive testing or chemical analysis on incoming materials and chemicals. TI and TI suppliers consider certain information to be proprietary, and thus CAS numbers and other limited information may not be available for release.

In no event shall TI's liability arising out of such information exceed the total purchase price of the TI part(s) at issue in this document sold by TI to Customer on an annual basis.

# **PACKAGE MATERIALS INFORMATION**

www.ti.com 14-Jul-2009

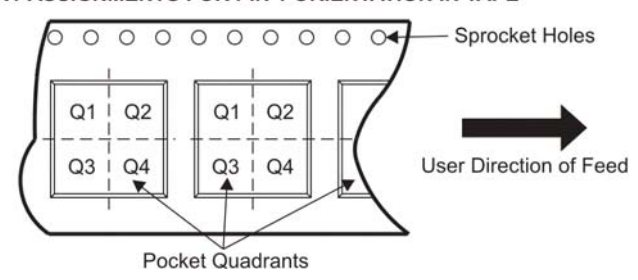
#### TAPE AND REEL INFORMATION

# REEL DIMENSIONS Reel Diameter Reel Width (W1)

# TAPE DIMENSIONS + K0 - P1 - B0 W

A0	Dimension designed to accommodate the component width
	Dimension designed to accommodate the component length
K0	Dimension designed to accommodate the component thickness
W	Overall width of the carrier tape
P1	Pitch between successive cavity centers

#### QUADRANT ASSIGNMENTS FOR PIN 1 ORIENTATION IN TAPE



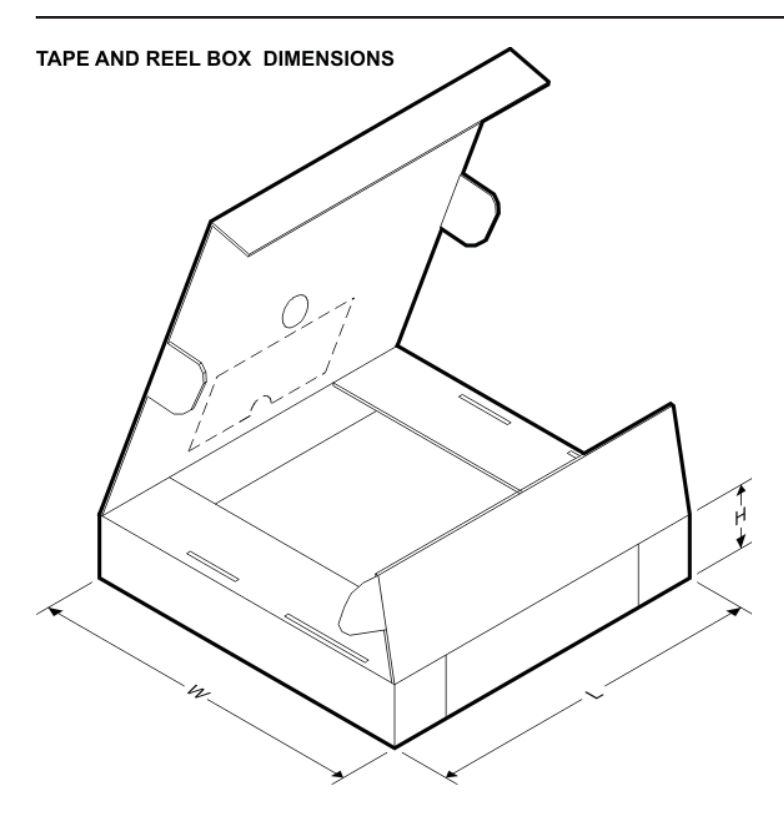
#### \*All dimensions are nominal

Device	Package Type	Package Drawing			Reel Diameter (mm)	Reel Width W1 (mm)	A0 (mm)	B0 (mm)	K0 (mm)	P1 (mm)	W (mm)	Pin1 Quadrant
OPA129UB/2K5	SOIC	D	8	2500	330.0	12.4	6.4	5.2	2.1	8.0	12.0	Q1



# PACKAGE MATERIALS INFORMATION

www.ti.com 14-Jul-2009

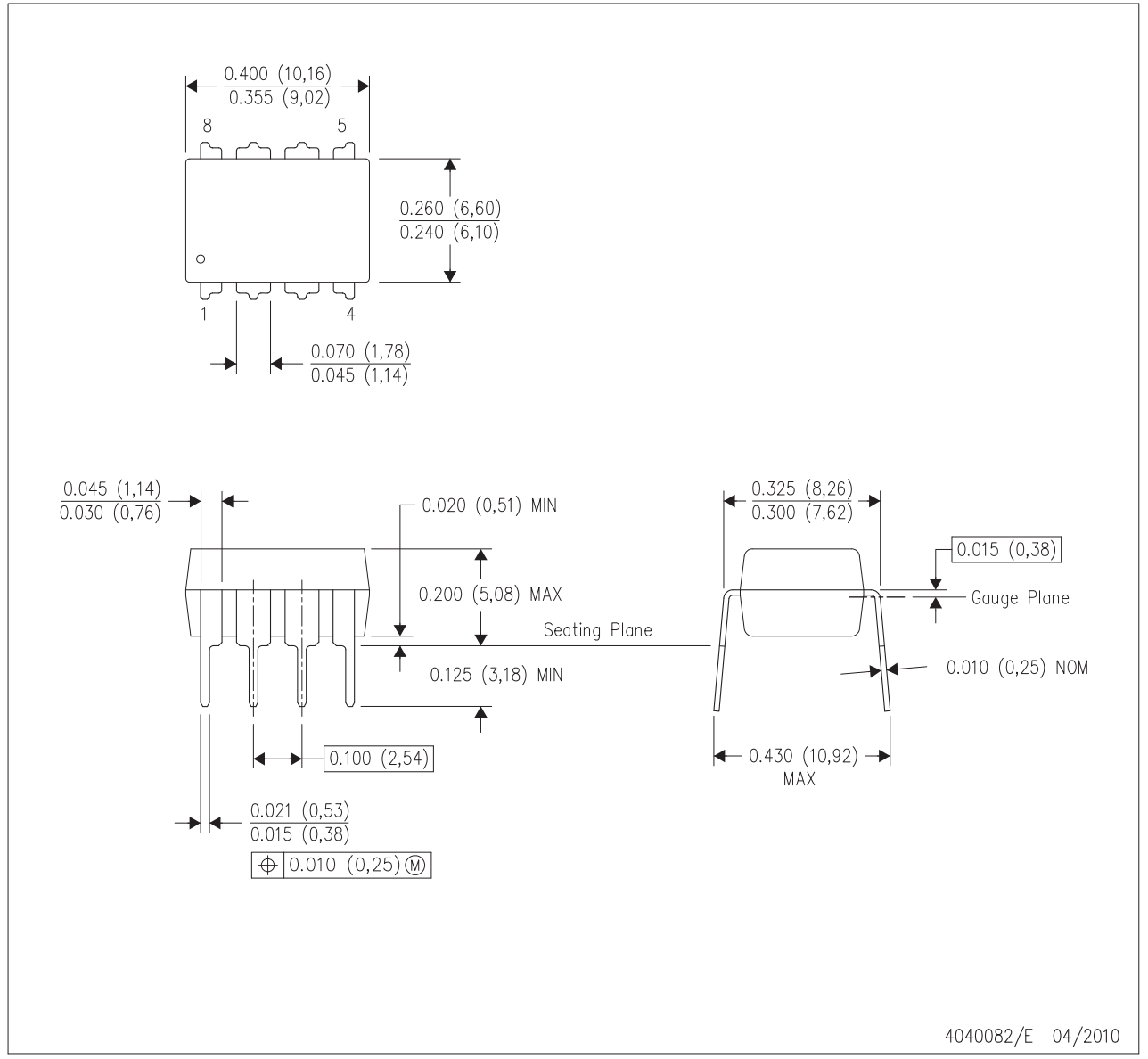


#### \*All dimensions are nominal

Device	Package Type	Package Drawing	Pins	SPQ	Length (mm)	Width (mm)	Height (mm)
OPA129UB/2K5	SOIC	D	8	2500	346.0	346.0	29.0

# P (R-PDIP-T8)

#### PLASTIC DUAL-IN-LINE PACKAGE



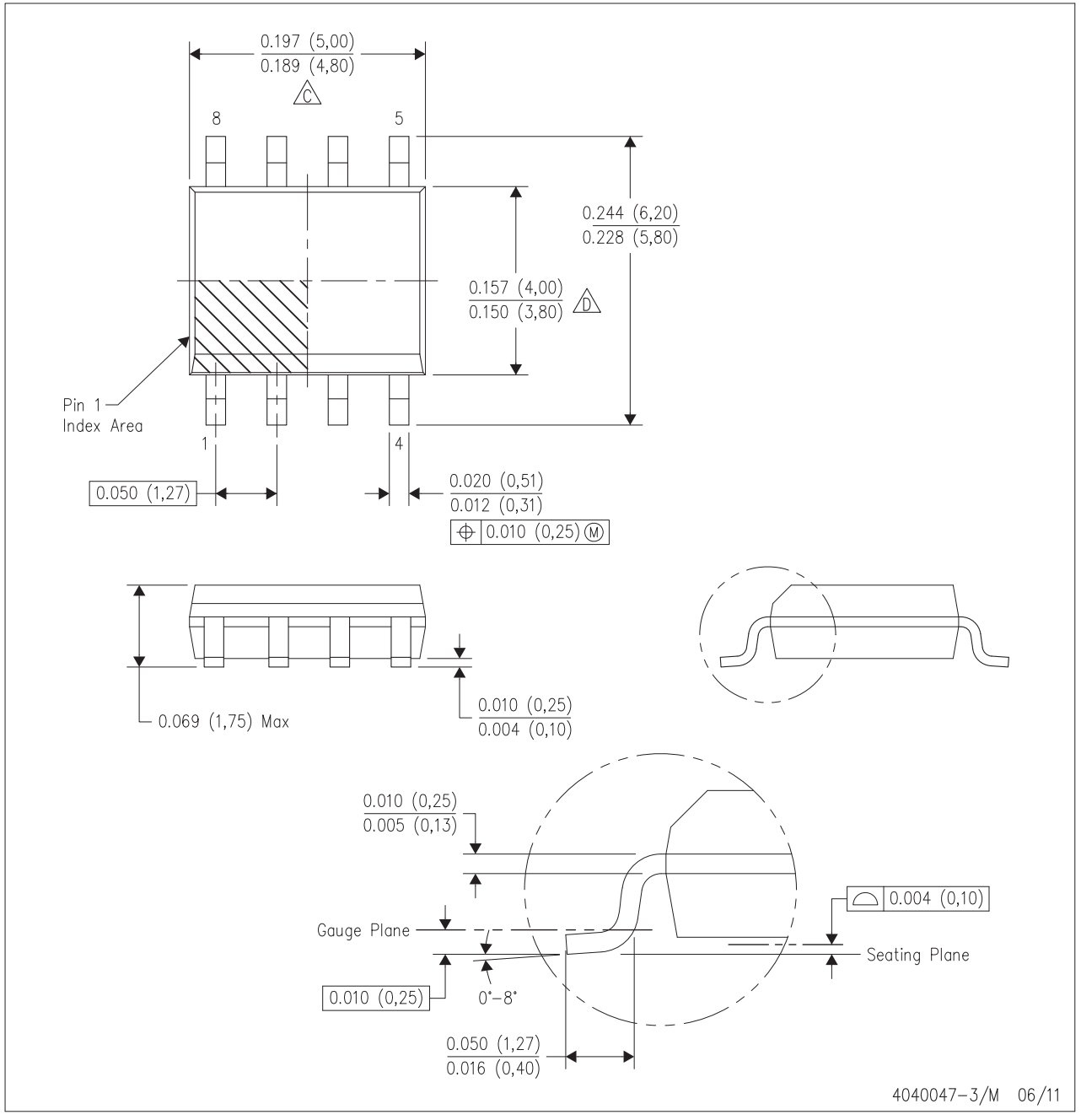
NOTES:

- A. All linear dimensions are in inches (millimeters).
- B. This drawing is subject to change without notice.
- C. Falls within JEDEC MS-001 variation BA.



# D (R-PDSO-G8)

#### PLASTIC SMALL OUTLINE



NOTES:

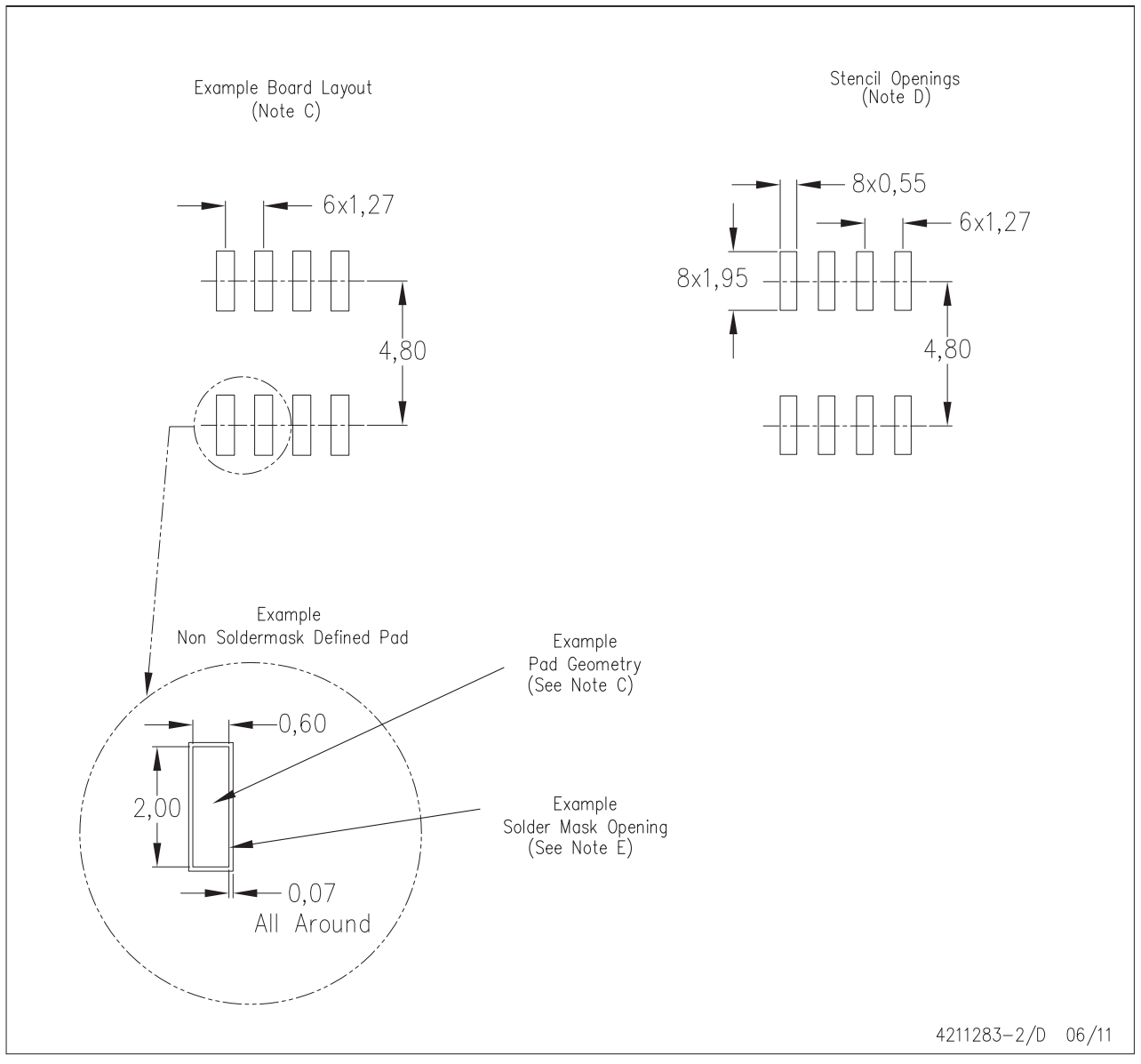
- A. All linear dimensions are in inches (millimeters).
- B. This drawing is subject to change without notice.
- 🖄 Body length does not include mold flash, protrusions, or gate burrs. Mold flash, protrusions, or gate burrs shall not exceed 0.006 (0,15) each side.
- Body width does not include interlead flash. Interlead flash shall not exceed 0.017 (0,43) each side.

  E. Reference JEDEC MS—012 variation AA.



# D (R-PDSO-G8)

# PLASTIC SMALL OUTLINE



NOTES:

- A. All linear dimensions are in millimeters.
- B. This drawing is subject to change without notice.
- C. Publication IPC-7351 is recommended for alternate designs.
- D. Laser cutting apertures with trapezoidal walls and also rounding corners will offer better paste release. Customers should contact their board assembly site for stencil design recommendations. Refer to IPC—7525 for other stencil recommendations.
- E. Customers should contact their board fabrication site for solder mask tolerances between and around signal pads.



#### **IMPORTANT NOTICE**

Texas Instruments Incorporated and its subsidiaries (TI) reserve the right to make corrections, modifications, enhancements, improvements, and other changes to its products and services at any time and to discontinue any product or service without notice. Customers should obtain the latest relevant information before placing orders and should verify that such information is current and complete. All products are sold subject to TI's terms and conditions of sale supplied at the time of order acknowledgment.

TI warrants performance of its hardware products to the specifications applicable at the time of sale in accordance with TI's standard warranty. Testing and other quality control techniques are used to the extent TI deems necessary to support this warranty. Except where mandated by government requirements, testing of all parameters of each product is not necessarily performed.

TI assumes no liability for applications assistance or customer product design. Customers are responsible for their products and applications using TI components. To minimize the risks associated with customer products and applications, customers should provide adequate design and operating safeguards.

TI does not warrant or represent that any license, either express or implied, is granted under any TI patent right, copyright, mask work right, or other TI intellectual property right relating to any combination, machine, or process in which TI products or services are used. Information published by TI regarding third-party products or services does not constitute a license from TI to use such products or services or a warranty or endorsement thereof. Use of such information may require a license from a third party under the patents or other intellectual property of the third party, or a license from TI under the patents or other intellectual property of TI.

Reproduction of TI information in TI data books or data sheets is permissible only if reproduction is without alteration and is accompanied by all associated warranties, conditions, limitations, and notices. Reproduction of this information with alteration is an unfair and deceptive business practice. TI is not responsible or liable for such altered documentation. Information of third parties may be subject to additional restrictions.

Resale of TI products or services with statements different from or beyond the parameters stated by TI for that product or service voids all express and any implied warranties for the associated TI product or service and is an unfair and deceptive business practice. TI is not responsible or liable for any such statements.

TI products are not authorized for use in safety-critical applications (such as life support) where a failure of the TI product would reasonably be expected to cause severe personal injury or death, unless officers of the parties have executed an agreement specifically governing such use. Buyers represent that they have all necessary expertise in the safety and regulatory ramifications of their applications, and acknowledge and agree that they are solely responsible for all legal, regulatory and safety-related requirements concerning their products and any use of TI products in such safety-critical applications, notwithstanding any applications-related information or support that may be provided by TI. Further, Buyers must fully indemnify TI and its representatives against any damages arising out of the use of TI products in such safety-critical applications.

TI products are neither designed nor intended for use in military/aerospace applications or environments unless the TI products are specifically designated by TI as military-grade or "enhanced plastic." Only products designated by TI as military-grade meet military specifications. Buyers acknowledge and agree that any such use of TI products which TI has not designated as military-grade is solely at the Buyer's risk, and that they are solely responsible for compliance with all legal and regulatory requirements in connection with such use.

**Applications** 

. - .

TI products are neither designed nor intended for use in automotive applications or environments unless the specific TI products are designated by TI as compliant with ISO/TS 16949 requirements. Buyers acknowledge and agree that, if they use any non-designated products in automotive applications, TI will not be responsible for any failure to meet such requirements.

Following are URLs where you can obtain information on other Texas Instruments products and application solutions:

**Products** 

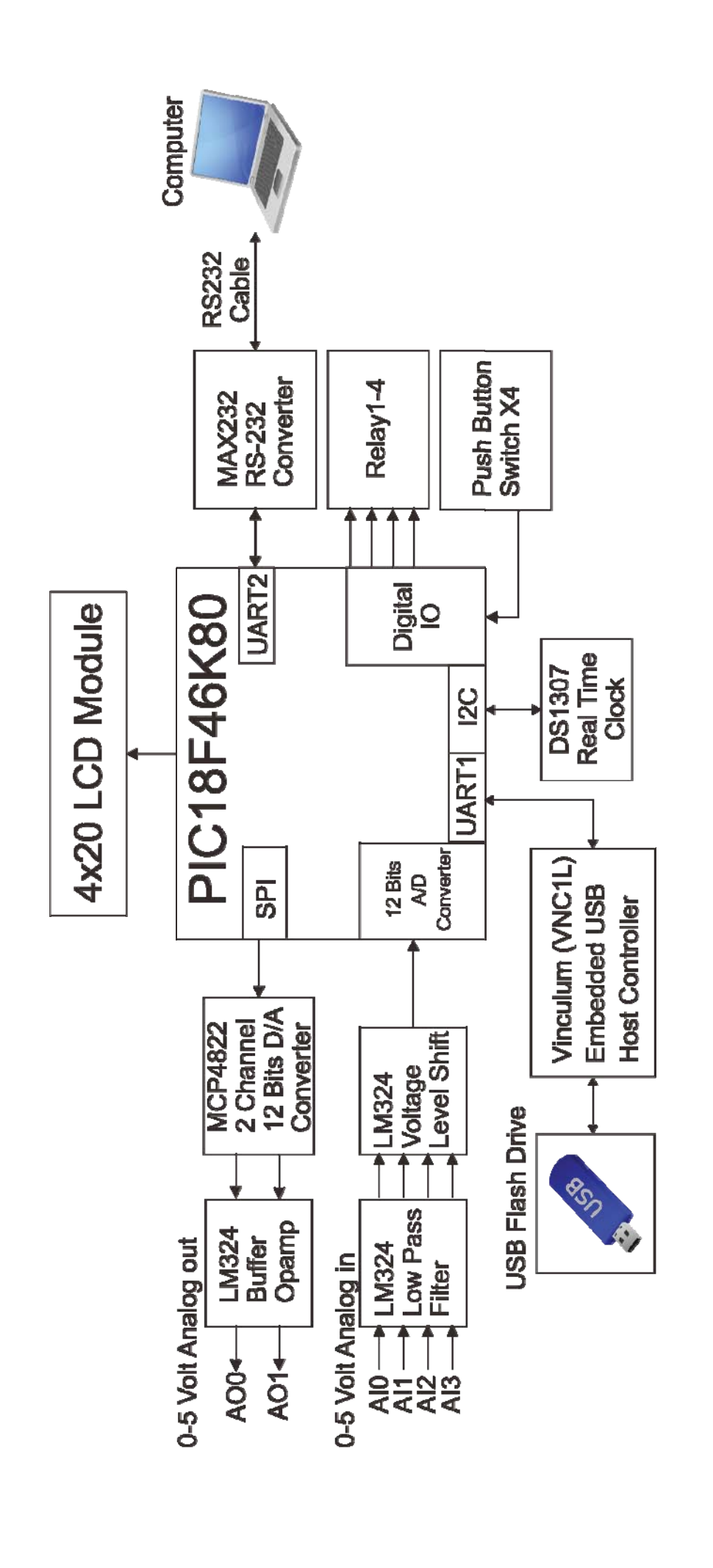
RF/IF and ZigBee® Solutions www.ti.com/lprf

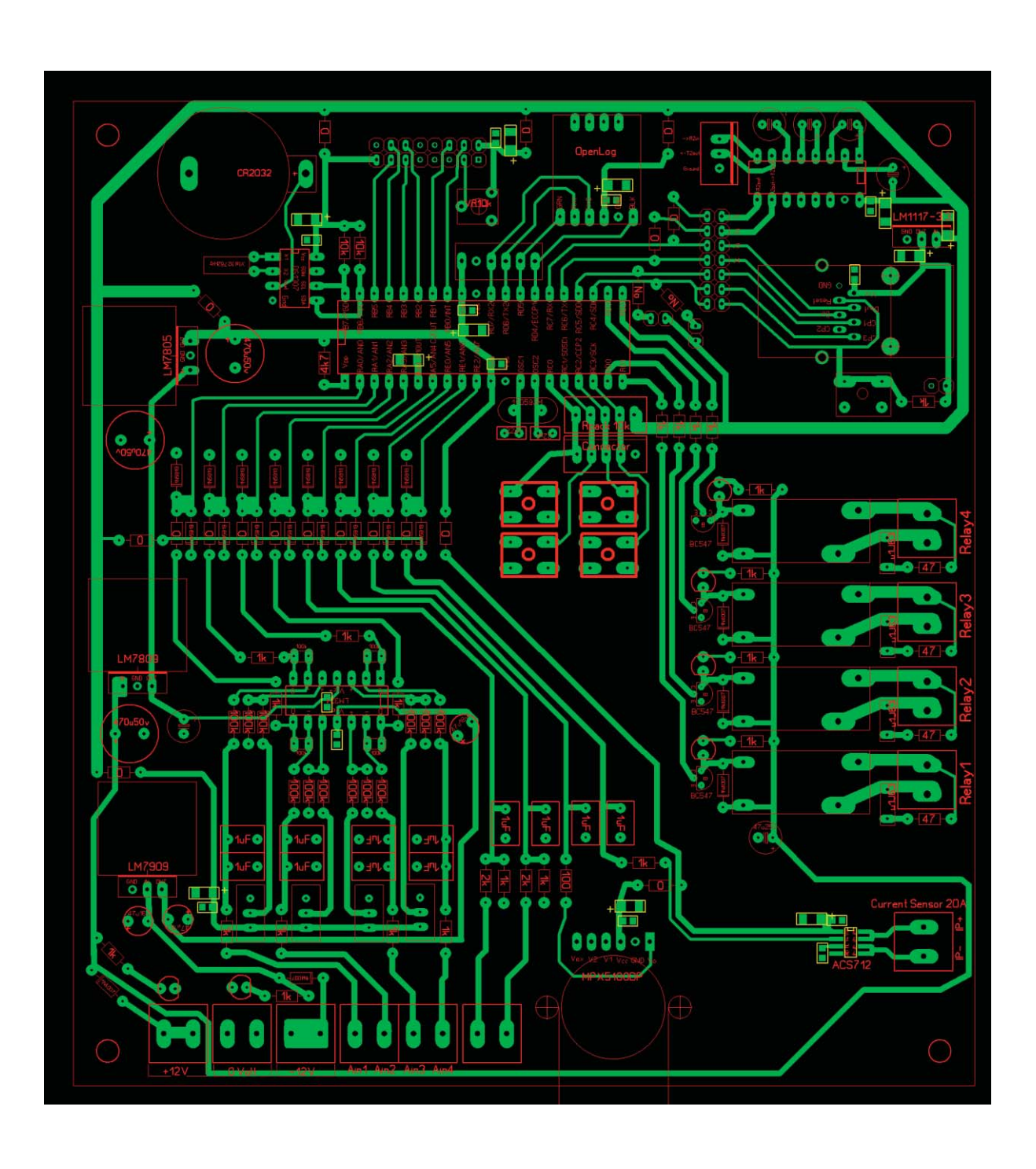
Audio	www.ti.com/audio	Communications and Telecom	www.ti.com/communications
Amplifiers	amplifier.ti.com	Computers and Peripherals	www.ti.com/computers
Data Converters	dataconverter.ti.com	Consumer Electronics	www.ti.com/consumer-apps
DLP® Products	www.dlp.com	Energy and Lighting	www.ti.com/energy
DSP	dsp.ti.com	Industrial	www.ti.com/industrial
Clocks and Timers	www.ti.com/clocks	Medical	www.ti.com/medical
Interface	interface.ti.com	Security	www.ti.com/security
Logic	logic.ti.com	Space, Avionics and Defense	www.ti.com/space-avionics-defense
Power Mgmt	power.ti.com	Transportation and Automotive	www.ti.com/automotive
Microcontrollers	microcontroller.ti.com	Video and Imaging	www.ti.com/video
RFID	www.ti-rfid.com	Wireless	www.ti.com/wireless-apps

TI E2E Community Home Page <u>e2e.ti.com</u>

# ภาคผนวก ค.5

วงจรหน่วยประมวลผลสัญญาณและข้อมูล





# ประวัติผู้วิจัย

# ผู้ช่วยศาสตราจารย์ ดร. พานิช อินต๊ะ

# ตำแหน่งปัจจุบัน

- ผู้ช่วยศาสตราจารย์ วิทยาลัยเทคโนโลยีและสหวิทยาการ มหาวิทยาลัยเทคโนโลยีราช มงคลล้านนา (ดอยสะเก็ด) จังหวัดเชียงใหม่
- ผู้ช่วยผู้อำนวยการฝ่ายวิจัยและบริการวิชาการ วิทยาลัยเทคโนโลยีและสหวิทยาการ มหาวิทยาลัยเทคโนโลยีราชมงคลล้านนา (ดอยสะเก็ด) จังหวัดเชียงใหม่
- อาจารย์ในบัณฑิตวิทยาลัย (อาจารย์พิเศษ) มหาวิทยาลัยเชียงใหม่
- หัวหน้ากลุ่มวิจัยการประยุกต์ใช้ไฟฟ้าสถิตในงานด้านพลังงานและสิ่งแวดล้อม วิทยาลัย เทคโนโลยีและสหวิทยาการ มหาวิทยาลัยเทคโนโลยีราชมงคลล้านนา (ดอยสะเก็ด) จังหวัดเชียงใหม่

#### การศึกษา

พ.ศ. 2546 – 2549	วิศวกรรมศาตรดุษฎีบัณฑิต สาขาวิศวกรรมเครื่องกล
	มหาวิทยาลัยเชียงใหม่
พ.ศ. 2544 – 2546	วิศวกรรมศาตรมหาบัณฑิต สาขาวิศวกรรมพลังงาน
	มหาวิทยาลัยเชียงใหม่
พ.ศ. 2541 – 2544	ครุศาสตร์อุตสาหกรรมบัณฑิต สาขาวิศวกรรมไฟฟ้า สถาบัน
	เทคโนโลยีราชมงคลล้านนา วิทยาเขตภาคพายัพ

### ประสบการณ์ทำงาน

- พ.ศ. 2555 ปัจจุบัน อาจารย์พิเศษ: ระดับบัณฑิตศึกษา ภาควิชาวิศวกรรมเครื่องกล คณะวิศวกรรมศาสตร์ มหาวิทยาลัยเชียงใหม่
- พ.ศ. 2554 ปัจจุบัน หัวหน้าโครงการ: การพัฒนาระบบการวัดและคัดแยกขนาด
   อนุภาคนาโนโดยใช้การวิเคราะห์ความสามารถในเคลื่อนตัวที่แตกต่าง
- พ.ศ. 2552 2555 ผู้ร่วมวิจัย: การพัฒนาเครื่องเก็บตัวอย่างสำหรับอากาศและฝุ่น ละอองลอยขนาดเล็กกว่า 2.5 และ 10 ไมครอนระดับการทดสอบภาคสนาม
- พ.ศ. 2554 ปัจจุบัน หัวหน้าโครงการ: การพัฒนาและปรับปรุงเครื่องตกตะกอนเชิง ไฟฟ้าสถิตสำหรับการกำจัดฝุ่นควันจากเตาเผาขยะชุมชน

- พ.ศ. 2554 2555 หัวหน้าโครงการ: การพัฒนาและปรับปรุงเครื่องตรวจวัดปริมาณ ความเข้มข้นเชิงจำนวนของอนุภาคนาโนแบบใช้หลักการเชิงไฟฟ้า
- พ.ศ. 2554 2556 หัวหน้าโครงการ: การปรับปรุง การสอบเทียบ และการทดสอบ ภาคสนามเครื่องวิเคราะห์ขนาดฝุ่นละอองในบรรยากาศแบบใช้หลักการเชิงไฟฟ้าสู่เชิง พาณิชย์ (ระยะที่ 1)
- พ.ศ. 2554 2555 หัวหน้าโครงการ: การออกแบบและสร้างห้องฆ่าเชื้อด้วย
   สนามไฟฟ้าแบบพัลส์สำหรับกระบวนการฆ่าเชื้อในน้ำนม
- พ.ศ. 2554 2555 หัวหน้าโครงการ: การพัฒนาเครื่องบำบัดอากาศภายในอาคาร สำหรับห้องปลอดความเป็นพิษโดยการผสมผสานเทคนิคเชิงไฟฟ้าสถิตและการกรอง
- พ.ศ. 2553 ปัจจุบัน ผู้ช่วยศาสตราจารย์: วิทยาลัยเทคโนโลยีและสหวิทยาการ มหาวิทยาลัยเทคโนโลยีราชมงคลล้านนา
- พ.ศ. 2553 ปัจจุบัน ผู้ช่วยผู้อำนวยการวิทยาลัยเทคโนโลยีและสหวิทยาการ:
   รับผิดชอบงานวิจัยและบริการวิชาการ
- พ.ศ. 2553 ปัจจุบัน หัวหน้าหน่วยวิจัยการประยุกต์ใช้ไฟฟ้าสถิตเพื่อพลังงานและ สิ่งแวดล้อม
- พ.ศ. 2552 2553 ผู้ร่วมวิจัย: การพัฒนาระบบกำจัดฝุ่นควันจากเตาเผาขยะชุมชน
   ขนาดไม่เกิน 1 ตันต่อวัน ได้รับทุนอุดหนุนจากสำนักงานพัฒนาวิทยาศาสตร์และ
   เทคโนโลยีแห่งชาติ เครือข่ายภาคเหนือ
- พ.ศ. 2552 2553 หัวหน้าโครงการ: การพัฒนาเครื่องวิเคราะห์และเก็บตัวอย่าง สำหรับอากาศและฝุ่นละอองลอยขนาดเล็ก PM 2.5 ได้รับทุนอุดหนุนจากสำนักงาน พัฒนาวิทยาศาสตร์และเทคโนโลยีแห่งชาติ เครือข่ายภาคเหนือ
- พ.ศ. 2551 2552 หัวหน้าโครงการ: การพัฒนาระบบกำจัดอนุภาคแขวนลอยจาก เตาเผาชีวมวลด้วยเทคนิคการตกตะกอนเชิงไฟฟ้าสถิต ได้รับทุนอุดหนุนจากสำนักงาน พัฒนาวิทยาศาสตร์และเทคโนโลยีแห่งชาติ เครือข่ายภาคเหนือ
- พ.ศ. 2551 2553 หัวหน้าโครงการ: โครงการพัฒนาเครื่องวิเคราะห์ปริมาณความ เข้มขันเชิงจำนวนของอนุภาคนาโนแบบใช้หลักการวัดประจุไฟฟ้าสถิตได้รับทุนอุดหนุน จากสำนักงานกองทุนสนับสนุนการวิจัย (ทุนพัฒนาศักยภาพในการทำงานวิจัยของ อาจารย์รุ่นใหม่)
- พ.ศ. 2550 ปัจจุบัน อาจารย์: วิทยาลัยเทคโนโลยีและสหวิทยาการ มหาวิทยาลัย เทคโนโลยีราชมงคลล้านนา

- พ.ศ. 2550 2552 ผู้ร่วมวิจัย: โครงการพัฒนาและปรับปรุงเครื่องวิเคราะห์ขนาด อนุภาคแขวนลอยในอากาศแบบใช้หลักการเคลื่อนตัวทางไฟฟ้าระดับการทดสอบ ภาคสนาม ได้รับทุนอุดหนุนโครงการวิจัย พัฒนา และวิศวกรรม สาขาเทคโนโลยี อิเล็กทรอนิกส์ งานวิจัยระบบตรวจวัดสิ่งแวดล้อม จากศูนย์เทคโนโลยีอิเล็กทรอนิกส์ และคอมพิวเตอร์แห่งชาติ สำนักงานพัฒนาวิทยาศาสตร์และเทคโนโลยีแห่งชาติ
- พ.ศ. 2549 2550 นักวิจัย: ศูนย์วิจัยพลังงาน มหาวิทยาลัยแม่โจ้
- พ.ศ. 2547 2549 ผู้ช่วยวิจัย: โครงการพัฒนาเครื่องวิเคราะห์ขนาดอนุภาคแขวนลอย
   ในอากาศแบบใช้หลักการเคลื่อนตัวทางไฟฟ้า ได้รับทุนอุดหนุนโครงการวิจัย พัฒนา
   และวิศวกรรม สาขาเทคโนโลยีอิเล็กทรอนิกส์ งานวิจัยระบบตรวจวัดสิ่งแวดล้อม จาก
   ศูนย์เทคโนโลยีอิเล็กทรอนิกส์และคอมพิวเตอร์แห่งชาติ สำนักงานพัฒนาวิทยาศาสตร์
   และเทคโนโลยีแห่งชาติ

# ผลงานวิจัยที่ได้รับการเสนอผลงานทางวิชาการและตีพิมพ์เผยแพร่

- ได้รับการตีพิมพ์ผลงานวิจัยในวารสารวิชาการทั้งระดับนานาชาติและระดับชาติ จำนวน มากกว่า 30 เรื่อง
- นำเสนอผลงานทางวิชาการทั้งระดับนานาชาติและระดับชาติ จำนวนมากกว่า 60 เรื่อง
- รายงานการวิจัยฉบับสมบูรณ์ 9 เล่ม
- หนังสือวิชาการ 2 เล่ม

# อื่น ๆ

- กองบรรณาธิการวารสารวิชาการนานาชาติ International Journal of Engineering and Advanced Technology (IJEAT), ISSN: 2249 – 8958
- ผู้ประเมินบทความในวารสารทางวิชาการระดับนานาชาติ ได้แก่
  - Micro & Nano Letters, Institution of Engineering and Technology (IET)
  - Journal of Electrostatics, Elsevier
  - Aerosol and Air Quality Research, Taiwan Association for Aerosol Research
  - Environmental Engineering Science, Mary Ann Liebert, Inc.
  - Maejo International Journal of Science and Technology, Maejo University
  - International Journal of Environmental Engineering, Inderscience Enterprises
     Limited
  - Journal of Mechanical Engineering Research, Academic Journals